Scientific
Research
Publishing

Journal of
Modern Physics

https://www.scirp.org/journal/jmp

Journal Editorial Board

Scientific Research Publishing

Table of Contents

The figure on the front cover is from the article published in Journal of Modern Physics, 2020, Vol. 11, No. 12, pp. 1911-1917 by Kai Wai Wong, Wan Ki Chow.

Journal of Modern Physics (JMP)
Journal Information

SUBSCRIPTIONS

SERVICES

COPYRIGHT

PRODUCTION INFORMATION

The Mathematical Origin of Gravitational Singularities

Kai Wai Wong[1], Wan Ki Chow[2]

[1]Department of Physics and Astronomy, University of Kansas, Lawrence, USA
[2]Department of Building Services Engineering, The Hong Kong Polytechnic University, Hong Kong, China
Email: kww88ng@gmail.com

Abstract

In this note we give a geometrical presentation to the 4D Riemannian curvature as it relates to the Newtonian gravity in the 4D Lorentz manifold. The compacting of the proper time as is necessary for the unification with the Maxwell electrodynamics, as given by Einstein and Kaluza-Klein, should the universe be only of 4D space-time, led to the concept of gravitational field singularity sinks known as black holes, that would not be acceptable under a 5D homogeneous manifold through which the 4D Lorentz manifold evolved by application of the Perelman-Ricci Flow entropy mapping, which is consistent with both Maxwell suggested magnetic monopole, the quantum Higgs vacuum theory and the Gell-Mann standard model for hadrons.

Keywords

Black Hole, Gravitational Field Singularities Within a Lorentz Manifold, Proper Time Compacting, Perelman Mappings as It Relates to Riemannian Curvature

1. Introduction

In order to understand gravity, it is necessary to start from Special Relativity, which states no matter can travel faster than the speed of light c in a 4D space-time manifold. Therefore, the 4D space-time manifold must be expressed in terms of the Lorentz manifold. Namely

$$(ct)^2 - (c\tau)^2 = \sum_{j=1}^{3} x_j^2 \tag{1}$$

where τ is a constant.

The Fourier representation is then given by

$$E^2 - \left(mc^2\right)^2 = \sum_{j=1}^{3}\left(cp_j\right)^2 \tag{2}$$

where $m > 0$ represents a mass.

In order that the 4D space-time covers the massless electromagnetic fields, which obeys the homogeneous 4D Maxwell manifold [1], where τ is 0, the 3D coordinates must be homogeneous, thus satisfying spherical symmetry, hence expressed in the Fermat's sum [2]

$$\left(ct\right)^2 = r^2 \tag{3}$$

where the Fermat's amplitude is the radius of a sphere.

It should be noted that should one replace τ as x_4 and moved to the r.h.s. in Equation (1), do NOT correspond to that we have a 5D homogeneous space-time manifold! [3] As electrodynamics is only given by the 4D homogeneous manifold. Hence, if it is expanded to a homogeneous 5D, it would result in a 5th potential field solution [4], namely the magnetic monopole potential as suggested by Maxwell. Should we take x_4 literally as the 4th space dimension, then τ is the result of a dimension projection from 5D into 4D [5]. In that case, and with space symmetry, the 4th space coordinate must be along "r" the Fermat's amplitude, since the 5D homogeneous manifold satisfies the Fermat's last theorem, and is given in terms of Euler representation by three independent angles having ranges π, 2π and 4π as shown rigorously in ref. [4], making it a degenerate radius for both the photons as well as a massless, charge 0, diagonal long range order Boson field, that is the Higgs fields [6], thus creating the Higgs Bose-Einstein vacuum that must occupy the universe wherever matter is absent. Hence if there is a gravitational field singularity region for masses in 4D, it would be removed by the outward pressure of the Higgs fields [7], thus eliminates such so-called Black Hole regions [8]. In fact, it would appear super bright as is observed at all galactic centers! And it explains why in galaxies stars spiral outward instead of collapsing into the galactic core [9].

2. The 4D Riemannian Curvature

To examine the gravity equation, we again must return to special relativity. Note the velocity of a moving mass depends on the observer's frame in relationship to the mass. Since Newtonian gravity is given w.r.t. the mass frame. Thus we must express the 4D coordinates in a covariant form. Hence it means x_μ must transform by the Riemannian curvature [10]:

$$x_\mu = \sum_{\nu=0}^{3} g_{\mu\nu} x^\nu \tag{4}$$

where

$$g_{\mu\nu} = \frac{\partial x_\mu}{\partial x_\nu} \tag{5}$$

Such that the line element ds is given by

$$ds^2 = \sum_{\mu,\nu} g^{\mu\nu} dx_\mu dx_\nu \tag{6}$$

By adding the 4 Maxwell potentials A_μ, $g^{\mu\nu}$ becomes $\gamma^{\mu\nu} - A^\mu A^\nu$ where $\gamma^{\mu\nu}$ is the space curvature when either μ or ν is fixed as 4, the proper time component and $\gamma^{\mu 4}$ becomes the time-space element, and A^4 either represents the monopole potential or in Einstein's case equal to 0, by closing the integral x_4 around itself, such that

$$ds^2 = \sum_{\mu,\nu} g^{\mu\nu} dx_\mu dx_\nu - \left(dx_4 - A_\mu dx^\mu \right)^2 \tag{7}$$

where x_4 is the proper time τ and NOT a 4th space coordinate. In fact this assumption on 4D space-time invalidates not just the absence of a monopole potential, but also the existence of a Bose-Einstein Higgs vacuum. Absence of it is problematic in the ability to justify the Gell-Mann Standard model [11]. Mathematically, it also invalidates the Perelman entropy Ricci-Flow mapping [12] that gives us the galactic Lorentz 4D manifold, and the Maxwell ghost w.r.t. non-symmetric photon distribution. Apart from these problems, a strict 4D space-time now leaves A_4' as a gravity potential φ_g choice. Thus produces

$$g_{\mu 4}' = g_{\mu 4} + g_{44} \partial_\mu g \tag{8}$$

when we identify $g_{\mu 4}'$ as the electromagnetic potential A_μ' and g_{44} as the unit vector 1, it gives us the Lorentz gauge transformation

$$A_\mu' = A_\mu - \partial_\mu f \tag{9}$$

Keeping in mind

$$\tau^2 = \sum_{\mu=0}^{3} \tau_\mu^2$$

This leads us to the linear line element for the EM unified 4D theory

$$ds = \delta \int d^4 x R_4 F_g + \delta \int d^4 x \left\{ -\frac{1}{4} F_{\mu\nu} F^{\mu\nu} \right\} F_g \tag{10}$$

where R_4 is the invariant derived from the 4D curvature tensors, and $g = \det g_{\mu\nu}$, which gives us the Maxwell potential equation along r, in the spherical coordinates, together with gravitational field F_g inside the Lorentz manifold. $F_{\mu\nu}$ is the electromagnetic tensor [12]. It is because both R_4 and g are given by the Riemannian curvature, leading to a non-linear differential equation for the gravitation field equation, and the existence of a singularity as r in the 4D Lorentz metric approaches 0, thus creating the so call Black holes [8]. This solution can be removed if the proper time τ as expressed in terms of x_4 is not in a closed loop as suggested by Einstein [10] since, when 3D space becomes 0, t^2 must become τ^2, thereby leaving a region as discussed by Wheeler as a worm hole [13]. While in the homogeneous 5D theory [5], leads to the presence of a Higgs vacuum filled with B.E. Higgs fields that carry the infinite quantum energies which would produce a repulsive pressure cancelling the gravitational attractive singular field solution as t approaches 0. Invalidating the concept of the existence of gravitation field singularities within the universe.

To compare to the Newtonian gravitation the gravity equation as given by Equation (10) in turn can be formulated following in the cylindrical space coordinate variables as we observed for the galactic structures in the universe, which in fact geometrically agrees with the Perelman-Ricci flow mapping [14] [15] obtained from the homogeneous 5D manifold, but not from the covariant of the 4D Lorentz manifold as Einstein assumed:

$$g_\varphi = \left(\frac{\partial z}{\partial r}\right)_\varphi = -g_{-\varphi} \tag{11}$$

Hence under the Perelman-Ricci flow mapping, the rate of mass creation can be expressed in terms of $\frac{\partial z}{\partial t} = \Gamma_z$ and $\left(\frac{\partial r}{\partial t}\right)_\varphi = \Gamma_r$ [3]. To explain that let $M(x_\mu)$ be the mass distribution within the Lorentz manifold, similar to Einstein theory [10]. The covariant mass distribution rate becomes

$$S_\mu = \frac{\partial M}{\partial x_\mu} \tag{12}$$

By applying the 3D cylindrical frame, the rate of mass density change becomes

$$S_t = \frac{\partial M}{\partial t}\left\{\frac{1}{\Gamma_z}\hat{z} + \frac{1}{\Gamma_r}\hat{r}\right\} \tag{13}$$

implying a non-symmetric mass density must be in the Lorentz manifold. In fact the value of G being small implies we have a very flat doughnut geometry for the Lorentz manifold containing a mass distribution [3] as in **Figure 1**. There, τ_0 varies [3] from an initial minimum value to τ as a function of h, the thickness of the galaxy given by:

$$h = c(\tau - \tau_0) \tag{13a}$$

and

$$r = \int_0^t v\,\mathrm{d}t \tag{13b}$$

where t is the galaxy age and v is dependent speed of expansion along r.

From Equation (10) as according to the Riemannian curvature in 4D, satisfies

$$g_\varphi = \left(\frac{\partial z}{\partial r}\right)_\varphi = \frac{\Gamma_z}{\Gamma_r} = \frac{1}{G} \tag{14}$$
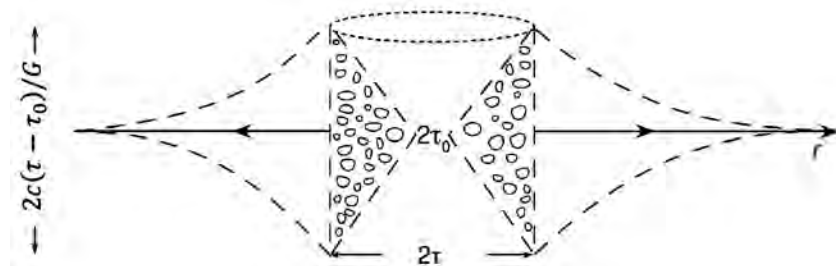
Figure 1. Doughnut structure galaxy model in cross section depicting a time-extended projection action.

Because Γ_z and Γ_r are functions of t, r, τ and A_μ. In order to satisfy Equation (14), Γ_z and Γ_r must be of identical functions multiplied with a proportionate constant G. By following Einstein and compacting τ, when r approaches 0, t must also approach 0, according to homogeneous 4D manifold. Therefore, this common function can be any arbitrary constant value C at $r = 0$. And according to uncertainty principle, and time reversal symmetry obeyed, energy must become + or − infinity at $r = 0$. Thus the gravitational field solution F_g within the Lorentz manifold must be singular at $r = 0$. With the + infinity equal to the creation of masses, such as in a galaxy around its bright core center. While the infinity energy than becomes a "black hole", that is an infinite sink for matter to be reverted back into pure energy. Such gravitation singularities can be removed if the mass creation rates Γ_z and Γ_r are not continuous functions in r and t. In fact pictorially such discontinuous solution resembles an inward rotating mass density vortex. To remove this inward spiral into $r = 0$, physically an increasing outward repulsive pressure must build up as r decreases towards 0. Or if we can just eliminate time reversal symmetry from the Lorentz manifold. Starting with a 5D homogeneous space-time, time reversal is disallowed. And via a Perelman-Ricci Flow mapping, such a natural outward pressure is available via the existence of a Higgs vacuum in the 5D universe, which exist as r is geometrically a degenerate coordinate filled with Higgs bosons, with the homogeneous Maxwell 4D becoming the boundary for the homogeneous 5D manifold. Hence there are NO black holes sinks in the universe, contrary to the theory of Einstein [10] and Penrose [16]. Meaning no matter can be reverted into pure energy, due to gravitational field singularities. Current astronomical observation cannot be interpreted as verification of the existence of black holes in the universe [17]. A spiral mass inward flow is like a fire whirl with attenuation swirling [18] [19] fluid flow requiring adding vorticity and thermally induced motion. It cannot be reverted to pure energy as interpreted.

3. Conclusions

There appear mathematical errors made originally by Einstein and furthered by Penrose and others. The mathematical errors came from the derivation of the covariant Lorentz 4D Riemannian curvature equation that leads to the gravity potential associated with a mass.

As explained in above, if the universe is a 5D homogeneous manifold, then the boundary must be given by the 4D homogeneous Maxwell manifold, and thus there exist massless charge-less quantum fields as suggested by Maxwell given by the 4 component electromagnetic potentials and the orthogonal 5th magnetic monopole potential. With that relationship, the homogeneous 5D is filled entirely with energy carried by the monopoles, which are bosons in the Bose-Einstein condensed state as given by Higgs. And the presence of mass is the result of dimension projection onto the Lorentz 4D, as represented by irreversible Perelman entropy mappings, through the excitation of the monopoles states,

and that matters are expelled by their presence, thus completely removes the gravitation singularity.

Acknowledgements

Conflicts of Interest

The authors declare no conflicts of interest regarding the publication of this paper.

References

[1] Maxwell, J.C. (1864) *Philosophical Transactions of the Royal Society of London*, **155**, 459-512. Reprinted in: The Scientific Papers of James Clerk Maxwell (W. D. Niven), Two Volumes Bound as One, Volume One, New York, Dover Publications, Inc., 1890, 526.

[2] Aczel, A.D. (1997) Fermat's Last Theorem: Unlocking the Secret of an Ancient Mathematical Problem. Penguin Press, London.

[3] Wong, K.W., Dreschhoff, G. and Jungner, H. (2014) The Five Dimension Universe: A Creation and Grand Unified Field Theory Model. Scientific Research Publication, USA.

[4] Wong, K.W., Dreschhoff, G., Jungner, H., Fung, P.C.W. and Chow, W.K. (2018) *Physics Essays*, **31**, 493-495. https://doi.org/10.4006/0836-1398-31.4.493

[5] Wong, K.W., Dreschhoff, G. and Jungner, H. (2012) The Homogeneous 5D Projection and Realization of Quark and Hadron Masses.

[6] Higgs, P.W. (1964) *Physical Review Letters*, **13**, 508-509.
https://doi.org/10.1103/PhysRevLett.13.508

[7] Fung, P.C.W. and Wong, K.W. (2015) *Journal of Modern Physics*, **6**, 2303-2341.
https://doi.org/10.4236/jmp.2015.615235

[8] Hawking, S. and Mlodinow, L. (2010) The Grand Design. Bantam Books, New York.

[9] Wong, K.W., Fung, P.C.W. and Chow, W.K. (2019) *Journal of Modern Physics*, **10**, 1548-1565. https://doi.org/10.4236/jmp.2019.1013103

[10] Einstein, A. (1916) *Annalen der Physik*, **49**, 769.
https://doi.org/10.1002/andp.19163540702

[11] Gell-Mann, M. (1964) *Physical Review Letters*, **12**, 155.
https://doi.org/10.1103/PhysRevLett.12.155

[12] Schwarz, A.J. and Doughty, N.A. (1992) *American Journal of Physics*, **60**, 150.
https://doi.org/10.1119/1.16935

[13] Wheeler, J.A. (1955) *Physical Reviews*, **97**, 511.
https://doi.org/10.1103/PhysRev.97.511

[14] Perelman, G. (2002) The Entropy Formula for Ricci Flow and its Geometric Applications.

[15] Perelman, G. (2003) Ricci Flow with Surgery on Three-Manifolds.

[16] Penrose, R. (2005) The Road to Reality—A Complete Guide to the Laws of the Universe. A.A. Knopf, New York.

[17] Gibney, E. and Castelvecchi, D. (2020) *Nature*, **586**, 347-348.
https://www.nature.com/articles/d41586-020-02764-w
https://doi.org/10.1038/d41586-020-02764-w

[18] Mueller, C.J., Driscoll, J.F., Reuss, D.L., Drake, M.C. and Rosalik, M.E. (1998) *Combustion and Flame*, **112**, 342-346, IN3-IN6, 347-358.
https://doi.org/10.1016/S0010-2180(97)00122-3

[19] Hung, H.Y., Han, S.S., Chow, W.K. and Chow, C.L. (2019) *Thermal Science*.
https://doi.org/10.2298/TSCI181004266H

Evaluation of the Fine Structure Constant

Adriano Alippi

Dept. of Basic and Applied Sciences for Engineering, Sapienza University of Rome, Rome, Italy
Email: adriano.alippi@uniroma1.it

Abstract

An equation is given for analytically defining the value of the fine structure constant, whose derivation follows two main steps, relative to the generation of electric charges and to the polarizability of vacuum due to virtual dipoles. The obtained value matches the experimental one by a factor lower than the relative standard uncertainty produced by the National Institute of Standards and Technology (NIST).

Keywords

Fine Structure Constant, Virtual Particles, Vacuum Permittivity

1. Introduction

The search for a theory that might give reasons for the value of constants in natural phenomena dates from the very beginning of man observing nature processes, and as new physics was going to be introduced into human knowledge, the problem stepped forward to include more fundamental constants. The modern problem was lucidly set by P. A. M. Dirac in a paper dated 1937 [1], where proper mention was given of the frantic efforts made by A. Eddington [2] in the field. Today, the values of fundamental constants are known with ever increasing precision [3] and efforts to give reasons of any single quantity or any link among different quantities are constantly under way and it would be inevitably tedious to cite even a limited group of them.

Probably, the so-called fine structure constant, from the name Arnold Sommerfeld used for it in 1916 in extending the Bohr model of the atom [4], stands as the most tricky character of the drama, for its receding way to be tracked and its adimensional nature. An endless number of articles treat the history and mystery of the constant and here we do only refer to a couple of them, relative to the earliest and to the most recent times [5] [6].

The present paper reports the process aimed at evaluating the fine structure

constant with a value that matches the experimental one reported by the National Institute of Standards and Technology (NIST) by a relative factor 8.4×10^{-11}, which is lower than the relative standard uncertainty [3]. That stands as a strong support for publicizing the obtained equation, in view of proper comments on the underlying procedure.

The question naively rises as to whether an Occam's razor approach would be successful in the struggle for defining the constant value. The way reported here follows two main steps, derived by the assumption that virtual particles [7] modify the electric permittivity of the vacuum, therefore the implicit value of the constant, as it results from the measured values of the contributing physical magnitudes. The two steps refer to the wave function describing the generation of electric charges in the so-called pair production phenomenon, and to the reduced permittivity of the vacuum in the absence of virtual particles. The procedure is based on the fundamental laws of electromagnetism and basic quantum physics and, as such, the referred literature is limited to basic texts.

2. Evaluating the Charge Value

The generation of an electric charge q is only possible with the contemporary generation of a second charge $-q$, allocated in the same point or, more properly, whose space-time distribution of the wave function completely matches that of the first charge, apart from a phase factor, that would be only observable at the interfering of the two waves. The two charges thus created do not produce any electric field in space, whose time variation would have a spherical symmetry that would not be consistent with the Maxwell laws of electromagnetism. However, they successively separate and create a dipole field in space. The charge value that attains the maximum probability is computed and successively that value is selected which allows the particles to separate. To this aim, let us construct the function ψ of either charge, say the positive one q, by applying the operator $\hat{q}$, corresponding to the derivative of ψ with respect to the conjugate variable of the charge itself, written as Θ:

$$-i\hbar \frac{\partial \psi}{\partial \Theta} = q\psi(q, \Theta).$$ (1)

Solution of the equation is

$$\psi = C e^{i\frac{q\Theta}{\hbar}},$$ (2)

with the constant C to be determined by initial conditions. Function Θ should be such that its product with quantity q shares the dimensions of the Planck constant h, equal then to those of the ratio between the electric flux $\Phi(\mathbf{E})$ and the particle velocity v. In addition, when generated, each charge would move away with velocity $\mathbf{v}$ in a direction opposite to that of the second charge and the electric field generated by it starts growing spherically outwards with velocity c from the point of generation.

The flux of the electric field may then be calculated on a plane normal to the

velocity, through the generation point. The surface for the evaluation of the flux can be closed with any half sphere surface at a proper distance where the electric field perturbation has not yet reached.

The flux derivative $\partial\Phi(E)/\partial v$ depends neither on v nor on time t, and stands for the Θ function to be considered, since the wave function in this way would not depend on space or time variables. Indeed, for a charge created at the origin of the coordinates at the time $t < 0$, that moves away along the positive x axis with a velocity v, the electric field in a point P = (0, 0, z) of the z axis at the time $t = 0$, is [5]

$$E = -\frac{q}{4\pi\varepsilon_0}\frac{\gamma}{r^3\left[1+\left(\gamma v_r/c\right)^2\right]^{3/2}}r \tag{3}$$

where r is the distance at the time $t = 0$ between the charge and the point P, v_r the component of the velocity vector v along r, c the velocity of light, ε_0 the dielectric constant and γ the factor $\gamma = 1/\sqrt{1-\beta^2}$, with $\beta = v/c$. The electric field flux through the plane $x = 0$ at time $t = 0$ may be, then, calculated by considering the cylinder geometry of the problem to obtain

$$\Phi(x=0, t=0) = \frac{q}{2\varepsilon_0}(\beta-1). \tag{4}$$

The function Θ can now be computed as the derivative of the flux expression reported above, and that however shall be considered as a density of the function with respect to the solid angle Ω, since the velocity v can be oriented along any direction:

$$\frac{d\Theta}{d\Omega} = \frac{d\Phi}{dv} \tag{5}$$

In addition, a factor 2 has to be taken into consideration for the electric field flux and its derivative, since an equal additional amount to it is contributed by the second charge, entangled with the first one. Finally, one obtains

$$\Theta = \frac{4\pi q}{\varepsilon_0 c}. \tag{6}$$

that has to be inserted into Equation (2) to give

$$\psi_+ = Ce^{4\pi i\frac{q^2}{\varepsilon_0 c\hbar}}, \tag{7}$$

being ψ_+ specified for the positive charge q. The wave function of the second charge of opposite sign $-q$ is equal to that of the first one, save for the sign in the exponent and a different constant C'. With regard to these constants, the probability of the generation of both particles $P_{\text{pair}} = |\psi_+ + \psi_-|^2$ vanishes at $q = 0$, so that we may assume $C' = -C$, and one may write

$$P_{\text{pair}} = |\psi_+ + \psi_-|^2 = \left[2\sin\left(\frac{4\pi q}{q_P}\right)^2\right]^2, \tag{8}$$

where the expression of the Planck charge unit $q_P = \sqrt{2\varepsilon_0 c\hbar}$ has been used.

Such a probability value, however, which is a maximum at

$$q_{\max} = \frac{q_P}{4\sqrt{2\pi}} = \frac{e}{4\sqrt{2\pi\alpha}} = 1.1675e, \qquad (9)$$

with $\alpha = (e/q_P)^2$ the fine structure constant, is not relative to a pair of particles experimentally observable, but only to the generation of a pair of opposite charges departing one from the other. These are just virtual particles which, in order to be detectable, must separate one from the other, in a process that is counteracted by the electrostatic attractive force between them. The process has no interpretation in classical physics, but could be only described by quantum physics. The quantum potential of Bohmian theory [8], for instance, would allow to localize two pointlike particles in different places at the very same time, permitting a finite force to overtake the attractive effect. The separation of the particles makes the wave function to collapse into a definite state, which corresponds to the maximum of probability with a minimum work. Since the electrostatic attractive force depends on a factor q^2/ε_0, the probability function in Equation (8) could be multiplied by this inverse factor and the maximum of the obtained overall function defines the state of the free particles:

$$P = P_{\text{gen}} \cdot P_{\text{sep}} \propto \frac{\sin^2\left(\dfrac{4\pi q}{q_P}\right)}{\left(\dfrac{4\pi q}{q_P}\right)^2} = \left(\frac{\sin \xi^2}{\xi}\right)^2 \qquad (10)$$

where $P_{\text{gen}} = P_{\text{pair}}$ is the probability of generating the pair and a similar notation P_{sep} is used for the separation process, although this is not a probability function. It is worth pointing that the zeroes and maxima of the P function do not depend on the multiplying coefficient of the single component functions, and this makes it possible to define the P function in just one variable $\xi = 4\pi q/q_P$, as reported in Equation (10).

The two functions P_{gen} and P_{sep} are represented in **Figure 1** vs. the parameter
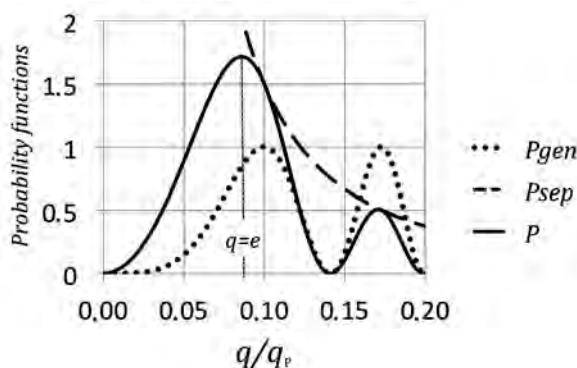
Figure 1. Probability functions vs. value of the charge, in Planck unit $q_P = \sqrt{2\varepsilon_0 ch}$. Units for each component function are arbitrarily chosen, in as much as the positions of maxima and minima in the product of functions P_{gen} and P_{sep} are not sensitive to normalization factors.

$q/q_P = \xi/(4\pi)$, where the two effects are identified, that counteract each other at low values of ξ, up to the first maximum, that is attained at $\xi_{max} = 1.07961158997447$. This value is not compatible with the known values of the involved constant and that is supposedly due to the presence of virtual particles in the vacuum, which affect the interaction between the true charges, by changing the electric permittivity of vacuum to its commonly known value ε_0.

Indeed, the maximum condition on function P sets a constrain on all the electromagnetic quantities involved, q, c and ε_0. The velocity c, however, is not to be considered affected by virtual particles, as it is suggested by its equality for electromagnetic and gravitational waves [9].

The ξ_{max} condition reduces then to a constrain on the electromagnetic interaction parameter q^2/ε_0. Charges originate with $\pm e$ values in an absolute vacuum that possesses an electric permittivity ε_{00}, and then access to reality in the real vacuum, whose permittivity is $\varepsilon_0 = \varepsilon_r \varepsilon_{00}$. Condition from Equation (10) should be then better written in the variable

$$\xi_0 = \frac{4\pi e}{\sqrt{2\varepsilon_{00} ch}} \tag{11}$$

whose ξ_{max} value sets the absolute vacuum permittivity at

$$\varepsilon_{00} = \frac{1}{2ch}\left(\frac{4\pi e}{\xi_{max}}\right)^2 = 8.753842149544 \times 10^{-12}\,\text{S.I.} \tag{12}$$

and $\varepsilon_r = 1.0114630423466$.

It has to be noted that function P attains its maximum for the variable ξ solving the equation

$$\tan \xi^2 = 2\xi^2, \tag{13}$$

with a value ξ_{max} whose squared value is $(4\pi)^2$ the fine structure constant value, increased by a factor due to the relative permeability factor ε_r, so that one may define a constant $\alpha_0 = \varepsilon_r \alpha = 0.00738100243079751$ in absolute vacuum, or $a_0^{-1} = 135.482952528$.

3. Evaluating the Vacuum Permittivity

The consistency of the procedure finds its validation in obtaining else way the value of the permittivity of the absolute vacuum, or the susceptibility of the real vacuum

$$\chi = \varepsilon_r - 1 = 0.0114630423466. \tag{14}$$

In order to prospect such validation, let us look for the polarization produced in the vacuum, when a uniform electric field E is present in a given volume of space. A number of virtual electric dipoles are constantly produced and annihilate in a way which depends upon the strength of the field E, each dipole lasting for a time Δt, inversely related to the energy needed to form it. The overall component of the dipoles along the electric field direction per unit volume

stands as the electric polarization vector $\boldsymbol{P}$ of the vacuum, and its ratio to the electric field equals the product of the susceptibility constant χ of the vacuum times its permittivity

$$\frac{\boldsymbol{P}}{\boldsymbol{E}} = \varepsilon_0 \chi . \tag{15}$$

In order to obtain the value of the permittivity, a procedure may be followed similar to the one previously followed for the charge maximum probability, by considering the product of the virtual dipole multiplied by its life-time ($\boldsymbol{p}\Delta t$). Indeed, the product of each charge times its displacement is to be taken into account in place of the dipole, so as to deal separately with the positive and the negative charge. The polarization electric field $\boldsymbol{E}_\mathrm{P}$ stands then as the conjugated variable, so that the contribution of the positive charge in the expression of the wave function may be written as

$$\psi_\mathrm{pol}^+ \propto \mathrm{e}^{i\frac{\boldsymbol{p}\cdot\boldsymbol{E}_\mathrm{P}\Delta t}{\hbar}} = \mathrm{e}^{i\frac{E_\mathrm{P}}{E}} , \tag{16}$$

where use has been done of the relation between time and energy. The wave function then writes as

$$\psi_\mathrm{pol} = \psi_\mathrm{pol}^+ + \psi_\mathrm{pol}^- \propto \sin\left(\frac{\boldsymbol{E}_\mathrm{P}}{\boldsymbol{E}}\right) = \sin\chi . \tag{17}$$

As for the case previously considered for the expected value of the charge, the expected value for the susceptibility χ will be the one that makes the function ψ_pol to attain its maximum at

$$\chi = \frac{\pi}{2}, \tag{18}$$

which is two orders of magnitude higher than the expected one. However, the electric polarization χ in the absolute vacuum is contributed by all the virtual particles, whose charge distribution follows the one previously reported in Equation (8), that gets its maximum for $\xi = \pi/2$, where $\sin\xi = 1$. Since the effective polarization in the real vacuum is contributed by those virtual charges alone that might interact with real charges, that is with electrons, the resulting maximum value $\pi/2$ has to be multiplied by the value the charge function attains for the electronic charge value, that is by $\sin\alpha$, with α the fine structure constant. Expression $\sin\alpha$ is obtained from Equation (8), save for the factor $1/8\pi$ in the phase expression. This is due to the electric field $\boldsymbol{E}$ aligning the dipoles along its own direction, so that no integration over the solid angle (4π) has to be taken into account and that each charge contributes to just one half of the dipole intensity.

An additional effect has to be considered for the final evaluation of the susceptibility, which is the normalization factor of the probability function. The interaction, indeed, of the real charges with the electronic charges in the virtual field makes the wave function denominator to be reduced by the probability of the electron pair in the virtual field, that is by the amount $\sin^2\alpha$. The interaction of a real charge, however, with one virtual pair finally releases an electronic

charge of the same sign, whose probability

$$\frac{1}{2}\frac{\sin^2 \alpha}{\left(\int\limits_{-\infty}^{+\infty}\sin x^2 dx\right)} = \frac{1}{2}\left(\frac{\sin \alpha}{\pi/2}\right)^2 \qquad (19)$$

has to be subtracted from the probability value $\sin^2 \alpha$ just reported above. Once, however, that this effect is taken into account, the function has to be newly normalized by subtraction of its probability term

$$\left(\frac{\sin \alpha}{\pi/2}\right)^2 \frac{\pi}{2}\sin \alpha . \qquad (20)$$

The real electric susceptibility χ_{real} will be finally written as

$$\chi_{\text{real}} = \frac{\pi}{2}\frac{\sin \alpha}{1-\sin^2 \alpha + \frac{1}{2}\left(\frac{\sin \alpha}{\pi/2}\right)^2 - \left(\frac{\sin \alpha}{\pi/2}\right)^2 \frac{\pi}{2}\sin \alpha}, \qquad (21)$$

which is set equal to

$$\chi_{\text{real}} = \frac{\alpha_0}{\alpha} - 1 , \qquad (22)$$

to give α = 0.00729735256868569, which matches the experimental value by a relative factor 8.41×10^{-11}. It should be noted that the α value of the fine structure constant is reported in the NIST data [3] with a standard uncertainty ranging from 0.0072973525682 to α = 0.0072973525704, between whose limit the value reported above is contained [10]. That sets a definite value to the relative ε_r permittivity of vacuum, as it results from Equation (14).

4. Conclusions

In conclusion, two steps are produced for analytically deriving the value of the fine structure constant. Firstly, a wave function is constructed describing the generation of two electrical charges in the so-called absolute vacuum that lately do separate as free charges in the real vacuum. In this way, the obtained value for the electrical permittivity results to be slightly higher than the experimental one, due to the effect of virtual charges acting in the separation process. A second step is then produced, in order to evaluate the contribution of this effect on the value of the permittivity through the introduction of a wave function for the polarization vector that leads to the value of the finite structure constant, equal to the one available in the NIST data.

The procedure relays on the search of the wave functions describing the underlining physical processes and on their relative maxima determination, and its validity really stands upon the optimum match between the derived numerical value of the fine structure constant and its experimental datum. Slight variations introduced into the procedure, particularly into the normalization function of the susceptibility, do greatly alter the deduced value in a way which seems to be impracticable for valuable results.

Acknowledgements

Conflicts of Interest

The author declares no conflicts of interest regarding the publication of this paper.

References

[1] Dirac, P.A.M. (1937) *Nature*, **139**, 323.
https://doi.org/10.1038/139323a0

[2] Eddington, A. (1942) *Proceedings of the Royal Physical Society*, **54**, 491-504.
https://doi.org/10.1088/0959-5309/54/6/303

[3] https://physics.nist.gov/cgi-bin/cuu/Value?alph

[4] Sommerfeld, A. (1916) *Annalen der Physik*, **51**, 1-94, 125-167.
https://doi.org/10.1002/andp.19163561802

[5] Kragh, H. (2003) *Archive for History of Exact Sciences*, **57**, 395-431.
https://doi.org/10.1007/s00407-002-0065-7

[6] Sherbon, M. (2019) Fine-Structure Constant from Sommerfeld to Feynman.
https://doi.org/10.31219/osf.io/hk8p5

[7] Jaeger, G. (2019) *Entropy*, **21**, 141. https://doi.org/10.3390/e21020141

[8] Bohm, D. (1952) *Physical Review*, **85**, 166-179.
https://doi.org/10.1103/PhysRev.85.166

[9] Abbott, B.P., LIGO and Virgo Collaborations (2017) *Physical Review Letters*, **119**, 161101-161117.

[10] Feynman, R.P. (1985) QED: The Strange Theory of Light and Matter. Princeton University Press, Princeton, 129-130.

Relativistic Approximations for Quantization and Harmony in the Schrödinger Equation, and Why Mechanics Is Quantized

Antony J. Bourdillon

UHRL, San Jose, CA, USA
Email: bourdillona@sbcglobal.net

Abstract

The initial purpose is to add two physical origins for the outstandingly clear mathematical description that Dirac has left in his Principles of Quantum Mechanics. The first is the "internal motion" in the wave function of the electron that is now expressed through dispersion dynamics; the second is the physical origin for mathematical quantization. Bohr's model for the hydrogen atom was "the greatest single step in the development of the theory of atomic structure." It leads to the Schrodinger equation which is non-relativistic, but which conveniently equates together momentum and electrostatic potential in a representation containing mixed powers. Firstly, we show how the equation is expansible to approximate relativistic form by applying solutions for the dilation of time in special relativity, and for the contraction of space. The adaptation is to invariant "harmonic events" that are digitally quantized. Secondly, the internal motion of the electron is described by a stable wave packet that implies wave-particle duality. The duality includes uncertainty that is precisely described with some variance from Heisenberg's axiomatic limit. Harmonic orbital wave functions are self-constructive. This is the physical origin of quantization.

Keywords

Wave Packet, Wave-Particle Duality, Harmony, Relativity, Dispersion Dynamics

1. Introduction

For the electron, Dirac's unspecified "internal motion", that is implied by relativity and quantum physics, is only fleetingly mentioned in his Principles [1]. That motion is here expressly analyzed in the wave packet, and this provides a

clear explanation for wave-particle duality. The model of the packet opposes one kind of *quantum theory* that is axiomatic and mathematical, (including: quantization; uncertainty limits; creation and annihilation operations; a supposedly unstable wave packet—even in absence of Newtonian force; unspecified reduction of the packet; etc.), against *physical quantum mechanics* that is empirical (including: quantization due either to stable and harmonic wave functions as in Bohr's hydrogen atom; or to conservation of mass; of particles; of charge; of energy; of momentum with classical wave-particle uncertainties; combined with continuous reduction of packets that are stable in the absence of external force; etc. [2]-[7]). Physically, this second set of properties is more substantial than the alternative mathematical representation by probabilistic statistics. The two representations frequently clash, not only in the wave packet but equally in neutrino induced radioactive decay (see Vasiliev [8]), and also in uncertainty as will be discussed below.

There are moreover, more profound differences: in mathematics it is convenient to simplify problems by abstractly limiting analysis; empirical physics, by contrast, includes evolving possibilities whether implicit in current theory, or whether perhaps measurable with future technology (as in the decay) and theory. A complete empirical physic is unattainable and noumenal. Each method has its merit at different phases of development in various fields in physics.

This merit is partly psychological: mathematical tautologies carry undeniable certainties: as a simple example, the summation 2 + 2 = 4 is certain because of number definition. Modulo 4, 2 + 2 = 10 is equally certain and for indistinguishable formal reasons. Sometimes postulates have extreme consequences: the imaginary number *i* underpins wave theory [9] and the whole of modern physics. Mathematical theories are in principle hypothetical. On the other hand, physical quantum mechanics is denied that tautological simplicity: hypothesis is to be falsified by measured fact [10] [11]. All hypotheses are equally true until one is falsified. Side-by-side, contradictory theories are normal in physics provided they are each, in principle, falsifiable, otherwise, any of them is physically meaningless. Meaningless also are editorial "opinions" that are not specifically verified by sufficient fact or consistent theory. Theoretical evolution is never complete. Some examples of these features are described in what follows[1].

Whereas mathematicians believe their axioms when they are consistent within restrictive incompleteness [12] [13]; in physics by contrast, only falsifiable propositions are admissible: they begin logically "true", and become unphysical upon

---

[1]In confirmation, A. Pais wrote that "It was [Einstein's] almost solitary conviction that quantum mechanics is logically consistent, but that it is an incomplete manifestation of an underlying theory in which an underlying objective reality is possible." [*Niels Bohr's Times* (1991) Oxford. ISBN 0-19-852049-2 p. 433]. Actually, in his EPR paper [Einstein, A., Podolsky, B. and Rosen, N., Phys. Rev. **47** 777-780 (19350] Einstein held that Bohr's theory is incomplete. The latter had claimed that *all* that can be known about an electron is its wave function, particularly with regard to momentum and position. This seems an unlikely theory since Gödel's mathematical theorems on completeness and consistency in axiomatic systems [12] [13]. This footnote does not contribute to the debate so much as outline background for arguments given in the text.

falsification[2]. In particular, Bohr's hydrogenic orbits were quantized by numbers in energetic series. Numerical quantization is an easy operation, but needs the physical model. Physically, the quantization is due to constructive interference, over time, in quantized and harmonic electronic wave functions. The physical model is not always given (e.g. intrinsic spin [3]); but the relativistic approximation to be described here is both mathematical and physical.

The Schrödinger equation is non-relativistic, but corrections can be made in various ways. By contrast, the well-known Klein-Gordon equation does include mass energy and is consistently represented in second order, as Lorentz covariant. Alternatively, any solution of the free Dirac equation [1] is, component-wise, a solution of the free Klein-Gordon equation. Electromagnetic interactions can be incorporated, forming the topic of scalar electrodynamics. Here we return to the simple inclusion of electromagnetism that is found in the Schrodinger equation, and include special relativity by incorporating the invariant event of harmonization. Approximate solutions at low relativistic energies can then be accounted more easily than occurs in a wide literature e.g. [14] [15].

2. Wave-Particle Duality and Harmonic Quantization

The physical wave packet replaces Dirac's mysterious "internal motion". The packet is the volume within which the energy of a photon or particle is contained: as in statistics, the normal shape is the Gaussian, in **Figure 1**. The dual wave-particle is described and explained by the stable wave packet ϕ:

$$\phi = A \cdot \exp\left(\frac{X^2}{2\sigma^2} + X\right) \quad \text{with } X = i\left(\bar{k}x - \bar{\omega}t\right) \tag{1}$$
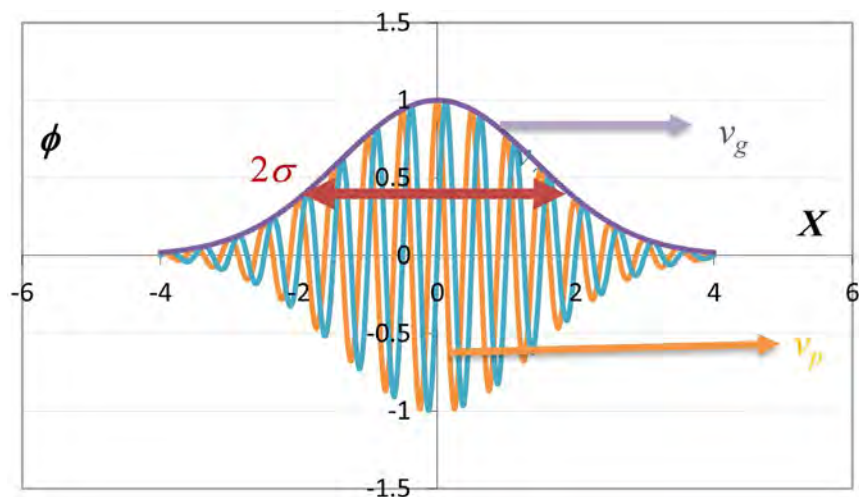
Figure 1. Stable wave packet (Equation (1)) containing envelope with group velocity v_g (purple arrow) and real (orange) and imaginary (blue) parts of the carrier wave having phase velocity v_P (horizontal orange arrow). The full width, at $\phi = 1/e$, is 2σ as shown by the red double arrow.

[2]Physics verifies; Mathematics intuits; understanding unifies: "In the idea of the will, the real and ideal are united." [*Hegel, G. W. F.* (1969). *Hegel's Science of Logic. Allen & Unwin.*]

Its mean angular frequency $\bar{\omega}$ and mean wave vector $\bar{k}$, together, stabilize the free packet through conservation laws in energy and momentum. Here, the propagation is represented as unidirectional, while the two transverse directions may be represented by the normalized amplitude $A(x, y, z)$. This packet represents not only optical photons described by solutions to Maxwell's equations, but it represents equally the free electrons used in an electron microscope column for imaging, or for astronomic photons that have travelled billions of light years. The figure describes a complex carrier wave in a Gaussian envelope.

The frequency in this packet is given by Planck's Law and is proportional to energy E:

$$E = \hbar\omega \tag{2}$$

that had been found quantized in photoemission from a bound atomic state. The reduced Planck constant is written $\hbar$. Bohr successfully applied this quantization to atomic spectra in the hydrogen atom: the wave orbitals harmonize as is represented provisionally on a planetary model (**Figure 2**) with red wave density amplitudes on a blue orbit.

In a particle, the displacements are not the real tensor fields known in electromagnetism; but components of a complex wave function. As Pauling observed, "[Bohr's] successful effort [at quantizing the spectrum of hydrogen], despite its simplicity, may be considered the greatest single step in the development of the theory of atomic structure [16]." Bound waves are harmonic on stationary states; otherwise the waves would self-annihilate. Of course, the constructive self-interference occurs on all three spatial dimensions (not just on the plane illustrated in **Figure 2**). The harmonization is provided in Schrödinger's curvilinear solutions to his equation, with three integral quantum numbers.

The free electron wave function is complex in **Figure 1**, but it is similar to quantized photons adapted from Maxwell's theory: the electromagnetic wave consists in two real components, an electric field **E** and lagging magnetic field **B** that is normal to both **E** and the direction of propagation along the orbit. The phase lag between the two fields is π/2 like the imaginary part of the particle wave function. The distinguishing difference is that the free electromagnetic
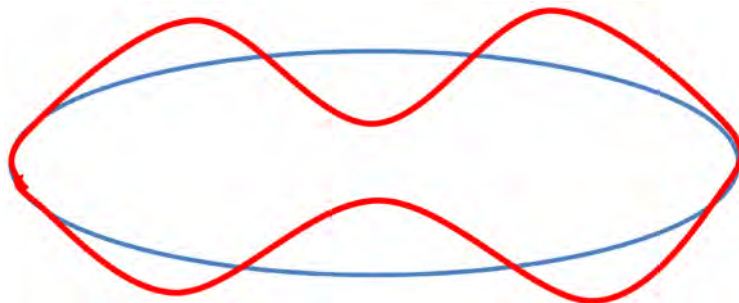
Figure 2. Schematic, 1-dimensional diagram showing three cycles of harmonic density functional red amplitude located on a blue orbit. The quantum number for this wave on this orbit is 4, but the full Schrödinger solution in curvilinear coordinates in 3-dimensions is more complicated [16].

wave has zero mass with group velocity equal to phase velocity, $v_g = v_p = c$, the speed of light *in vacuo*.

Prior to Bohr's success with quantized solutions for the hydrogen atomic states, Einstein had described the special theory of relativity: physical laws are invariant in all inertial reference systems. This includes the special case of *c*. There are several consequences that are summarized for the present discussion. In whatever inertial reference frame, the energy *E*, momentum *p*, and rest mass m_0, are related by Einstein's formula:

$$E^2 = p^2 c^2 + m_0^2 c^4 \tag{3}$$

which is often written in terms of relativistic mass *m*:

$$E = m'c^2 = \frac{m_0 c^2}{\left(1 - \beta^2\right)^{1/2}} \tag{4}$$

with $\beta = v_g / c$. Applying Planck's law (Equation (2)) and de Broglie's subsequent hypothesis $p = h_i / \lambda = \hbar k \simeq h_j / \lambda_i$, with *j* = *x*, *y* or *z* Cartesian components. Equation (3) is transformed:

$$\omega^2 = p^2 c^2 + m_0^2 c^4 / \hbar^2 \tag{5}$$

with derived values in dispersion dynamics [2] [3]:

$$\frac{d\omega}{dk} \cdot \frac{\omega}{k} = v_g \cdot v_p = c^2 \tag{6}$$

including second derivative curvature, which is most easily derived in simplified units, $c = 1 = \hbar$:

$$\frac{d^2\omega}{dk^2} = \frac{1}{m_{\text{eff}}} = \frac{a}{F} \tag{7}$$

where m_{eff} is a relativistic effective mass, equal to the ratio of force *F* to acceleration *a* in Newton's second law of motion. In consequence, since *F* depends on a physical law and is invariant in all inertial reference systems $d^2\omega/dk^2 < 0 \supset a < 0$ *i.e.* reversed. (When, as occurs for conducting electrons in electrostatic crystal fields, the electron energy-dispersive curvature is negative, so also is the Coulombic acceleration). Equations (3)-(7) are the essential formulae in Dispersion Dynamics. They are generally consistent with the Klein-Gordon equation that is likewise frame invariant.

3. Properties of the Wave Packet

Consider Equation (1) as the product of two wave components and normalizer $\phi = A\phi_1 \cdot \phi_2$. The envelope ϕ_1 is real; the carrier wave ϕ_2 is complex. The wave packet in **Figure 1** combines three essentials of modern physics: the particle, the wave and relativity.

Firstly, the purple envelope group, ϕ_1, carries the corpuscular properties (energy and momentum) that Newton claimed for light. These properties were extended to particles and supported quantized events in Plank's law and de

Broglie's hypothesis. Optics of light and electrons are almost the same, bur with the noteworthy exceptions of finite mass in the latter, along with slower group velocities $v_g < c$.

Secondly, the green and orange complex oscillations, ϕ_2, within the group cause the diffractive interference that was systematically described by Huygens, Fresnel, Fraunhofer *et al.* The oscillations also determine the harmonies that quantize stationary states established by Schrödinger's solutions for the hydrogen atom. Whereas the carrier wave determines the principal features of interference, diffraction etc.; the values of the real product $\phi_2(x,t)*\phi_2(x,t) = e^0$ are everywhere constant in all space and time, so that the oscillations carry neither energy nor momentum: *the frequency spectrum in ϕ_2 has no influence on the stability of the wave group envelope*, ϕ_1, though the energy and momentum of the packet do indeed depend on its frequency ω and wave-vector $k = 2\pi/\lambda$. Meanwhile, the oscillations cause the harmonization of stationary carrier waves, at orbits or boundaries, during emission or absorption. This is the consequence of constructive self-interference.

Thirdly, the wave properties of X in these functions are subject to the relativistic invariance of physical laws in all inertial reference systems. Equations (3)-(7) are some of its consequences. Figure 1 and Equation (1) describe the principal qualities of free particles (whether having zero or finite rest mass) in quantum physics.

Group and phase velocities of the relativistic wave functions are plotted elsewhere [2] [3]. The absolute value of the carrier wave ϕ_2 is constant with x and t; *energy transport is described by its envelope ϕ_1*.[3] The elastic union between the carrier wave ϕ_1, and group envelope ϕ_2, is a significant characteristic of wave-particle duality. The wave packet is the physical explanation for the dual phenomena.

4. Uncertainty and Stability

In axiomatic and mathematical quantum theory [1] built on quantized, stationary states $\phi(\bar{k}, \bar{\omega})$, Heisenberg's Uncertainty Principle (HUP) is the axiom used to describe transition relationships in energy and time, or in momentum and space: $\Delta p_i \cdot \Delta x_j = (\hbar/2)\delta_{ij}$ where $i, j = 0, 1, 2$ or 3 in four dimensions, and δ_{ij} is the Dirac delta. The usage is not universal: some authors omit the HUP [17]; others criticize it [18]. In Dispersion Dynamics by contrast, the uncertainties inherent in wave-particle duality are concisely and precisely described at an elementary physical level: on the central, rest frame ($m' = m_0$, $x = 0$) in cases $X = 0$, Equation (1) yields, by direct inspection, the component uncertainty $\Delta t = 2\sigma_x^2$ and by Fourier transform, $\Delta\omega = 2/\sigma_x^2$, since the Fourier transform of a Gaussian is Gaussian. The combined uncertainty, $\Delta t \cdot \Delta\omega = 4$, *i.e.* independent of σ_x. Likewise, for cases $t = 0$, $\Delta x = 2\sigma^2$ and $\Delta k_x = 2/\sigma_x^2$ and $\Delta x \cdot \Delta k_x = 4$. The joint Uncertainties are 8 times greater than the extreme limit in the equivalent

---

[3]A simple example is the bow wave excited by a speedboat.

HUP, *i.e.* after generalizing dimensions using Equation (2) etc. As examples, consider uncertainties, at various heights, that are accurately calculated about the near field for the case of Fresnel diffraction of electrons through a narrow slit (Table 1). Figure 3 is an aerial image [19] [20].

Notice firstly that by Newton's first law of motion, "Any particle continues in a state of rest or uniform motion in a straight line except in so far as it is compelled by applied external force to change that state." This law is true in his corpuscular theory, and it is true for the plane-wave, incident beam before entering the thin slit. This acts as an external force that changes the transverse uncertainty in a systematic way. It is not necessary to cite an uncertain HUP to describe how this happens; the stable wave packet in conventional wave optics provides the simple, methodical explanation [2] [6]. Indeed the stable wave packet itself provides the uncertainty "limit" that is itself uncertain in HUP. The derivation was given in the previous paragraph, and can be written in normal 4-dimensional relativistic notation:

$$\Delta k_i \cdot \Delta x_j = 4\delta_{ij} \text{, where } i, j = 0, 1, 2 \text{ or } 3 \tag{8}$$

This is a more precise value than is given in the HUP. It can be generalized to terms of energy and momentum by multiplication by the constant $\hbar$, while the limit itself fundamentally physical: it is the immediate consequence of wave-particle duality.

Table 1. Various uncertainties illustrated in Figure 3, with explanations in legend. Notice anomalous uncertainties at the Critical Condition in column c. The *x*-direction is downwards.

Uncertainty \ Level	a	b	c	d
ω	$m'c^2/\hbar$			
$\Delta\omega$	$2e/\hbar$ rad/s	<--	<--	<--
Δt	$4\hbar/2e$ s	<--	<--	<--
k_x	$2\pi/\lambda$			
Δk_x	$\Delta\omega/v_g$ m^{-1}	~ <--	~ <--	~ <--
Δx	$4/\Delta k_x$ m	~ <--	~ <--	~ <--
Δk_y	0	0	$-6/s$	$8s/G\lambda$
Δy	∞	$2s$	$2s/3$	$\sim G\lambda/2s$
Δk_z	0	<--	<--	<--
Δz	∞	<--	<--	<--
Dual uncertainty			$\Delta k_y \cdot \Delta y \simeq -4$	$\Delta k_y \cdot \Delta y \simeq 4$

Explanatory notes: Column a, line 1: in simple units, ω is the relativistic mass, *i.e.* m_0 + kinetic energy; line 2: energy line width in the electron microscope; line 3: from dual uncertainty (Equation (8)); line 4: de Broglie hypothesis; line 5: From relativity (Equation (5)) $\omega d\omega = kdkc^2$; $\Delta k = \Delta\omega\dfrac{\omega}{kc^2} = \dfrac{\Delta\omega}{v_g}$; line 6: From wave dual uncertainty. Column c, line 7: The critical condition $kc^2 v_g$; line 8: From wave dual uncertainty *in this case abnormally small*. Column d, line 9: zero in far field diffraction; line 10: from wave dual uncertainty.
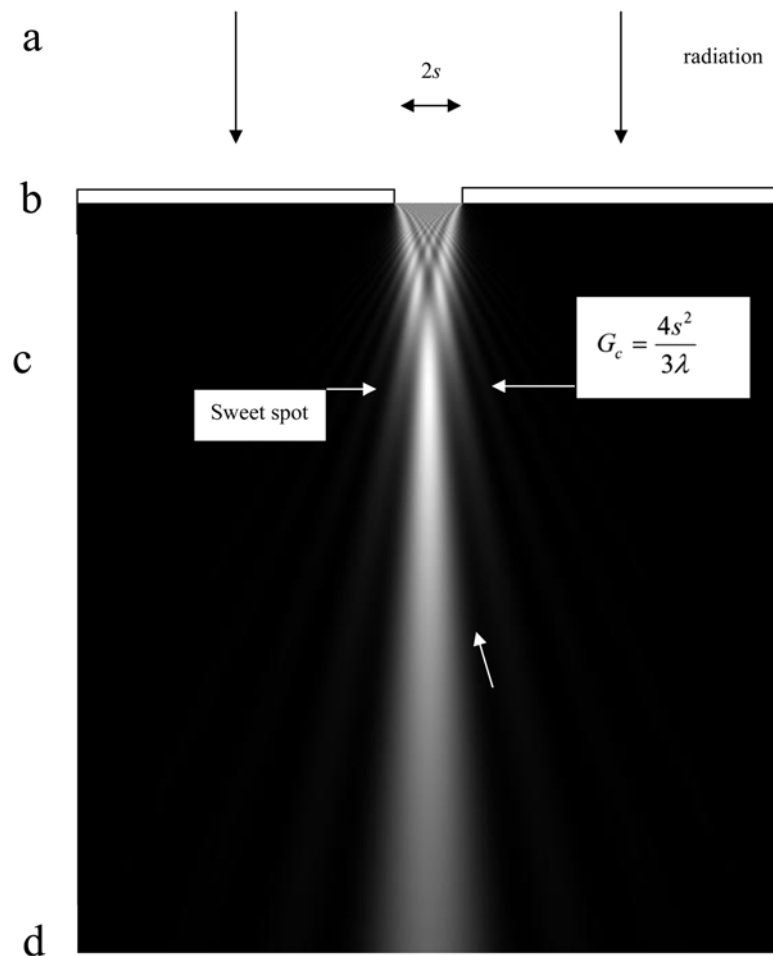
Figure 3. Aerial image calculated for an incident parallel incidence (level a) after emergence of a 100 KV, wavelength λ, electron beam from a slit, of width s, in a gold mask 10 μm thick (level b) [19] [20]. Notice the focusing effect at the "Critical Condition".

Wave uncertainty not only complements the fact of wave-particle duality; it is more precise than the HUP and includes otherwise anomalous situations such as the Critical condition in near field. Dual wave uncertainty is also necessary in engineering applications [20], where precision has more value than mathematical oversimplification.

A further example of the increased precision is the fact that the wave optics demonstrates, through the wave function $X(k, x, \omega, t)$, a necessary relation between transverse σ_y and σ_z, with $\sigma_{|k|}$ in the direction of propagation. This relation is neglected in the HUP but is exemplified in **Table 1**, cell a5. Many other examples of precision are predicted in the wave particle: the amplitude A depends on the divergence of σ, expressed vectorially; the transverse wavelength λ_y lengthens as the beam spreads, etc.

Moreover, the table illustrates the various ways in which the free wave packet is stable; but becomes partly unstable by the presence of applied external forces such as the narrow slit in **Figure 3**. Wave optics supplies a degree of determina-

cy, within limits provided by wave particle duality. Experimental evidence requires it, for example as the condition' for proximity lithography (level c), and also in far field (level d), where the horizontal intensity profile approaches the Gaussian distribution. Precise uncertainty is a core property in wave-particle duality.

Notice further in Table 1, that when $x > G_o$ the critical gap, then $\Delta y \cdot \Delta k_y > \hbar/2\pi$ which is divergent; but when $x < G_o$ $\Delta y \cdot \Delta k_y < 0$ and convergent. By contrast, the HUP is indiscriminate and inaccurate.

In concluding this section, notice that Heisenberg's principle correctly interprets the particle as a field, but his estimate is excessively restrictive when compared with known photon and electron optics. In orbital motion, the uncertainty is restricted by harmonies in the wave function. In measurement by reduction of the wave packet, (e.g. absorptive scintillation events in an interference pattern) multiple restrictions apply from sensing or emitting equipment. The HUP shows that "point particles" [3] are actually extended, and that the Copenhagen probabilistic theory of the wave function is mathematical, not physical

5. Limitations of the Schrodinger Equation

Compare with Equation (3) the Schrödinger equation in 3-dimensions which may be written for a system of j particles bound to a central potential V [16]:

$$\sum_{j=1}^{N} \frac{\hbar^2}{2m_j} \nabla_j^2 \Psi - V\Psi_{j=1} = -i\hbar \frac{\partial \Psi}{\partial t} \tag{9}$$

where ∇^2 represents the Laplacian for the jth particle, and the first term represents the summation of kinetic energy of the interacting particles; the second represents their electrostatic potentials; and the third term their energy W_n, or eigenvalues when expressed in matrix form for various quantized states. The equation is complementary to the free particle, 3-dimensional Equation (1) when its amplitude A is small; σ is large; and the function is made harmonic. In particular $\left\langle \phi^* \left| \frac{\partial}{\partial x} \right| \phi \right\rangle \simeq ik_x$, or $ip_x/\hbar$; while $\left\langle \phi^* \left| \frac{\partial}{\partial t} \right| \phi \right\rangle \simeq -i\omega$, or $-iE/\hbar$. However, equation (9) is not consistent with Equation (3): in Schrödinger's equation the masses m_i are treated as constant and disregarded, and this is typically applied approximately in calculations of atomic structure. In relativity by contrast, particle masses vary with rest frame, and they sometimes absorb the major part of the kinetic energy: $E = m'c^2 = m_0 c^2 / \left(1 - \beta^2\right)^{1/2}$, where $\beta = v_g/c$. Moreover, in relativity (Equation (3)) the three variables occur regularly in powers of 2, while the potential energies must be addedconsistently with Equation (9). Thus:

$$E_n = \hbar \omega_n = W_n' + m_0 c^2 \tag{10}$$

where W' requires correction for relativistic contraction in space, with increasing β, and for dilation in time. Both E_n and W_n are functions of momentum, and therefore vary with rest frame. These features are implied in the Klein-Gordon equation.

By contrast, Dirac factorized Equation (3) into two first order equations designed to operate on rank 4 matrix eigenvectors [1]. His antiparticles have negative rest mass and positive kinetic energy, which is problematic when $k = -m_0 c$, since solutions for ω and k become singular. Moreover, he uses Heisenberg dynamics to claim the speed of the electron equal to c, and this contradicts special relativity. Given the facts inherent in Dispersion Dynamics, we explore a different path that uses the advantage of quantized and *harmonic* self-constructive orbits (**Figure 2**) that are invariable events in any relativistic frame.

A paradigm solution that is enabled by these equations is the relativistic correction for eigenvalues of the Schrodinger equation. Calculate initially, the electronic, non-relativistic, solution using a preferred method such as the linear combination of atomic orbitals; Slater orbitals; hydrogenic wavefunctions etc. For illustration, consider hydrogenic functions. Treat the relativistic state as a perturbation on the non-relativistic state. We will account for changes in eigenvalues and eigenstates with length contractions, time dilations, and expectation values for momentum, velocity, mass etc.

The hydrogenic eigenvalues W_n for quantum states n are given by [16]:

$$W_n \simeq \frac{\mu Z^2}{\hbar^2} \frac{e^4}{n^2} = \frac{Z^2}{a_0} \frac{e^2}{n^2} \tag{11}$$

for electrons with rest mass m_e and charge e orbiting nuclear charge Z. The Bohr radius $a_0 = \hbar^2 / (\mu e^2)$; and principal quantum number is n; where for atomic number N and nuclear rest mass m_N, the reduced mass for an electron is:

$$\mu = \frac{m_e \cdot m_N}{m_e + m_N} \simeq m_e \quad \text{when } m_N \gg m_e \tag{12}$$

Notice that W_n depends on the inverse of the Bohr radius which has the dimension of length:

$$W_n = \frac{2Z^2 e^2}{a_0 n^2} = \hbar \omega_n \tag{13}$$

Then, the relativistic radial contraction corresponds to wavelength shortening and frequency growth: as time dilates, frequency shifts blue.

$$a' = a_0 \left(1 - \beta^2\right)^{1/2}; \quad \omega_n' = \omega_n \left(1 - \beta^2\right)^{-1/2} \tag{14}$$

From these results are found approximate mean radii $\langle r_n \rangle$ for hydrogenic wavefunctions, and corresponding eigenvalues W_n' for states n.

In the non-relativistic approximation, the frequency is W_n/h and phase velocity for the mean orbit is $v_p = 2\pi a_0 W_n/h$. In relativity, $\beta = v_p/c = c/v_p$ for a free particle, so that $v_g = \hbar c^2 / (a_0 W_n)$, *i.e. independent of β*, in an observer frame, because fixed by the harmonic nature of the hydrogenic motion.[4]

---

[4]More generally, Equation (3) and Equation (5) are related: $E_n'^2 = W_n'^2 + m_0^2 c^4 = \left(K' + V'\right)^2 + m_0^2 c^4$ where again the primes indicate relativistically corrected values even though some are independent of rest frame, while V can be expressed by the vector potential **A**. In case $W_n \ll m_0 c^2$, the virial theorem gives, typically for a ground state, $W_n \simeq V'/2$, where the potential is negative. Then $k^2/2m_0 \simeq -V/2$,

6. Reactions to force in Crystal Fields

In Dispersion Dynamics, as an immediate consequence of special relativity, particles react to force fields by accelerations that follow Equation (7): the force and acceleration are negative in negative dispersive curvature and *vice versa*. Electrons moving in negative curvature are often called "holes", and these are typically observed by positive coefficients in the Hall effect, most notably in high temperature superconductors [2] [5] (HiTc). The Hall effect demonstrates fundamental dynamic effects in electrons accelerated by electric crystals fields and applied magnetism. In superconductors, Dispersion Dynamics provides further explanation for extraordinary conduction where physical forces seem, *prima facie*, to disappear: inside the superconductor, the electric field E = 0 because of zero resistivity; the magnetic field (in a type I superconductor) B = 0 by the Meissner-Ochsenfeld effect; P = 0 [21] [22] the momentum of the Cooper pair; the charge in the high temperature superconductor Q = 0 in the Wannier excitons; and the spin S = 0, because the positive Hall coefficients in HiTc shows the paired electrons are s-like and orthonormal. What then is left for the dynamics of the measured supercurrent? We suppose that the wave packet is reduced in Newtonian time by energy injection at electrodes so releasing electrons formerly bound into pairs by the superconducting gap [2].

More generally in condensed matter, relativistic effects become increasingly significant as binding energies or transport energies approach the rest mass energy of the electron m_ec^2. This occurs in deep core states in heavy atoms and in electron microscopes.

7. Conclusion

Given wave-particle duality that exists in the wave packet, *harmonic events* in a self-constructive wave function are Lorentz covariant and therefore subject both to normal time dilation in special relativity, and to space contraction. Atomic orbital radii and eigenvalues, such as those derived from the Schrödinger equation, can be used in approximation to account for relativistic effects in spatial and temporal accounting over a range of physical properties. These are significant at energies that approach the rest mass energy of the electron, as in core state scattering of electrons in EXAFS (extended X-ray absorption fine structure) from heavy elements, and in electron microscopes, especially in high energy instruments used for imaging thick or heavy specimens. The relativistic approximations are comparatively simple. They add many applications, previously described, for dispersion dynamics that are derived from the wave packet in special relativity. The applications add physical consistency to mathematical axioms that are chosen to represent quantization in energy states, sometimes with uncertain approximations.

Conflicts of Interest

The author declares no conflicts of interest regarding the publication of this paper.

References

[1]   Dirac, P.A.M. (1958) Principles of Quantum Mechanics. 4th Edition, Oxford University Press, Oxford.

[2]   Bourdillon, A.J. (2017) Dispersion Dynamics in the Hall Effect and Pair Bonding in HiT$_c$. Nova Science, Hauppauge.

[3]   Bourdillon, A.J. (2018) *Journal of Modern Physics*, **9**, 2295-2307.
https://doi.org/10.4236/jmp.2018.913145

[4]   Bourdillon, A.J. (2018) *Journal of Modern Physics*, **9**, 1304-1316.
https://doi.org/10.4236/jmp.2018.96079

[5]   Bourdillon, A.J. (2017) *Journal of Modern Physics*, **8**, 483-499.
https://doi.org/10.4236/jmp.2017.84031

[6]   Bourdillon, A.J. (2015) *Journal of Modern Physics*, **6**, 2011-2020.
https://doi.org/10.4236/jmp.2015.614407

[7]   Bourdillon, A.J. (2015) *Journal of Modern Physics*, **6**, 463-471.
https://doi.org/10.4236/jmp.2015.64050

[8]   Vasiliev, B. (2020) *Journal of Modern Physics*, **11**, 1263-1278.
https://doi.org/10.4236/jmp.2020.116055

[9]   Wittgenstein, L. (1956) Remarks on the Foundations of Mathematics. Tr. Anscombe, G.E.M., MIT, Cambridge.

[10]   Popper, K.R. (1959) The Logic of Scientific Discovery. Hutchinson, London.
https://doi.org/10.1063/1.3060577

[11]   Popper, K.R. (1982) Quantum Theory and the Schism in Physics. Hutchinson, London.

[12]   Gödel, K. (1931) *Monatshefte für Mathematik und Physik*, **38**, 173-198.
https://doi.org/10.1007/BF01700692

[13]   Nagel, E. and Newman, J.R. (1959) Gödel's Proof. Routlegde & Kegan Paul, Abingdon-on-Thames.

[14]   Devian, C. and Bertrand, J. (2020) *Journal of Modern Physics*, **11**, 1263-1278.
https://doi.org/10.4236/jmp.2020.119079

[15]   De Peralta, L. (2020) *Journal of Modern Physics*, **11**, 788-802.
https://doi.org/10.4236/jmp.2020.116051

[16]   Pauling, L. and Wilson, E.B. (1935) Introduction to Quantum Mechanics. McGraw-Hill, New York.

[17]   Isaacs, A. (1990) Concise Dictionary of Physics. Oxford University Press, Oxford.

[18]   Olszewski, S. (2015) *Journal of Modern Physics*, **6**, 22-626.
https://doi.org/10.4236/jmp.2015.65067

[19]   Bourdillon, A.J., Boothroyd, C.B., Kong, J.R. and Vladimirsky, Y. (2000) *Journal of Physics D: Applied Physics*, **33**, 2133. https://doi.org/10.1088/0022-3727/33/17/307

[20]   Bourdillon, A.J. and Vladimirsky, Y. (2006) X-Ray Lithography—On the Sweet Spot. UHRL, San Jose.

[21]   Bardeen, J., Cooper, L.N. and Schrieffer, J.R. (1957) *Physical Review*, **106**, 162-164.
https://doi.org/10.1103/PhysRev.106.162

[22]   Bardeen, J., Cooper, L.N. and Schrieffer, J.R. (1957) *Physical Review*, **108**, 1175-1204.
https://doi.org/10.1103/PhysRev.108.1175

The Two Relativistic Rydberg Formulas of Suto and Haug: Further Comments

Espen Gaarder Haug

Norwegian University of Life Sciences, Ås, Norway
Email: espenhaug@mac.com

Abstract

In a recent paper, we [1] discussed that Suto [2] has pointed out an interesting relativistic extension of Rydberg's formula. In that paper, we had slightly misunderstood Suto's approach, something we will comment on further here. The relativistic Suto formula is actually derived from a theory where the standard relativistic momentum relation is changed. The relativistic Rydberg formula we presented and mistakenly thought was the same as Suto's formula is, on the other hand, derived to be fully consistent with the standard relativistic energy-momentum relation. Here we will point out the differences between the formulas and correct some errors in our previous paper. The paper should give deeper and better intuition about the Rydberg formula and what it represents.

Keywords

Rydberg's Formula, Relativistic Extension, Compton Wavelength

1. Introduction

A considerable number of papers have been published on relativistic corrections of the Rydberg states, see for example [3] [4]. However, the main focus of these papers tends to be corrections based on relativistic quantum mechanics. Even if relativistic quantum mechanics is very powerful, this seems to give a limited intuition on why the Rydberg formula is non-relativistic, and how we can adjust the Rydberg formula to make it relativistic. Here we will look directly at the Rydberg formula and how it can be modified based on special relativistic effects without looking into relativistic quantum mechanics. The relativistic quantum mechanical approach may be considerably better in prediction power, but the main advantage with the approach here is that it gives energy and additional intuition about the non-relativistic versus relativistic Rydberg states.

Since we use a series of variables and parameters, we will start by providing a list of symbols (Table 1), as a preface to our paper.

The well-known Rydberg [5] formula is given by

$$\frac{1}{\lambda} = R_\infty Z^2 \left(\frac{1}{n_1^2} - \frac{1}{n_2^2} \right) \tag{1}$$

where R_∞ is Rydberg's constant, which has a value of 10,973,731.568160(21) m^{-1} (NIST CODATA 2018 value). Even though the formula is very simple, it is hard to gain much intuition from it. The Rydberg constant can be rewritten as

$$R_\infty = \frac{m_e e^4}{8\epsilon_0^2 h^3 c}$$

$$R_\infty = \frac{\dfrac{\hbar}{\bar{\lambda}_e} \dfrac{1}{c} \left(\sqrt{\dfrac{\hbar}{c}} \sqrt{\alpha} \sqrt{10^7} \right)^4}{8\epsilon_0^2 h^3 c}$$

$$R_\infty = \frac{\dfrac{\hbar^3}{\bar{\lambda}_e} \dfrac{1}{c^3} \alpha^2 \left(10^7 \right)^2}{8 \left(\dfrac{1}{4\pi c^2 10^{-7}} \right)^2 h^3 c}$$

Table 1. Symbol list.

Symbol	Represents
h	Planck constant
$\hbar$	reduced Planck constant
c	speed of light
v	velocity of the electron
Z	atomic number
R_∞	Rydberg constant
n_1	the principal quantum number of an energy level
n_2	the principal quantum number of an energy level for the atomic electron transition
ϵ_0	vacuum permittivity
α	Fine structure constant
e	elementary charge
λ	Photon wavelength
λ_e	Compton wavelength electron
$\bar{\lambda}_e$	Reduced Compton wavelength electron
m_e	rest mass of electron
m_P	rest mass of proton
p	momentum
E	energy
E_k	kinetic energy

$$R_\infty = \frac{\dfrac{\hbar^3}{\bar{\lambda}_e}\dfrac{1}{c^3}\alpha^2}{8\dfrac{1}{16\pi^2 c^4}h^3 c}$$

$$R_\infty = \frac{1}{2}\frac{\hbar}{h}\frac{1}{\bar{\lambda}_e}\alpha^2$$

$$R_\infty = \frac{1}{2}\frac{\dfrac{h}{2\pi}}{h}\frac{1}{\bar{\lambda}_e}\alpha^2$$

$$R_\infty = \frac{\alpha^2}{2\bar{\lambda}_e} \tag{2}$$

And we can rewrite this as

$$R_\infty = \frac{\alpha^2}{2\dfrac{h}{m_e c}} = \frac{\alpha^2 m_e c}{2h} \tag{3}$$

(In the former paper, we had incorrectly used the Compton wavelength rather than the reduced Compton wavelength in the beginning of this derivation and thus we incorrectly got $R_\infty = \dfrac{\alpha^2}{2\dfrac{h}{m_e c}} = \dfrac{\alpha^2 m_e c}{4\pi\hbar}$. However, we made another error further down that canceled this error out and therefore we obtained the right result with respect to the Rydberg formula.)

This is standard knowledge, so we have shown nothing new so far. Let us now replace this in Rydberg's formula, which gives

$$\frac{1}{\lambda} = \frac{\alpha^2 m_e c}{2h}Z^2\left(\frac{1}{n_1^2} - \frac{1}{n_2^2}\right)$$

$$h\frac{c}{\lambda} = Z^2\left(\frac{1}{2}m_e\frac{\alpha^2 c^2}{n_1^2} - \frac{1}{2}m_e\frac{\alpha^2 c^2}{n_2^2}\right) \tag{4}$$

where $\dfrac{\alpha^2 c^2}{n_1^2}$ can be seen as v_1^2 and $\dfrac{\alpha^2 c^2}{n_2^2}$ as v_2^2. In other words, we can write this as

$$E = h\frac{c}{\lambda} = \frac{Z^2}{2\pi}\left(\frac{1}{2}m_e v_1^2 - \frac{1}{2}m_e v_2^2\right) \tag{5}$$

Since $\dfrac{1}{2}mv^2$ is the well-known approximation of the kinetic energy when $v \ll c$ (the first term of a Taylor series approximation), the Rydberg formula is clearly non-relativistic. Even though this is known, we have not seen any relativistic extension of the formula before Suto's paper [2]. However, before we discuss his formula, we will briefly show how we arrived at our relativistic version of the Rydberg formula. Since $\dfrac{1}{2}mv^2$ is the approximation for $v \ll c$, we simply replaced this approximation by the full relativistic kinetic energy

$E_k = mc^2\gamma - mc^2$, where, as usual, $\gamma = \dfrac{1}{\sqrt{1 - v^2/c^2}}$. This gives

$$
\begin{aligned}
E &= \left(\frac{m_e c^2}{\sqrt{1 - v_1^2/c^2}} - m_e c^2 - \frac{m_e c^2}{\sqrt{1 - v_2^2/c^2}} - m_e c^2 \right) \\
&= \left(\frac{m_e c^2}{\sqrt{1 - v_1^2/c^2}} - \frac{m_e c^2}{\sqrt{1 - v_2^2/c^2}} \right)
\end{aligned}
\tag{6}
$$

where $v_1 = Z\alpha c/n_1$ and $v_2 = Z\alpha c/n_2$, and we also have that $m_e = \dfrac{h}{\lambda_e}\dfrac{1}{c}$, where λ_e is the Compton [6] wavelength of the electron. The equation can then be rewritten as

$$
h\frac{c}{\lambda} = \left(\frac{\dfrac{h}{\lambda_e}c}{\sqrt{1 - \dfrac{Z^2\alpha^2}{n_1^2}}} - \frac{\dfrac{h}{\lambda_e}c}{\sqrt{1 - \dfrac{Z^2\alpha^2}{n_2^2}}} \right)
$$

$$
\frac{1}{\lambda} = \left(\frac{1}{\lambda_e \sqrt{1 - \dfrac{Z^2\alpha^2}{n_1^2}}} - \frac{1}{\lambda_e \sqrt{1 - \dfrac{Z^2\alpha^2}{n_2^2}}} \right)
\tag{7}
$$

We mistakenly thought that the formula we presented in the last paper was the same as Suto's relativistic Rydberg formula. However, Suto's [2] relativistic formula is (his equation 48)

$$
\frac{1}{\lambda} = \left(\frac{1}{\lambda_e \sqrt{1 + \dfrac{\alpha^2}{n_2^2}}} - \frac{1}{\lambda_e \sqrt{1 + \dfrac{\alpha^2}{n_1^2}}} \right)
\tag{8}
$$

where λ is the photon wavelength, and λ_e is the Compton wavelength of the electron.

While our new relativistic formula should be consistent with the standard energy momentum relation $E^2 = p^2 c^2 + m^2 c^4$, where p is the momentum, the Suto formula is not consistent with this, but it is consistent with the modified energy momentum relation that he presented in the same paper as $m_e^2 c^4 - p_n^2 c^2 = m_n^2 c^4$. The Taylor expansion of our relativistic formula is

$$
\begin{aligned}
\frac{1}{\bar{\lambda}} = \frac{1}{\bar{\lambda}_e} \Bigg(&\left(1 - \frac{Z^2\alpha^2}{2n_1^2} + \frac{3Z^4\alpha^4}{8n_1^4} + \frac{5Z^6\alpha^6}{16n_1^6} + \cdots \right) \\
&- \left(1 - \frac{Z^2\alpha^2}{2n_2^2} + \frac{3Z^4\alpha^4}{8n_2^4} + \frac{5Z^6\alpha^6}{16n_2^6} + \cdots \right) \Bigg)
\end{aligned}
\tag{9}
$$

And the Taylor series expansion of Suto's formula is

$$\frac{1}{\bar{\lambda}} = \frac{1}{\bar{\lambda}_e}\left(\left(1 - \frac{\alpha^2}{2n_1^2} - \frac{3\alpha^4}{8n_1^4} + \frac{5\alpha^6}{16n_1^6} + \cdots\right) - \left(1 - \frac{\alpha^2}{2n_2^2} - \frac{3\alpha^4}{8n_2^4} + \frac{5\alpha^6}{16n_2^6} + \cdots\right)\right) \quad (10)$$

We incorrectly pointed out that Suto might have made a mistake and there was a sign error in his series expansion, but this is actually not the case. This was because we thought his formula was identical to the one that we had derived[1].

When expanded to hold for any atom, the Suto formula, based on his energy momentum assumption, must likely be:

$$\frac{1}{\lambda} = \left(\frac{1}{\lambda_e\sqrt{1 + \frac{Z^2\alpha^2}{n_2^2}}} - \frac{1}{\lambda_e\sqrt{1 + \frac{Z^2\alpha^2}{n_1^2}}}\right) \quad (11)$$

while our relativistic extension of the Rydberg formula is

$$\frac{1}{\lambda} = \left(\frac{1}{\lambda_e\sqrt{1 - \frac{Z^2\alpha^2}{n_1^2}}} - \frac{1}{\lambda_e\sqrt{1 - \frac{Z^2\alpha^2}{n_2^2}}}\right) \quad (12)$$

In other words, we have recently gotten two relativistic Rydberg formulas; one consistent with the standard relativistic energy momentum relation (the Haug formula) and one consistent with what we can call a somewhat alternative theory of Suto.

In general, we would think the formula that is consistent with the standard relativistic energy momentum relation is more correct and consistent. However, it is not necessarily easy to test out which one is superior, as the hydrogen atom is known to be best described by the relativistic Dirac [7] wave equation.

2. Length Contraction and Length Expansion of the Compton Wavelength

In the Suto formula, the Compton wavlength of the electron looks like it is extended in length due to velocity of the electron, since in the denominator we have $\lambda_e\sqrt{1 + \frac{Z^2\alpha^2}{n_2^2}}$ and $\lambda_e\sqrt{1 + \frac{Z^2\alpha^2}{n_1^2}}$, while in our relativistic formula we have standard relativistic length contraction, $\lambda_e\sqrt{1 - \frac{Z^2\alpha^2}{n_2^2}}$ and $\lambda_e\sqrt{1 - \frac{Z^2\alpha^2}{n_1^2}}$ of the Compton wavelength of the electron, as observed from the laboratory frame that the electron is moving relative to. We would find it strange if the Compton wave should undergo length expansion because of motion and not length contraction as measured with Einstein-Poincaré synchronized clocks. Einstein-Poincaré synchronized clocks are simply indicating we assume the one-way speed of light is the same as the round trip speed of light when we synchronize the clocks over

---

[1]We apologize for missing this, but we are taking steps to correct that here.

distance.[2]

It seems that the methodology we have laid out basically only takes into account that the electron moves parallel to the laboratory frame. In other words, our model seems to be 2-dimensional. However, if in reality the reduced Compton wavelength represents a radius of a sphere rather than a length, then this length contraction will likely be correct for electrons moving in any direction as observed from the laboratory frame with Einstein-Poincaré synchronized clocks. There could naturally be a series of other corrections needed to fit observations, such as relativistic quantum mechanical effects. There should also be several interesting angles to investigate further: how close we can get to predicting observations with non-quantum mechanical models, for example.

3. Table Calculations

In Table 2, we look at the Lyman series. This is for a hydrogen atom where we hold $n_1 = 1$ and in this table let n_2 vary from 2 to 7. We see that the Haug formula predicts a slightly shorter wavelength than the non-relativistic Rydberg formula, while the Suto formula predicts a slightly longer wavelength than the non-relativistic formula. Table 3 shows predictions from the three formulas for the Balmer series, where we have $n_1 = 2$ and let n_2 vary from 3 to 7. The first column in Table 3 is from real observations. The real observations in this case have been done in air, so we have adjusted all the three formulas by the refraction index in air; this simply means we need to divide the formulas by the refraction index in air, which is about 1.00029. One can find observation studies done in a vacuum and in air; when comparing theoretical predictions against observations it is naturally important to know how the observations have been done the medium matters.

Table 2. The table shows the Lyman series calculated from the non-relativistic formula, the Haug relativistic formula, and the Suto relativistic formula. The difference-column shows the difference in percent between the relativistic formula predictions and the non-relativistic formula predictions for the Haug and Suto formulas. The Haug relativistic formula predicts a slightly shorter wavelength than the non-relativistic formula, and the Suto formula predicts a slightly longer wavelength. The Haug formula seems to be consistent with relativistic length contraction (also of waves).

n_2	Non-Relativistic	Haug	Difference	Suto	Difference
2	121.568	121.562	−0.0050%	121.575	0.0050%
3	102.573	102.569	−0.0044%	102.578	0.0044%
4	97.255	97.251	−0.0042%	97.259	0.0042%
5	94.975	94.971	−0.0042%	94.979	0.0042%
6	93.781	93.778	−0.0041%	93.785	0.0041%
7	93.076	93.072	−0.0041%	93.080	0.0041%

[2]Whether or not such synchronization is fully valid is an ongoing discussion, see for example [8] [9], but that is outside the scope of this paper.

Table 3. The table shows the Balmer series calculated from the non-relativistic formula, the Haug relativistic formula, and the Suto relativistic formula. The difference column is the difference in percent between the relativistic formula predictions and the non-relativistic formula predictions for the Haug and Suto formulas. The Haug relativistic formula predicts a slightly shorter wavelength than the non-relativistic formula, and the Suto formula predicts a slightly longer wavelength. The Haug formula seems to be consistent with relativistic length contraction (also of waves). The observations are from the Atomic Spectra NIST Standard Reference Database 78 Version 5.7, and are done in air, so we have made an adjustment based on the refraction index in all formulas based on air. If this adjustment is not done, our prediction is far off, as expected.

n_2	Observed in air	Non-relativistic in air	Difference	Haug in air	Difference	Suto in air	Difference
3	656.28	656.279	−0.0001%	656.270	−0.0016%	656.289	0.0013%
4	486.13	486.133	0.0006%	486.127	−0.0007%	486.139	0.0018%
5	434.05	434.047	−0.0007%	434.042	−0.0018%	434.052	0.0005%
6	410.17	410.175	0.0011%	410.170	0.0000%	410.179	0.0022%
7	397.005	397.008	0.0009%	397.004	−0.0002%	397.013	0.0020%

Since Table 2 and Table 3 are covering hydrogen atoms, we have also adjusted all of the formulas by multiplying by one divided by the adjusted mass $\frac{m_P}{m_P + m_e}$, where m_P is the proton mass, and m_e is the electron mass. First of all, observations for the hydrogen atom are likely not accurate enough to distinguish between the non-relativistic and relativistic formulas, but we leave that for future discussion. For the hydrogen atom, the Lyman series is where the differences between the three formulas are the greatest, so there is no reason to look at the Paschen, Brackett, Humphreys, or Pfund series in addition, as the differences between non-relativistic and relativistic predictions would be even smaller. To test out the formulas, one would likely need to look at much heavier hydrogen-like atoms, as the electrons move much faster, in general, and therefore relativistic effects would play a bigger role. Still, one likely needs a relativistic wave equation to include all necessary adjustments, another issue to consider in this framework.

In our original table, there was a typo in the spreadsheet that resulted in incorrect values from our relativistic Rydberg formula. Below, we present the corrected tables (Table 4 and Table 5); here we have not adjusted the formulas based on the reduced mass, so the difference in values will be the same in any of the formulas, even if we multiply each predicted wavelength with one divided by the reduced mass: $\frac{m_P}{m_P + m_e}$.

4. Conclusion

We have shown that the relativistic extensions of the Rydberg formula given by Suto and Haug are two different formulas. The Haug relativistic Rydberg formula

Table 4. The table shows the Rydberg formula predictions and the relativistic predictions for the first 137 elements. As we can see, the difference increases between the two models. Here we are just looking at the case $n_1 = 1$ and $n_2 = 2$.

Atomic #	Rydberg formula	Relativistic formula	Diff.	Diff. %	Atomic #	Rydberg formula	Relativistic formula	Diff.	Diff. %
1	121.5023	121.4962	(0.0061)	−0.005%	71	0.0241	0.0181	(0.0060)	−32.9%
2	30.3756	30.3695	(0.0061)	−0.020%	72	0.0234	0.0175	(0.0060)	−34.2%
3	13.5003	13.4942	(0.0061)	−0.045%	73	0.0228	0.0168	(0.0060)	−35.4%
4	7.5939	7.5878	(0.0061)	−0.080%	74	0.0222	0.0162	(0.0060)	−36.8%
5	4.8601	4.8540	(0.0061)	−0.125%	75	0.0216	0.0156	(0.0060)	−38.1%
6	3.3751	3.3690	(0.0061)	−0.180%	76	0.0210	0.0151	(0.0060)	−39.5%
7	2.4796	2.4736	(0.0061)	−0.245%	77	0.0205	0.0145	(0.0060)	−41.0%
8	1.8985	1.8924	(0.0061)	−0.320%	78	0.0200	0.0140	(0.0060)	−42.5%
9	1.5000	1.4940	(0.0061)	−0.406%	79	0.0195	0.0135	(0.0060)	−44.0%
10	1.2150	1.2090	(0.0061)	−0.502%	80	0.0190	0.0130	(0.0059)	−45.6%
11	1.0042	0.9981	(0.0061)	−0.607%	81	0.0185	0.0126	(0.0059)	−47.3%
12	0.8438	0.8377	(0.0061)	−0.724%	82	0.0181	0.0121	(0.0059)	−49.0%
13	0.7189	0.7129	(0.0061)	−0.9%	83	0.0176	0.0117	(0.0059)	−50.8%
14	0.6199	0.6138	(0.0061)	−1.0%	84	0.0172	0.0113	(0.0059)	−52.7%
15	0.5400	0.5339	(0.0061)	−1.1%	85	0.0168	0.0109	(0.0059)	−54.6%
16	0.4746	0.4686	(0.0061)	−1.3%	86	0.0164	0.0105	(0.0059)	−56.6%
17	0.4204	0.4144	(0.0061)	−1.5%	87	0.0161	0.0101	(0.0059)	−58.6%
18	0.3750	0.3689	(0.0061)	−1.6%	88	0.0157	0.0098	(0.0059)	−60.8%
19	0.3366	0.3305	(0.0061)	−1.8%	89	0.0153	0.0094	(0.0059)	−63.0%
20	0.3038	0.2977	(0.0061)	−2.0%	90	0.0150	0.0091	(0.0059)	−65.3%
21	0.2755	0.2695	(0.0061)	−2.2%	91	0.0147	0.0087	(0.0059)	−67.7%
22	0.2510	0.2450	(0.0061)	−2.5%	92	0.0144	0.0084	(0.0059)	−70.2%
23	0.2297	0.2236	(0.0061)	−2.7%	93	0.0140	0.0081	(0.0059)	−72.8%
24	0.2109	0.2049	(0.0061)	−3.0%	94	0.0138	0.0078	(0.0059)	−75.5%
25	0.1944	0.1884	(0.0061)	−3.2%	95	0.0135	0.0075	(0.0059)	−78.4%
26	0.1797	0.1737	(0.0061)	−3.5%	96	0.0132	0.0073	(0.0059)	−81.3%
27	0.1667	0.1606	(0.0061)	−3.8%	97	0.0129	0.0070	(0.0059)	−84.4%
28	0.1550	0.1489	(0.0061)	−4.1%	98	0.0127	0.0067	(0.0059)	−87.6%
29	0.1445	0.1384	(0.0060)	−4.4%	99	0.0124	0.0065	(0.0059)	−91.0%
30	0.1350	0.1290	(0.0060)	−4.7%	100	0.0122	0.0062	(0.0059)	−94.6%
31	0.1264	0.1204	(0.0060)	−5.0%	101	0.0119	0.0060	(0.0059)	−98.3%
32	0.1187	0.1126	(0.0060)	−5.4%	102	0.0117	0.0058	(0.0059)	−102.2%
33	0.1116	0.1055	(0.0060)	−5.7%	103	0.0115	0.0056	(0.0059)	−106.3%
34	0.1051	0.0991	(0.0060)	−6.1%	104	0.0112	0.0053	(0.0059)	−110.6%
35	0.0992	0.0931	(0.0060)	−6.5%	105	0.0110	0.0051	(0.0059)	−115.1%
36	0.0938	0.0877	(0.0060)	−6.9%	106	0.0108	0.0049	(0.0059)	−119.9%
37	0.0888	0.0827	(0.0060)	−7.3%	107	0.0106	0.0047	(0.0059)	−125.0%

Continued

38	0.0841	0.0781	(0.0060)	−7.7%	108	0.0104	0.0045	(0.0059)	−130.4%
39	0.0799	0.0738	(0.0060)	−8.2%	109	0.0102	0.0043	(0.0059)	−136.1%
40	0.0759	0.0699	(0.0060)	−8.6%	110	0.0100	0.0041	(0.0059)	−142.1%
41	0.0723	0.0662	(0.0060)	−9.1%	111	0.0099	0.0040	(0.0059)	−148.6%
42	0.0689	0.0628	(0.0060)	−9.6%	112	0.0097	0.0038	(0.0059)	−155.4%
43	0.0657	0.0597	(0.0060)	−10.1%	113	0.0095	0.0036	(0.0059)	−162.8%
44	0.0628	0.0567	(0.0060)	−10.6%	114	0.0093	0.0035	(0.0059)	−170.7%
45	0.0600	0.0540	(0.0060)	−11.2%	115	0.0092	0.0033	(0.0059)	−179.1%
46	0.0574	0.0514	(0.0060)	−11.7%	116	0.0090	0.0031	(0.0059)	−188.3%
47	0.0550	0.0490	(0.0060)	−12.3%	117	0.0089	0.0030	(0.0059)	−198.1%
48	0.0527	0.0467	(0.0060)	−12.9%	118	0.0087	0.0028	(0.0059)	−208.9%
49	0.0506	0.0446	(0.0060)	−13.5%	119	0.0086	0.0027	(0.0059)	−220.6%
50	0.0486	0.0426	(0.0060)	−14.1%	120	0.0084	0.0025	(0.0059)	−233.4%
51	0.0467	0.0407	(0.0060)	−14.8%	121	0.0083	0.0024	(0.0059)	−247.4%
52	0.0449	0.0389	(0.0060)	−15.4%	122	0.0082	0.0022	(0.0059)	−263.0%
53	0.0433	0.0372	(0.0060)	−16.1%	123	0.0080	0.0021	(0.0059)	−280.4%
54	0.0417	0.0357	(0.0060)	−16.9%	124	0.0079	0.0020	(0.0059)	−299.9%
55	0.0402	0.0342	(0.0060)	−17.6%	125	0.0078	0.0018	(0.0059)	−321.9%
56	0.0387	0.0327	(0.0060)	−18.3%	126	0.0077	0.0017	(0.0059)	−347.1%
57	0.0374	0.0314	(0.0060)	−19.1%	127	0.0075	0.0016	(0.0060)	−376.2%
58	0.0361	0.0301	(0.0060)	−19.9%	128	0.0074	0.0015	(0.0060)	−410.2%
59	0.0349	0.0289	(0.0060)	−20.8%	129	0.0073	0.0013	(0.0060)	−450.8%
60	0.0338	0.0278	(0.0060)	−21.6%	130	0.0072	0.0012	(0.0060)	−500.2%
61	0.0327	0.0267	(0.0060)	−22.5%	131	0.0071	0.0011	(0.0060)	−562.0%
62	0.0316	0.0256	(0.0060)	−23.4%	132	0.0070	0.0009	(0.0060)	−642.0%
63	0.0306	0.0246	(0.0060)	−24.3%	133	0.0069	0.0008	(0.0061)	−751.3%
64	0.0297	0.0237	(0.0060)	−25.3%	134	0.0068	0.0007	(0.0061)	−912.6%
65	0.0288	0.0228	(0.0060)	−26.3%	135	0.0067	0.0005	(0.0061)	−1184.2%
66	0.0279	0.0219	(0.0060)	−27.3%	136	0.0066	0.0003	(0.0062)	−1794.2%
67	0.0271	0.0211	(0.0060)	−28.4%	137	0.0065	0.0001	(0.0064)	−11,232.7%
68	0.0263	0.0203	(0.0060)	−29.5%					
69	0.0255	0.0195	(0.0060)	−30.6%					
70	0.0248	0.0188	(0.0060)	−31.7%					

Table 5. The table shows the Rydberg formula predictions and the relativistic predictions for the first 137 elements. As we can see, the difference increases between the two models. Here we are just looking at the case $n_1 = 1$ and $n_2 = 2$.

Atomic #	Rydberg formula	Relativistic formula	Diff.	Diff. %	Atomic #	Rydberg formula	Relativistic formula	Diff.	Diff. %
1	121.5023	121.4962	−0.0061	−0.0050%	71	0.0241	0.0144	−0.0097	−67.6%
2	30.3756	26.0315	−4.3440	−16.7%	72	0.0234	0.0139	−0.0096	−68.9%

Continued

3	13.5003	11.0414	−2.4589	−22.3%	73	0.0228	0.0134	−0.0094	−70.2%
4	7.5939	6.0710	−1.5229	−25.1%	74	0.0222	0.0129	−0.0093	−71.6%
5	4.8601	3.8329	−1.0272	−26.8%	75	0.0216	0.0125	−0.0091	−73.0%
6	3.3751	2.6374	−0.7377	−28.0%	76	0.0210	0.0121	−0.0090	−74.5%
7	2.4796	1.9247	−0.5549	−28.8%	77	0.0205	0.0116	−0.0088	−76.0%
8	1.8985	1.4659	−0.4326	−29.5%	78	0.0200	0.0112	−0.0087	−77.6%
9	1.5000	1.1533	−0.3467	−30.1%	79	0.0195	0.0109	−0.0086	−79.2%
10	1.2150	0.9308	−0.2842	−30.5%	80	0.0190	0.0105	−0.0085	−80.9%
11	1.0042	0.7668	−0.2373	−31.0%	81	0.0185	0.0101	−0.0084	−82.6%
12	0.8438	0.6425	−0.2013	−31.3%	82	0.0181	0.0098	−0.0083	−84.4%
13	0.7189	0.5460	−0.1729	−31.7%	83	0.0176	0.0095	−0.0082	−86.2%
14	0.6199	0.4696	−0.1503	−32.0%	84	0.0172	0.0092	−0.0081	−88.1%
15	0.5400	0.4081	−0.1319	−32.3%	85	0.0168	0.0088	−0.0080	−90.1%
16	0.4746	0.3579	−0.1168	−32.6%	86	0.0164	0.0085	−0.0079	−92.2%
17	0.4204	0.3163	−0.1042	−32.9%	87	0.0161	0.0083	−0.0078	−94.3%
18	0.3750	0.2815	−0.0935	−33.2%	88	0.0157	0.0080	−0.0077	−96.5%
19	0.3366	0.2521	−0.0845	−33.5%	89	0.0153	0.0077	−0.0076	−98.8%
20	0.3038	0.2270	−0.0768	−33.8%	90	0.0150	0.0075	−0.0075	−101.2%
21	0.2755	0.2054	−0.0701	−34.1%	91	0.0147	0.0072	−0.0075	−103.7%
22	0.2510	0.1867	−0.0643	−34.5%	92	0.0144	0.0070	−0.0074	−106.3%
23	0.2297	0.1704	−0.0593	−34.8%	93	0.0140	0.0067	−0.0073	−109.0%
24	0.2109	0.1561	−0.0548	−35.1%	94	0.0138	0.0065	−0.0073	−111.8%
25	0.1944	0.1436	−0.0509	−35.4%	95	0.0135	0.0063	−0.0072	−114.7%
26	0.1797	0.1324	−0.0473	−35.8%	96	0.0132	0.0061	−0.0071	−117.7%
27	0.1667	0.1225	−0.0442	−36.1%	97	0.0129	0.0058	−0.0071	−120.9%
28	0.1550	0.1136	−0.0414	−36.5%	98	0.0127	0.0056	−0.0070	−124.2%
29	0.1445	0.1056	−0.0389	−36.8%	99	0.0124	0.0054	−0.0070	−127.7%
30	0.1350	0.0984	−0.0366	−37.2%	100	0.0122	0.0053	−0.0069	−131.3%
31	0.1264	0.0919	−0.0346	−37.6%	101	0.0119	0.0051	−0.0068	−135.1%
32	0.1187	0.0860	−0.0327	−38.0%	102	0.0117	0.0049	−0.0068	−139.1%
33	0.1116	0.0806	−0.0310	−38.4%	103	0.0115	0.0047	−0.0067	−143.3%
34	0.1051	0.0757	−0.0294	−38.8%	104	0.0112	0.0045	−0.0067	−147.7%
35	0.0992	0.0712	−0.0280	−39.3%	105	0.0110	0.0044	−0.0067	−152.3%
36	0.0938	0.0671	−0.0267	−39.7%	106	0.0108	0.0042	−0.0066	−157.2%
37	0.0888	0.0633	−0.0254	−40.2%	107	0.0106	0.0040	−0.0066	−162.4%
38	0.0841	0.0598	−0.0243	−40.7%	108	0.0104	0.0039	−0.0065	−167.9%
39	0.0799	0.0566	−0.0233	−41.2%	109	0.0102	0.0037	−0.0065	−173.7%
40	0.0759	0.0536	−0.0223	−41.7%	110	0.0100	0.0036	−0.0065	−179.8%
41	0.0723	0.0508	−0.0214	−42.2%	111	0.0099	0.0034	−0.0064	−186.3%

Continued

42	0.0689	0.0483	−0.0206	−42.7%	112	0.0097	0.0033	−0.0064	−193.3%
43	0.0657	0.0459	−0.0199	−43.3%	113	0.0095	0.0032	−0.0064	−200.8%
44	0.0628	0.0436	−0.0191	−43.9%	114	0.0093	0.0030	−0.0063	−208.8%
45	0.0600	0.0415	−0.0185	−44.4%	115	0.0092	0.0029	−0.0063	−217.3%
46	0.0574	0.0396	−0.0178	−45.1%	116	0.0090	0.0028	−0.0063	−226.6%
47	0.0550	0.0378	−0.0172	−45.7%	117	0.0089	0.0026	−0.0062	−236.6%
48	0.0527	0.0360	−0.0167	−46.3%	118	0.0087	0.0025	−0.0062	−247.4%
49	0.0506	0.0344	−0.0162	−47.0%	119	0.0086	0.0024	−0.0062	−259.2%
50	0.0486	0.0329	−0.0157	−47.7%	120	0.0084	0.0023	−0.0062	−272.1%
51	0.0467	0.0315	−0.0152	−48.4%	121	0.0083	0.0021	−0.0062	−286.3%
52	0.0449	0.0301	−0.0148	−49.1%	122	0.0082	0.0020	−0.0061	−302.0%
53	0.0433	0.0289	−0.0144	−49.8%	123	0.0080	0.0019	−0.0061	−319.5%
54	0.0417	0.0277	−0.0140	−50.6%	124	0.0079	0.0018	−0.0061	−339.1%
55	0.0402	0.0265	−0.0136	−51.4%	125	0.0078	0.0017	−0.0061	−361.3%
56	0.0387	0.0255	−0.0133	−52.2%	126	0.0077	0.0016	−0.0061	−386.6%
57	0.0374	0.0244	−0.0130	−53.0%	127	0.0075	0.0015	−0.0061	−415.8%
58	0.0361	0.0235	−0.0126	−53.8%	128	0.0074	0.0013	−0.0061	−450.0%
59	0.0349	0.0226	−0.0123	−54.7%	129	0.0073	0.0012	−0.0061	−490.7%
60	0.0338	0.0217	−0.0121	−55.6%	130	0.0072	0.0011	−0.0061	−540.2%
61	0.0327	0.0209	−0.0118	−56.6%	131	0.0071	0.0010	−0.0061	−602.1%
62	0.0316	0.0201	−0.0115	−57.5%	132	0.0070	0.0009	−0.0061	−682.3%
63	0.0306	0.0193	−0.0113	−58.5%	133	0.0069	0.0008	−0.0061	−791.8%
64	0.0297	0.0186	−0.0111	−59.5%	134	0.0068	0.0006	−0.0061	−953.2%
65	0.0288	0.0179	−0.0108	−60.6%	135	0.0067	0.0005	−0.0062	−1224.9%
66	0.0279	0.0173	−0.0106	−61.7%	136	0.0066	0.0003	−0.0062	−1835.0%
67	0.0271	0.0166	−0.0104	−62.8%	137	0.0065	0.0001	−0.0064	−11,273.7%
68	0.0263	0.0160	−0.0102	−63.9%					
69	0.0255	0.0155	−0.0101	−65.1%					
70	0.0248	0.0149	−0.0099	−66.3%					

is consistent with the standard relativistic energy momentum relation, and the Suto formula is based on an alternative theory, with a modified relativistic energy momentum formula. It is too early to say whether or not these relativistic extensions of the Rydberg formula can tell us anything new that is consistent with observations, as it is likely that relativistic quantum mechanical corrections would be needed for that. We encourage others to look further into this, and we hope to do so some time in the future as well.

Acknowledgements

Conflicts of Interest

The author declares that there is no conflict of interest regarding the publication of this paper.

References

[1] Haug, G.E. (2020) *Journal of Modern Physics*, **110**, 528-534. https://doi.org/10.4236/jmp.2020.114035

[2] Suto, K. (2020) *Journal of Modern Physics*, **11**, 294-303. https://doi.org/10.4236/jmp.2020.112018

[3] Drake, G.W.F. and Yan, Z.C. (1992) *Physical Review A*, **460**, 2378. https://doi.org/10.1103/PhysRevA.46.2378

[4] Le Bigot, E.O., Jentschura, U.D., Evers, J., Mohr, P.J. and Keitel, C.H. (2005) *Journal of Physics B: Atomic, Molecular and Optical Physics*, **380**, 97. https://doi.org/10.1088/0953-4075/38/2/008

[5] Rydberg, J.R. (1890) *Philosophical Magazine*, **29**, 331-337. https://doi.org/10.1080/14786449008619945

[6] Compton, A.H. (1923) *Physical Review*, **210**, 483. https://doi.org/10.1103/PhysRev.21.483 https://journals.aps.org/pr/abstract/10.1103/PhysRev.21.483

[7] Dirac, P. (1928) *Proceedings of the Royal Society of London*, **117**, 610. https://doi.org/10.1098/rspa.1928.0023

[8] Spavieri, G., Rodriguez, M. and Sanchez, A. (2018) *Journal of Physics Communications*, **80**, 1. https://doi.org/10.1088/2399-6528/aad5fa

[9] Spavieri, G., Gillies, G., Haug, E.G. and Sanchez, A. (2019) *Journal of Modern Optics*, **66**, 2131-2141. https://doi.org/10.1080/09500340.2019.1695005

Physics of Clocks in Absolute Space-Time

Edwin Eugene Klingman

Cybernetic Micro Systems, Inc., San Gregorio, CA, USA
Email: klingman@geneman.com

Abstract

20th century physics experimentally established beyond doubt the fact that moving clocks read differently from "static" clocks. This fact is typically interpreted as support for special relativity. On the other hand, the same century produced proof that clocks at various locations in the gravitational field also read differently, and this fact is explained by general relativity, which is, in general, not Lorentz transformable. This paper establishes a common framework for the physics of clocks in these different situations.

Keywords

Relativity, Time Dilation, Space-Time Ontology, Clock Slowdown, Inertial Clocks, Absolute Space and Time, Inertial Mass, Covariance Principle, Ideal Clocks

1. Introduction

Numerous 20th century physics experiments proved beyond doubt that clock measurements vary based on clock position and velocity in a local gravitational field. The global positioning system (GPS) is based upon these facts. Interestingly, despite the reality of the local gravitational fields, the theory that deals with velocity-based clock changes (special relativity) [1] ignores local gravity, assuming that it has no relevance. General relativity, on the other hand, is based on a metric representation of gravity in its treatment of clock changes [2]. Both theories focus on ideal clocks in space and time and ignore inertial mass contributions to the phenomena. Our modern world operates on the GPS that combines velocity and position in the local gravitational field. These are almost never treated together in special relativity texts, due to the imagined absence of gravity in special relativity theory.

The best-known clock experiments are Hafele-Keating [3], which treats clocks in relative motion in a local gravitational field; and Pound-Rebka [4], which

treats clocks displaced relative to local gravitational field. In both instances, local gravity establishes the preferred local absolute coordinate system, with the origin in both cases being the local center-of-mass. In special theory moving clocks slow down and there exists no preferred frame; however in order to interpret the fact that clocks speed up or slow down according to whether they move East or West, one must define a preferred frame at the center-of-mass. These facts demand treatment based on local absolute coordinates and that is the goal of this paper.

The plan of this paper is as follows.

Section 1, the Introduction, summarizes the 20th century consensus that "time dilation" occurs and is physically real, with one aspect attributed to special relativity and another to general relativity.

Section 2 provides a novel overview of ideal clocks versus real inertial clocks.

Section 3 provides relevant background and context from 21st-century experimental physics, and formulates a novel physical, rather than mathematical, basis for the Minkowski invariance.

Section 4 develops a geometric algebra formulation of invariance following Hestenes. After relating his multi-vector to our photon model of invariance, we derive a relation based upon the fact that measurements of clocks in relative motion vary in such a way that an invariance relation is preserved across frames in relative motion. Unlike other derivations of this relation, ours is based upon the assumption of absolute space and time. Apparent differences in time are given a novel interpretation.

Section 5, physics in absolute space and time, differs from Hestenes' derivation that is based on Lorentz transformation. Our derivation of physics in absolute space yields the classical Hamiltonian that is generally believed to be based on relativistic space-time. This is a significant novel result that forms the basis for the inertial analysis of clocks in motion.

Section 6, the physics of inertial clocks, introduces the idea of real physical clocks as opposed to the "ideal" clocks of relativity. It lays the groundwork for the physics of the following sections.

Section 7 on time measurement analyzes the basis of atomic clocks. It is a review and summary of the physics underlying atomic clocks. There is little new physics in the section but it provides details that show the commonality of the simple harmonic oscillator approach for inertial clocks.

Section 8 analyzes clocks in relative motion, derives the key result of this paper, based on the covariance principle of physics applied to identical clocks in separate coordinate frames. This result does not apply to special relativity theory because it is based on kinetic energy difference between the accelerated clock and the stationary clock, and the effect on inertial mass due to the equivalent mass of this energy. In special relativity there is no preferred frame and the mass in question is reset to rest mass in every frame, preventing the physical basis of our analysis, *i.e.* the difference in kinetic energy of the two inertial clocks. In our theory local absolute space defines the preferred frame; the novel physics is

straightforward, yielding exactly the clock behavior determined by 20th century physics.

Section 9 discusses the rationale used earlier to justify the derivation of the invariance relation, and clarifies the rationale based on the physics results just derived. It then applies this reasoning to the Hafele-Keating experiment. The actual results support our theory in absolute space and time, and it is necessary to depart from special relativity to explain these experimental results.

Section 10 treats positional dependence in the local absolute frame. It derives the formula for inertial clocks based on our energy theory that interprets both kinetic energy and gravitational energy in the same context. This interpretation differs from the generally unrelated interpretations of clock behavior in special and general relativity texts, but physical results are the same.

Section 11 discusses analysis of classical and quantum clocks in the context of a 2020 paper. The assumptions underlying the quantum treatment of clocks are similar to our assumptions concerning energy and absolute time and space, and differ from the Lorentz-based assumptions of special relativity.

Section 12 provides a summary of the paper.

2. Overview Inertial Clocks versus Ideal Clocks

Ideal clocks operate in a geometric universe; real clocks operate in a physical universe with inertial mass. The geometric model rotates time into space via Lorentz transformation on coordinates, while inertial clock models bring the relativistic $\gamma(v,c)$-factor into the definition of inertial mass $m = \gamma m_0$ and that is the extent of which γ enters the physics. Length contraction and velocity addition do not appear in energy-time theory. Newtonian dynamics based on $F = ma$ show an inverse relation between inertial mass m and acceleration a for constant force F. Physically this exhibits the fact that inertia resists acceleration and hence clocks that have been accelerated in absolute space slow-down. Time plays no variable role in this dynamic; universal time is the same everywhere in the universe; it does not "flow differently" with local circumstances. One key principle in operation is *conservation of energy* and periodic transfer of energy associated with disturbances in the media. Another key principle is the *covariance principle*: Physics must not change, regardless of change in coordinate-based formalism. The time-based dependence of thermodynamic systems is seen in the $\gamma(v,c)$ function across all inertial clocks, based primarily upon the covariance of physics across frames in relative motion.

3. Relevant Background

The fundamental theories of "clock change" attribute the change to geometric transformation; the Lorentz transformation in special relativity and generalized space-time transformations in general relativity, which is, in general, not space-time Lorentz transformable. In this sense the physics is somewhat compartmentalized, with "flat-space" geometry describing velocity-based clock change and "curved

space-time" geometry describing position-based change. This is further complicated by the fundamental proposition that <u>no</u> coordinate system can affect physics. Therefore, to remove whatever confusion accompanies these geometric formulations, we desire physics-based, rather than geometry-based, formulation. To establish such we begin with the existence of photons as disturbances in a gravitational field.

A major event occurred in 2017 when both photons and gravitons were detected from inspiraling neutron stars [5]. After traveling through gravitational fields for 1 billion years, the photon-disturbance and graviton-disturbance arrived at earth within roughly a microsecond of each other, establishing for the first time the equivalence of the speed of light in a gravitational field and the speed of gravity waves in the same field.

Light waves derive from Maxwell's equations with the speed given by $c = 1/\sqrt{e_0 \mu_0}$, while gravitational waves derive from Heaviside-Einstein linear equations based on Newton's gravitational constant G. As the waves propagate in the same medium, we relate ε and μ to G and derive Equation (1). Will [6] discusses the $TH\varepsilon\mu$ formalism relating ε and μ to G.

$$c = \frac{1}{\sqrt{\varepsilon_0 \mu_0}} \Rightarrow \left[\varepsilon(G)\mu(G)\right]^{-1/2} = \left[\left(\frac{-1}{4\pi G}\right)_{\varepsilon}\left(\frac{-4\pi G}{c^2}\right)_{\mu}\right]^{-1/2} = \left(c^{-2}\right)^{-1/2} = c \quad (1)$$

Based on this detection, we know that photons and gravitons obey propagation law $|x| = ct$. It is this basic physical law that we wish to build upon, rather than upon geometry independent of material reality. To do so we describe change in position $\mathrm{d}x$ of the photon during a change in time, duration $\mathrm{d}t$, as given by $|\mathrm{d}x| = c\mathrm{d}t$. A vector magnitude is equal to the scalar distance. Hestenes, in Geometric Calculus, defines an entity $X = ct + x$ which is a multi-vector scalar travel distance and travel direction representing the photon in our development. An associated entity, $\tilde{X} = ct - x$ represents an anti-photon, or photon moving in the opposite direction ($-x$) for the same time t as shown in **Figure 1**.

The position multi-vector does not relate space to time other than as a disturbance traversing space for a given time. As this disturbance in the field has energy and momentum, we develop an energy-time theory of clocks rather than a space-time theory. Our goal is to formulate a theory of inertial clock slowdown, compatible with both special and general relativity.
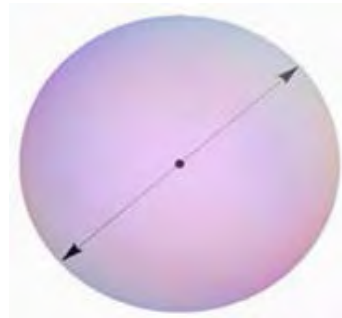
Figure 1. Photon propagation.

Since we are dealing with coordinate systems we begin by recalling that <u>no</u> coordinate system can affect physics. Coordinates are names or labels of "points" in time and space and have no effect at all on physical reality. When a chosen coordinate system is applied to local reality, physical measurements performed are expressed in terms of changes detected in local time or space, $\mathrm{d}t$ or $\mathrm{d}x$ respectively. Thus, had we chosen a different, "primed" coordinate frame, measurements would be expressed in terms of $\mathrm{d}t'$ or $\mathrm{d}x'$ respectively.

Einstein's *Principle of Covariance* stipulates that laws of physics should be the same in *all* coordinate frames. Time and space are related in local absolute frames via one parameter, the speed of light c such that $x = \pm ct$, ($\mathrm{d}x = \pm c\mathrm{d}t$). With this absolute relation between time and space, we obtain two key physics relations with $c = 1$: *distance* and *invariance*:

$$\mathrm{d}s^2 = \mathrm{d}t^2 + \mathrm{d}x^2 \to \infty \quad \text{Pythagorean distance in 4-space,}$$

$$\mathrm{d}s^2 = \mathrm{d}t^2 - \mathrm{d}x^2 = 0 \quad \text{Minkowski invariance in 4-space.}$$

4. Geometric Algebra Formulation of Invariance

Following Hestenes [7], we define *geometric algebra multi-vector* $X = ct + \boldsymbol{x}$ $\Rightarrow \mathrm{d}X = c\mathrm{d}t + \mathrm{d}\boldsymbol{x}$ and conjugate $\tilde{X} = ct - \boldsymbol{x}$ $\Rightarrow \mathrm{d}\tilde{X} = c\mathrm{d}t - \mathrm{d}\boldsymbol{x}$. From these it follows that

$$X\tilde{X} = 0. \tag{2}$$

and also that $X\tilde{X}' = 0$ when $X' = ct' + \boldsymbol{x}'$. These *invariance relations* apply in <u>all</u> frames in which *time-based distance* is defined by the speed of light. For generality, we define invariance with respect to frames in relative motion at speeds slower than light. Consider one rest frame to have its origin at the local center-of-mass and a moving frame that moves with velocity $\boldsymbol{v}$ with respect to the rest frame, such that $\boldsymbol{x} = \boldsymbol{v}t$. If we replace $\boldsymbol{x}$ in our X multi-vector by $\boldsymbol{v}t$ we obtain $X = ct + \boldsymbol{v}t$ and $\tilde{X} = ct - \boldsymbol{v}t$. Unfortunately, this destroys invariance, since $X\tilde{X} \neq 0$ and $X\tilde{X}' \neq 0$. However, invariance is such a powerful part of 20th century physics we attempt to rescue the concept by declaring measurements performed in two different frames yield

$$\frac{\mathrm{d}}{\mathrm{d}t}\left(X\tilde{X} - X\tilde{X}'\right) = 0 \tag{3}$$

If this is true, we have found *an invariance relation relating two frames* in relative motion – an absolute reference frame S and a frame S' moving with respect to S. This will allow us to develop physics that is valid in either frame. The frames move with velocity $\boldsymbol{v}$ and $\boldsymbol{v}'$, respectively, so we proceed to differentiate Equation (3);

$$\frac{\mathrm{d}}{\mathrm{d}t}\left[\left(c^2 - v^2\right)t^2 - \left(c^2 - v'^2\right)t'^2\right] = 0 \Rightarrow \frac{\mathrm{d}}{\mathrm{d}t}\left[\left(c^2 - v^2\right)t^2\right] = \frac{\mathrm{d}}{\mathrm{d}t}\left[\left(c^2\right)\tau^2\right], \tag{4}$$

where we have replaced t' by τ with no change of meaning, and we have arbitrarily set $v' = 0$ (and adjusted v if necessary). Thus v is the relative velocity of the two frames, with primed frame S' moving with velocity $\boldsymbol{v}$ with

respect to the unprimed (absolute) frame S. Clearly $t \neq \tau$ and the relationship between t and τ is a function of relative velocity $\boldsymbol{v}$; $t = \gamma(v)\tau$. A subtlety that may go unnoticed is that the invariance in question is not a geometric relation; it is in support of *covariance of physics equations*, where the variables represent measurements. The "time durations" $\mathrm{d}t$ and $\mathrm{d}t'$ represent clock readings in the unprimed and primed coordinate frames respectively. For example, at 1:41:20 in his Stanford video on special relativity [8] Leonard Susskind asks: "*what is this quantity t'?*" He answers: "*It's the reading of a moving clock.*" That is also our answer: t and t' represent clock readings (time measurements) in frames in relative motion. We complete the calculation and then interpret the result.

$$2t\left(c^2 - v^2\right) = \left(c^2\right)2\tau \frac{\mathrm{d}\tau}{\mathrm{d}t} \Rightarrow \left(1 - \frac{v^2}{c^2}\right) = \frac{\tau}{t}\frac{\mathrm{d}\tau}{\mathrm{d}t} \Rightarrow \frac{1}{\gamma}\frac{\mathrm{d}\tau}{\mathrm{d}t} \Rightarrow \frac{1}{\gamma^2} \tag{5}$$

Thus

$$\gamma(v) = \frac{1}{\sqrt{1 - v^2/c^2}} \quad \text{for constant } v \neq v(t). \tag{6}$$

If absolute time t is measured by a clock in the absolute frame, then apparent time τ, associated with the moving frame, will be that measured by an identical clock in the moving frame S'. Thus we may view $\gamma(v)$ as a *clock calibration factor* that must be satisfied for our invariance to hold true for all moving frames. To know that our clocks are "identical", we compare them at rest in the preferred frame, and then accelerate them to velocity v of the target frame. The acceleration of clocks is undetermined in relativity, but the added kinetic energy is equivalent to added mass and hence the inertia of the clocks will change. To analyze this we develop physics based on the invariance relations we have found.

5. Physics in Absolute Time and Space

The unprimed system S is considered to be at rest in the local absolute framework while the primed system is moving with velocity $\boldsymbol{v} = \dot{\boldsymbol{x}}$ in the rest frame. From Equation (2) and Equation (3) we obtain $\left(\Delta X\right)\left(\Delta \tilde{X}\right) = c^2\left(\Delta t\right)^2 - \left(\Delta \boldsymbol{x}\right)^2$ and $\left(\Delta X'\right)\left(\Delta \tilde{X}'\right) = c^2\left(\Delta \tau\right)^2 - \left(\Delta \boldsymbol{x}'\right)^2$. Let $\Delta \boldsymbol{x} = \boldsymbol{v}\Delta t$ and $\Delta \boldsymbol{x}' = \boldsymbol{v}'\Delta \tau$. If invariance is preserved, and we set $\boldsymbol{v}' = 0$ we obtain Hestenes' relation:

$$\left(\Delta X'\right)\left(\Delta \tilde{X}'\right) = c^2\left(\Delta \tau\right)^2 = \left(\Delta X\right)\left(\Delta \tilde{X}\right). \tag{7}$$

Divide both sides of the equation by $\Delta \tau$ twice, yielding

$$\left(\frac{\Delta X}{\Delta \tau}\right)\left(\frac{\Delta \tilde{X}}{\Delta \tau}\right) = c^2 \tag{8}$$

If $\Delta \tau \to \mathrm{d}\tau$ then four-velocity V is the entity $\left(\mathrm{d}X/\mathrm{d}\tau\right)$ with conjugate $\tilde{V} = \mathrm{d}\tilde{X}/\mathrm{d}\tau$, hence

$$V\tilde{V} = \left(\frac{\mathrm{d}X}{\mathrm{d}\tau}\right)\left(\frac{\mathrm{d}\tilde{X}}{\mathrm{d}\tau}\right) = c^2 \tag{9}$$

As Hestenes observes: "*Unlike three-velocities, the four-velocity has a constant magnitude independent of the particle history.*" The Minkowski invariance is key. Though Hestenes derives his relations from the Lorentz transformation, we have not, and will not, invoke Lorentz herein, because it does not carry through to the gravitational aspects of clocks.

Recall that $X(t) = ct + x(t)$, $\tilde{X}(t) = ct - x(t)$, therefore

$$\frac{dX}{dt} = c + \frac{dx}{dt} = c + v \ . \tag{10}$$

If moving clock time τ is used, and $X(\tau) = ct(\tau) + x(\tau)$ then

$$\frac{dX}{d\tau} = \frac{dt}{d\tau}\left(c + \frac{dx}{dt}\right) = \gamma(c + v) \tag{11}$$

since $t = \gamma\tau$ then $dt = \gamma d\tau \Rightarrow \gamma = dt/d\tau$. Although the above development appears geometric, we stipulate that physics involves inertial mass; therefore we introduce mass into the development. We do so with the right-hand terms of Equation (11) and multiply these by the rest mass m_0 of a particle, to obtain $m_0\gamma(c + v)$. The four-vector has the form *scalar* plus *vector*, with $\gamma m_0 c$ = scalar and $\gamma m_0 v$ = vector. Since γ is dimensionless $\gamma m_0 v$ has units of momentum:

$$p = mv \ . \tag{12}$$

If this is to make sense, we define the inertial mass m to be

$$m \equiv \gamma m_0 \tag{13}$$

implying that inertial mass increases with velocity, yielding rest mass at $v = 0$. This relation has been confirmed countless times in twentieth century particle physics. [9] Thus $P = m_0 V$. The scalar $\gamma m_0 c$ has units of momentum, but no obvious interpretation. If we multiply and divide by c we obtain $\gamma m_0 c^2/c$. Since $\gamma m_0 c^2$ has units of energy, we define $E = \gamma m_0 c^2$ as particle energy. Four-momentum $P = m_0 V = \left(\dfrac{E}{c} + p\right)$ implies a conjugate $\tilde{P} = m_0\tilde{V} = \left(\dfrac{E}{c} - p\right)$ thus $P\tilde{P} = \dfrac{E^2}{c^2} - p^2$ while Equation (9) shows that

$$P\tilde{P} = m_0 V m_0 \tilde{V} = m_0^2 V\tilde{V} = m_0^2 c^2 \ , \tag{14}$$

hence

$$\frac{E^2}{c^2} - p^2 = m_0^2 c^2 \ . \tag{15}$$

We now have a four-momentum invariance relation based on scalar E plus 3-vector momentum p. This dynamical energy-momentum relation is the essence of particle physics. The rest mass is found by setting $p = 0 \Rightarrow E(0) = m_0 c^2$. The energy expression $E(p) = \left(m_0^2 c^4 + c^2 p^2\right)^{1/2}$ implies the classical Hamiltonian [10]

$$H(p) = E(p) = \left(m_0^2 c^4 + c^2 p^2\right)^{1/2} \ . \tag{16}$$

This key invariance relation in physics, the Hamiltonian, was derived based

on local absolute space and universal time. A Legendre transformation allows us to transform a function of some variable into another function of another variable without losing any information. Classical physics can be formulated in terms of Lagrangian $L = T - V$ where T is kinetic energy and V is potential energy. Application of Legendre transform to a Lagrangian produces a Hamiltonian $H = T + V$. Legendre transformations do not lose any information; they are self-inverse. So in going from Lagrangian to Hamiltonian we lose no information; a second application of Legendre, this time to the Hamiltonian, will restore the original information, in the form of the Lagrangian. Thus our Hamiltonian derived from absolute time and space should transform into the appropriate Lagrangian formulation. In Hamiltonian $H = T + V$ for a free particle ($V = 0$) only the kinetic energy, $T = m_0 v^2 / 2$, is used. The total energy scalar defined above is $E = \gamma m_0 c^2$. For velocities much less than the speed of light we expand total energy as

$$E = \gamma m_0 c^2 = m_0 c^2 \left(1 - \frac{v^2}{c^2}\right)^{-1/2} \cong m_0 c^2 + m_0 v^2 / 2 \tag{17}$$

Ignoring rest energy $m_0 c^2$ the free particle kinetic energy is $T = m_0 v^2 / 2$, hence our absolute time and space Hamiltonian maps into classical non-relativistic mechanics as required.

6. The Physics of Inertial Clocks

We required only that clocks be constructed identically, but we never specified physically real clock construction. Clocks are sometimes conceptualized as *time transducers* but physical transducers such as piezoelectric devices convert mechanical stress into voltage, and voltage into mechanical stress. There exists no *time transducer* that converts time into something else that can be measured. *All clocks count cycles*; hence constructing a clock depends on designing a device that cycles with stable period. All useful time-measurement devices consist of multiple particles or subsystems and thus are subject to thermodynamic considerations [11] where:

"*Thermodynamics deals with matter and interactions between matter.*"

Multiple subsystems are typically partitioned into a system of interest and its surroundings, and "*Work refers to an interchange between a system and its surroundings.*" Our clocks are material in nature, hence *inertial*, and considered as non-intrusive entities present at the origin of the inertial reference frame of interest, or wherever else it is desirable to measure time in said frame.

7. Time Measurement: The Diatomic Molecule Vibrational states

Thermodynamic systems are modeled as subsystems that exchange energy within themselves and with their surroundings. Atomic clocks provide accurate time measurement devices, so we begin by modeling the vibrational state of a diatomic molecule, consisting of nuclear masses m_1 and m_2 and several elec-

trons. Our partitioning framework involves *exchange interactions* between all charged particles. The fact that low mass electrons quickly adjust to any change of position of the relatively massive, slow-moving nuclei suggests that we partition the system into two nuclei embedded in a distributed charge environment [12] as seen in **Figure 2**.

Instantaneous actions are based on force exchange; it is convenient to interpret an integral over forces: $\boldsymbol{F} = -\nabla \phi$, $\phi = \int \boldsymbol{F} \cdot \mathrm{d}\boldsymbol{x}$, where ϕ is the relevant potential. The diatomic molecule's nuclei are a distance r apart and are surrounded by several electrons. The force of electric interaction is $\approx q_1 q_2 / r_{12}^2$ for the nuclei and $\approx q_1 q_e / r_{1e}^2$ between nucleus q_1 and a q_e electron, r_{1e} distant. The Schrödinger equation potential energy is made up of *electron-electron*, *electron-nucleus, and nucleus-nucleus* coulomb interactions obtaining a set of electronic energy levels dependent on r, denoted by $u_e(r)$. If the masses are assumed constant, the nuclear mass $m_n = m_1 = m_2$ is many thousands of times greater than electron mass m_e so velocity v_e of the electron is many times greater than the nuclear velocity. **Figure 3** represents a relatively stationary nucleus in the cloud of fast-moving electrons which also interact with themselves. If all electrons were positioned between the two nuclei the positively charged nuclei would be attracted toward the center. If no electrons were located between the nuclei, the nuclei would force each other apart. The *Born-Oppenheimer* approximation considers the nuclei fixed, while studying the electrons in motion. For nuclei fixed a distance r apart, the potential energy is made up of the sum of all coulomb interactions. Let the dependence of the ground state electronic energy on internuclear distance be $u_e(r)$, with typical form shown in **Figure 3**.
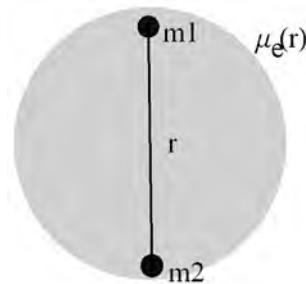
Figure 2. Diatomic molecule.
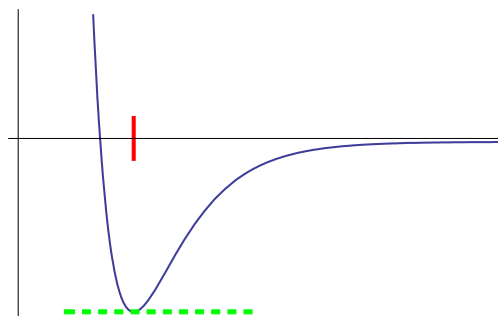
Figure 3. Ground state: electron energy $\mu_\varepsilon(r)$.

Following Hill, we choose coordinates x, y, z, r, θ, ϕ where x, y, z refers to the position of the center of mass, r is a separation on an axis ξ connecting the two nuclei, m_1 and m_2, and θ and ϕ describe the orientation of axis ξ, associated with vibration of the nuclei along ξ and the rotation of ξ about z. Our interest is in the *vibrational states*; we restrict ourselves to small vibrations near the bottom of the potential well. If the ground state electronic energy is a stable configuration, the nuclei effectively exist in stable *surroundings*; the diatomic molecule is partitioned into a system of two nuclei in a surrounding electron "bath", labeled $u_e(r)$. We can investigate the (relatively slow) motion of the two nuclei in the coordinate system x, y, z, r, θ, ϕ on the axis ξ connecting the two nuclei, m_1 and m_2; and θ and ϕ describe the orientation of axis ξ, as seen in **Figure 4**. Thus, in addition to the electron energy states, there exist energy states associated with vibration of the nuclei along ξ and the rotation of ξ about z. As our interest is in the *vibrational states*, it is customary to replace the actual $u_e(r)$ with a parabola which fits $u_e(r)$ in the neighborhood of its minimum, since, if a stable physical configuration exists, the state exists at a local minimum or ground energy. The Taylor series expansion around the local minimum at r_0 is

$$u_e(r) = u_e(r_0) + \frac{du_e}{dr}(r - r_0) + \frac{1}{2}\frac{d^2 u_e}{dr^2}(r - r_0)^2 + \cdots \tag{18}$$

The linear term vanishes near the minimum since $\left. \dfrac{du_e}{dr} \right|_{r=r_0} = 0$ so if

$\Delta u_e(r) = u_e(r) - u_e(r_0)$ then

$$\Delta u_e(r) = \frac{1}{2}\left.\frac{d^2 u_e}{dr^2}\right|_{r=r_0}(r - r_0)^2. \tag{19}$$

The energy change Δu_e represents work done on, or by, the system. Following Hill [13], the inter-nuclear distance is $r = \xi_2 - \xi_1$, where the line between the center of the two nuclei is the ξ-axis with arbitrary origin and ξ_2 (location of nuclear mass m_2) $> \xi_1$.

$$u_e = \frac{k}{2}\left(\xi_2 - \xi_1 - r_0\right)^2. \tag{20}$$
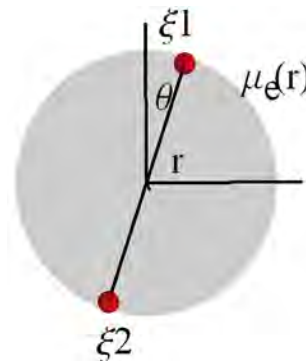
Figure 4. Vibration axis.

Newton's equation of motion is $f = ma$; force is the derivative of the potential $f = -\nabla u$, hence

$$m_1 \ddot{\xi}_1 = -\frac{\mathrm{d}u_e}{\mathrm{d}\xi_1} = k\left(\xi_2 - \xi_1 - r_0\right) \tag{21}$$

$$m_2 \ddot{\xi}_2 = -\frac{\mathrm{d}u_e}{\mathrm{d}\xi_2} = k\left(\xi_2 - \xi_1 - r_0\right) \tag{22}$$

Multiply Equation (21) by $-m_2$, Equation (22) by m_1, add the equations, and divide by $m_1 + m_2$ to obtain

$$\mu \ddot{x} = -kx \tag{23}$$

where $x = r - r_0$ and $\mu = \dfrac{m_1 m_2}{m_1 + m_2}$. Equation (23) is the equation of motion of the 1D harmonic oscillator with "reduced" mass μ. The cycle frequency of the classical motion is $2\pi\nu = \sqrt{k/\mu}$, but what exactly is cycling? In literally every clock system, *energy* cycles through two conjugate modes of the system, capable of at least temporary storage of energy; typically *kinetic energy of the system* exchanged with *potential energy of the environment* that the system is linked to; inherently thermodynamic. If potential energy is considered zero at $r = r_0$ then kinetic energy is maximum at r_0. As r decreases, the ions come closer together and repel each other more strongly, slowing down the ions according to $\mathrm{d}p/\mathrm{d}t = -kx$ where $F = \mathrm{d}p/\mathrm{d}t = -\nabla\left(kx^2/2\right)$. When $x = r - r_0$ is negative ($r < r_0$) the change in momentum is positive, forcing the ions apart from each other. When x is positive, the ions are far apart and the electron cloud attracts both more strongly. A parabola that approximates the potential minimum is symmetric, changing the sign of the force when r crosses r_0, reversing the cycle of motion. If $x \sim \sin \omega t$ where ω is the circular frequency $\omega = 2\pi/\Delta T$ then $x = \sin \omega t$, $\dot{x} = \omega \cos \omega t$, and $\ddot{x} = -\omega^2 \sin \omega t$ hence

$$\ddot{x} + \omega^2 x = 0. \tag{24}$$

Generally speaking, every system capable of vibrating around a minimum potential energy (an approximate parabolic shape) will oscillate as a sine wave function of time plus a phase. It is the *act-of-counting oscillation cycles* that measures time. From our derivation of absolute physics we have $p = mv$ hence $\dot{p} = m\ddot{x} = -kx$, thus

$$\ddot{x} + \left(k/m\right)x = 0 \Rightarrow \quad \omega^2 = k/m, \omega = \sqrt{k/m} \tag{25}$$

The ions move slowly compared to the surrounding electrons so the oscillating speed of the ions is nonrelativistic. This motion is internal to the clock mechanism, which may itself be moving with velocity v with respect to our rest frame. We analyze this clock motion next.

8. Analysis of Clocks in Relative Motion: The Covariance Principle

The only meaningful way to say that clocks tell the same time is to construct

them identically in some place side-by-side and observe time measurements. This is readily done; vast numbers of clocks exist, all of which count cycles based on some appropriate oscillating mechanism. Assume that we have two identical clocks initially at rest. Twentieth century physics tells us that *one of the clocks will slow down* if the clocks are in uniform relative motion, but *which clock?* The answer is whichever clock is accelerated to velocity v with respect to the other clock, which remains at rest. In other words, when we *apply work or transfer kinetic energy* to a clock, it slows down. We make use of the *covariance of the physics equations* in two separate frames, S and S', where S is the rest frame and S' is the frame that moves with velocity v as measured in the S frame, both shown in Figure 5. The equation of motion has the same form in both frames:
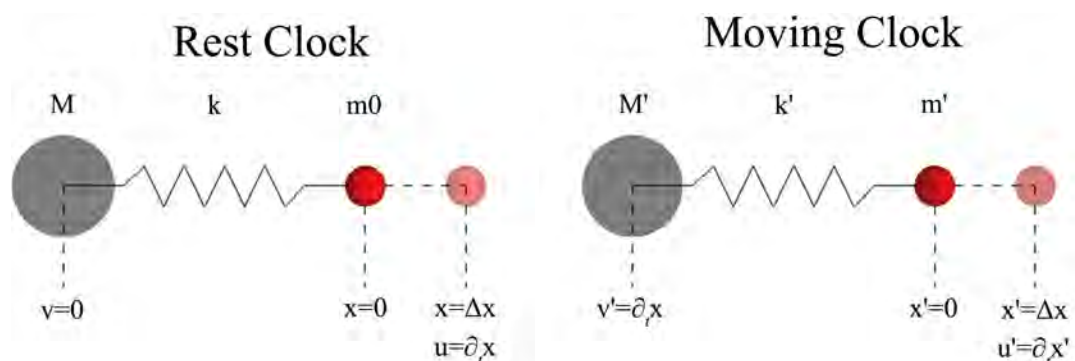
$$\frac{\mathrm{d}\boldsymbol{p}}{\mathrm{d}t} = -k\boldsymbol{x}, \quad \frac{\mathrm{d}\boldsymbol{p}'}{\mathrm{d}t'} = -k'\boldsymbol{x}' \tag{26}$$

Newton's law $\boldsymbol{F} = \mathrm{d}\boldsymbol{p}/\mathrm{d}t$ for the clock at rest has restoring force on the sprung mass $\boldsymbol{F} = -k\Delta\boldsymbol{x}$. We assign an equivalent relation $\boldsymbol{F}' = \mathrm{d}\boldsymbol{p}'/\mathrm{d}t' = -k'\boldsymbol{x}'$ to the clock in motion, where $x' = \Delta x$ is the stretch of the spring and we assume $k' = k$. Velocity $\boldsymbol{v}_0$ of the rest clock is zero in absolute space, while the velocity of sprung mass m_0 of the rest clock is $\boldsymbol{u} = \mathrm{d}\boldsymbol{x}/\mathrm{d}t = \dot{\boldsymbol{x}}$. The moving clock is assumed to be initially at rest, and then to be accelerated to velocity v, so the velocity of the sprung mass m' of the moving clock is $\boldsymbol{v} + \boldsymbol{u}'$ in absolute space with $\boldsymbol{v} = \mathrm{d}\boldsymbol{x}/\mathrm{d}t$ and $\boldsymbol{u}' = \mathrm{d}\boldsymbol{x}'/\mathrm{d}t = \dot{\boldsymbol{x}}'$. In these terms the momentum of the sprung mass of the rest clock is given by $\boldsymbol{p} = m_0(\boldsymbol{v}_0 + \boldsymbol{u})$ while the momentum of the sprung mass of the moving clock is $\boldsymbol{p}' = m'(\boldsymbol{v} + \boldsymbol{u}')$. We write equations of motion of such mass in both unprimed (rest) and primed (moving) frames:

$$\frac{\mathrm{d}\boldsymbol{p}}{\mathrm{d}t} = m_0\frac{\mathrm{d}\boldsymbol{u}}{\mathrm{d}t} = m_0\ddot{\boldsymbol{x}} = -k\boldsymbol{x}, \quad \frac{\mathrm{d}\boldsymbol{p}'}{\mathrm{d}t'} = m'\frac{\mathrm{d}}{\mathrm{d}t'}(\boldsymbol{v}+\boldsymbol{u}') = -k\boldsymbol{x}' \tag{27}$$

so

$$\frac{\mathrm{d}}{\mathrm{d}t'} = \frac{\mathrm{d}}{\mathrm{d}t/\gamma} = \gamma\frac{\mathrm{d}}{\mathrm{d}t} \Rightarrow \frac{\mathrm{d}\boldsymbol{p}'}{\mathrm{d}t'} = m'\frac{\mathrm{d}}{\mathrm{d}t'}(\boldsymbol{v}+\boldsymbol{u}') = \gamma m'\frac{\mathrm{d}\boldsymbol{u}'}{\mathrm{d}t} = -k\boldsymbol{x}'. \tag{28}$$

Figure 5. Diagrams with relevant parameters for rest and moving clocks.

Since $\boldsymbol{u}' = \dfrac{\mathrm{d}\boldsymbol{x}'}{\mathrm{d}t}$ and $m' = \gamma m_0$ we have $\dfrac{\mathrm{d}\boldsymbol{p}'}{\mathrm{d}t'} = \gamma m' \dfrac{\mathrm{d}^2 \boldsymbol{x}'}{\mathrm{d}t^2} = -k\boldsymbol{x}'$

$\Rightarrow \gamma^2 m_0 \ddot{\boldsymbol{x}}' = -k\boldsymbol{x}'$.

Summarizing:

$$\frac{\mathrm{d}\boldsymbol{p}'}{\mathrm{d}t'} \Rightarrow \frac{\mathrm{d}^2 \boldsymbol{x}'}{\mathrm{d}t^2} + \left(\frac{\omega_0}{\gamma}\right)^2 \boldsymbol{x}' = 0 \Rightarrow \ddot{\boldsymbol{x}}' + \omega'^2 \boldsymbol{x}' = 0 \tag{29}$$

$$\frac{\mathrm{d}\boldsymbol{p}}{\mathrm{d}t} \Rightarrow \frac{\mathrm{d}^2 \boldsymbol{x}}{\mathrm{d}t^2} + \omega_0^2 \boldsymbol{x} = 0 \Rightarrow \ddot{\boldsymbol{x}} + \omega_0^2 \boldsymbol{x} = 0 \tag{30}$$

In terms of universal time t, the equation of motion of the rest clock yields frequency ω_0, while the frequency of the moving clock yields $\omega' = \omega_0/\gamma$. This establishes *time dilation* for inertial clocks in relative motion in universal time and space.

Should one become confused over $\boldsymbol{x}$ and $\boldsymbol{x}'$ above, the equations of motion for sprung-mass treat $\boldsymbol{x}$ and $\boldsymbol{x}'$ as the position variables for m and m' respectively, $\boldsymbol{x}$ can be replaced by $\boldsymbol{x}_m$ and $\boldsymbol{x}'$ be replaced by $\boldsymbol{x}'_{m'}$ such that the relevant velocities are denoted by:

$$\boldsymbol{u} = \frac{\mathrm{d}\boldsymbol{x}}{\mathrm{d}t} \equiv \frac{\mathrm{d}\boldsymbol{x}_m}{\mathrm{d}t} \quad \text{and} \quad \boldsymbol{u}' = \frac{\mathrm{d}\boldsymbol{x}'}{\mathrm{d}t} \equiv \frac{\mathrm{d}\boldsymbol{x}'_{m'}}{\mathrm{d}t}, \tag{31}$$

and every step can be carried out using these explicit mass-based position coordinates. Of course one obtains the same final results. Equation (29) and Equation (30) are *formulated in terms of universal time*, *t*, as should be expected in a theory of absolute time and space. The frequency ω' of the moving oscillator is less than rest frequency ω_0 since $\gamma > 1$. Frequency ω_0 is inversely related to the rest clock period: $\omega_0 \sim 1/\Delta t$ and frequency ω' of the moving oscillator is inversely related to the period of the moving clock $\omega' \sim 1/\Delta t'$. From these we obtain $\dfrac{\omega_0}{\omega'} = \gamma = \dfrac{\Delta t'}{\Delta t}$. Since *clocks tell time by counting periods* let us assume an absolute time period ΔT is measured by each clock. If the rest clock counts n periods (Δt) during ΔT and the moving clock counts n' periods ($\Delta t' = \Delta \tau$) then we obtain

$$\Delta T = n\Delta t = n'\Delta t' \tag{32}$$

where n and n' are the *respective readings of the clocks in S and S'*. From Equation (32) we derive

$$\frac{n}{n'} = \frac{\Delta t'}{\Delta t} = \gamma \tag{33}$$

hence $n = \gamma n'$. Thus the clock moving with velocity v runs more slowly by a factor equal to the inertial factor γ. This *clock slowdown* agrees with relativistic *time dilation* but is based on *absolute time*. For instance, the derivative $\mathrm{d}/\mathrm{d}t'$ refers to the change in something with respect to the time measured in the moving system. Thus $\mathrm{d}t'$ represents time measured in S' and $\mathrm{d}t$ represents time measured in rest frame *S*. But these times are <u>clock readings</u> n and n', hence $n \sim \mathrm{d}t$ and $n' \sim \mathrm{d}t'$ and we obtain

$$\frac{n}{n'} = \frac{\mathrm{d}t}{\mathrm{d}t'} = \gamma. \tag{34}$$

These readings are multiples of the clock *tick* or oscillation periods, denoted by Δt and $\Delta t'$ respectively for rest and moving frames. These terms are *inverse* to the respective frequencies: $\omega_0 \sim 1/\Delta t$, $\omega' \sim 1/\Delta t'$. In terms of clock periods, the relations *appear* reversed: $\frac{\Delta t'}{\Delta t} = \gamma$. So *do not confuse clock reading* $\mathrm{d}t$ *with rest clock period* Δt, *or* $\mathrm{d}t'$ *with* $\Delta t'$.

For a spring-based clock $\boldsymbol{f} = -k\boldsymbol{x}$ the frequency of oscillation of the moving clock is $\omega' = \omega_0/\gamma$ thus the moving clock "runs slower" than the clock at rest. The increase in inertial mass is the equivalent mass of the kinetic energy of the moving clock gained when the moving clock was accelerated from rest to velocity $\boldsymbol{v}$ in the absolute frame. The key fact is that:

Our analysis of inertial clocks leads to exactly $\omega' = \omega_0/\gamma \Rightarrow \mathrm{d}t/\mathrm{d}\tau = \gamma$ *the clock relationship that was experimentally confirmed in the twentieth century.*

9. "Calibration" vs. Thermodynamics

In our absolute time and space derivation of invariance leading to the Hamiltonian, the rest frame clock measures universal time t while the moving clock measurement is t'. Invariance between frames is preserved if clocks yield $\mathrm{d}t = \gamma(v)\mathrm{d}t'$ with $\gamma(v) = \left(1 - v^2/c^2\right)^{-1/2}$. How can one *calibrate* two clocks in this way? We cannot *construct* both clocks in the rest frame such that they can be calibrated for all mutual velocity $\boldsymbol{v}$. Clocks must be constructed *identically;* there is no way to build such calibration into the moving clock since we choose which clock is to remain at rest and which is to be accelerated to velocity $\boldsymbol{v}$. Yet while a *calibration* perspective fails, the *thermodynamics* of clock oscillators yields *exactly* the required $\gamma(v)$ relation, regardless of which clock accelerates from rest.

In deriving physics from the invariance relation, we sought to justify the invariance itself, in order to be able to apply the invariance *if* the γ constraint was met. Application of the invariance, combined with mass, yielded $\gamma(v)$ such that $m = \gamma m_0$ with $\boldsymbol{p} = m\boldsymbol{v}$ and $E = mc^2$. This relation applies to *all* inertial mass and therefore to *all* harmonic oscillators, and hence *all* clocks. Thus clocks are effectively *self-calibrating* for *all* velocities, exactly preserving the invariance relation that yields the energy Hamiltonian.

In energy-time theory, based on universal simultaneity and preferred local frame, space-time symmetry is thermodynamically unrealistic: In the real world, say Denver, a plane taking off in any direction is predicted by space-time symmetry to run slower than the clock at the Denver airport. Of course this does not happen. As Hafele and Keating first showed, clocks on planes taking off to the east slow down, while clocks on planes taking off to the west speed up. As *the rotating earth is not an inertial reference frame*, thermodynamic theory addresses reality. The west-to-east velocity of the Denver airport is approximately 500 miles per hour, so the clock at Denver airport has associated velocity and

momentum and energy $\{E, \boldsymbol{p}\} \sim \{mc^2, m\boldsymbol{v}\}$ going *west-to-east*. When Bob takes off from Denver heading east, he *adds to* the clock's local absolute velocity; its inertial mass will increase, its resistance to acceleration will increase, and his clock will slow down. But when Alice heads out for San Francisco, she will add a velocity component *east-to-west* that *subtracts from* the local absolute west-to-east velocity and thus travels slower; so Alice's clock does *not* slow down as she flies west, *it speeds up*, exhibiting the effect of a preferred frame. That is, a preferred frame is required to predict clock slowdown vs. speedup.

10. Positional Dependence in the Local Field

Our above thermodynamic analysis is based not on space-time symmetry, but on inertial mass $m = m_0 \gamma(v)$; inertial factor $\gamma(v)$ relates to inertial mass, not to space and time. We extend this relation to general relativity [14] as

$$m = m_0 \gamma(\dot{\boldsymbol{r}}) e^{\phi(r)} \tag{35}$$

Here the mass of the particle depends upon the kinetic energy in a local absolute gravitational field as well as its position-dependent energy within a gravitational field with potential ϕ. This inertial relation explains clock-slowing, as known and practiced in GPS.

Our "gravity free" definition of inertial mass, $m = \gamma m_0$ was found to include the kinetic energy in addition to rest mass: $m = m_0 \left(1 - v^2/c^2\right)^{1/2}$. In a gravitational field the energy of a mass depends upon the Newtonian potential $\phi = GM/r$ so let us naïvely add the gravitational term $2\phi/c^2$ to the kinetic energy term as follows

$$m = m_0 \left[1 - \left(\frac{v^2}{c^2} + \frac{2\phi}{c^2}\right)\right]^{-1/2} \Rightarrow m_0 \left[1 + \frac{1}{2}\frac{v^2}{c^2} + \frac{\phi}{c^2}\right] \tag{36}$$

yielding inertial mass and associated energies:

$$\underset{\text{total energy}}{mc^2} = \underset{\text{rest}}{m_0 c^2} + \underset{\text{kinetic}}{m_0 v^2/2} + \underset{\text{gravitational}}{m_0 \phi} \tag{37}$$

This formulation demonstrates the dependence of inertial mass on velocity $\dot{\boldsymbol{r}}$ through the local gravitational field and on position $\boldsymbol{r}$ in the local gravitational field. Our simple addition of the gravitational potential $\phi = GM/r$ is only intuitively justified, however Poisson and Will [13] derive the same result in orthodox fashion based on the action

$$S = -m_0 c^2 \int d\tau = \int L dt \tag{38}$$

where $d\tau$ is the proper time after clock slowdown (speedup) is considered, and the Lagrangian

$$L = -mc\sqrt{-\eta_{\alpha\beta} \frac{dr^\alpha}{dt} \frac{dr^\beta}{dt}} \tag{39}$$

is evaluated as

$$L = -mc\sqrt{1 - \frac{2\phi}{c^2} - \frac{v^2}{c^2}} \tag{40}$$

in which case

$$L = -m_0 c^2 + m_0 v^2 / 2 + m_0 \phi \,. \tag{41}$$

As explained in Section 5, our energy-time Hamiltonian is completely compatible with the classical Lagrangian approach, therefore the Lagrangian in Equation (41) yields physics in agreement with Equation (37). We again see that the time-dependence of clocks follows from energy-based analysis rather than geometry.

11. Analysis of Classical and Quantum Clocks

The issue of inertial clocks is one of current interest: Paige, Plato, and Kim [15] analyze classical and non-classical time dilation for quantum clocks. Quantum mechanics assumes universal time, and their analysis starts from a Hamiltonian modified to account for the *inertial mass of internal energy* as well as kinetic energy. Thus their key assumptions agree with our treatment of inertial clocks, and their clocks are also assumed to be based on composite particles, bringing thermodynamic aspects into play. They, too, view energy and inertial mass as equivalent, and they utilize the same relativistic Hamiltonian that we derived herein. In this context their predicted classical clock behavior agrees with our analysis and with experiment.

For non-classical analysis, quantum aspects such as the *Uncertainty Principle* complicate the picture: with momentum boosts it becomes impossible to define the exact position of the origin of the frame. Purely quantum aspects such as superposition, entanglement also complicate issues, but predicted differences are too small to measure with shifts about 10^{-10} smaller than observed.

The analysis of quantum clocks shares our key assumptions: universal time, relativistic Hamiltonian, and inertial mass. Their results show that clocks run slower by the inverse factor of γ. Of major significance: their analysis, like our analysis, is based on physics, not on geometry.

12. Summary

The 20th century essentially began with Einstein's relativistic $E = mc^2$ Lorentz transformation on time and space, differentiating "modern" physics from the pre-relativistic classical physics of Newtonian absolute space and time. The Lorentz rotation of time into space and space into time predicted "length contraction" and "time dilation", and led to the relativistic Hamiltonian of Equation (16). Muon physics and Hafele-Keating essentially nailed down physicist's belief in time dilation and length contraction despite that, per Rindler, "*no direct experimental verification of length contraction has yet been attempted.*" Lorentz-based "velocity addition" has also been challenged [16] based on accelerator physics; the experimental basis of special relativity is more of a mixed bag than is perhaps generally recognized. Nevertheless no one seriously questions "time dilation" as an empirical fact.

Yet while physics provides a means of understanding nature by focusing on changes in systems over time, our intuition provides a means of understanding focused on the direct perception of truth or fact, independent of any reasoning process. Mermin [17] says "*… relativity reveals the nature of time to be shockingly different from what has been taken completely for granted.*" This mismatch between intuitive understanding of time and Einstein's relativistic theory of time is so pronounced that the journal *Foundations of Physics* last year published three papers [18] [19] [20] in a special issue focused on this problem.

Despite the lack of experimental verification of length contraction and of velocity addition, the Lorentz transformation is built-into modern physics at the root: the *action principle* and the Lagrangian formulation of physics are basic to all fields of physics and employ the Lorentz transformation from the beginning. This is almost unanimously interpreted as support for space-time rotation, although the excellent relativity text by Lucas and Hodgson summarizes the many derivations of the Lorentz transformation and concludes:

"*… if we insist on retaining Newtonian dynamics, and the Newtonian definition of velocity and acceleration, then we can still obtain relativistically correct results if we pay the price of allowing the mass to depend on the velocity.*"

This is *exactly* the assumption behind our treatment of inertial clocks. However, the relativistic proposition of "no preferred frame" forbids this interpretation by systematically "resetting" inertial mass to rest mass in *every* frame, thereby "throwing away" the differential kinetic mass responsible for clock-slowing in our energy theory.

Although our assumption of absolute space was hinted at in Equation (1), there is a literature on "gravity as aether" that even Einstein appeared to subscribe to in later years. This assumption is strengthened by the 2017 detection of gravitational waves and light waves from inspiraling neutron stars, and also receives little-recognized support from Michelson-Gale experiments [21].

It was also noted in this paper that the Hafele-Keating "time dilation" experiments do <u>not</u> fit the special relativity theory as one must violate the no-preferred-frame proposition in order to explain the East-West dichotomy.

In summary, we recall Hestenes remark on physical modeling:

"*everything we know about physical space-time is known through its representation by some model, so when we are thinking about space-time and its properties, we're actually thinking about the model. (…) however we **attribute an independent existence** to space-time which might not be accurately represented by our model (…) so we must keep the distinction clear when considering the possibility that the model is wrong.*"

When Hestenes says "*we attribute an independent existence to …*", he is speaking of ontology. He is warning here that our "model" may not correspond to reality. Physicists who regard ontology as metaphysics are comfortable switching ontology as necessary, for example, invoking a forbidden *preferred frame* if needed to explain clock *speedup* when flying west. We note simply that our model, based on inertial clocks in absolute space and time, appears compati-

ble with all experimental results. It is unlikely that nature maintains a *geometric* ontology and an *inertial mass* ontology, just for the satisfaction of physicists who have learned one model or another.

Our treatment of inertial clocks as simple harmonic oscillators, subject to thermodynamic analysis, has yielded dynamical behavior consistent with the experimental record. The approach is based on physical phenomena rather than geometry, and assumes universal time and preferred spatial frames associated with local center-of-mass. The result we have achieved is formulated in local absolute space, identified with local center-of-mass, and universal time, t. The theory is compatible with Hafele-Keating and with Pound-Rebka experiments and agrees with treatments of clock slowdown in special relativity and general relativity. In this mathematical theory of physics we have avoided some thorny ontological issues. For example, Poisson and Will's excellent gravity text states:

"*Time flows at a rate that depends on position in a gravitational field.*"

Alternatively, one could state that time does not "flow" at that rate; instead, energy-time conservation dictates that inertial clocks measure time at that rate. The inertial mass of the clock oscillator incorporates the mass-equivalent of kinetic energy and the potential energy of the gravitational field; the resultant change in oscillator frequency is counted and the changed count represents the clock reading or time measurement. This thermodynamic interpretation establishes the common framework we sought for "clock slowing" in special and general relativity.

Acknowledgements

Conflicts of Interest

The author declares no conflicts of interest regarding the publication of this paper.

References

[1]   Rindler, W. (1991) Introduction to Special Relativity. 2nd Edition, Oxford University Press, New York.

[2]   Ohanian, H. and Ruffini, R. (2013) Gravitation and Spacetime. 3rd Edition, Cambridge University Press, New York. https://doi.org/10.1017/CBO9781139003391

[3]   Hafele, T. and Keating, R. (1972) *Science*, **177**, 166-168. https://doi.org/10.1126/science.177.4044.166

[4]   Pound, R. and Rebka, V. (1959) *Physical Review Letters*, **3**, 439. https://doi.org/10.1103/PhysRevLett.3.439

[5]   Abbott, B., *et al.* (2017) *Physical Review Letters*, **119**, Article ID: 161101.

[6]   Will, C. (2018) Theory and Experiment in Gravitational Physics. 2nd Edition, Cambridge Press, Cambridge.

[7]   Hestenes, D. (1986) New Foundations for Classical Mechanics. 2nd Edition, Kluwer

Academic Pub., Dordrecht. https://doi.org/10.1007/978-94-009-4802-0

[8] Susskind, L. (2012) Special Relativity Lecture 1. Stanford Video Series.
https://youtu.be/toGH5BdgRZ4

[9] Lucas, J. and Hodgson, P. (1990) Space-Time and Electromagnetism. Clarendon Press, Oxford.

[10] Kauffmann, S. (2018) Dirac Theory's Breaches of Quantum Correspondence and Relativity; Nonrelativistic Pauli Theory's Unique Relativistic Extension.
https://vixra.org/abs/1810.0114
https://vixra.org/abs/1901.0228

[11] Reynolds, W. (1965) Thermodynamics. 2nd Edition, McGraw-Hill, New York.

[12] Hill, T. (1960) An Intro to Statistical Thermodynamics. Dover Publications, New York.

[13] Poisson, E. and Will, C. (2014) Gravity. Cambridge University Press, Cambridge.

[14] Robertson, S. (2019) *Prespacetime Journal*, **10**, 621-626.

[15] Paige, A., Plato, A. and Kim, M. (2020) *Physical Review Letters*, **124**, Article ID: 160602. https://doi.org/10.1103/PhysRevLett.124.160602

[16] Cannoni, M. (2016) Lorentz Invariant Relative Velocity.

[17] Mermin, D. (2005) It's about Time. Princeton University Press, Princeton.
https://doi.org/10.1515/9781400830848

[18] Rovelli, C. (2019) *Foundations of Physics*, **49**, 1325-1335.
https://doi.org/10.1007/s10701-019-00312-9

[19] Thyssen, P. (2019) *Foundations of Physics*, **49**, 1336-1354.
https://doi.org/10.1007/s10701-019-00294-8

[20] Ben-Yami, H. (2019) *Foundations of Physics*, **49**, 1355-1364.
https://doi.org/10.1007/s10701-019-00306-7

[21] Klingman, E. (2018) Everything's Relative, or Is It?
http://vixra.org/pdf/1812.0424v1.pdf

Making Drug Discovery More Efficient Applying Statistical Entropy to Biology

Philip D. Houck

Department of Medicine (Division of Cardiology) Baylor Scott & White Health, Temple, TX, USA
Email: Philip.Houck@bswhealth.org

Abstract

Biology without governing principle makes predications impossible. Observations lead to some successful therapies, and to unexpected failures. Erwin Schrödinger attempted to quantify biology with the concept of negative entropy. These insights lead to fundamental principles of biologic entropy. The quantification of negative entropy is difficult to calculate since the number of parts of the body and the way these parts are arranged is very large (atomistic disorder). There can be approximations that answer questions such as why females live longer, and why a lower body temperature predicts longevity. This concept can reveal the culprit of diabetes II; understanding the microbiome can reduce its entropy by increasing the entropy of its host. The real advantage of statistical entropy is finding new drugs and predicting viral mutations based on energetics and negative entropy. The misfolding of a protein will increase the entropy of an individual with the result of early death. The calculations of biologic entropy require the knowledge of each developmental step, and the statistical possibilities of the next step. If the step is crucial to maintain low entropy, a carrier protein will assure the energetics of the step is favorable. This protein is the target of new therapies.

1. Introduction

Erwin Schrödinger was a famous early 20th century physicist who first proposed the concept of negative entropy to explain the ordering of life. He also conjectured the existence of a memory molecule that preserves life information from one generation to the next. Erwin Schrödinger (1944), "What Is Life? The Phys-

ical Aspect of the Living Cell". The excerpt below is based on lectures delivered under the auspices of the Dublin Institute for Advanced Studies at Trinity College, Dublin, in February 1943.

"How would we express in terms of the statistical theory the marvelous faculty of a living organism, by which it delays the decay into thermodynamical equilibrium (death)? We said before: 'It feeds upon negative entropy', attracting, as it were, a stream of negative entropy upon itself, to compensate the entropy increase it produces by living and thus to maintain itself on a stationary and fairly low entropy level. If D is a measure of disorder, its reciprocal, l/D, can be regarded as a direct measure of order. Since the logarithm of l/D is just minus the logarithm of D, we can write Boltzmann's equation thus:

$$-(\text{entropy}) = k \log(1/D).$$

Hence the awkward expression 'negative entropy' can be replaced by a better one: entropy, taken with the negative sign, is itself a measure of order. Thus, the device by which an organism maintains itself stationary at a fairly high level of the orderliness (=fairly low level of entropy) really consists continually sucking orderliness from its environment. This conclusion is less paradoxical than it appears at first sight. Rather could it be blamed for triviality? Indeed, in the case of higher animals we know the kind of orderliness they feed upon well enough, viz. the extremely well-ordered state of matter in more or less complicated organic compounds, which serve them as foodstuffs. After utilizing it they return it in a very much degraded form, not entirely degraded, however, for plants can still make use of it (These, of course, have their most power supply of 'negative entropy' the sunlight).

Entropy = $k \log D$, where k is the so-called Boltzmann's constant = (3.2983 × 10^{24} cal./C), and D a quantitative measure of the atomistic disorder of the body in question [1]".

The above introduction by Erwin Schrödinger states best the difference between life and physical properties of the universe. Attempts to justify statistical entropy as a force of biology; explaining evolution and other difficult biological questions are explored in the paper "Should negative entropy be included in the fundamental laws of biology?" [2]. The key to understanding negative entropy in biology is the determination of atomistic disorder, D.

D is the sum of all the parts and all the possible ways the parts fit together. The human body has 50 trillion cells of roughly 300 cell types. The human also has 500 trillion bacteria and even more viruses and fungi in the microbiome inhabiting the gut, skin, airway, and every organ system. In addition, each cell has the entire information to make another individual with the molecule predicted by Schrödinger identified as Deoxyribonucleic acid DNA. In Men there are 46 chromosomes and in women there are 45 with one of the X chromosomes blocked, since it is a duplicate. Four base pairs describe 20,000 genes that encode 2 million proteins. Separate structures called mitochondria may have been parasitic bacteria that now live within our cells symbiotically. The proteins consisting

of 20 amino acids build cell organelles surface markers messenger RNA and the means to communicate between all our cells. The structure of proteins and the folding of branch chains is a complex entropic question adding significantly to atomistic disorder. D is a very big number [2]. Computations must be approximated. A huge number of small equations need to be solved to find the source of environmental energy.

The equation is useful and can give insight to mysteries that perplex biological scientist. Why do women live longer than men? The first question was addressed in the paper "Why is there a young woman advantage? Why is it lost? Applying the Laws of Biology to Men and Women" [3]. Men are more complex having 46 chromosomes as opposed to 45 in women. Men live less; approximated $(1 - 45/46) \times$ average death age of females. Table 1 lists some principles of biologic entropy.

Why does a low body temperature predict a longer life? Negative entropy is temperature dependent and humans have an approximate temperature of 310 K°. A lower body temperature suggests a lower state of entropy. Entropy is not time dependent but is temperature dependent [4]. The lower the temperature the less entropy.

Biologic age seems to be time dependent since it is observed that old people are closer to death. Older individuals have had more processes occur than younger individuals. The processes are time dependent. After a process is completed, statistical possibilities will be available for the next step. The number of possibilities is the atomistic disorder. The favored completed process is the lowest energy requiring state. In biology there is ordering of disorder taking energy from the environment. Biologic age is reduced by efficiently accepting energy from the environment. Other pathways could be statistically chosen and represents noise in a biological process. Entropy is not reduced and biologic age increases pushing patients to an early death. If the process is critical to survival, there will

Table 1. Fundamental principles of biologic entropy.

- Health is defined as maintaining low entropy
- Disease is a failure to maintain low entropy
- Entropy, introducing changes in DNA, favors evolution so life can survive in a changing environment
- Fetal development is an ordering of substrates and requires negative entropy with the energy supplied by the environment
- Repair of Injury depends on the developmental state. Prior to birth, injury is directed toward complete functional repair (negative entropy). After birth, repair is directed toward rapid return of partial function at the expense of achieving complete repair (positive entropy)
- Age is a state of increasing entropy
- Biologic processes are time dependent ordered by information provided by DNA. At the end of each process there are statistical possibilities for the next step. The energy required for this step is negative entropy = $k *$ LOG $(1/D)$.
- A strategy that saves energy by supplying a catalyst, carrier protein, or electromagnetic force assures the next critical step has the lowest energy.
- Drug discovery finds the catalyst, carrier protein, or electromagnetic force that favors negative entropy

be a mechanism that lowers the energy requirement to assure a successful process. One mechanism of securing the correct pathway is carrier proteins that can reduce the energy required to complete the critical step. These carrier proteins are targets for new drug discoveries.

Information science and negative entropy is a way of quantifying biological systems making systems biology more predictable. Each pathway in systems biology has a probabilistic outcome based the total possible interactions for the next step. An additional carrier protein may or not be present to assure the outcome if the desired outcome requires more energy. Quantification can be added to the multiple arrows and diagrams required in system analysis. Quantification can suggest a missing element that could serve as a drug target.

2. Current Pharmacological Short Falls

Pharmacology had not kept pace with new discoveries in biology. Pharmacological principles are mired in the receptor hypothesis and pharmacokinetics. The search is for protein and receptor matches, downstream effects and regulators of the response. Twenty thousand genes provide codes to make two million proteins. Researchers are invested in their proteins and tease out mechanisms of actions hoping their protein is the solution to human suffering. These targets of new therapies are elusive, often found serendipitously or teased out of simple analysis of single cells or simple organisms. A newer approach of systems biology is intensely complex and involves pathways within multiple organelles and interaction between cells. This approach also leads to new drug discoveries in a painfully slow manner. Escape pathways, inhibitors, and alternate stimulations/inhibitions lead to unexpected failures. The proteins are often abandoned. The more information obtained the more complex systems biology becomes. Since proteins are encoded by similar genes, they can have the same basic structure and can influence another pathway that was totally unsuspected. The drug industry is flourishing with a new technique of modifying receptors or proteins by antibodies to upregulate or down regulate pathways. The development identifies, purifies, elicits properties, and fulfills the 5 steps of drug approval. The estimated cost per drug approaches 3 Billion dollars [5]. The cost of identifying all 2 million proteins is a Quadrillion (10^{15}) \$ (Table 2).

Once the drug has come to market, the clinician finds new attributes of the drug not predicted by pharmacokinetics or systems biology. An example of new attributes is HMG CoA Reductase Inhibitors (Statins) that lower cholesterol but also modifies the immune system and increases circulating stem cells [6] [7]. The latter discovered effects are more important in decreasing myocardial infarction,

Table 2. Steps in the development of drugs.

1) Discovery and development
2) Pre-clinical Research
3) Clinical Research
4) FDA Review
5) FDA Post-Market Safety Monitoring

surviving infections, reducing perioperative complications, and repair of the fatty liver despite warning of its use with liver enzyme elevation. Pleomorphic benefits are attributed to properties of 3-hydroxy-3-methylglutaryl-coenzyme (HMG-CoA) reductase inhibitors. The pleomorphic effects escaped the basic scientist who only considered this molecule in lipid metabolism. Statins appear to have a negative entropy affect. The mechanism of interaction with the immune system that promotes repair over destruction is still not known. The property that reduces inflammation is observed and not understood. The answer is complex requiring knowledge the interaction of the drug with all the parts of the body. When energy of the desired outcome exceeds the energy of entropy a catalyst, carrier protein, or electromagnetic force is required to assure success, repair over decay. Statins provide this function favoring repair over decay. Table 3 proposes why current methods of drug discovery are inefficient.

3. Example of Entropy and Disease

Diabetes II is a modern disease first described in 1936 by Dr. Himsworth. He describes a disease of elevated glucose with excess insulin [10]. The disease is very commonly associated with abdominal obesity, elevated blood pressure, atherogenic dyslipidemia, insulin resistance manifested as glucose intolerance, and pro-inflammatory, and pro-thrombotic states. The cause of the disease is not elucidated. Entropy should be suspected. The greatest source of entropy is the virome followed by the microbiome. The changing diet of excess calories, carbohydrates, modern invention of agriculture; favors the microbiome as the strongest entropic energy in this disease. Glucose and carbohydrates are easy for bacteria to consume and process [11]. Taking this energy from the environment lowers the microbiome's entropy. It is to the bacteria's favor to elevate glucose in

Table 3. Criticism of current techniques.

1) There are no fundamental laws of biology used to model health and disease. Biology, lingering in observation, is not a science [8].

2) There is only one Cell. Subspecialty silos partition cardiovascular drugs, cancer therapies, and diabetes drugs failing to acknowledge that there is only one cell. Therefore, drugs in one discipline may have used in other disciplines that are undiscovered.

3) Biological system noise is dismissed. Carrier proteins that in themselves have no biologic activity can allow proteins to fold in a preferred manner permitting function, partially block a receptor, or the misfolded proteins lead to a serious disease [9].

4) Using surrogate risk factors for biological measured defects is inefficient and does not account for individual compensation. Biological biomarker measures should select patients for drug therapies to increase the efficiency of studies. Some biologic markers are pivotal representing a major shift in biologic balance identifying disease and treatment of disease.

5) Inflammation is a term explaining all chronic disease states. Inflammation can increase or decrease entropy. The state of the immune system that perpetuates these states is not measured. Knowledge to characterize immune system malfunction is necessary.

6) Drugs in normal subjects may not behave the same as in diseased states due to disease activation of genes that are not present in normal subjects.

7) The study of energetics in protein folding, molecular interactions, and influence of the electromagnetic environment on protein formation is in its infancy, complex, and poorly organized.

the host. If the bacteria make a protein that partially blocks the insulin receptor or attaches to insulin making it less likely to fit in to the receptor; glucose will become more abundant since the human cells are unable to process the glucose. This simple protein lowers the microbiome entropy and raises the human entropy. Finding the protein and neutralizing its effects represents a new therapy. Entropy supports more research in the microbiome to solve the disease state of diabetes II. Observational medicine is slowly getting to the same conclusion but painfully slow. Table 4 taken from "Should negative entropy be included in the fundamental laws of biology?" [2] demonstrates other diseases of entropy.

4. Roadmap to the Future

Biology must be quantified. Calculation of energy of every sequence of embryological development from two cells to an entire organism. The entropic energy for two cells to become one is 3.67×10^{-23} cal supplied by the carbohydrate in semen. The subsystems of DNA replication, gene activation, protein production must be quantified in all the possible outcomes. The energy requirement and noted discrepancies between entropy and the energy available from the environment are calculated. New drugs will be found to explain the discrepancies. Once the energies and processes are described the origin of life could be modeled.

Unfortunately, the number of permutations and calculations to describe every step in the development of a human would take to the end of our sun. The good news is once a calculation is performed it does not have to be performed again.

Table 4. Diseases of entropy and interventions.

Disease/Affliction	Component of life	Defect Promoting Increased Entropy	Entropy Intervention
Age	Chromosomes	Failure to copy DNA correctly	Increase Telomere length
Age	Cells	Decreased stem cells	Increase stem cells
Age/red cell aplasia	Types of Cells	Lack of red cell precursor	Replace Red Cell Precursor
Age/Hutchinson-Gilford's progeroid syndrome	Genes	mutation in LMNA	Replace Gene
Evolution	Base pairs	Point mutation	Depending on the environment this could be helpful or harmful in entropy
Alzheimer's Dementia	Protein Folding	Abnormally folded amyloid beta protein	Inhibit protein productionRefold miss-folded protein
Amyloidosis	Proteins, Protein Chains, Protein Folding	beta-pleated sheet conformation	Inhibit protein productionRefold miss-folded protein
Prion Disease "mad cow disease"	Protein Folding	Miss-folded protein of a normally produced protein	Inhibit protein productionRefold miss-folded protein
Sickle cell Anemia	Proteins, Protein Folding	Mutation Glu to Val distorts B-subunit	Replace Gene
Parkinson's Disease	Protein Folding	Non-functioning chaperone Protein	Infuse functioning chaperone protein
Anoxic Brain Injury	Cells	Apoptosis	Cooling protocols, a sink for excess entropy

Piecemeal calculations can give insight and useful information. The largest contributor to biologic entropy is the virus which is relatively small and can be potentially studied so that every step of its production can be sequenced, and energy of that step calculated. The virus is subject to mutations and these mutations could be predicted understanding the energetics of its development. Vaccines could be produced prior to the mutation so that endemics could be halted.

Information science and negative entropy is a way of quantifying biological systems making systems biology more predictable. Each pathway in systems biology has a probabilistic outcome based on all the possible interaction for the next step. An additional carrier protein may or not be present to assure the outcome if the desired outcome requires more energy. Quantification can be added to the multiple arrows and diagrams required in system analysis. Quantification can suggest a missing element that could serve as a drug target.

5. New Physics from Biology

Erwin Schrödinger was interested in life to discover new physics. He was fascinated how life preserved order at least for a fraction of time. The universe appears to have order for a greater fraction of time, and the energy to preserve this order is under intense investigation. Physicists have invented dark matter and dark energy to explain the orderly motion of stars in galaxies. Erwin Schrödinger, a physicist gave insight to biologist helping them understand a property of life negative entropy. As a cardiologist I would like to imagine how the Universe maintains order. Perhaps, space time has a thickness, a Planck length where light can travel as wave and emerge as a particle. Particles can emerge from either side of space time and be entangled over space while still being connected in space time. Cosmologists should look within Space time to find the energy that explains the ordering of galaxies. Imagine writing relativistic equation including space time thickness. Singularities are no longer a mathematical construct just a very large number.

6. Conclusion

Life is complicated. Biology lacks fundamental principles not allowing predictive models. Erwin Schrödinger pondered upon this weakness of biology and proposed negative entropy as a means of quantifying biologic processes. He did not provide the solution only the path forward. The solution is not trivial and requires energetics to every protein twist, bonds between receptors and proteins. The processes of life from intercellular protein production to cell differentiation, assembly, and repair needs catalogued. Successful sequencing of DNA over the last 50 years pales to the task of quantifying life. Drugs will still be discovered serendipitously, but energetics can be applied to specific disease processes such as amyloid related dementia, a disease of protein mal formation. Processes lowering entropy can extend life and reduce disease burden. Entropic forces point to the microbiome as an important predictor of health and disease. Age

represents a failure to maintain low entropy. Determining the failure to lower entropy as we age will be new drug targets. The concept of negative entropy was not well received in the lectures by Erwin Schrödinger; but, as he said "entropy, taken with the negative sign, is itself a measure of order." New physics and understanding the order of the Universe will arise from application of the second law of thermodynamics statistical entropy.

Conflicts of Interest

The author declares no conflicts of interest regarding the publication of this paper.

References

[1] Erwin, S. (1944) What Is Life?: The Physical Aspect of the Living Cell. Based on Lectures Delivered under the Auspices of the Dublin Institute for Advanced Studies at Trinity College, Dublin, in February 1943. Chapter 6 Order, Disorder and Entropy.

[2] Houck, P.D. (2014) *OA Biology*, **2**, 7.

[3] Houck, P.D. (2014) *JCVD*, **10**, 1-8.

[4] Ben-Naim, A. (2020) *Entropy*, **22**, 430.
https://doi.org/10.3390/e22040430

[5] Wouters, O.J., McKee, M. and Luyten, J. (2020) *JAMA*, **323**, 844-853.
https://doi.org/10.1001/jama.2020.1166

[6] Ridker, P., Danielson, E., Fonseca, F., *et al.* (2009) *The Lancet*, **373**, 1175-1182.
https://doi.org/10.1016/S0140-6736(09)60447-5

[7] Vasa, M., Fichtlscherer, S., Adler, K., *et al.* (2001) *Circulation*, **103**, 2885-2890.
https://doi.org/10.1161/hc2401.092816

[8] Houck, P.D. (2015) *Medical Hypotheses*, **85**, 266-271.
https://doi.org/10.1016/j.mehy.2015.05.011

[9] Argyrou, A. (2020) The Misfolding of Proteins. In: Vlamos, P., Ed., *GeNeDis* 2018, Advances in Experimental Medicine and Biology, Vol. 1195, Springer, Cham, 249-254.
https://doi.org/10.1007/978-3-030-32633-3_33

[10] Himsworth, H.P. (1936) *Lancet*, **I**, 127-130.
https://doi.org/10.1016/S0140-6736(01)36134-2

[11] Houck, P.D. and de Oliveira, J.M.F. (2013) *Medical Hypotheses*, **80**, 637-642.
https://doi.org/10.1016/j.mehy.2012.11.019

Space-Time Curvature Mode Quanta

Philipp Kornreich[1,2]

[1]1090 Wien, Austria
[2]King of Prussia, PA, USA
Email: pkornrei@syr.edu

Abstract

Einstein theorized that Gravity is not a force derived from a potential that acts across a distance. It is a distortion of space and time in which we live by masses and energy. Consistent with Einstein's theory, a model of space-time curvature modes and associated curvature quanta in slightly warped space-time generated by a light Photon is derived. Both a Schrödinger and a Second Quantized representation of the space-time curvature mode quanta are calculated and are fourth rank tensors. The eigenvalues of these equations are radii of curvature, not energy. The Eigenfunctions are linear functions of the components of the tensor that describes the curvature of space-time.

Keywords

Photons, Phonons, Gravity, General Relativity, Space-Time, Radius of Curvature, Tensor

1. Introduction and Summary

Consistent with Einstein's [1] description of the effect of gravity being a distortion of space and time, a model of **space-time curvature modes** generated by a light Photon is derived. The space-time curvature modes are derived from Einstein's Field Equation in the limit of slightly warped space-time. A Quantum Mechanical model of the space-time modes is obtained. Both a Schrödinger and a Second Quantized representation of the space-time mode quanta are derived. The eigenvalues of these equations are radii of curvature, not energy. The Eigenfunctions are linear functions of the components of the tensor that describes the curvature of space-time. Since light does not interact to first order with isotropic Minkowski space, an Earth-like mass is used to warp space-time and facilitate the interaction of the light wave and the space-time curvature modes. Flat Minkowski space-time does not have modes or quanta. Only curved space-time

has modes and mode quanta that can interact.

The space-time curvature modes called gravity Phonons [2] are different than the Electromagnetic Field modes which also have quanta called Photons. The Electromagnetic Field modes exist in space-time. The space-time curvature modes are modes of the curvature of space-time itself. The space-time curvature modes are modes of a description of the vacuum. This derivation is only valid for slightly warped space-time. It is not valid in the vicinity of Black Holes, Neutron stars, or similar objects. Space-time in most of the Universe is only slightly curved.

The reason we don't feel or hear the space-time curvature modes is that the curvature is very slight. Even the Sun with its huge mass produces only a slight curvature in space-time. If a sphere is fitted to the space-time curvature produced by the Sun, it would need a radius equal to the distance light travels in 5 days and 3.5 hours. The radius of this sphere is the **radius of curvature** that characterizes the modes.

Einstein [1] theorized in 1915 that Gravity is not a force derived from a potential that acts across a distance. The effect of gravity is a distortion of space and time by masses and energy. For example, one mass moves towards another mass because it travels through space and time that is warped to make the masses travel towards each other. This has been verified by astronomical observations and experiments. Einstein also postulated the existence of wave-like space-time modes. This too has been verified by the Laser Interferometer Gravity-Wave Observatory—LIGO [3] experiment.

In this paper, equations derived from the General Relativity Theory (GRT) and verified by astronomical observations or experiments are employed at every step of the calculations.

Because this space-time curvature mode model is only valid for slightly warped space-time, it is only scale-invariant within a limited range of space-time curvature amplitudes.

The space-time curvature mode quanta are fourth rank tensors, and massless Bosons, that propagate with the speed of light. Light Photons are vector components derived from the Maxwell Electromagnetic Theory and have a spin angular momentum of 1. The space-time curvature modes are fourth rank tensors derived from the GRT and have spin angular wave vector of 4. The example of gravity Phonons calculated here has a very large radius of curvature of $R_C = 5769.812126$ Light Years. Gravity is a very weak force. Space-time curvature modes affect the momentum and energy of objects propagating through it, and the momentum and energy of the objects affect the curvature of space-time.

Note, that this is only a mathematical model that is valid for a limited range of Nature, and in this region of Nature it is only an approximation.

The gravity Phonons, like other wave quanta, can form entangled states [4] [5]. *Since gravity Phonons have radii of curvature with Astronomical dimensions and few losses,* **entangled gravity Phonon states can link structures over in-**

terstellar distances.

The eccentric motion of moons and planets also produces space-time wave modes. For example, the space-time wave mode generated by the Moon's eccentric orbit has a period of 27 days 7 hours, 12 minutes, and a wavelength of $7.071264665 \times 10^{14}$ m or 27.3 Light Days. Because the wavelength is much larger than the 2.667 light seconds size of the system, the motion of the Lunar system can be modeled by Newtonian Classical Mechanics.

In the late part of the 19'th century it was thought that like sound, which is a mode of the atoms in a material, electromagnetism is a mode of a substance that was named Luminiferous Aether. The Michelson-Morley experiment [6] and Einstein's calculation showed that there is no Luminiferous Aether of which electromagnetic effects are modes. Electromagnetic modes can propagate through space-time. But the electromagnetic waves are not modes of space-time.

The electromagnetic wave discussed in this paper is affected by the curvature of space-time, and the electromagnetic wave affects the curvature of space-time. If the Michelson-Morley experiment could have been performed at a higher accuracy, the interaction of the light and space-time would have been discovered. Light propagates differently in different directions due to the Earth not being an ideal sphere, and also due to the gravity effects of the Moon, the Sun, Jupiter, and the effect of other solar system objects. These effects are described by the GRT.

Sakharov [7] and Puthoff [8] derive the effect of gravity from quantum fluctuations of the vacuum. Boccaletti [9] calculated the effect of a light wave on the curvature of space-time subject to a steady electromagnetic field.

Bryce C. DeWitt [10] [11] [12] attempts to derive a Quantum theory of gravity from the GRT starting with a General Relativistic Lagrangian. His derivation is intended to be applicable to all gravity values. He wrote 3 papers but he was unable to produce a Quantum Mechanical model of gravity in a form that has useful applications.

There are a large number of publications describing unsuccessful attempts to develop models of Quantized Gravity called Gravitons [6] [7] [8] [10] [11] [12]. A number of these models use Maxwell's Equations modified by gravitational Potentials [10]. Others use Lagrangeans of Metric tensor components. This is similar to Einstein's equation of motion derived by a variational method. These run into difficulty with Gauge Normalization resulting in terms that go to infinity.

Professor Wytler C. dos Santos [13] derives the effect of gravity on electromagnetic fields expressed by the Einstein-Maxwell equation and the Rainich condition. Using the Electromagnetic Stress tensor he derives the Ricci tensor of Einstein's Field Equation. He calculates the effect of Maxwell's equation on the Riemann Curvature tensor. This derivation is in flat Minkowski space. Therefore, Professor dos Santos result is to second order in the Electromagnetic Field tensor components. The derivation in this paper uses a space-time that has a cur-

vature due to a mass, and thus the effects calculated are to first order in the Electromagnetic Field tensor components.

Professor Rovelli [14] in his "Zakopane Lectures on Loop Gravity" describes Loop-Quantum-Gravity. He postulates Curvature Operators. These operators are similar to the operators used in this paper. The Curvature operators in this paper are derived from the Riemann Christoffel tensor and show that such operators are only valid for slight space-time curvatures. The Loop-Quantum-Gravity models space as a lattice of triangles with Plank length dimensions. Half integer spins are associated with the triangle edges. "Loop Quantum Gravity" [15] is also based on this discrete space-time model. It results in Gravity Quanta that can couple to elementary particles. This implies a very large amplitude of Gravity Quanta which is inconsistent with a weak gravity force.

The Quantum Mechanical model of Gravity derived in this paper is based on the GRT which has been verified by observations and experiments rather than use postulated quantities.

2. Einstein's Field Equation for Slightly Curved Space-Time

Note: Numbers such as {8} in curly brackets denote equation numbers in the literature.

To describe the effect of the energy of the light wave on the curvature of space-time, Einstein's Field Equation is used. In Einstein's Field Equation, the Einstein tensor describes the curvature of space-time, and the Stress tensor describes the effect of the light wave energy density. The derivation is for slightly warped space-time only. The lightwave does not interact with flat isotropic Minkowski space to first order in the coordinate components.

The Metric tensor in curved space-time describes the transformation from one coordinate system to another coordinate system that is located at an infinitesimal distance away. The two coordinate systems are tilted with respect to each other. Thus, the Metric tensor describes the local tilt of the two coordinate systems. The components of the Metric tensor describe the effect of mass and energy. This is the curvature of space-time. Einstein called the Metric Tensor the Fundamental Tensor.

The components of the Metric tensor for isotropic Minkowski space are only constant for rectangular coordinates. For curvilinear coordinates, for the same isotropic space-time, the Metric tensor has components that are functions of the coordinates. Therefore, this derivation is restricted to rectangular coordinates. After the calculation, the result can be transformed into any arbitrary coordinates. The metric tensor has the following properties:

$$\text{a)} \ g^{\alpha\tau}g_{\tau\beta} = \delta^{\alpha}_{\beta} \qquad \text{b)} \ g^{\alpha\tau}g_{\tau\alpha} = \delta^{\alpha}_{\alpha} \quad \text{therefore} \quad \text{c)} \ g^{\alpha\tau}g_{\tau\alpha} = 4 \qquad (1)$$

The Metric tensor components $g_{\mu\nu}$ for the case of slightly warped space-time can be approximated as follows:

$$\text{a)} \ g_{\mu\nu} \approx \eta_{\mu\nu} + h_{\mu\nu} \quad \text{where} \quad \text{b)} \ \partial_{\alpha}\eta_{\mu\nu} = 0 \quad \text{c)} \ \left(\partial_{\alpha}h_{\mu\nu}\right)\left(\partial_{\beta}h_{\mu\nu}\right) \ll \partial_{\alpha}\partial_{\beta}h_{\mu\nu} \quad (2)$$

The tensor components $h_{\mu\nu}$ are small parameters. An Earth-like mass is used to warp space-time slightly to facilitate the Photon space-time curvature mode interaction. The Metric tensor components depend on both the Earth-like mass and the energy of the light beam.

A four-dimensional Riemann space with a signature $- + + +$ is used. It consists of the three spatial dimensions and time. The time coordinate t is multiplied by the velocity of light c in free space so that this coordinate, too, has dimensions of space $x_0 = jct, x_1, x_2, x_3$. Greek subscripts $\mu = 0, 1, 2,$ and 3 denote four-dimensional coordinates and Latin subscripts $a = 1, 2,$ and 3 denote three-dimensional coordinates. The volume V_4 and area S_3 of a four-dimensional sphere is

$$\text{n Dimensions} \quad a)\ V_n\left(R_n\right) = \frac{\pi^{\frac{n}{2}}}{\Gamma\left(\frac{n}{2}+1\right)}R_n^n \quad\quad b)\ S_{n-1}\left(R_n\right) = \frac{dV_n\left(R_n\right)}{dR_n} \tag{3}$$

$$\text{4 Dimensions} \quad c)\ V_4\left(R_4\right) = \frac{\pi^2}{2}R_4^4 \quad\quad\quad d)\ S_3\left(R_4\right) = 2\pi^2 R_4^3$$

where $\Gamma\left(\frac{n}{2}+1\right)$ is the Gamma function of $\frac{n}{2}+1$. The "Surface" S_3 in four-dimensions has dimensions of volume in three-dimensional space. Here R_4 is the radius of the four-dimensional sphere which is not the same as the radius R of the three-dimensional sphere. The Schwarzschild ratio $\frac{r_{ss}}{R_\oplus}$ of the Earth-like mass is $1.390705726 \times 10^{-9}$. The ratio of the radius R_4 of a four-dimensional sphere to the radius R of the corresponding three-dimensional sphere is constant for all sizes of the sphere. Therefore, the Schwarzschild ratio is the same for the three or four-dimensional sphere.

For a mass M, modeled as a point mass, the radius r_{ss} is the distance from the center of the mass M to the point at which a test mass m has to have an escape velocity equal to the speed of light c. This distance is the Schwarzschild radius r_{ss}.

$$\frac{r_{ss}}{R_\oplus} = \frac{2M_\oplus G}{c^2 R_\oplus} \tag{4}$$

where $M_\oplus = 5.9724 \times 10^{24}\,\text{kg}$ is the Earth-like mass. $r_{ss} = 8.87071165\,\text{mm}$ is the Schwarzschild radius [16] and $R_\oplus = 6378137\,\text{m}$ is the radius of the Earth-like mass.

The g_{00} component of the Metric tensor can be approximated by the effect of the time dilation calculated by Einstein [1] in the chapter "*The Foundation of the GRT*" section 22 "*Behavior of Rods and Clocks in the Static Gravitational Field. Bending of Light Rays. Motion of the Perihelion of a Planetary Orbit.*" on page 160 using g_{00} from equation {70}. This equation for {g_{00}} is also the Schwarzschild metric [17] or Schwarzschild solution.

$$a)\ g_{00} \approx \frac{1}{\sqrt{1+\dfrac{r_{ss}}{R_4}}} \quad\quad b)\ 1+h_{00} \approx 1-\frac{r_{ss}}{2R_4} \tag{5}$$

where $\dfrac{r_{ss}}{R_4} = 1.390705726 \times 10^{-9}$ is the Schwarzschild ratio of the Earth-like mass. The distance vector with components x'_μ in the vicinity of the mass $M_\oplus$ is approximately equal to the product of the metric tensor with components $g_{\mu\nu}$ times the distance vector far from the mass with components x_ν.

$$a)\; x'_\mu = g_{\mu\nu}x_\nu \quad b)\; x'_\mu \approx \sqrt{1-\frac{r_{ss}}{R_4}}x_\mu \quad c)\; x'_\mu \approx \frac{r_{ss}}{R_4}x_\nu \quad d)\; R'_\oplus \approx \sqrt{1-\frac{r_{ss}}{R_4}}R_\oplus \qquad (6)$$

Einstein's Field equation [1] has the following form:

$$\frac{c^4}{8\pi G}G_{\mu\nu} + g_{\mu\nu}\Lambda \quad = \quad T_{\mu\nu} \qquad (7)$$

Curvature of space-time = Energy density

where $G_{\mu\nu}$ is a component of the Einstein tensor, $T_{\mu\nu}$ is a component of the Stress tensor and Λ is Einstein's Cosmological Constant. The cosmological constant Λ is neglected here. The components of the Einstein tensor $G_{\mu\nu}$ have dimensions of curvature $\dfrac{1}{\text{distance}^2}$.

The GRT has always given results in agreement with observations and experiments. Therefore the effect of the energy of the light wave on the curvature of space-time, predicted by the GRT must also be correct.

The Stress tensor has two parts. A part due to the energy density u_E of the light beam and a part due to the energy density u_{EM} of the interaction of the light beam and the mass.

The part of the Stress tensor that depends only on the energy density of the light beam is the Electromagnetic Stress tensor calculated in **Appendix A**. Without losing generality one can assume that the light electric field is aligned along the x_1 axis and it can be assumed to be a plane wave. As is shown in **Appendix A**, Equation (A6), the Electromagnetic Stress Tensor [18] in this case has only 4 non zero components $T_{00}(\text{Light})$, $T_{30}(\text{Light})$, $T_{03}(\text{Light})$, and $T_{33}(\text{Light})$ all equal, to within a plus or minus sign, to the Electromagnetic Energy density $\varepsilon_0 E_1^2$. The energy density u_E of the light beam is:

$$a)\; u_E = E_1^2\varepsilon_o \quad b)\; u_E = n\hbar\omega \quad c)\; T_{\mu\nu}(\text{Light}) = e_{\mu\nu}n\hbar\omega \qquad (8)$$

$n = 1.14527 \times 10^{13} \dfrac{\text{Photons}}{\text{m}^3}$ is the density of incident solar Photons at the Equator on top of the atmosphere, and $\omega = 3.756087441 \times 10^{15}$ radians per second is the frequency of the light beam at the peak of the Black Body radiation curve of the Sun. The Sun's temperature is 5778°K. The tensor components $e_{\mu\nu}$ from Equation (A5) have the following values $e_{00} = 1$, $e_{30} = -1$, $e_{03} = -1$, $e_{33} = 1$, and all other components of this tensor are equal to zero. This term does not change with the direction of the light beam, it is symmetric, and depends on even powers of the coordinate components only. The effect of the Earth-like mass $M_\oplus$ on the Light electromagnetic wave with a Photon density n and wave vector $\dfrac{\omega}{c}$ is to

deflect it. The relativistic energy density $\rho'c^2$ of the Earth-like mass is equal to the relativistic mass times the square of the velocity of light divided by the surface S_3 of a four-dimensional sphere. Using Equation (4) for $\dfrac{r_{ss}}{R_4}$ one obtains

$$\text{a) } \rho'c^2 = \frac{M_\oplus c^2}{S_3\sqrt{1-\dfrac{r_{ss}}{R_4}}} \qquad \text{b) } \rho'c^2 \approx \frac{M_\oplus c^2}{2\pi^2 R_4^3}\left(1+\frac{r_{ss}}{2R_4}+\cdots\right) \tag{9}$$

$$\text{c) } \rho'c^2 \approx \frac{M_\oplus c^2}{2\pi^2 R_4^3}+\frac{M_\oplus^2 G}{2\pi^2 R_4^4}+\cdots \qquad \text{where} \quad \text{d) } r_{ss} = \frac{2M_\oplus G}{c^2}$$

By using Equation (8b) and the second term on the right of Equation (9c) to form the interaction energy density u_{EM} of the light beam and the Earth-like mass:

$$\text{a) } u_{EM} = \sqrt{\frac{M_\oplus^2 G}{2\pi^2 R_4^4}n\hbar\omega} \qquad \text{b) } T_{\mu\nu} = e_{\mu\nu}\sqrt{\frac{M_\oplus^2 G}{2\pi^2 R_4^4}n\hbar\omega} \tag{10}$$

The energy density u_{EM} of the interaction of the light beam and the space-time curvature modes are not symmetric and can be a linear function of the coordinates. The much smaller energy density u_E of the light beam does not depend on the direction of the light beam. It is symmetric and depends to second-order on the coordinates. It has been neglected.

$$u_{EM} = 1616.138805\,\frac{\text{Joules}}{\text{m}^3} \qquad u_E = 4.536471695\times 10^{-6}\,\frac{\text{Joules}}{\text{m}^3}$$

The radius R_4 of the four-dimensional sphere is calculated from the radius $R_\oplus$ of the three-dimensional sphere by setting the S_3 equal to the three-dimensional volume of the sphere. Substituting Equation (10b) into Einstein's Field Equation, Equation (7).

$$\frac{c^4}{8\pi G}G_{\mu\nu} = e_{\mu\nu}\sqrt{\frac{M_\oplus^2 G}{2\pi^2 R_4^4}n\hbar\omega} \tag{11}$$

The Einstein Tensor with components $G_{\mu\nu}$ is a function of the Ricci tensor with components $R_{\mu\nu}$ and the scalar curvature $R_{\alpha\alpha}$.

$$G_{\mu\nu} = R_{\mu\nu} - \frac{1}{2}R_{\alpha\alpha}g_{\mu\nu} \tag{12}$$

The Ricci tensor with components $R_{\mu\nu}$ is equal to the contraction over the indices ρ and $\tau = \rho$ of the Riemann-Christoffel tensor with components $B^\rho_{\mu\nu\tau}$. The Riemann-Christoffel tensor with components $B^\rho_{\mu\nu\tau}$ describes the curvature of space-time. It describes the transport $B^\rho_{\mu\nu\tau}V_\rho$ of a covariant vector with components V_ρ around an infinitesimal size volume in curved space-time. The difference of the vector V when transported clockwise and counter-clockwise back to the same point is a measure of the curvature of space-time. Therefore, the Riemann-Christoffel tensor is equal to the difference between two similar tensors $A^\rho_{\mu\nu\tau}$ and $A^\rho_{\mu\tau\nu}$ shown in reference [1] in section 12 "The Riemann-Christoffel Tensor", equation {42} and the preceding discussion. The route of the vector can

be modeled by a path with four turning points. The index μ is the number of each turning point. At each turning point μ, a rotation matrix associated with a clockwise path has indices ντ, and the rotation matrices associated with the counter-clockwise path have indices τν.

The first Riemann-Christoffel tensor contravariant index describes the index of the components ρ of the vector V. The second Riemann-Christoffel tensor covariant index describes the turning point number μ. The row and column numbers ν and τ of the rotation matrices at the turning points provide another two covariant Riemann-Christoffel tensor indices. Thus, the Riemann-Christoffel tensor $B^\rho_{\mu\nu\tau}$ is a fourth-rank tensor with 4 indices ρ, μ, ν and τ. In a flat Minkowski space, the vector V has the same form after being transported around the infinitesimal volume clockwise or counter-clockwise and thus, the Riemann-Christoffel tensor is equal to zero.

The Riemann-Christoffel tensor is also equal to the commutation relation of two covariant derivatives [1]. In flat space, the covariant derivatives reduce to ordinary derivatives that commute. Thus, in flat Minkowski space, the commutation relation of two derivatives is equal to zero, and therefore, the Riemann-Christoffel tensor is equal to zero.

This description has too much unnecessary data to just describe the curvature of the space-time. Certainly, the initial direction of the vector V with component indices ρ is irrelevant. It is, also, sufficient to describe the new direction acquired by the vector V at each turning point by a vector with index ν or τ, rather than describing the turning process by a matrix with indices ν and τ. This leaves the tensor describing the curvature of space-time with just two indices, μ and ν. Thus, the Riemann-Christoffel tensor describing the curvature of space-time can be reduced to a second-rank tensor, the Ricci tensor with indices μ and ν. The conversion of the fourth-rank Riemann-Christoffel tensor to the second-rank Ricci tensor, with components $R_{\mu\nu}$ can be accomplished by taking the inner product of the vector V with components V_ρ and a vector with components that have indices equal to the row numbers τ of the matrices at the turning points. A vector with components with indices equal to the column numbers ν of the matrices at the turning points can also be used. Thus, the Riemann-Christoffel tensor is contracted over the two indices ρ and τ to obtain the Ricci tensor $R_{\mu\nu}$.

$$R_{\mu\nu} = B^\rho_{\mu\nu\rho} \qquad (13)$$

The Riemann-Christoffel tensor was derived in Reference [1], page 141 equation {43}:

a) $B^\rho_{\mu\nu\tau} = -\partial_\tau \Gamma^\rho_{\mu\nu} + \partial_\nu \Gamma^\rho_{\mu\tau} - \Gamma^\alpha_{\mu\nu}\Gamma^\rho_{\alpha\tau} + \Gamma^\alpha_{\mu\tau}\Gamma^\rho_{\alpha\nu}$

b) $B^\rho_{\mu\nu\tau} \approx -\partial_\tau \Gamma^\rho_{\mu\nu} + \partial_\nu \Gamma^\rho_{\mu\tau}$ where $\partial_\alpha\partial_\beta h^{\alpha\beta} \gg \left(\partial_\mu h^{\alpha\beta}\right)\left(\partial_\alpha h^{\mu\beta}\right)$ (14)

c) $R_{\mu\nu} \approx -\partial_\rho \Gamma^\rho_{\mu\nu} + \partial_\nu \Gamma^\rho_{\mu\rho}$

The Christoffel symbol $\Gamma^\rho_{\mu\nu}$ is a function of the derivatives of the Metric tensor components. The Metric tensor components are of the order of the Schwarzschild

ratio $\frac{r_{ss}}{R} = 1.3907 \times 10^{-9}$. Therefore, *the last two terms of* Equation (14a) *consisting of products of Christoffel symbols are of the order of* 1.934 × 10⁻¹⁸, *and thus can be neglected which simplifies the calculation*. The Christoffel symbols $\Gamma^{\rho}_{\mu\nu}$ are obtained from reference [1] Einstein's Equation of Motion, equation {20d} and equations {21} and {23} on page 182, given here by:

$$a)\ \Gamma^{\rho}_{\mu\nu} = -\frac{1}{2}g^{\rho\alpha}\left[\partial_{\nu}g_{\mu\alpha} + \partial_{\mu}g_{\nu\alpha} - \partial_{\alpha}g_{\mu\nu}\right]$$

$$b)\ \Gamma^{\rho}_{\mu\nu} \approx -\frac{1}{2}\eta^{\rho\alpha}\left[\partial_{\nu}h_{\mu\alpha} + \partial_{\mu}h_{\nu\alpha} - \partial_{\alpha}h_{\mu\nu}\right]$$

(15)

where $\eta^{\rho\alpha}$ is a Minkowski Metric tensor component for a Riemann space with a signature − + + +. Note from Equations (15) that the Christoffel symbol components are functions of the derivatives of the Metric tensor components. The Metric tensor components $h_{\mu\nu}$ shown in Equations (1) and (2) are very small. For slightly warped space-time the Metric tensor components $g_{\mu\nu}$ of Equation (2) can be approximated by the Minkowski tensor components $\eta_{\mu\nu}$. Substituting Equation (15b) into Equation (14c)

$$R_{\mu\nu} \approx \frac{1}{2}\eta^{\rho\alpha}\left(\partial_{\rho}\partial_{\mu}h_{\nu\alpha} - \partial_{\rho}\partial_{\alpha}h_{\mu\nu} - \partial_{\nu}\partial_{\mu}h_{\rho\alpha} + \partial_{\rho}\partial_{\alpha}h_{\mu\rho}\right)$$

(16)

The trace of the Ricci tensor can be calculated from Equation (16)

$$\frac{1}{2}R_{\gamma\gamma} \approx \frac{1}{4}\eta^{\rho\alpha}\left[\partial_{\rho}\partial_{\gamma}h_{\gamma\alpha} - \partial_{\rho}\partial_{\alpha}h_{\gamma\gamma} - \partial_{\gamma}\partial_{\gamma}h_{\rho\alpha} + \partial_{\gamma}\partial_{\alpha}h_{\gamma\rho}\right]$$

(17)

Substituting Equation (16) and Equation (17) into Equation (12).

$$G_{\mu\nu} = \frac{1}{2}\eta^{\rho\alpha}\left(\partial_{\rho}\partial_{\mu}h_{\mu\alpha} - \partial_{\rho}\partial_{\alpha}h_{\mu\nu} - \partial_{\nu}\partial_{\mu}h_{\rho\alpha} + \partial_{\nu}\partial_{\alpha}h_{\mu\rho}\right)$$
$$-\frac{1}{4}\eta^{\mu\nu}\eta^{\rho\alpha}\left(\partial_{\rho}\partial_{\beta}h_{\beta\alpha} - \partial_{\rho}\partial_{\alpha}h_{\beta\beta} - \partial_{\beta}\partial_{\beta}h_{\rho\alpha} + \partial_{\beta}\partial_{\alpha}h_{\beta\rho}\right)$$

(18)

Equation (18) *for Einstein's tensor can be written in terms of a fourth-rank tensor with components* $s^{\alpha\beta}_{\mu\nu}$.

$$\partial_{\alpha}\partial_{\beta}s^{\alpha\beta}_{\mu\nu} = G_{\mu\nu}$$

(19)

Since the gradient vector with components ∂_{α} is covariant and the inner product $\partial_{\alpha}\partial_{\beta}s^{\alpha\beta}_{\mu\nu}$ contracts to $G_{\mu\nu}$, the tensor with components $s^{\alpha\beta}_{\mu\nu}$ must be partially contravariant. The tensor components $s^{\alpha\beta}_{\mu\nu} = s^{\alpha\beta}_{\mu\nu}\left(h_{\rho\tau}\right)$ are linear functions of the Metric tensor components. For example, the G_{33} component of the Einstein tensor derived from Equation (18) is:

$$G_{33} \approx \frac{1}{2}\begin{bmatrix}\partial_0 & \partial_1 & \partial_2 & \partial_3\end{bmatrix}\begin{bmatrix}h_{33} & 0 & 0 & -h_{03} \\ 0 & h_{22} & -h_{21} & 0 \\ 0 & -h_{12} & h_{11} & 0 \\ -h_{30} & 0 & 0 & h_{00}\end{bmatrix}\begin{bmatrix}\partial_0 \\ \partial_1 \\ \partial_2 \\ \partial_3\end{bmatrix}$$

(20)

After multiplying out Equation (20) all derivatives have to be moved to the left like in Equation (19). The differentiation operators ∂_{μ} operate on the Metric tensor components that describe the effect of the Earth-like mass and the light

electromagnetic field. Substituting Equation (10b) and Equation (19) into Equation (7) to obtain for Einstein's Field Equation in the limit of slightly warped space-time.

$$a) \quad \frac{c^4}{8\pi G}\left(\partial_\alpha\partial_\beta s_{\mu\nu}^{\alpha\beta} + \partial_\alpha^{Earth}\partial_\beta^{Earth} s_{\mu\nu}^{\alpha\beta}\right) = e_{\mu\nu}\sqrt{\frac{M_\oplus^2 G}{2\pi^2 R_4^4}n\hbar\omega}$$

$$b) \quad \frac{c^4}{8\pi G}\left(\partial_\alpha\partial_\beta s_{\mu\nu}^{\alpha\beta} + K_\alpha K_\beta s_{\mu\nu}^{\alpha\beta}\right) = e_{\mu\nu}\sqrt{\frac{M_\oplus^2 G}{2\pi^2 R_4^4}n\hbar\omega}$$

(21)

Equation (21) has dimensions of energy density. Equation (21b) is in the form of a Hamiltonian. The canonical variables are the momentum components $-j\partial_\alpha$ and the curvature vector components K_α. The first term $\partial_\alpha\partial_\beta s_{\mu\nu}^{\alpha\beta}$ of Equation (21a) describes the part associated with the effect of the interaction energy density of the light beam and the Earth-like mass.

The terms $\partial_\alpha^{Earth}\partial_\beta^{Earth} s_{\mu\nu}^{\alpha\beta} = K_\alpha K_\beta s_{\mu\nu}^{\alpha\beta}$ appearing in Equation (21a) and Equation (21b) describe the part associated with the curvature of space-time due to the Earth-like mass. This is similar to equation {7} in "Physical and Geometric Interpretation of the Ricci Tensor and Scalar Curvature" by L. C. Loveridge [19]. The tensor with components $s_{\mu\nu}^{\alpha\beta}$ is dimensionless.

3. Schrödinger Formulation of Space-Time Curvature Modes

Equation (21b), derived from the GRT, bears a resemblance to a tensor form of Schrödinger's equation. Here $-j\partial_\alpha$ is a component of a momentum vector operator and K_α is a curvature vector potential operator. K_α stands for Krümmung, curvature in German. *By multiplying* Equation (21b) *by* $\frac{8\pi G}{c^4}$ *one obtains a tensor Schrödinger like equation for curvature instead of energy.* The equation instead of having an energy Eigenvalue, as the conventional Schrödinger equation, this equation has a curvature Eigenvalue $\frac{1}{R_{EM}^2}$.

$$\partial_\alpha\partial_\beta\psi_{\mu\nu}^{\alpha\beta} + V_{\alpha\beta}\psi_{\mu\nu}^{\alpha\beta} = \frac{\eta_{\alpha\beta}}{R_{EM}^2}\psi_{\mu\nu}^{\alpha\beta}$$

(22)

$\eta_{\alpha\beta}$ are components of the Minkowski Metric tensor and $\psi_{\mu\nu}^{\alpha\beta}\left(h_{\lambda\rho}\right)$ is a dimensionless tensor wave function of a space-time curvature mode. The tensor wave functions $\psi_{\mu\nu}^{\alpha\beta}\left(h_{\lambda\rho}\right)$ are linear functions of the components of the Metric tensor components $h_{\lambda\rho}$ that describe the curvature of space-time due to the light beam and Earth-like mass. The eigenvalues of these equations are radii of curvature, not energy.

$$a) \quad \psi_{(\mu\nu)}^{\alpha\beta} = ws_{\mu\nu}^{\alpha\beta} \qquad b) \quad 1 = \frac{1}{V_{4\text{-Volume}}}\int_{4\text{-Volume}}\psi_{\alpha\beta(\mu\nu)}^*\psi_{(\mu\nu)}^{\alpha\beta}d^4x$$

(23)

No summation over subscripts in brackets is not implied. This derivation of a Quantum Mechanical formulation is only valid for slightly curved space-time. Since this is a straightforward derivation from Einstein's Field Equation no

Gauge requirements are necessary. From Equation (21) the square of the reciprocal of the radius of curvature R_{EM} is:

$$\frac{1}{R_{EM}^2} = e_{\mu\nu} \frac{8\pi G}{c^4} \sqrt{\frac{M_\oplus^2 G}{2\pi^2 R_4^4} n\hbar\omega} \tag{24}$$

where $R_{EM} = 5.45866374 \times 10^{19}\,\text{m}$ or $R_{EM} = 5769.812126$ Light Years.

4. Formulation Second Quantized Form of Space-Time Curvature Modes

Dividing Equation (21b) by $\sqrt{\dfrac{M_\oplus^2 G}{2\pi^2 R_4^4} n\hbar\omega}$, using Equation (24) in the resulting equation and expanding the ensuing equation.

$$e_{\mu\nu} = \frac{1}{2}\Big[\big(\boldsymbol{K}_\alpha + j\partial_\alpha\big)\big(\boldsymbol{K}_\beta - j\partial_\beta\big)R_M^2 s_{\mu\nu}^{\alpha\beta} + \big(\boldsymbol{K}_\alpha - j\partial_\alpha\big)\big(\boldsymbol{K}_\beta + j\partial_\beta\big)R_M^2 s_{\mu\nu}^{\alpha\beta}\Big] \tag{25}$$

The $j\partial_\alpha$ and $\boldsymbol{K}_\alpha$ curvature operators don't commute.

$$-j\partial_\alpha \boldsymbol{K}_\beta R_{EM}^2 s_{\mu\nu}^{\alpha\beta} + j\boldsymbol{K}_\alpha \partial_\beta R_{EM}^2 s_{\mu\nu}^{\alpha\beta} = e_{\mu\nu} \tag{26}$$

Similar to the derivation of the quantization of the Electromagnetic Field by G. M. Wysin [20] in equations {43} and {44} the state raising and state lowering operators are defined.

$$\text{a) } \boldsymbol{b}_\alpha^\dagger \exp\big(-jq_a x_a\big) \equiv \frac{R_{ME}}{\sqrt{2}}\big(\boldsymbol{K}_\alpha - j\partial_\alpha\big)$$

$$\text{b) } \boldsymbol{b}_\alpha \exp\big(jq_a x_a\big) \equiv \frac{R_{ME}}{\sqrt{2}}\big(\boldsymbol{K}_\alpha + j\partial_\alpha\big) \tag{27}$$

The state raising and state lowering operators are dimensionless curvature operators. Here $\exp\big(-jq_\tau x_\tau\big)$ represents a forward traveling space-time wave mode and $\exp\big(jq_\tau x_\tau\big)$ represents a reverse traveling space-time wave mode. The **gravity Phonon** number state wave functions $|m_\lambda\rangle$ form a Hilbert space. The state raising vector component operators $\boldsymbol{b}_\alpha^\dagger$ and state lowering vector component operators $\boldsymbol{b}_\alpha$ are operators on the gravity Phonon Hilbert space.

$$\text{a) } \boldsymbol{b}_\alpha s_{\mu\nu}^{\alpha\beta} |m_\lambda\rangle = \hat{a}_\alpha s_{\mu\nu}^{\alpha\beta} \sqrt{m}\,|(m_\lambda - 1)\rangle$$

$$\text{b) } \boldsymbol{b}_\alpha s_{\mu\nu}^{\alpha\beta} |0_\lambda\rangle = 0 \tag{28}$$

$$\text{c) } \boldsymbol{b}_\alpha^\dagger s_{\mu\nu}^{\alpha\beta} |m_\lambda\rangle = \hat{a}_\alpha s_{\mu\nu}^{\alpha\beta} \sqrt{m+1}\,|(m_\lambda + 1)\rangle$$

$\hat{a}_\beta$ is a component of a unit vector in four dimensional space. The commutation relations of the $\boldsymbol{b}_\alpha$ and $\boldsymbol{b}_\beta^\dagger$ are:

$$\boldsymbol{b}_\beta \boldsymbol{b}_\alpha^\dagger - \boldsymbol{b}_\beta^\dagger \boldsymbol{b}_\alpha = e_{\mu\nu}$$

$$\text{where } \boldsymbol{b}_\beta \boldsymbol{b}_\alpha^\dagger = \boldsymbol{b}_\alpha^\dagger \boldsymbol{b}_\beta \quad \text{for } \alpha \neq \beta \tag{29}$$

Substituting Equation (27) into Equation (25) and dividing the result equation by R_{EM}^2.

$$C_{\mu\nu} = \frac{1}{2R_{EM}^2}\left(\boldsymbol{b}_\alpha \boldsymbol{b}_\beta^\dagger + \boldsymbol{b}_\alpha^\dagger \boldsymbol{b}_\beta\right) \tag{30}$$

where $C_{\mu\nu}$ is a curvature Hamiltonian tensor. Since the Metric tensor is symmetric, the tensor with components $s_{\mu\nu}^{\alpha\beta} = s_{\mu\nu}^{\beta\alpha}$ and $s_{\mu\nu}^{\alpha\beta} = s_{\nu\mu}^{\alpha\beta}$ is also symmetric. The tensor with components $s_{\mu\nu}^{\alpha\beta}$ is a linear function the components $h_{\alpha\beta} = h_{\beta\alpha}$ of the Metric tensor. Substituting Equation (29) into Equation (30) to obtain a curvature Hamiltonian tensor $C_{\mu\nu}$ in second quantized form for the gravity Phonons is:

$$C_{\mu\nu} = \frac{1}{R_{EM}^2}\left(\boldsymbol{b}_\alpha^\dagger \boldsymbol{b}_\beta s_{\mu\nu}^{\alpha\beta} + \frac{1}{2}e_{\mu\nu}\right) \tag{31}$$

The gravity Phonon ground state from Equation (31) is:

$$\text{a)} \quad \langle 0_\lambda | C_{\mu\nu} | 0_\lambda \rangle = \frac{1}{R_{EM}^2}\langle 0_\lambda | \left(\boldsymbol{b}_\alpha^\dagger \boldsymbol{b}_\beta s_{\mu\nu}^{\alpha\beta} + \frac{1}{2}e_{\mu\nu}\right) | 0_\lambda \rangle$$

$$\text{b)} \quad \langle 0_\lambda | C_{\mu\nu} | 0_\lambda \rangle = \frac{1}{2R_{EM}^2}e_{\mu\nu} \tag{32}$$

The tensor wave functions that describe the components of the Metric tensor can be calculated from the Curvature Hamiltonians of Equation (22) and Equation (31). The Metric tensor components describe the curvature of space-time due to the Earth-like mass and the energy of the light beam.

5. Conclusions

Both a Schrödinger and second quantized formulations of space-time curvature quanta are derived. The tensor wave functions that describe the components of the Metric tensor can be calculated from the Curvature Hamiltonians. The Metric tensor components describe the effect of the Earth-like mass and the energy of the light beam.

Einstein [1] theorized in 1915 that Gravity is not a force derived from a potential that acts across a distance. Gravity is a distortion of space and time by masses and energy. For example, a test mass moves towards another mass because it travels through space and time that is warped in such a way as to make the test mass travel towards the other mass. Einstein also postulated the existence of wave-like space-time modes. These too, have been verified by the LIGO experiment [3].

In this paper, equations derived from the GRT and verified by astronomical observations or experiments are employed at every step of the calculations.

A model of space-time curvature modes in slightly warped space-time generated by a light Photon is derived. Since an electromagnetic wave does not interact with isotropic space-time, to first order, an Earth-like mass is used to warp space-time to facilitate the Photon space-time curvature mode interaction. Each space-time curvature mode is a fourth-rank tensor and can have any number of curvature quanta, called gravity Phonons. Gravity Phonons have very large radii

of curvature in agreement with gravity being a weak force. The gravity Phonons are fourth-rank tensors, massless Bosons, have a spin angular wave vector of 4, and propagate with the speed of light. Energy and momentum are conserved because curved space-time causes a change in energy and momentum of the electromagnetic wave, and the energy of the electromagnetic wave causes a change of the curvature of space-time. Because this model is only valid for slightly warped space-time, it is only scale invariant within a limited range of space-time curvature amplitudes.

A large number of publications describing unsuccessful attempts to develop models of Quantized Gravity called Gravitons have been published. A number of these models use Post Newtonian Maxwell's Equations modified by gravitational potentials. These run into difficulty with Gauge Normalization resulting in terms that go to infinity. The other approach uses "Loop Quantum Gravity". It uses a lattice of triangles with Plank distance and Plank time sides to calculate the gravity energy quanta. This results in huge energy quanta amplitudes, not consistent with gravity being a very weak force. Therefore, in order to derive a Quantum Mechanical model of Gravity, one has to calculate space-time curvature mode quanta rather than use Gravitational potentials or Plank space and time to formulate gravity energy quanta.

Space-time is only slightly warped throughout most of the Universe except in the vicinity of Black Holes and Neutron Stars. For example, space-time at the surface of the sun has a radius of curvature of approximately 5.165 Light Days. Thus, gravity Phonons are a suitable Quantum Mechanical description of most of space-time in the Universe.

The space-time curvature quanta, like electromagnetic wave quanta, can form entangled states [4] [5]. Photons are vector quantities while gravity Phonons are fourth-rank tensors. Gravity Phonons have radii of curvature with Astronomical dimensions, therefore entangled gravity Phonon fourth-rank tensor states can link structures over interstellar distances.

Acknowledgements

Conflicts of Interest

The author declares no conflicts of interest regarding the publication of this paper.

References

[1] Einstein, A., Lorentz, H.A., Weyl, H. and Minkowski, H. (1952) The Principles of Relativity. Dover Publishing Co., Mineola.

[2] Kornreich, P. (2019) *Journal of Modern Physics*, **10**, 1674-1695.

[3] Abbott, B.P., *et al.* (2016) *Physical Review Letters*, **116**, Article ID: 061102.

[4] Liao, S.-K., Young, H.-L., Liu, C., Shentu, G.-L., Li, D.-D., Lin, J., Dai, H., Zhao, S.-Q., Li, B., Guan, J.-Y., Chen, W., Lin, Y.-H., Pan, G.-S., Pelc, J.S., Fejer, M.M., Liu, W.-Y., Yin, J., Ren, J.-G., Wang, X.-B., Zhang, Q., Peng, C.-Z. and Pan, J.-W. (2017) *Nature Photonics*, **11**, 509-513. https://doi.org/10.1038/nphoton.2017.116

[5] Krenn, M., Malik, M., Erhard, M. and Zeilinger, A. (2017) *Philosophical Transactions of the Royal Society A*, **375**, Article ID: 20150442. https://doi.org/10.1098/rsta.2015.0442

[6] Shankland, R.S. (1964) *American Journal of Physics*, **32**, 16-35. https://doi.org/10.1119/1.1970063

[7] Sakharov, A.D. (1967) *Doklady Akademii Nauk SSSR*, **177**, 70-71.

[8] Puthoff, H.E. (1989) *Physical Review A*, **39**, 2333-2342. https://doi.org/10.1103/PhysRevA.39.2333

[9] Boccaletti, D., De Sabbata, V., Fortini, P. and Gualdi, C. (1970) *Il Nuovo Cimento B* (1965-1970), **70**, 129-146. https://doi.org/10.1007/BF02710177

[10] DeWitt, B.C. (1967) *Physical Review*, **160**, 1113-1147. https://doi.org/10.1103/PhysRev.160.1113

[11] DeWitt, B.C. (1967) *Physical Review*, **162**, 1195-1239. https://doi.org/10.1103/PhysRev.162.1195

[12] DeWitt, B.C. (1967) *Physical Review*, **162**, 1239-1256. https://doi.org/10.1103/PhysRev.162.1239

[13] dos Santos, W.C. (2016) Introduction to Einstein-Maxwell Equations and Rainich Conditions.

[14] Rovelli, C. (2011) Zakopane Lectures on Loop Gravity. Centre de Physique Theorique Luminy, Case 907, F-13288, EU.

[15] Engle, J., Pereira, R. and Rovelli, C. (2007) *Physical Review Letters*, **99**, Article ID: 161301. https://doi.org/10.1103/PhysRevLett.99.161301

[16] Schwarzschild, K. (1916) Über das Gravitationsfeld eines Massenpunktes nach der Einsteinschen Theorie. Sitzungsberichte der Deutschen Akademie der Wissenschaften zu Berlin, Klasse fur Mathematik, Physik, und Technik, 189.

[17] Eddington, A.S. (1922) Mathematical Theory of Relativity. UP, Cambridge, 85-93.

[18] McDonald, K.T. (2013) Relativistic Harmonic Oscillator. Joseph Henry Laboratory, Princeton University, Princeton.

[19] Loveridge, C.L. (2004) Physical and Geometric Interpretation of the Ricci Tensor and Scalar Curvature.

[20] Wysin, G.M. (2011) Quantization of the Free Electromagnetic Field, Photons and Operators. Department of Physics, Kansas State University, Manhattan.

Appendix A

The electromagnetic field tensor described here is only valid for gravity-free space. Any additions to the electromagnetic field tenser due to the effect of the Earth-like mass are small parameters. When these small parts of the electromagnetic Tensor are multiplied by the small terms describing the space-time curvature one obtains very small second-order terms that can be neglected. The $T_{\mu\nu}$ component of the Electromagnetic Stress Tensor is given by:

$$\text{a) } T_{\mu\nu} = \frac{1}{\mu_o}\left[F_{\mu\alpha}\eta^{\alpha\beta}F_{\beta\nu} - \frac{1}{4}\eta_{\mu\nu}F^{\alpha\beta}F_{\alpha\beta}\right] \qquad \text{b) } \eta^{\mu\beta}F_{\beta\alpha}\eta^{\alpha\nu} = F^{\mu\nu} \qquad (A1)$$

The contravariant Electromagnetic field tensor with components $F^{\mu\nu}$ and the covariant Electromagnetic field tensor with components $F_{\mu\nu}$ are:

$$\text{a) } F^{\mu\rho} = \begin{bmatrix} 0 & -\dfrac{E_1}{c} & -\dfrac{E_2}{c} & -\dfrac{E_3}{c} \\ \dfrac{E_1}{c} & 0 & -B_3 & B_2 \\ \dfrac{E_2}{c} & B_3 & 0 & -B_1 \\ \dfrac{E_3}{c} & -B_2 & B_1 & 0 \end{bmatrix} \qquad \text{b) } F_{\rho\nu} = \begin{bmatrix} 0 & \dfrac{E_1}{c} & \dfrac{E_2}{c} & \dfrac{E_3}{c} \\ -\dfrac{E_1}{c} & 0 & -B_3 & B_2 \\ -\dfrac{E_2}{c} & B_3 & 0 & -B_1 \\ -\dfrac{E_3}{c} & -B_2 & B_1 & 0 \end{bmatrix} \qquad (A2)$$

and where $\eta^{\alpha\beta}$ is a component of the Minkowski Metric tensor for a Riemann space signature $+ - - -$.

$$\eta^{\alpha\beta} = \begin{bmatrix} 1 & 0 & 0 & 0 \\ 0 & -1 & 0 & 0 \\ 0 & 0 & -1 & 0 \\ 0 & 0 & 0 & -1 \end{bmatrix} \qquad (A3)$$

Substituting Equation (A2) and Equation (A3) into Equation (A1a)

$$T_{\mu\nu} = \frac{1}{\mu_o}\begin{bmatrix} \dfrac{E_1^2+E_2^2+E_3^2}{c^2} & -\dfrac{E_2B_3-E_3B_2}{c} & \dfrac{E_1B_3-E_3B_1}{c} & -\dfrac{E_1B_2-E_2B_1}{c} \\ -\dfrac{E_2B_3-E_3B_2}{2} & -\dfrac{E_1^2}{c^2}+B_3^2+B_2^2 & -\dfrac{E_1E_2}{c^2}-B_1B_2 & -\dfrac{E_1E_3}{c^2}-B_1B_3 \\ \dfrac{E_1B_3-E_3B_1}{c} & -\dfrac{E_1E_2}{c^2}-B_1B_2 & -\dfrac{E_2^2}{c^2}+B_3^2+B_1^2 & -\dfrac{E_2E_3}{c^2}-B_2B_3 \\ -\dfrac{E_1B_2-E_2B_1}{c} & -\dfrac{E_1E_3}{c^2}-B_1B_3 & -\dfrac{E_2E_3}{c^2}-B_2B_3 & -\dfrac{E_3^2}{c^2}+B_2^2+B_1^2 \end{bmatrix}$$

$$-\frac{1}{2}\left[\dfrac{E_1^2+E_2^2+E_3^2}{c^2} - B_1^2 - B_2^2 - B_3^2\right]\begin{bmatrix} 1 & 0 & 0 & 0 \\ 0 & -1 & 0 & 0 \\ 0 & 0 & -1 & 0 \\ 0 & 0 & 0 & -1 \end{bmatrix} \qquad (A4)$$

The Electric field and the Magnetic Flux density pseudo vectors of a Plane-wave propagating in the 3 direction are:

$$\text{a) } \mathbf{E} = \hat{\mathbf{a}}_1 E_1 \exp\left(j\omega t - j\frac{\omega x_3}{c}\right)$$

$$\text{b) } B_2 = \frac{E_1}{c} \tag{A5}$$

where the Electric field vector is in the 1 direction. Substituting Equation (A5) into Equation (A4)

$$\text{a) } T_{\mu\nu} = \varepsilon_o E_1^2 \begin{bmatrix} 1 & 0 & 0 & -1 \\ 0 & 0 & 0 & 0 \\ 0 & 0 & 0 & 0 \\ -1 & 0 & 0 & 1 \end{bmatrix} \qquad \text{b) } T_{\mu\nu} = \varepsilon_o E_1^2 e_{\mu\nu} \tag{A6}$$

where ε_0 is the dielectric constant of free isotropic space.

Standard Model Particles with Mass Treated as Spheres with Finite Radii

T. R. Mongan

Sausalito, CA, USA
Email: tmongan@gmail.com

Abstract

The particle physics Standard Model involves three charge 0 neutrinos, three charge e leptons, three charge $(2/3)e$ quarks, and three charge $-(1/3)e$ quarks, where e is electron charge. However, the Standard Model cannot explain why there are three generations of particles in each charge state and makes no predictions relating to quark and lepton masses. This analysis, treating Standard Model particles as spheres with radii 1/4 the particle Compton wavelength, explains three, and only three fermions are in each charge state and relates first generation quark masses to the electron mass.

Keywords

Standard Model Extension, Fermions Generations, Electron and First Generation Quark Masses

1. Introduction

The particle physics Standard Model cannot explain why there are three generations of quarks and lepton, and makes no predictions relating quark and lepton masses [1]. Furthermore, the Standard Model as presently constituted:

- must be modified to accommodate neutrino mass to account for oscillations between neutrino states as they propagate through space;
- treats fundamental particles as point particles with angular momentum $\hbar/2$, or $\hbar$. Angular momentum is usually defined for rotating objects extended in space and, regarding point particles with angular momentum, we might ask what is rotating.
- is formulated in quantum field theory, based on continuum mathematics with infinite degrees of freedom. However, the holographic principle [2], developed from quantum mechanics, general relativity, and black hole thermodynamics, indicates only a large, but finite, number [~10^{122}] of bits of in-

formation will ever be available to describe the observable universe, suggesting quantum field theory approximates an underlying discrete theory.

- involves point fermions with infinite energy density and physical theories involving infinities are logically complicated and debatable [3].

This analysis, treating Standard Model particles with mass as spheres with finite radii, addresses these important issues. In particular, it explains why three, and only three fermions are in each charge state and relates first generation quark masses to electron mass.

2. Standard Model Particle Masses

Masses m_i, in (MeV/c²), of charged Standard Model fermions [4] are in **Table 1**. Compton wavelengths are $l_i = \hbar c/m_i$, with $\hbar$ Planck's constant, $c = 3 \times 10^{10}$ cm/sec the speed of light, $\hbar c = 197.32$ MeV·F, $1\,\text{F} = 1 \times 10^{-13}$ cm, and charges in fractions of electron charge e.

Neutrino masses are estimated using known [5] quantities

$$a^2 = m_2^2 - m_1^2 = 7.37 \times 10^{-5} \left(\text{eV}\right)^2 \quad \text{and} \quad b^2 = m_3^2 - \frac{1}{2}\left(m_1^2 + m_2^2\right) = 2.50 \times 10^{-3} \left(\text{eV}\right)^2,$$

assuming neutrino mass sum Σ_ν equals upper bound [6] $\Sigma_\nu = 0.12$ eV. $\Sigma_\nu = \sqrt{m_2^2 - a^2} + m_2 + \sqrt{m_3^2 + b^2 - \left(a^2/2\right)}$, solved by successive approximation, results in $m_1 = 0.030$ eV, $m_2 = 0.031$ eV, and $m_3 = 0.059$ eV. Massive fundamental bosons are W$^\pm$ with mass 80.4 GeV/c², Z with mass 91.2 GeV/c², and Higgs with mass 125 GeV/c².

3. Treating Fundamental Fermions as Godel Systems

This analysis describes fundamental fermions as spherical shells with radius $\dfrac{l}{4}$ rotating around an axial core centered on the axis of rotation, with half of any fermion charge on the shell surface at each end of the axis of rotation. Fundamental fermions are then represented by Godel solutions of Einstein's equations, with average matter density ρ equal average fermion mass density, pressure

Table 1. Mass, wavelengths, and charge of charged standard model fermions.

Fermion	Mass m_i (MeV/c²)	Wavelength l_i (F)	Charge
Electron	0.511	386	e
Up quark	2.16	91.4	$2e/3$
Down quark	4.67	42.3	$-e/3$
Strange quark	93	2.12	$-e/3$
Muon	105.7	1.87	e
Charm quark	1270	0.155	$2e/3$
Tau lepton	1777	0.111	e
Bottom quark	4180	0.0472	$-e/3$
Top quark	173,000	0.00114	$2e/3$

$\left(\dfrac{1}{2}\right)\rho c^2$ from negative vacuum energy density $-\left(\dfrac{1}{2}\right)\rho c^2$, and effective internal gravitational constant G_f determined by $\omega = 2\sqrt{\pi G_f \rho}$. Charge is on the shell at the axis of rotation, so rotation does not cause radiative loss of energy by accelerated charge. Rotation axis orientation is unknown until z component of fermion angular momentum is measured, so fermion mass appears sinusoidally distributed on a disk of radius $(l/4)$ perpendicular to the line of sight.

4. Mass and Pressure Distribution in Fundamental Fermions Allow only Three Fermions in Each Charge State

Fundamental fermions, considered as spheres with size characterized by Compton wavelengths l, have three associated geometric quantities, volume $\sim l^3$, surface area $\sim l^2$, and diameter $\sim l$. Mass and pressure distribution in fundamental fermions identifies three wavelengths in each charge state as solutions of a cubic equation $Al^3 + Bl^2 + Cl = 0$. Describing mass and pressure distribution in terms of surface and linear elements requires minimum shell thickness and core radius near the Planck length $l_P = \sqrt{\dfrac{\hbar G}{c^3}}$. In each charge state $\dfrac{ne}{3}$, with $n = 0, 1, 2$ or 3, total fermion mass is the sum of mass equivalent of pressure, $\dfrac{m}{2}$, in the volume, mass equivalent of surface pressure $\dfrac{\pi}{4} S l^2$, and core mass Ll. So

$$\frac{4}{3}\pi\rho\left(\frac{l}{4}\right)^3 = \frac{4}{3}\pi\frac{\rho}{2}\left(\frac{l}{4}\right)^3 + 4\pi S\left(\frac{l}{4}\right)^2 + 2L\left(\frac{l}{2}\right).$$

Written as $Al^3 - Bl^2 - Cl = 0$, with $A = \dfrac{\pi}{96}\rho$, $B = \dfrac{\pi S}{4}$, and $C = 2L$, the discriminant $B^2C^2 - 4AC^3$ is positive regardless of the sign of B and the equation has three real roots corresponding to three fermion Compton wavelengths in a charge state. Nickalls [7] showed wavelengths $l = \dfrac{\hbar}{mc}$ satisfying the equation correspond to projections on the l axis, defined by an angle Θ, of vertices of an equilateral triangle. Θ is the angle between two lines starting at the center of the triangle, one parallel to the l axis and one extending to the rightmost vertex of the equilateral triangle. Nickall's parameters $l_N = -\dfrac{B}{3A} = -\dfrac{8S}{\rho}$, $\delta^2 = l_N^2 - \dfrac{C}{3A} = l_N^2 - \dfrac{64L}{\rho}$, $3l_N = l_1 + l_2 + l_3$, and

$$\delta^2 = \frac{(l_1 - l_N)^2}{4} + \frac{(l_2 - l_3)^2}{12},$$

identify roots $l_1 = l_N + 2\delta\cos\Theta$, $l_2 = l_N - \delta\left(\cos\Theta - \sqrt{3}\sin\Theta\right)$, and $l_3 = l_N - \delta\left(\cos\Theta + \sqrt{3}\sin\Theta\right)$ corresponding to fermion Compton wavelengths in a charge state. Three positive Compton wavelengths in each charge state require negative surface mass equivalent density $S = -\dfrac{\rho l_N}{8}$, $\delta^2 < l_N^2$ in each charge state, and positive mass per unit core length $L = \dfrac{\rho}{64}\left(l_N^2 - \delta^2\right)$. Negative S results from positive shell vacuum energy density

$\left(\dfrac{1}{2}\right)\rho c^2$, opposite the negative vacuum energy density $-\left(\dfrac{1}{2}\right)\rho c^2$ in the volume.

Then negative pressure equivalent mass inside the shell counters positive pressure equivalent mass in the volume. With no net pressure at the fermion surface, no force acts to increase or decrease fermion size, necessary for stable fundamental fermions as Godel solutions within our universe. Total fundamental fermion mass $= \dfrac{\pi}{48}\rho l^3$, surface mass $= -\dfrac{\pi}{32}\rho l_N l^2$, and core mass $= \dfrac{\pi}{64}l\left(l_N^2 - \delta^2\right)$, so surface mass multiple of total mass $= -\dfrac{3}{2}\dfrac{l_N}{l}$ and core mass multiple of total mass $= \dfrac{3}{4}\dfrac{\left(l_N^2 - \delta^2\right)}{l^2}$. Surface mass and core mass multiple increase with decreasing l because smaller fermion volume at smaller l decreases volume occupied by positive pressure from negative vacuum energy density of Godel solutions, while (surface mass)/(core mass) $= -\dfrac{2l_N l}{\left(l_N^2 - \delta^2\right)}$ increases with l.

5. Angular Velocity and Internal Gravitational Constant from Angular Momentum $\hbar/2$

Fermion spheres with radius $\dfrac{l}{4}$ and core radius r have moment of inertia $I = \dfrac{2}{5}\dfrac{m}{2}\left(\dfrac{l}{4}\right)^2 + \dfrac{2}{3}\dfrac{\pi}{4}Sl^2\left(\dfrac{l}{4}\right)^2 + \dfrac{1}{2}Llr^2$, with negligible last term because $r \ll l$. Angular velocity $\omega = \dfrac{\hbar}{2I} = \dfrac{8c}{\left(0.2l - l_N\right)}$ and tangential speed of points on the spherical shell equator as multiple of the speed of light $\dfrac{v_T}{c} = \dfrac{\omega l}{4c} = \dfrac{2l}{\left(0.2l - l_N\right)}$.

$\dfrac{v_T}{c} > 1$ for lowest mass fermions in each charge state, with closed time-like curves within those Godel solutions acceptable in fundamental fermions unchanging from creation to annihilation. From $\omega = 2\sqrt{\pi G_f \rho}$, $\dfrac{G_f}{G} = \dfrac{3l^4}{l_P^2\left(0.2l - l_N\right)^2}$.

6. Charge and Ground State Fundamental Fermion Mass

Ground state fundamental fermions constituents of atoms and molecules, differ from other generation fundamental fermions by having core mass less than total mass, tangential speeds $\dfrac{v_T}{c} > 1$, and larger internal gravitational constants. With fine structure constant $\dfrac{e^2}{\hbar c} = \dfrac{1}{137}$, electrostatic potential energy of fundamental fermions from repulsion between equal surface charges at the rotation axis is $\left(\dfrac{ne}{6}\right)^2 \bigg/ \left(\dfrac{l}{2}\right) = n^2\dfrac{me^2}{9\hbar c} = n^2\dfrac{m}{1233}$. If electrostatic potential energy is the same for

all charged ground state fundamental fermions and electron mass $m_e = 0.511\,\text{MeV}$, up quark mass $m_u = 4m_e = 2.04\,\text{MeV}$ and down quark mass $m_d = 9m_e = 4.60\,\text{MeV}$, well within quark mass error bars [4]. All charged fundamental fermion masses and charges can be related to election charge and mass.

7. Massive Standard Model Bosons as Spheres with Finite Radii

Treating massive Standard Model bosons as spheres with finite radii and an internal gravitational constant is simpler than for fundamental fermions. $W^{\pm}$ and Z bosons as uniform spheres with moment of inertia $I = \dfrac{2}{5}mr^2$ and radius $r = \dfrac{l}{4}$ have angular momentum $\hbar = I\omega$, so $\omega = \dfrac{40\hbar}{ml^2}$. For Godel systems with internal gravitational constant G_i, $\omega = 2\sqrt{\pi G_i \rho}$, resulting in $\dfrac{G_i}{G} = \dfrac{25}{3}\left(\dfrac{l}{l_P}\right)^2$, where Planck length $l_P = 1.62 \times 10^{-20}\,\text{F}$. Higgs bosons are treated as static Einstein solutions of general relativity with matter energy density ρc^2 and positive vacuum energy density $\dfrac{1}{2}\rho c^2$, opposite the negative vacuum energy density of Godel solutions. The Friedmann equation for the radius of those closed, homogeneous, isotropic systems with internal gravitational constant G_i is

$$\left(\frac{dR}{dt}\right)^2 - \frac{8\pi G_i}{3}\left[\rho c^2 \left(\frac{R_0}{R}\right)^3 + \frac{1}{2}\rho c^2\right]\left(\frac{R}{c}\right)^2 = -c^2, \text{ with } \left(\frac{dR}{dt}\right) = 0, \quad R = R_0 = \frac{l_H}{4},$$

and Higgs Compton wavelength l_H, resulting in $\dfrac{G_i}{G} = \dfrac{1}{12}\left(\dfrac{l_H}{l_P}\right)^2$.

8. Conclusions

Considering fundamental fermions as spherical shells rotating around an axial core, identified with Godel solutions to Einstein's equations, in each charge state,

- three fermion wavelengths specify volume, surface, and core mass as multiples of total fermion mass, and
- each fermion mass and wavelength specify angular velocity, tangential speed of points on the shell equator, and effective internal fermion gravitational constant.

Electrostatic potential energy in ground state fundamental fermions, from repulsion between equal surface charges at the rotation axis, is identical if up quark mass $= 4m_e = 2.04\,\left(\text{MeV}/\text{c}^2\right)$ and down quark mass $= 9m_e = 4.60\,\left(\text{MeV}/\text{c}^2\right)$.

Acknowledgements

Conflicts of Interest

The author declares no conflicts of interest regarding the publication of this paper.

References

[1]   https://home.cern/science/physics/standard-model

[2]   Bousso, R. (2002) *Reviews of Modern Physics*, **74**, 825. arXiv:hep-th/0203101
      https://doi.org/10.1103/RevModPhys.74.825

[3]   Hilbert, D. (1926) *Mathematische Annalen* (Berlin), **95**, 161.
      Ellis, G., Meissner, K. and Nicolai, H. (2018) *Nature Physics*, **14**, 770.
      https://doi.org/10.1038/s41567-018-0238-1

[4]   Zyla, P., *et al.*, (Particle Data Group) (2020) *Prog. Theor. Exp. Phys.*, **2020**, 083C01.

[5]   Capozzi, S., Lisi, E., Marrone, A., Montanino, D. and Palazzo, A. (2016) *Nuclear Physics B*, **908**, 1-14. [arXiv:1601.07777]
      https://doi.org/10.1016/j.nuclphysb.2016.02.016

[6]   Vagnozzi, S. (2109) Cosmological Searches for the Neutrino Mass Scale and Mass Ordering. Stockholm University PhD Thesis. [arXiv:1907.08010]

[7]   Nickalls, R. (1993) *The Mathematical Gazette*, **77**, 354-359.
      https://doi.org/10.2307/3619777

Manifestation of Color Confinement in the YY Model for Atomic Nuclei

—With Implication to Colors, Anti-Colors and Interactions

Hongguang Yang, Weidong Yang

Munich, Germany
Email: hgyang2013@gmail.com

Abstract

In this paper, a manifestation of the well-known color confinement from the QCD (quantum chromodynamics) in the newly developed YY model for the atomic nucleus is presented. There is a wonderful correspondence between the structural requirements from the YY model and some elementary properties of the color dynamics from QCD. The open questions in the YY model, namely the holding forces for triple nodes and for pairing space links, are exactly covered by the three-color compensation or by the paired color anti-color balance. We will see what colors and anti-colors do mean in the YY model, how up quarks and down quarks get assigned a color or anti-color. We will discover some relationships between gluon-based interactions as described in the standard model and pairing space links in the YY model.

Keywords

Quantum Chromodynamics QCD, Color Confinement, YY Model for Atomic Nucleus, Pairing Space Link PSL, Triple Space Link TSL, Colored up Quark, Colored Down Quark, Colored Hydrogen Nucleus, Colored Helium Nucleus, Colored Helium Isotope Nucleus, Color Confinement Aggregate State CCAS, Color-Balanced PSL, Tumbling of Colored PSLs

1. Introduction

The YY model (Ref. [1] and [2]) was first introduced several months ago. The most important subatomic particles (up quark, down quark, neutron and proton) and some complex nuclei (deuterium, tritium and helium) have been described in their structural (spatial) constitutions. A basic understanding of the YY model with its schematic description approach is required to follow the color

dynamic interpretations here. The content of this paper is a further step in the development of the YY model considering the knowledge artifacts from the standard model and its extension approaches (Ref. [3] [4] [5] [6] [7]).

An important result of the current paper (Sections 2, 3, 4, 5 and 6) will be the assignment of quantum colors to the structural constructs of the YY model, in particular to the up and down quarks, giving an interpretation of the color confinement of the QCD for selected atomic nuclei, from a neutron and a proton, to the complex helium nucleus. The mechanism is applicable to all nuclei described by the YY model.

The other results of the current paper (Section 7) will be the interpretation of the interaction mechanism by color anti-color pairs, which cause the color exchange of two building quarks of an atomic nucleus. Again, the YY model will provide a more detailed plausible visualization of the color anti-color pairs and how they mediate color exchanges. There is a close analogy to the gluon-based interactions.

Furthermore, a very interesting fact will be worked out: The structural make-up of an atomic nucleus can assume a number of defined states, the so-called "Color Confined Aggregate State CCAS" (Section 6). Each CCAS is well described. The set of all CCASs for a certain nucleus can act as a kind of "quantum aggregate". Considerations are made about the relationship to gluon interactions and quantum nature (Section 8).

2. Assignment of Colors to PSL and Quarks

The YY model introduced the "**Pairing Space Link (PSL)**" for building the spatial structure of each atomic nucleus. A PSL consists of a Yang and a Yin, which are marked with "+" and "−" respectively. If we assign a color to them, e.g. "red", we get a colored PSL in Figure 1.

Figure 1. Pairing space link and its coloring in red.

As will be seen later, it is reasonable to consider the Yang end as **red** and the Yin end as **anti-red**. This is an important aspect of the YY model for the color manifestation, it associates three colors (red, green and blue) with the positive pool (Yang) and their anti-colors consequently with negative pool (Yin), without using cyan, magenta and yellow.

The YY model described the up quark as an energetic and materialized state combination of two Yang's and a PSL, whereas a down quark is simply an energetic and materialized Yin (Figure 2, left parts). If an up quark is colored green, this means that the PSL is green and the head is white (green, blue and red). To say that a down quark is colored yellow simply means to color its Yin through the yellow (Figure 2, middle and equivalent right-hand side).
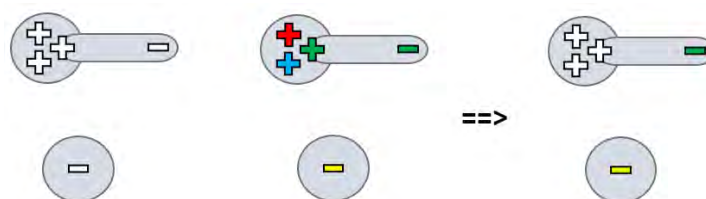
Figure 2. Up quark and down quark (left) and their coloring in green and yellow.

As will be seen later, it is reasonable to consider the color of this up quark simply as **green**, without necessarily distinguishing between green and anti-green. Similarly, it is reasonable to consider the color of this down quark as **yellow**, without necessarily distinguishing between yellow and anti-yellow.

3. Color Confinement within Simple Hadrons

Based on the structural description of a neutron and a proton in the YY-model (**Figure 3**, left parts) and based on the color assignments to the quarks in the last section, it is easy to understand the color confinement within a neutron and a proton nucleus (**Figure 3**, right parts).
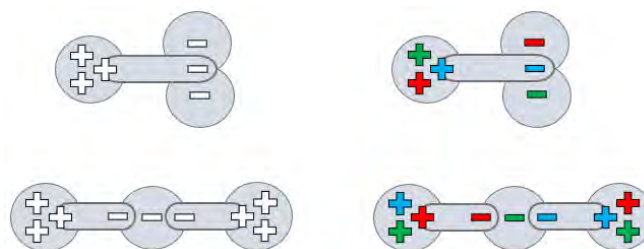
Figure 3. Neutron and proton, their coloring to a confined state.

This current coloration can be considered as an enclosed state: The neutron as an aggregate has assumed a confined state with a blue PSL. Similarly, the proton, as an aggregate, has assumed a confined state with the red and blue PSLs. The current color of each PSL can be understood as a spontaneous state which is "fixed by an observation": For the neutron the PSL color can also take on red or green. For the proton, the colors of two PSLs can take on red-green or blue-green.

4. Manifestation of Colors, Anti-Colors and Color Confinement in YY Model

In summary, the colors and anti-colors manifest themselves in (or are associated with) the constituting parts Yang and Yin of the PSL, **Figure 4**.

The difference between a color and an anti-color is just the different assignments: The color is assigned to yang and the anti-color is assigned to yin. The three PSLs in **Figure 4** are called "color-balanced" or "color-symmetric", because the yang and its counter-part yin have the same color. As will be seen (Section 7), interactions will make use of "unbalanced" PSLs, for example the color pair green anti-red.
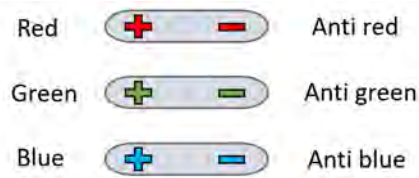
Figure 4. PSL colored in red - anti red, green - anti green or blue - anti blue.

The color confinement in the YY model states that each triple node of yang (or of yin) must be tricolor in red, green and blue (or anti-red, anti-green and anti-blue) to yield white, electrically positively (or negatively) charged, **Figure 5**.
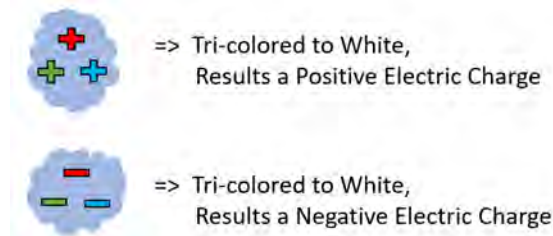

Figure 5. Triple color-charged nodes, resulting a positive or negative electrical charge.

5. Assignment of Colors to TSL

The YY model introduced also the "**Triple Space Link (TSL)**" for constructing complex atomic nuclei. Conceptually, this is a combination of three pairing space links, PSLs. Physically, however, a TSL with triple yang's on the central node (**Figure 6**, upper left) has a much stronger binding than a TSL with triple yin's on the central node (**Figure 6**, lower left). The colored TSLs result in **Figure 6** on the right, considering the color confinement (red - green - blue yield white in the center).
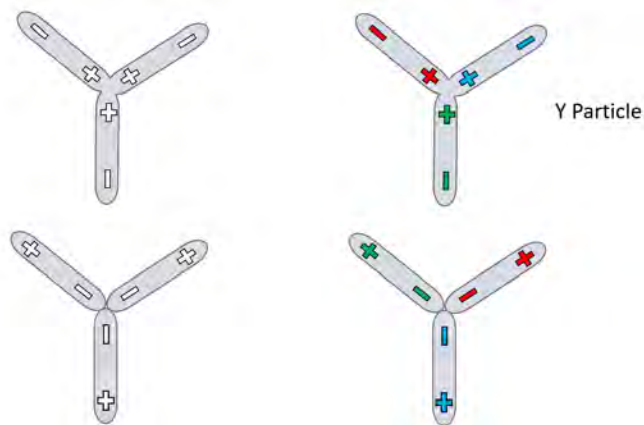

Figure 6. Triple space links, positive and negative centered, and their coloring.

Although the research focus here is on color handling, it should be mentioned that a triple space link with a yang node corresponds to a **Y particle**, which is predicted by the YY model, stable and not necessarily elementary, upper right part of

Figure 6. All nuclear transmutations described by the YY model reserve the triple yang nodes, while triple yin nodes are recombined with quarks and other TSLs, see **Figure 7**: The shaded parts are all possible combinations on yin nodes.
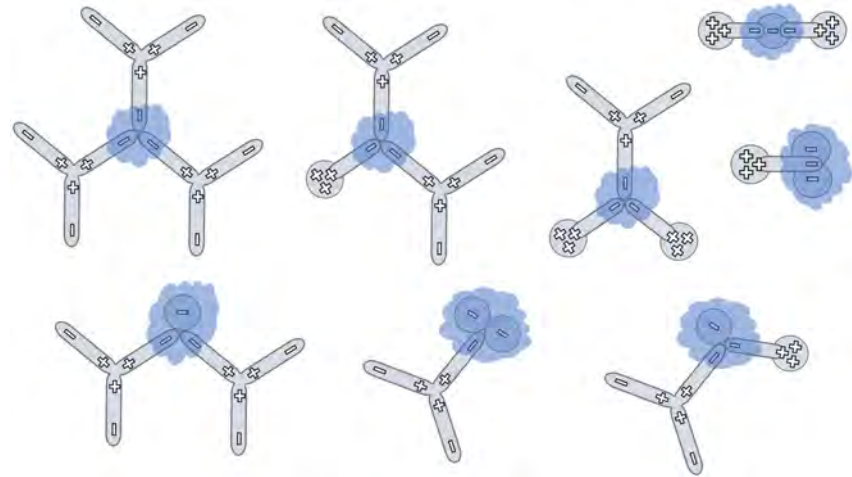

Figure 7. All possible combinations for TSLs with yin nodes.

Based on these color assignments, the YY model is able to balance each complex atomic nucleus to white through colors and anti-colors and to form hadron aggregates.

## 6. Color Confinement within Complex Atomic Kernels

The YY model describes a complex atomic nucleus, e.g. the main proton isotope H^2 (deuterium), by using TSL to combine its **neutronhead** (upper part with two down quarks), **protonhead** (lower right part with one down quark) and **protonids** (left and right parts, all up quarks), following the construction rules defined in the YY model (e.g. Internal Charge Balance ICB), **Figure 8**.
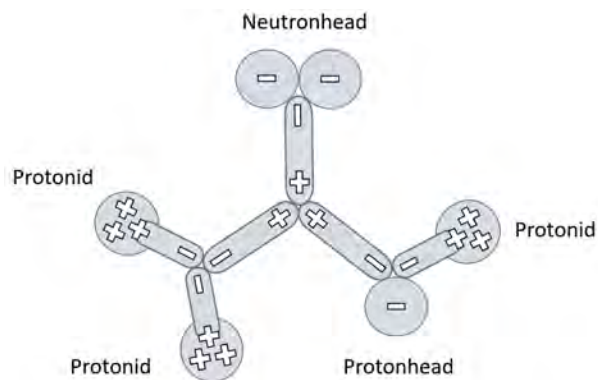
Figure 8. YY model description for atomic nucleus of deuterium.

By coloring all constructing parts (yang's, yin's and consequently PSLs and TSLs), by forcing tri-color compensation at each node (red green blue to white or ant-red anti-green anti-blue to white) and by forcing pairing color balancing

(red anti-red, green anti-green or blue anti-blue), many special color aggregates may be derived. **Figure 9** shows three examples of them.
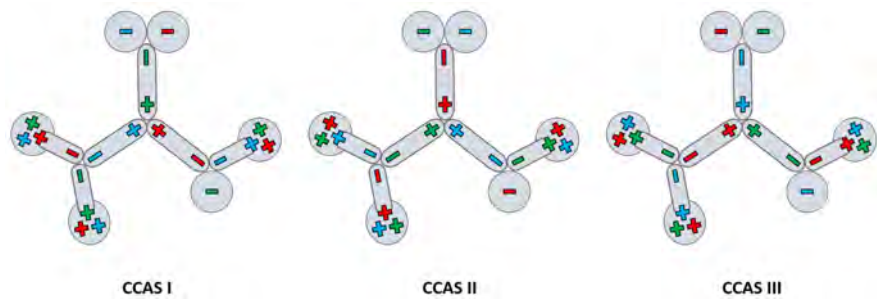
Figure 9. Three samples of color confined aggregate states (CCAS) for a deuterium nucleus.

They are special because compensating all node colors will result the entire aggregate white. We call this combination "Color Confined Aggregate States CCAS". Obviously, there are more such states beyond that showed in **Figure 9**. It is easy to obtain them by recombining the colors and by following the confinement requirement.

The introduction of the term CCAS is important in considering each atomic nucleus as a conceptual aggregate of a series of slightly different varied color distributions. At this stage of understanding, any CCAS can be considered as a state fixed by observing a quantum system that is determined by the uncertainty: One knows the three possible colors (red, green und blue) for a given PSL, but a certain color (e.g., green) is associated with a fixed state.

It must be possible to map the described coloring behavior of structures and states to the solution space resulting from the theories of symmetric and asymmetric groups, as well as of quantum fields. Further investigations of CCAS and its relation to the standard model are necessary.

Following the descriptions, more complex atomic kernels (tritium, helium and one of its isotope) are given for just one of their all possible CCASs.
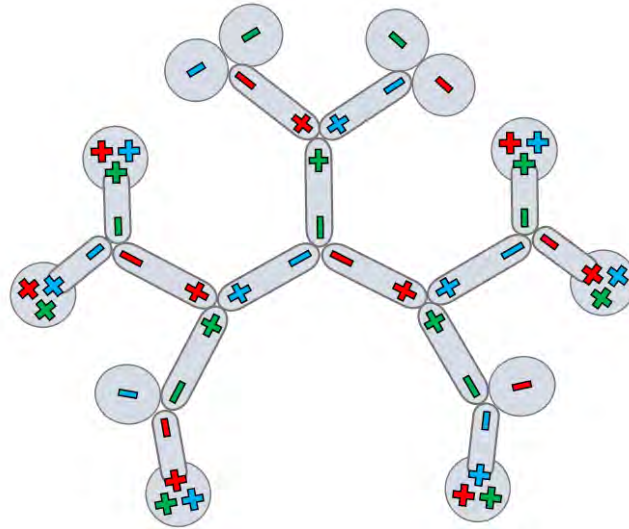
Firstly, the proton isotope H^3 (tritium) consists of one proton (one protonhead) and two neutrons (two neutronheads) as shown in **Figure 10**.
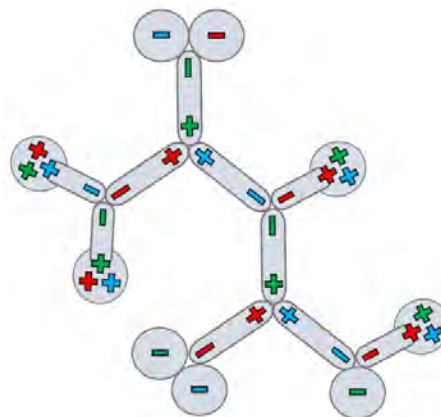
Figure 10. A color confined aggregate state (CCAS) for a tritium nucleus.

For the next, the helium He^4 consists of two protons (two protonheads) and two neutrons (two neutronheads), **Figure 11**.

Figure 11. A color confined aggregate state (CCAS) for a helium nucleus.

Finally, the helium isotope He^3 consists of two protons (two protonheads) and one neutron (one neutronhead) as shown in **Figure 12**.
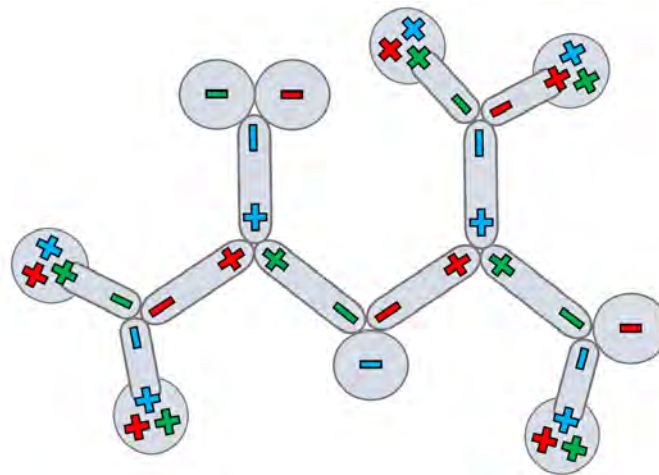
Figure 12. A Color confined aggregate state (CCAS) for a helium isotope nucleus.

7. Interaction Mechanism by Colored PSLs

All states described before are "color confined" because all triple nodes (TSLs) are white and all paring space links (PSLs) are balanced. Now the aspect of interaction is considered: How the color of a quark is transmitted to another quark, *i.e.* the both quarks exchange their colors – this is illustrated by using the example of the deuterium nucleus.

Figure 13 illustrates a change of state from "CCAS I" (color confined) to a new "Not Confined State A": The upper right down quark (anti-red) and the

linked PSL (anti-green) exchange their colors, so that this down quark becomes anti-green and the PSL receives the anti-red and is now charged to a pair of green anti-red.
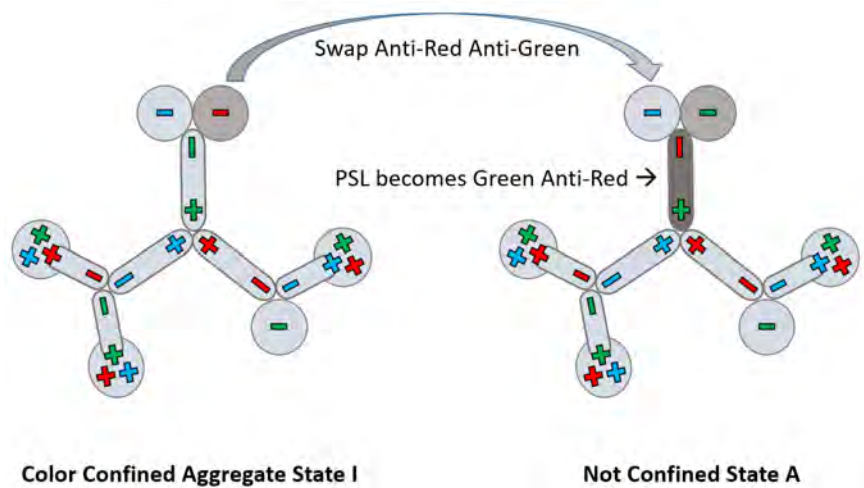
Figure 13. Change of state by swapping the colors of a down quark and the linked PSL.

This participating PSL is now "unbalanced" because it contains two different colors. Therefore, the whole aggregate is called "not confined".

The next change of state is from "Not Confined State A" to "Not Confined State B", Figure 14: The unbalanced PSL (green ant-red) forces itself to balance by pulling the red color at the triple node and giving its green to the adjacent PSL, which loses its red.
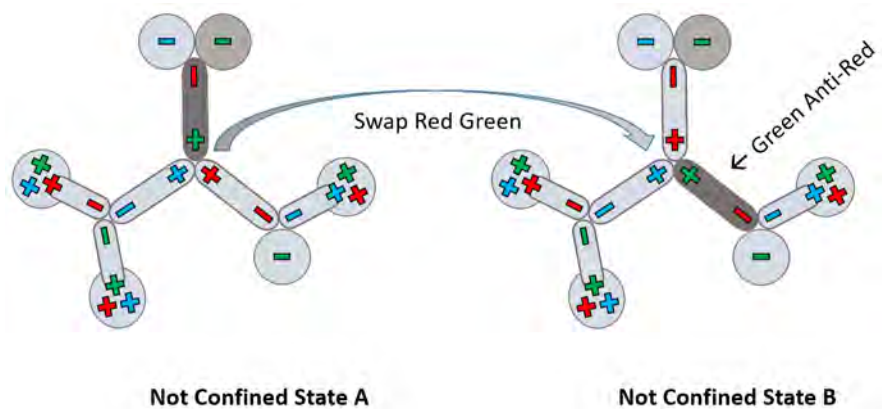
Figure 14. Change of state by swapping the colors of green and red of two linked PSLs.

The first unbalanced PSL gets its color re-balanced and changed its color from original green to current red, whereas the second balanced PSL now becomes unbalanced (green anti-red). It is equivalent to a tumbling movement of the pair green anti-red alongside the PSL chain.

The further change of state from "Not Confined State B" to "CCAS II" (color confined) is done by swapping the anti-red of the unbalanced PSL and the an-

ti-green of the down quark on the low part, Figure 15.

Not Confined State B   **Color Confined Aggregate State II**
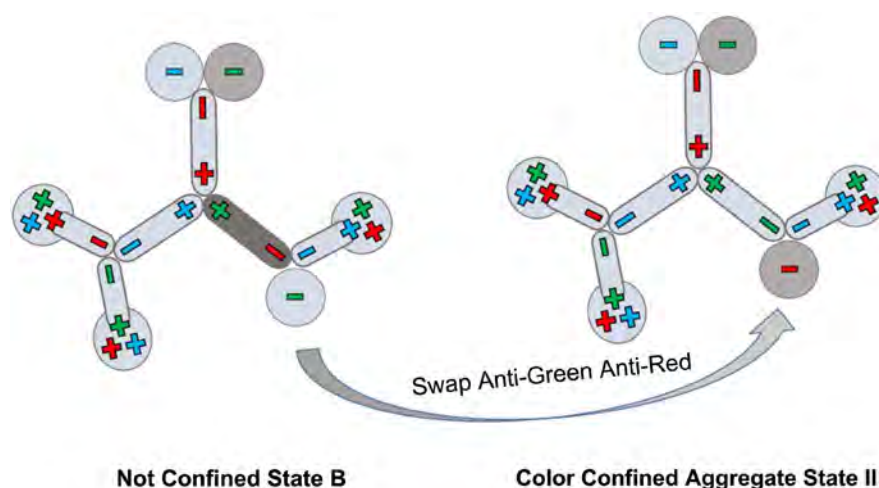
Figure 15. Change of state by swapping the colors of anti-green of down quark and anti-red of PSL.

The end effect of all these interactions is the color exchange of two down quarks, from the original anti-red anti-green to anti-green anti-red. All interactions are submitted by the green anti-red PSL, which runs along the structural chain by "tumbling". The entire aggregate changed its state from "CCAS I" to "CCAS II", with both color state confined.

If we consider only the relay effect of the color and the anti-color, the ending quark of color changes is clearly determined by the three following factors:

➤ Color of the starting up quark or Anti-color of the starting down quark;

➤ Anti-color of the first PSL;

➤ The current CCAS, will determine the travel path and the end quark.

In addition, the color exchanges of the two down quarks are "path-symmetric": The change of state from "CCAS II" to "CCAS I" is transmitted by the same pair of green anti-red and follows the same travel path (backwards). Also note that all participating PSLs on the path before and after the change are alternately green and anti-red. This means that the pair of remotely exchanging quarks "will" follow a path with alternating colors of their own.

The previously shown case was the (anti-) color exchange of two down quarks. By the same mechanism two up quarks exchange their colors. The color of an up quark and the (anti-) color of a down quark can also be exchanged with each other and vice versa.

At the end of this section, Figure 16 shows another change of states (CCAS X to CCAS Y) by exchanging the colors of two up quarks, without drawing "not confined" intermediate states.

In Figure 16, the neutronhead (upper node) and one protonid (low node) that do not participate in the exchange are marked in white – also due to the three compensating colors red, green and blue, respectively anti-red, anti-green and anti-blue.
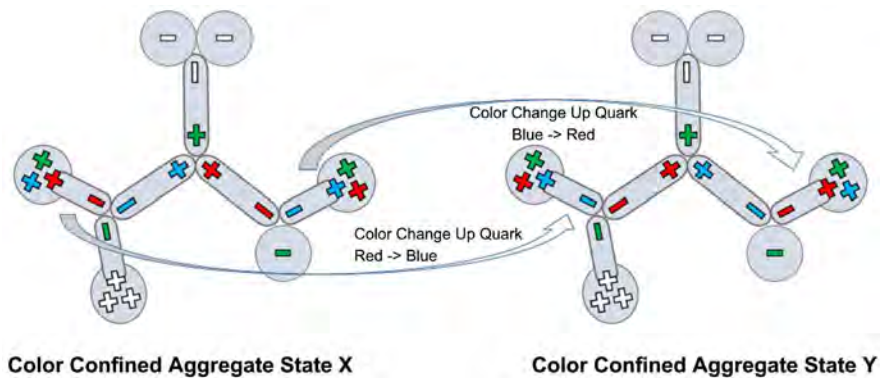
Figure 16. State change by swapping colors of two up quarks (Red $\leftrightarrow$ Blue).

8. Further Considerations

The manifestation of the color confinement from the standard model is closely related to the color assignment to the structural constructs (yang and yin) from the YY model. "Confinement" in the sense of the YY model means that each positively charged node is colored by red, green, blue, whereas each negatively charged node is colored by anti-red, anti-green and anti-blue. A color is always assigned to a yang node, whereas an anti-color is always assigned to a yin node. The "confinement" in the YY model also requires that each PSL must be color balanced (either red anti-red or green anti-green or blue anti-blue).

The color exchange of the quarks takes place via the interaction mechanism described above. It is transmitted by the "unbalanced PSLs" as an asymmetric color and anti-color pair. It is therefore very similar to the interactions transmitted by gluons, which form the basis of the strong forces in the standard model. There is much potential for studying the internal relationships between the gluons and the PSLs. For example, it is conceptually simple to represent the unbalanced PSLs in **Figures 13-15** as gluon tubes (Ref [8] and [9]). All this is logical, and the question is justified how this color exchange should be performed statically or dynamically.

The cause of the initial color change is unclear (for example, the change of state from "CCAS I" to "Not Confined State A" in **Figure 13**). Possibly there is some kind of "ghost" inside or around the aggregate that causes the color change. It is also unclear whether the color change of several quark pairs occurs simultaneously and whether and how the tumbling PSLs interfere with each other, especially on the TSL node. In view of the color changes described by the standard model, the two similar questions arising from this are also not yet answered properly.

There are two possible ways to gain a better understanding, which can lead to achieve interesting results through more in-depth research.

One is based on the idea that the strong forces that hold the surrounding quarks of an atomic nuclear aggregate interact statically (TSL nodes, electrically positive and negative alternating, plus PSL links, color and anti-color balanced). The nucleus must always be a CCAS. The detailed color change mechanism as a

thinking aid of the standard model becomes imaginary. This consideration requires a multiple solution of the quantum field potential for the entire aggregate—think of a flock of birds finding its flight formation interactive and self-organized.

The other way is the "vertical" superposition of the multiple color states by considering them as quantum possibilities in a broader sense the Schrödinger cat analogy: In the whole kernel aggregate, the colors of the PSLs change within the possible values, forced by the "color rotations" of the adjacent TSLs. The symmetry between the color confined aggregate states is broken locally by an observation that provides an immediate snapshot. This way is more compatible to the usual interpretation of interactions for strong forces.

Finally, we mention the main difference between the methodological approach of the YY model and other schematic approaches to nuclear models, such as preon model (Ref [10]) or molecular nucleon model (Ref [11]). The YY model uses well-known basic artifacts of the standard model to build an architecture that allows to include more and more facts in a clear and consistent way. Regarding the color considerations of this paper, which are based on the model construction of the last paper, the authors believe that the goal of this approach has been achieved.

Conflicts of Interest

The authors declare no conflicts of interest regarding the publication of this paper.

References

[1] Yang, H. and Yang, W. (2020) Extending Standard Atomic Kernel Model with New Interpretation of Strong Forces. https://arxiv.org/abs/2006.15695

[2] Yang, H. and Yang, W. (2020) A Generic Description Model for the Structure of Atomic Nucleus with New Interpretation of the Strong Forces. *Journal of Modern Physics*, **11**, 1132-1156. https://doi.org/10.4236/jmp.2020.118071

[3] Di Giacomo, A. (2006) Confinement of Color: Open Problems and Perspectives. *AIP Conference Proceedings*, **842**, 216. https://arxiv.org/abs/hep-lat/0602011 https://doi.org/10.1063/1.2220230

[4] Di Giacomo, A. (2007) Recent Progress on Color Confinement. *AIP Conference Proceedings*, **964**, 348. https://arxiv.org/abs/0710.1164 https://doi.org/10.1063/1.2823875

[5] Braun, J., Gies, H. and Pawlowski, J.M. (2007) Quark Confinement from Color Confinement. https://arxiv.org/abs/0708.2413

[6] Hansson, J. (2000) A Simple Solution to Color Confinement. https://arxiv.org/abs/hep-ph/0011060

[7] Tornqvist, N.A. (2007) The Scalar Mesons, Symmetry Breaking, Three Colors and Confinement. https://arxiv.org/abs/hep-ph/0606041

[8] Ying, C. (2020) Confinement and the Global SU(3) Color Symmetry. https://arxiv.org/abs/2010.00431

[9] Baker, M., Cea, P., Chelnokov, V., Cosmai, L., Cuteri, F. and Papa, A. (2019) Isolat-

ing the Confining Color Field in the SU(3) Flux Tube. *The European Physical Journal C*, **79**, Article Number: 478. https://arxiv.org/abs/1810.07133 https://doi.org/10.1140/epjc/s10052-019-6978-y

[10] Dugne, J.J., Fredriksson, S. and Hansson, J. (2002) Preon Trinity: A Schematic Model of Leptons, Quarks and Heavy Vector Bosons. *Europhysics Letters*, **60**, 188. https://doi.org/10.1209/epl/i2002-00337-8

[11] Ho, V.B. (2020) Molecular Structure of Atomic Nucleus. *Journal of Modern Physics*, **11**, 1395-1409. https://doi.org/10.4236/jmp.2020.119087

Scientific Research Publishing

Virus Destruction by Resonance

Auguste Meessen

UC Louvain, Louvain-la-Neuve, Belgium
Email: auguste@meessen.net

Abstract

Viruses and other microbes can be inactivated in a selective way by subjecting them to an oscillating electric field of adequate frequency. Royal R. Rife discovered this method already about 100 years ago. He proved its efficiency by means of high resolution microscopes and in 1934, by controlled clinically tests. However, these results seemed to be unbelievable, since the underlying mechanism was not yet understood. Actually, we are faced with three problems: 1) the functioning of Rife's supermicroscopes, 2) his observation that bacteria can undergo size reduction, and 3) the decisive resonance phenomenon. We explain the high magnification and resolving power of Rife's microscopes and show that new discoveries confirm that the postulate of invariable forms of bacteria has to be abandoned. Then we prove that forced oscillations of virus spikes lead to a peculiar resonance, because of nonlinear effects. It causes total destruction of the virus by rupture of its coating. The same theory applies to bacteria and nanobacteria, because of their pili. The worldwide coronavirus pandemic, the constant threat of unpredictable mutations and the now available explanations should make it obvious that biophysical methods cannot be neglected anymore.

Keywords

Rife, Microscope, Virus, Pleomorphism, Cantilever, Resonance

1. Introduction

Royal Raymond Rife (1888-1971) was an outstanding scientific inventor, who wanted to help humanity by discovering and fighting still unknown causes of sickness and death. His achievements and the opposition that he encountered were described in the remarkable book of Barry Lynes [1]. In his youth, Rife had been impressed by the discoveries of Louis Pasteur and Robert Koch during the second half of the 19th century. They used microscopes to see lethal microbes. They could then isolate and culture them. When the resulting entities caused

always the same sickness after repeated cycles, the next step was to find specific vaccines to help their recognition by our immune system. Rife suspected that cancer does also result from microbes, but that they are too small to be seen by means of standard optical microscopes.

This limitation results from the wave nature of light. It leads to interference effects. The physicist Ernst Abbe, working for the Carl Zeiss Company, established even in 1873 a relation between the best possible resolving power of optical microscopes and the wavelength of light. It is at best of about $\lambda/3$, where λ is the wave length for visible light. The limit is thus about 180 nm, but for ultra violet light, $\lambda < 400$ nm. The Carl Zeiss Company developed therefore UV fluorescence microscopes. The light source was an intense electric arc lamp and the UV light was concentrated on the specimen by means of quartz lenses. Since the specimen converted this light by fluorescence into visible light, the objective and ocular were glass lenses. In 1913, the Carl Zeiss Company was ready to sell this new type of microscopes [2].

Rife started in 1917 to construct himself a better microscope for visible light and finished it in 1922 [1]. It magnified up to 17,000 times, while the best standard optical microscopes could only reach 2000 - 2500 times. Moreover, the images were well-contrasted, with unprecedented high resolution. How this was achieved remained an unsolved puzzle. Rife constructed even more powerful optical microscopes. His second one was finished in 1929 and the third one in 1933. He called it a "universal microscope", because of its great adaptability. It could even magnify up to 60,000 times.

These supermicroscopes allowed him to make extraordinary discoveries, but they contradicted the beliefs of medical authorities. Using only conventional microscopes, they were unable to observe what Rife saw by means of his supermicroscopes. Moreover, Rife discovered the cancer microbe, although it was generally assumed that cancer is not an infectious sickness. Science progresses, of course, by discovering previously unknown facts and by explaining them, but that may require correcting previous assumptions. Unfortunately, it is very difficult to modify deeply rooted ideas. One objective of this article is to illustrate this fact by analyzing Rife's discoveries and achievements, to show the complementarity of experimental and theoretical methods.

It has been claimed [3], for instance, that it is impossible to reach the high resolution of Rife's microscope, by repeating the standard theory. It is also incorrect to believe that Rife did suppress the interference effects [4]. The Nobel Prize in Chemistry of 2014 was actually awarded for the development of *super-resolved microscopy* [5]. This was achieved by using powerful lasers, while Rife succeeded with purely classical means. Nevertheless, his name has been wiped out from official medical and scientific literature.

Fortunately, some documents were preserved and their analysis did help us to uncover the secret that escaped attention. Moreover, they provide first-hand information about the discoveries that Rife made with his new microscope. The

first one concerned the existence of "nanobacteria", resulting from size-reduction of known bacteria. They are more virulent, but Rife discovered also a method to destroy them, by resonance. To observe both phenomena very clearly, he constructed the more powerful microscopes. The size of typical bacteria is of the order of 1000 nm. For viruses, it ranges from about 400 to 20 nm, but their existence had already been established at about 1900 by means of porcelain filters with very narrow pores. The filtrate contained no bacteria, but remained virulent. This fact justified Rife's conviction that these mysterious entities should be observable by means of better microscopes.

A description of his universal microscope was published in 1944 by a scientific journal [6]. It mentioned also other new optical microscopes and compared them with electron microscopes, developed in the 1930th. Their magnification is greater and allows for instance to determine the size of the polio virus. It is merely 30 nm. The diameter of the spherical core of the Covid-19 virus is 85 nm and it carries 20 nm long spikes. However, electron microscopes can only yield images of dead microbes. The article of 1944 insisted thus on the "great interest" of the new type of optical microscopes, since they allow scientists to penetrate the unseen world of the minute and disease-causing organism when they are still living and active.

This was essential for Rife, but how did he acquire the competence for his apparently impossible achievements? We know that he began medical studies in 1905 at John Hopkins University in Maryland, but he broke them off. His aim was to construct as soon as possible a better microscope and to find the cancer microbe. It has been reported [7] that he married in 1912 and moved then to San Diego, California. Speaking German, he travelled often before WWI to Germany for the US Navy. Rife provided himself reliable information in 1960, by answering 137 questions of the lawyer of his collaborator John Crane [8]. He was on trial, since the powerful American Medical Association (AMA) had decided to abolish the Rife/Crane cancer therapy. It was declared to be bogus, even without examining Rife's methods and results. After Rife's trial, orchestrated already in 1939 by AMA, he was forced to stop his research. He was bankrupt and desperate. His laboratory had been raided. His microscopes were made unusable and documents were stolen. They included also movies of the behavior of the tiny living beings that Rife made visible. He took refuge in Mexico. Even his written answers of 1960 were not allowed to appear in court during Crane's trial in 1961, but they were conserved.

Rife's answered (to question Q.38) that he acquired his expertise in optics by working for 6 years with Hans Lukel, who was Carl Zeiss's scientist in the USA. Rife mentions there also that he made "all the photomicrographs for the Atlas of Parasites which was done at the University of Heidelberg". This book was published in 1914 and contained more than thirteen hundred colored lithographs [9]. Our inquiries at the archives of the universities of Heidelberg and Gießen, as well as at the Carl Zeiss History Support in Jena revealed no recorded or easily accessible traces. The authors of the book did only thank their academic col-

leagues. Anyway, it took nine years before Rife felt ready to begin his own research (Q.39). The link [8] provides photographs of his microscopes and the copy of a certificate, where the Institute for Scientific Research of the Andean Anthropological Expedition recognized Rife's "outstanding contributions to science" and the attribution of a Research Fellowship in biochemistry. Rife confirmed this (Q.135-137) and added that he studied *bacteriology* at John Hopkins University (Q.56). He acquired there a PhD diploma, since he signed a scientific paper [10] with this title and was often called Dr. Rife.

When he was running out of financial resources, he took a job as chauffeur of the multi-millionaire Henry Timken. He manufactured ball bearings and Rife provided a way to control their quality by constructing an X-ray machine. Timken valued his creativity and technical abilities, demonstrated in various ways. Impressed by Rife's competence and his strong motivation to construct better microscopes for identifying the cancer microbe, Timken offered him a laboratory at Point Loma, California, with full equipment and financial support.

Rife constructed there his microscopes and the basement provided facilities for 1000 animals with precisely controlled air-conditioning (Q.10). There were about 800 albino rats, but also Guinea pigs and rabbits (Q.59). In 1929, a local newspaper published an article about Rife's extraordinary microscope and his fascinating discoveries [11]. The journalist praised his competence in bacteriology, chemistry, metallurgy and engineering. Rife had developed methods to observe and document previously unobservable living entities. He found even a technique to destroy harmful microbes, but "refuses to make money from it". He is concerned with pure science and wants to free humanity from cancer and other dreadful sicknesses.

In his interview [8], Rife provides important details concerning his research and the difficulties that he encountered. He did use cancer tissues and prepared over 15,000 slides, since he was convinced that his microscope should allow him to see the microbe that causes cancer, but it remained hidden. He tried numerous molecules for staining and this lasted over 10 years, to no avail (Q.22). Eventually, he thought that chemical substances might destroy the mini-microbes and started therefore to exploit other capabilities of his microscope. Although this was time-consuming, it allowed him to select a color that made microbes visible by their own luminescence, without having to add some staining substance. It was also necessary to discover a method for multiplying the microbes that he expected to be present in cancer tissue. He found that they had to be cultured in the "K medium", developed by the microbiologist Arthur Kendall. This medium is protein based, but poor in peptones (polypeptides and amino acids). It was superior to all other ones (Q.29 and 30). Nevertheless, the decisive breakthrough was quasi-accidental [12].

"After many long procedures and unsuccessful attempts", Rife had fortuitously placed a test tube near an argon discharge tube. It ionizes air and produces O_2^- ions, becoming ozone. Rife noted some cloudiness, but the microscope re-

vealed nothing special. After incubation during 24 hours at 37.5˚ on K-medium, the solution was "teeming with cancer virus". These entities were very small and motile, but easily discernable by means of their purplish fluorescence. Their proliferation resulted from subjecting bacteria to stress. Since Rife had been searching these mysterious entities during many years, he called them X-bacteria or simply "BX". To verify if they did really cause cancer, he inoculated albino rats with a solution, derived from human breast cancer tissue. In almost 3 to 4 days there appeared a lesion at the point of inoculation in the mammary gland of these rats. Pathological examination disclosed typical malignancy. Rife mentioned that the same procedure was repeated 411 times with identical results (Q. 24). He wanted to be absolutely sure.

The culprit of cancer or at least a new possible cause had thus been uncovered. It was a tiny ovoid particle, about 50 nm large and 70 nm long. Its motility indicated that it was flagellated [10]. Rife observed also with his supermicroscope that these BX entities could be transformed again into bacteria or fungi, according to the medium where they were living. In their reduced form, they could not be destroyed by UV radiation or X-rays, but they were killed after two days at 42˚C. The newspaper article [11] attracted the attention of Dr. Arthur Kendall, who had developed the K medium. He was professor and head of the department of bacteriology at the Northwestern University in Chicago and wanted to check the reality of these amazing claims.

He invited Rife in 1931 to bring his microscope to his institution, where he used a type of bacteria that he had cultured himself. In their "filterable state", they appeared in Rife's scope as tiny, motile granules of turquoise-blue color. These observations were so astonishing, that the whole procedure was repeated eight times. In 1931, Prof. Dr. Kendall published with Rife an article [10] that described these experiments and their results. Kendall was then invited to speak in 1932 at a meeting of the Association of American Physicians. Dr. Thomas Rivers, virologist at the Rockefeller Foundation, tried to get Kendall's talk cancelled. This was not accepted, but Rivers went immediately to the podium after his talk to express fierce opposition. He impressed the audience by daring to address Dr. Kendall as if he were a liar.

Dr. Rivers and Dr. Zinser, bacteriologist at Harvard, had tried to reproduce Kendall's results. They did use the K-medium, but their observations were made with conventional optical microscopes. Without Rife's supermicroscope and his method to provoke luminescence, they were unable to see the relevant nanoparticles. Moreover, they believed in *monomorphism*, advocated by Louis Pasteur. He had attributed infectious diseases to bacteria of specific size and form. A similar postulate is used for classifications in botany and zoology, but metamorphosis is not impossible. Since Rife and Kendall were facing *ideology*, Dr. Edward Rosenow, who was heading the Mayo Foundation's Experimental Bacteriology program at Rochester, Minnesota, wanted to check the facts. He spent 3 days at Kendall's laboratory where Rife's microscope was still installed and reported his

observations in Science [13]. He wrote: "there can be no question of the existence of filterable turquoise blue bodies". They appear in large numbers in filtrates of cultures of infected tissues and constitute a "stage in the development of microorganisms."

Rife mentioned in his interview [8] that the BX entities are actively moving around (Q. 51), but that he found a method to "devitalize all microorganisms as desired" (Q.19). It required EM waves of particular frequency, depending on the kind of microbes. This frequency was determined by observing the microbes with his microscope (Q.76). Some types did then "explode or disintegrate" and other types did aggregate (Q.80). This happened for various types of bacteria (Q.78), but they were never affected by inadequate frequencies (Q.118). This observation led to the development of the "ray machine". Its production was continued by John Crane when Rife fled to Mexico, but Crane was prosecuted. AMA accused him, though it refused to test his system (Q.131). The American Cancer Society was interested, until they found out that Crane and Rife were not medical doctors (Q.127).

However, Dr. Milbank Johnson, Professor of Physiology and Clinical Medicine at the University of Southern California, gathered in 1934 a Research Committee to test the clinical efficiency of Rife's cancer therapy. Sixteen terminally ill patients with different types of malignancies were selected and treated with the instrument that produced an oscillating electric field of the required frequency for deactivating the BX entities. The sessions lasted only 3 *minutes*, *every third day*. The patients felt neither pain nor any other sensation, but "the virus or bacteria is destroyed and the body then recovers itself" [1]. The interval between treatments was needed to eliminate the toxic debris. "After 3 months, 14 of these hopeless cases were signed off as clinically cured by the staff of five medical doctors". Other ones participated in overviewing this test and the pathologist of the group, Dr. Foord, certified the healing. The two other patients were cured after 20 more days [7]. The first cancer clinic that used the Rife technology was opened in 1934 and the Rife Beam Ray Company was operating in 1938. That was intolerable for the powerful AMA. The capitalistic pharma industry wanted also to prevent the development of alternative forms of medical treatments, of course, but had merely to encourage AMA's request of legal prohibition and its use of other methods of coercion. This procedure has been analyzed in the context of social anthropology, related to science and technology [14]. It is necessary, indeed, to realize that it was profoundly unjust, unscientific and even harmful, by preventing possible cure.

The structure of this article results from the need to solve three basic problems. *Section* 2 describes Rife's supermicroscope and explains its functioning. *Section* 3 justifies the concept of pleomorphism. *Section* 4 provides a detailed scientific explanation of the physical mechanism of targeted microbe destruction by resonance. This part illustrates also the usefulness of physical reasoning for solving scientific riddles, even in medicine. *Section* 5 presents conclusions and

some recommendations.

2. Optical Supermicroscopes

2.1. Rife's Universal Microscope

The basic principles of microscopy result from the laws of geometrical optics. All light rays that emerge from a point A and pass through a lens L do converge at the point A'. To determine its position, it is sufficient to consider two rays, as shown in Figure 1. The ray that passes through the center of a thin lens is not deviated, while the ray passing through the focal point F is refracted by the lens to become parallel to its symmetry axis. This applies even to combinations of thin lenses. The position of the image A' of A is determined by 5 parameters: their distances D and d from the plane of the lens, their heights H and h above and below the symmetry axis, as well as the focal length f of the lens L. Indeed,

$$\frac{1}{f} = \frac{1}{d} + \frac{1}{D} \quad \text{and} \quad \frac{H}{h} = \frac{D}{d} \tag{1}$$

Analogous relations apply to the second lens L'. Since the rays that emerge from A' and pass through this lens are refracted as if they did emerge from I, this is a virtual image. The global magnification is the product of the magnifications provided by the objective and ocular lenses.

Rife modified this system to get a much greater magnification by increasing the distance D. He did that by intercalating many prisms as indicated in Figure 2. We represent there only a narrow bundle of rays, forming a beam that would coincide with the symmetry axis if it were not deviated. Rife stated in his description [15] that the beam was subjected to "21 light bends". There are only 20
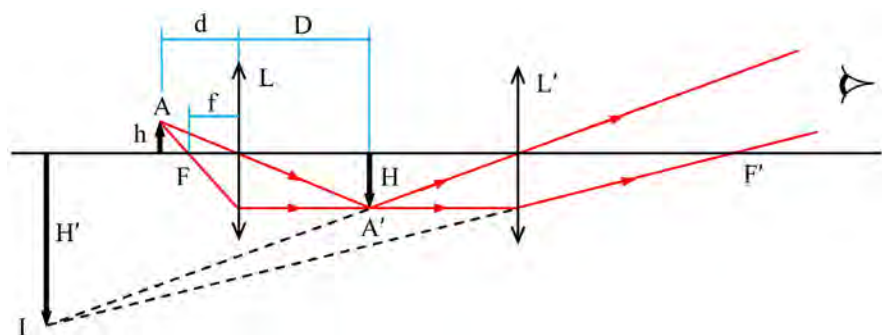
Figure 1. Successive formation of two images A' and I of the point A in optical microscopes.
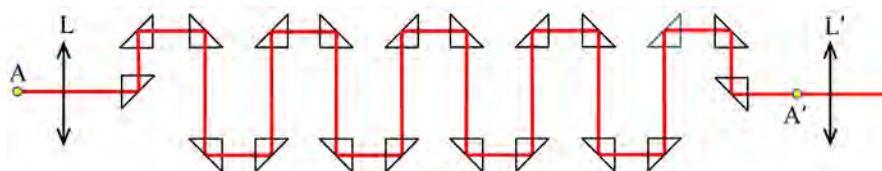
Figure 2. Rife achieved great magnification by increasing the distance D between the lens L and A'.

prisms, but the image A' does also produce a deviation to yield the image I. Rife insisted that the rays of light have to remain *nearly parallel*, although the rays emerging from the lens L are converging. The 90˚ prisms did thus not simply act like mirrors. One of their faces was slightly concave. Every time before the rays would tend to meet, they were thus made less convergent. This stratagem required extremely high precision, since the total deviation from the ideal one could not exceed one wavelength.

The distance that light rays traveled zigzag fashion was 449 mm, while the length of the barrel was only 229 mm. For usual microscopes it is 160 - 190 mm. All prisms and lenses were made of block-crystal quartz. The barrel and screws were made of "magnalium". This AL/Mg alloy was very expensive, but it has the same thermal dilatation coefficient as quartz. Figure 1 shows that both focal distances f and f' should be as small as possible. Rife opted thus for a pair of identical, high-quality objectives with quartz lenses, developed by Zeiss. Why did Rife not follow the contemporary trend to improve resolution by using UV light? It would not be converted everywhere into visual light when it passes through the specimen, but is dangerous for visual observation. Though it could be eliminated by a filter, Rife preferred to use a normal light source, since his initial intention was to use chemical staining.

Rife knew that molecular fluorescence results from processes that are represented in Figure 3(a). The curves show how the energy E depends for the ground state and the first excited state on the structure parameter s. Photons of blue or near ultraviolet light can thus excite an electron from the most probable ground state to another possible state. The molecule modifies then its configuration before emitting a photon of lower energy. Since absorption and emission of a photon are instantaneous processes, they are represented by vertical transitions. There are also vibrational states, leading to spectral bands instead of lines, but we can simplify the graph, since the essential point is that molecules, which can rapidly lose any excess energy. However, it was necessary that the light source could provide light of any required color to elicit optimal fluorescence.

An electric arc is a very intense light source, but there are spectral lines. Rife preferred thus an incandescent filament. It yields a continuous spectrum and Rife did use a special filter to select the adequate color. It had been invented in 1889 by the ophthalmologist Risley and is represented in Figure 3(b). Indeed,
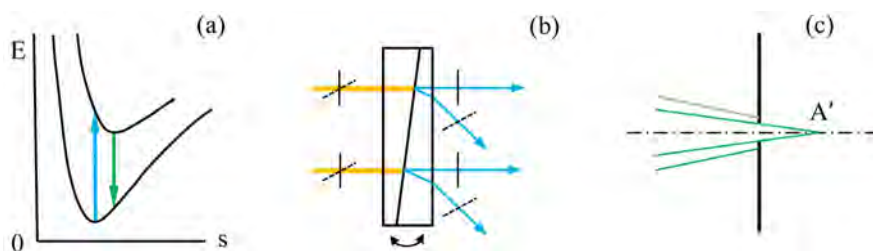
Figure 3. (a) Molecular luminescence is optimal when it is excited by light of a particular color. (b) It was selected by a Risley filter. (c) Rife's secret was a pinpoint filter near A'.

two identical 90˚ prisms can be rotated with respect to one another, while their oblique faces remain in contact. At normal incidence light is only refracted at the interface. This leads to dispersion, but by rotating the prisms with respect to one another, we get only light of a particular color that leaves the second prism at normal incidence. Since quartz is birefringent, the angle of refraction depends not only on the color, but also on the polarization of light waves. Rife could thus produce polarized light of any desired color. This is useful for mineralogy, since thin slices reveal then colored parts.

Figure 3(c) represents the pinpoint filter that Rife did place before the first image A', but he did not mention it in his dialogue with Crane [16]. He stated there (#43) that the universal microscope has "a resolution of 31,000 times and a magnification of 60,000 times". These values have often been repeated, without explaining how they were determined, but Rife mentioned that he used a Zeiss silver coated slide, carrying 800 lines per mm with perfect definition. They were thus separated by 1.25 μm. Under a standard microscope, there appeared 40 - 60 of these lines with distortions, due to spherical aberration of the lenses. "Under the universal microscope, we see only 1 - 3 lines and they are perfectly parallel through the entire field" (#44 and 45). The greater magnification kept only the central part of usual images. Rife claimed that "the resolution is 31,000 times", which is unusual, but he considered that the sharpness of the image reached at least half the separation of the lines.

The high resolution remained very puzzling, since Feynman noted in his famous lectures on physics (I, 27-7) that we might build a "system of lenses that magnifies 10,000 diameters, but we still could not see two points that are too close together." We mentioned already that the resolving power of optical microscopes is limited by interference effects. However, Rife answered only to Cranes question concerning this limit (#43) that the lack of sharpness is due to "factors of error that come into the field of optics by the illumination and things of all sort." The use of a pinpoint filter just before the first image was not mentioned. Even in the article of 1944, Rife noted merely [6] that "if one pierces a black strip of paper or cardboard with the point of a needle and then brings the card up close to the eye so that the hole is in the optic axis, a small brilliantly lighted object will appear larger and clearer, revealing more fine detail." This hint has not been perceived, but Rife's method is equivalent to a recent discovery [5], that deserved even a Nobel prize.

2.2. Modern High-Resolution Microscopes and Diffraction

Stephan Hell, who pioneered the use of lasers for high resolution optical microscopy, explained the basic idea in his Nobel lecture [16]. He began with underlining the advantage of minimally invasive optical microscopy with respect to electronic microscopy. However, the resolution of optical microscopes is limited and "scientists believed throughout the 20th century" that this barrier cannot be overcome". Knowledge of Rife's achievement had been wiped out, but Hell

thought that "so much new phenomena were discovered" that higher resolution of optical microscopes should be realizable. He was teaching biophysical chemistry in Göttingen and attributed the difficulty to the fact that light is emitted by *different molecules* inside a small volume of the specimen. They are exited together and emit light by the molecular processes that were depicted in **Figure 3(a)**. Since it is impossible to excite only a very small group of molecules, he tried to find out if we can "manage to keep some molecules dark".

Searching an answer to this question, he found that physics knows about *stimulated emission* of radiation. Einstein discovered this phenomenon in 1917 by proving that it accounts for Planck's spectrum of EM radiation in an oven or any cavity at sufficiently high temperature. With lasers, it is possible to silence excited molecules by "stimulated emission depletion" (STED). This process is represented in a simplified way in **Figure 4(a)**. Blue laser light (1) of moderate intensity is absorbed by a molecule. An electron is there raised from the ground state S_o to the first excited state S_1. The molecule relaxes, by changing its configuration. The interrupted line represents this loss of energy, since it is sufficient to represent the initial and final excited state to account for **Figure 3(a)**. Light emission result from the transition (2) in **Figure 4(a)**, but stimulated emission (2') can be caused by intense laser light of the adequate frequency. The excited state is then constantly emptied and normal light emission is quenched.

Figure 4(b) represents the spatial domains of illumination by means of the two lasers. These light distributions cannot be point-like, but it is possible to produce a blob of blue light (1) and to superpose a ring of very intense green light (2'). It abolishes light emission in this ring and leaves only the small central spot where light emission (2) is still possible.

Once the spell was broken, other scientists did tackle the same problem during the two last decades and discovered various methods to solve it. They were reviewed in a comprehensive and interesting way [17]. The basic technique consisted always in separating light emission in space or time. How could Rife succeed already in the 1920th to reach high resolution without lasers? To understand this fact, it is useful to return to basics.

Grimaldi's careful observation in 1660 of the shadow cast by a rod revealed that it cannot be explained by geometrical optics, unless light rays that pass close to obstacles are divided (at least) in two rays. This led to the concept of "diffraction".
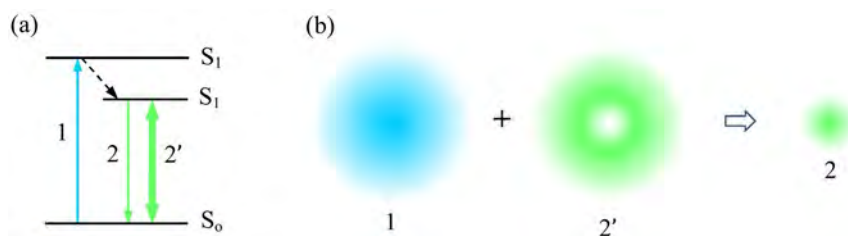
Figure 4. (a) Transitions between energy levels, used for high-resolution microscopy by the method of stimulated emission depletion (STEP). (b) Superposed illuminations and the resulting emission.

Grimaldi thought already that light may not be constituted of particles that are moving along straight lines in any homogeneous medium. Young's famous double slit experiment of 1801 proved that light is propagating *like* waves. It was then generally believed that there are "light waves", but Planck discovered in 1900 that there are grains of light energy and Einstein proved in 1905 that they are particles. These photons do not always move along a single well-defined trajectory, but do also allow for interference.

In 1815, Fraunhofer discovered spectral lines in sunlight by improving the quality of lenses and prisms, but he did also use gratings with many equidistant narrow slits. The resulting interference decomposes white light in different colors. Fraunhofer found that a single slit produces also a set of closely spaced interference fringes. Even when light encounters a screen with a small circular hole of radius r, as shown in **Figure 5(a)**, it does produce a brilliant spot of light that is surrounded by fainter rings. Fresnel explained this fact in 1819 by considering that all points inside this hole emit spherical light waves, but on the symmetry axis, they do always interfere constructively with one another. **Figure 5(b)** shows that for the angle θ with respect to the symmetry axis, light emitted by any pair of points that are radially separated by the distance r interferes destructively for monochromatic light of given wavelength λ, when

$$r\sin\theta = \lambda/2 \qquad (2)$$

For other angles the wave amplitudes are not opposite to one another. Fresnel calculated the resulting variation of the light intensity and found that it varies as indicated in **Figure 5(c)**. It is even the square of a Bessel function. The arrows define the width of the central spot, resulting from relation (2).

Distant stars are point-like light sources, but for telescopes, their image is a spot of light that is surrounded by rings of decreasing intensity. This was proven in 1835 and led to the term "Airy disc". It is represented in **Figure 6(a)**, when light intensities are represented in black/white inversion. **Figure 6(b)** recalls that all light rays that emerge from the point A and pass through the lens L will converge at the point A'. Ernst Abbe realized in 1873 that a microscope is thus equivalent to a circular hole of radius

$$r = 0.61\frac{\lambda}{2NA} \quad \text{where} \quad NA = n\sin\theta \qquad (3)$$
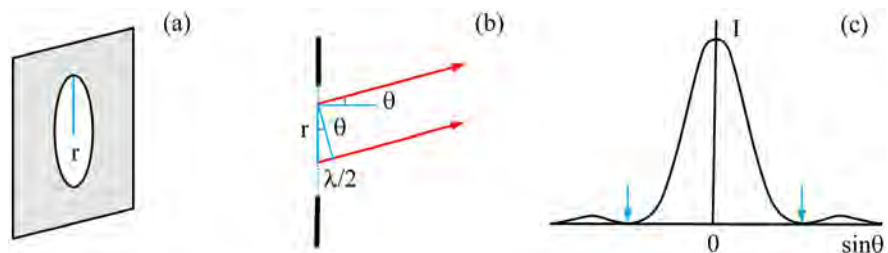
Figure 5. (a) Light passing through a small circular opening leads to interference. (b) It is always destructive for a particular angle θ. (c) The angular distribution of the resulting light intensity I yields a central blob, surrounded by fainter luminous rings.
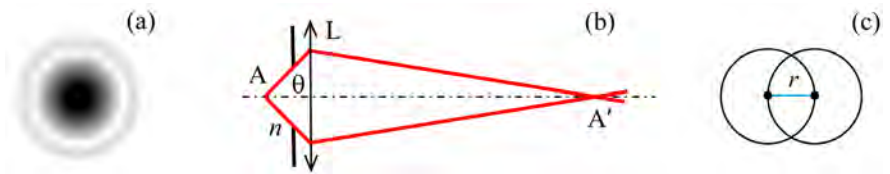
Figure 6. (a) Black/white image of an Airy disc. (b) Formation of the first image in a microscope. (c) The resolving power *r* defines the smallest distance between separable point-like sources.

The value of *r* results from (2) and the fact that light rays are refracted by the lens. *NA* is called the "numerical aperture" of the lens system, since it depends on the angular opening θ of the diaphragm and the index of refraction *n* of the medium between the specimen and the lens. It refracts light wave, but on the other side of the lens L there is air, where *n* = 1. **Figure 6(c)** shows that the blurred image of two points near A can only be separated when their separation is greater than *r*. The *resolving power* of microscopes is thus defined by (3). Abbe concluded that the resolution of optical microscopes can be improved by filling the space between the sample and the lens with a transparent fluid, where $n \approx 1.5$. Immersion does thus reduce *r* from $\lambda/2$ to $\lambda/3$.

2.3. Rife's Method and Other Supermicroscopes

It has been asserted [3] that Rife could not overcome the diffraction barrier and that he did suppress it by applying the principle of reversibility [4]. Sorry, this principle is only valid in geometrical optics, since it implies that the direction of propagation of light is irrelevant for light rays. Diffraction of light that passes through a small circular hole or a narrow slit results from interference and cannot be eliminated, but **Figure 4** showed that the difficulty can be bypassed. How could Rife also do that without lasers?

Rife's contact with the Zeiss Company and his own observations made him aware of diffraction phenomena, but he found a very simple way to reduce their effects. He combined very high magnification with a pinpoint filter, which reduces the size of the Airy disc at A', as shown in **Figure 3(c)**. Probably, Rife did not mention this filter to protect his invention. It is even impossible to verify that he did use a pinhole filter, since his microscopes were dismantled. Rife constructed in 1932 a supermicroscope for a friend, who was a watchmaker and may have given advice for high precision tooling. This instrument was sold on auction in 2009, but the objective and ocular lens systems were missing, as well as the pinpoint filter [18].

It is very remarkable that *Gaston Naessens* (1924-2018) developed in 1949 another type of optical supermicroscopes with specialists of the Leitz Company in Wetzlar, Germany. This instrument reached a magnification of 30,000 and a sufficiently high resolution to see very small living entities. Naessens called them "somatides" and his microscope a "somatoscope". He observed that these somatides resulted from changes of size and form of normal bacteria. They could

pass through a simple or a complex life-cycle [19]. This is demonstrated in a short and very interesting video [20]. His microscope was also based on bioluminescence, but the exciting radiation was very intense UV and blue light of fixed wavelengths, respectively of 185 nm and 330 nm. Since excitation like that of Figure 3(a) requires a specific color, this was achieved by means of magnetic and electric fields, modifying molecular spectra in an adaptable way.

Since we ignore if he did also use a pinhole filter to achieve very high resolution, we wonder if other methods might have been used. This is conceivable, since Figure 7(a) accounts for excitation by means of UV light that allows for transitions (1) between the ground state S_o and a higher exited state S_2. The energy is then reduced, by modifying the configuration parameter s of the molecule. However, the curve $S_2(s)$ cuts the curve $S_1(s)$. The exited electron goes then over to the lower energy state, which allows for immediate light emission (2), called *fluorescence*. However, the excited electron can also go over from S_1 to another state T. It is a triplet state, since the spin of the excited electron has been reversed. We get thus an electron pair, where the total spin is 1 instead of 0 for singlet S states and the transition $T \rightarrow S_o$ is forbidden. The electron is thus trapped until it is thermally excited to reach again the level S_1. This allows for retarded light emission, known as *phosphorescence*. Since there is no fixed phase relation anymore with the exciting light, the emitted light waves are incoherent and cannot interfere.

Another method consists in placing a pinpoint filter precisely at the point A', as shown in Figure 7(b). This has mainly the advantage of improving depth sharpness, since light emerging from other planes than at A will not be focalized in the image plane A'. This type of *confocal microscopy* was invented and patented in the 1950th [21]. It allowed for laser scanning. Optical microscopy made thus remarkable progress, but the pioneers, Rife and Naessens were unjustly discarded from the list of honorable scientists.

They did use their microscopes for observing that bacteria can reduce their size and developed then methods for fighting sicknesses. Rife did this by resonance and Naessens by discovering drugs that he could observe to be efficient, but he was prosecuted for illegal exercise of medicine [22]. Rife and Naessens did not belong to the required corporation or caste. This mentality is akin to *racism*, since it was not even deemed necessary to check if their observations were correct and if their treatments were helpful or not.
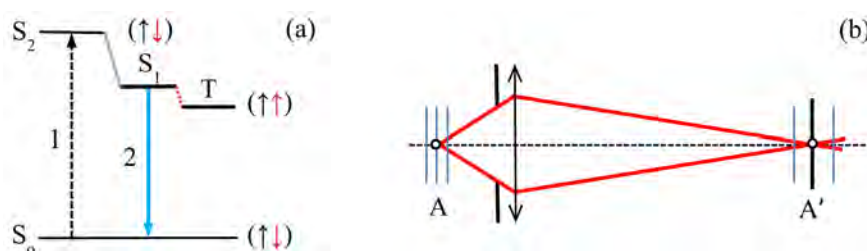
Figure 7. (a) Excitation of fluorescence and phosphorescence. (b) Confocal microscopy.

3. Biological Discoveries and Medical Applications

3.1. Pleomorphism Revisited

Antoine Béchamp, a compatriot of Pasteur, proved already by extensive experimentation that the size and form of bacteria can be modified [23]. He introduced the term *pleomorphism*, meaning more possible forms. He found that the smaller entities survive in chalk, but can reacquire their usual size and even become fungi. In 1886, Béchamp described "microzymas" (small ferments) that subsist as living entities after the death of organs, although it was believed that nothing can survive. These microzymas can also be present in living beings, where they cause diseases, but Pasteur did fiercely defend his conviction that all infectious diseases are only due to microbes of external origin. Béchamp was doctor of pharmacy and professor of chemistry. He became a medical doctor and then professor of medicine. He was a member of the French Academy, like Louis Pasteur, who was a chemist. Pasteur made very important discoveries, but was quite intolerant. He had even a feud with Robert Koch [24] and reacted so aggressively against Béchamp that monomorphism prevailed by docile consent of colleagues.

Nevertheless, Mrs. Henri of the Pasteur Institute in Paris observed in 1914 that anthrax bacilli change their form when they are subjected to ultraviolet light [25]. Monomorphism was also contested by the Swedish Biologist Ernest Almquist [26]. He wrote in 1922: "Nobody can pretend to know the complete life cycle and all the varieties of even a single bacterial species. It would be an assumption to think so."

Rife was not aware of these controversies or not interested. His aim was to observe the tiny microbes that he expected to exist. He succeeded and found even that "any alteration of artificial media (for culturing bacteria) or slight metabolic variation in tissues will induce an organism of one group to change over into any other organism included in that same group". These transformations are reversible, but the *bacillus typhosus* yields always turquoise-blue luminescent entities. For the *bacillus coli* it has a mahogany color, for *tuberculosis* it is emerald green and for the BX purplish-red.

Rife found that inoffensive bacteria become virulent when their size is reduced. He thought therefore that bacteria do not produce themselves diseases, but the microorganisms that result from their transformation. "If the metabolism of the human body is perfectly balanced or poised, it is susceptible to no disease". Rife added nine years later [12]: "with a pure culture of bacillus coli, by altering the media as little as two parts per million by volume, we can change that organism in 36 hours". In the initial medium, the micro-organism becomes again a bacillus coli. Continued microscopic study and stop motion photography confirmed the reversibility and revealed that the BX allows for "many changes and cycles."

In experimental animals, the BX produces "a typical tumor with all the pathology of true neoplastic tissue, from which we can again recover the BX mi-

cro-organism". They are even abundantly present. To be absolutely sure of this astounding result, Rife repeated these observations several hundred times. It should be noted that he tended to use the term "virus" for any type of filterable microbes, since the specific mode of virus reproduction was not yet known. The biologist Gaston Naessens observed pleomorphism in more detail. He presented clear evidence in a video [27] that the somatid found in blood can have a simple lifecycle or one with 16 different stages. Can these facts simply be negated, since they are not observable with standard optical microscopes? The books of Lynes [1] and Bird [23] denounce the enormous lack of scientific honesty in regard to the discoveries of Rife and Naessens.

Fortunately, it is possible to rediscover what is happening in Nature. Emmy Klieneberger-Nobel published in 1951 a thorough study of filterable forms of bacteria. She used a phase-contrast microscope, developed in 1942. It converts subtle phase changes of light waves passing through the specimen into amplitude modifications. They are made perceptible by reducing the amplitude of the background waves. This method made it possible to discover reversible changes of various types of bacteria, resulting from modifications of their environment [28]. According to her long list of references, she was not aware of the discoveries of Rife and Naessens, but the reality of pleomorphism was confirmed.

Kurath and Morita demonstrated in 1983 that marine bacteria are able to adapt themselves for survival under conditions of nutrient starvation [29]. The geologist Robert Folk discovered in the early 90th that precipitation of carbonates in hot springs of central Italy is due to modified bacteria. He studied them by scanning electron microscopy (SEM), proving that heir average size was 200 nm. In 1994, Folk attributed the observed carbonate precipitation to negatively charged cell walls. They attract Ca^{++} ions, neutralized by CO_3 ions, which yields chalk ($CaCO_3$) [30].

Kajander and Ciftcioglu proved in 1998 that blood can contain nanobacteria, associated with Ca^{++}, CO_3 and PO_4 [31]. Nanobacteria act then as crystallization centers that lead to the formation of kidney stones. The calcified envelope seems to provide a shelter for survival, since SEM micrographs revealed that they are still able of division. It appeared also that these nanobacteria are covered with a "hairy layer". Transmission electron microscopy (TEM) confirmed the existence of this coat of mineralized whiskers.

However, the existence of nanobacteria raised controversies, since it was generally believed that bacteria have to be big enough to accommodate DNA or RNA, as well as the required enzymes for autonomous replication. The opposition to the concept of pleomorphism resurged, but now because of molecular genetics. Ciftcioglu, Kajander *et al.* responded in 2006 by more facts: pathological calcification caused by nanobacteria does also account for gallstones, arterial heart disease, prostatitis, cancer and Alzheimer's disease [32]. They stated that research in this area has been "paralyzed for decades by attributing the calcifications to insignificant, passive, degenerative processes of aging".

The dermatologist Milton Wainwright published already in 1990 a book [33], where he presented important results concerning microbiological causes of cancer. He discovered that *scleroderma*, a rare form of cancer that leads to hardening of the skin and inevitably to death, is caused by microbes. Other outstanding physicians and medical research scientists had also demonstrated in the meantime that various forms of cancer result from nanobacteria, but the medical establishment did recklessly reject all proofs that contradicted the standard dogma. Wainwright's book of 2005 provides ample proof of this kind of "medical politics" [34].

Milton Wainwright recalled the battle between pleomorphism and monomorphism [35], since it is still going on. By dismissing this possibility, "we may be missing something of fundamental importance". A review [36] concluded in 2011 that "the evidence that nanobacteria exist in the human body and are closely associated with many kinds of diseases is now overwhelming". Nevertheless, it came still in 2011 to a categorical denial [37]. It refereed unjustly to a study of Ciftcioglu and McKay [38]. It was much more careful and mentioned that calcifying nanoparticles "do not fit the typical definition of life", but it could be too restrictive. Smaller forms have detrimental effects on human health and should be the "focus of future effort."

Cantwell insisted again in 2014 on existing evidence that cancer is caused by pleomorphic bacteria [39]. More and more justifications of the relevance of modified forms of bacteria in human pathologies have been published. Russian scientists presented in 2012 a review [40] where coccoid nanobacteria were reported to appear in sea water, soil, sedimentary and granite rocks, the Greenland ice sheet, glaciers and permafrost soils, as well as in humans and insects, for instance. Their size can be reduced to about 150 nm. This article contains several micrographs showing that ultramicrobacteria can make contact with one another by means of hair-like appendices. Banfield's team at the University of California, Berkeley, collected nanobacteria by filtering acetate-amended ground water [41]. These cells were immediately deep-frozen to prevent deterioration and brought to the laboratory, where they were analyzed by CryoTEM. It appeared that these nanobacteria are even quite common and well-adapted for survival under adverse conditions. A widely published micrograph [42] shows a coated spherical particle. Its diameter is close to 300 nm and its surface is covered with numerous *pili*, radiating outwards. Their length is about 50 nm. Their presence attracted our attention and will turn out to be very important.

Lida Mattman was an outstanding microbiologist. She confirmed pleomorphism and described the life cycle of various bacteria. Her textbook [43] concentrated on "cell wall deficient forms". They could result from an adaptation to increase protection against natural antibiotics, but they remained hidden in blood, though they are damaging. "Current bacteriology holds the belief that each cell species has only one simple form and retains it by reproduction". Nevertheless, they are able to "pass through stages with markedly different morphologies".

Dennis Claessen and his group at the Institute of Biology in Leiden discovered filamentous bacteria that are present in soils. He called them "actinomycetes". In response to stress, they can become cell wall deficient [44]. This may be a transient state, but also a lasting one. Pr. Claessen commented in an interview: "It gives a whole new understanding of the flexibility of microorganisms under stress and their ability to adapt to their environment." He published an article in 2019, where he reviewed recent progress concerning *stress induced* wall deficiency and pleomorphism [45]. He concluded that during the last decade, it became increasingly clear that "cells have a wide range of defense mechanisms to cope with various stresses." This is also clinically relevant, since morphological plasticity can cause reinfections.

It is particularly noteworthy that Rife discovered that deadly nanobacteria did thrive in tissues that had been treated by α, β and γ radiation or cobalt 60 gamma rays [46]. The idea that cancer results only from mutations, due to radiation damage and some chemical substances, needs revision, since we were not aware of pleomorphism, caused by stress.

3.2. Rife's Method for Producing EM Waves

His aim was not only to see small microbes, causing sicknesses and death, but also to destroy them. He suspected already 1915 that this might be possible by subjecting them to oscillating electric fields. He declared [8] that systematic experimentation started in 1920. At that time radio amateurs were very active. The carrier wave for radio frequencies had initially been produced by means of a sequence of sparks (in German: Funken, meaning also radio-emission). The sparks result from high tension, obtained by means of a Ruhmkorf induction coil and an interrupter. The electric field accelerates some stray electrons that become then able to ionize air molecules. This produces more free electrons in avalanche fashion, but recombination processes lead to a spark and rapid discharge. This is also relevant for lightning.

When it was realized that electrons can be emitted by a hot filament, it became possible to fabricate luminous diodes. However, Lee De Forest used a vacuum tube and invented the triode, where the amplified electron flux can be controlled. This "audion" could thus modulate a high frequency carrier wave at audio frequencies and was patented in 1908. Public broadcasting began in 1922 from the Eifel tower in Paris and in 1926, NBC started radio emissions in the USA, but Dr. Rife wanted only to produce radio waves of limited range. Their frequency should be adaptable and stable to allow for selective action on particular microbes. Being technically gifted and very creative, he did that by combining two existing inventions.

On one hand, the German physicist and glassblower Geissler had created in 1857 a *gas discharge tube*, still used today as a source of colored light. It consists of a sealed glass vessel that contains a noble gas at low pressure and two electrodes. There is no hot filament, but a constant high potential difference is ap-

plied to these electrodes. The resulting field accelerates free electrons that will then ionize atoms. At low pressure, they are diffused by collisions before emitting light. The whole tube becomes thus luminous and the color depends on the chosen gas.

On the other hand, Coolidge invented in 1913 an *X-ray tube* that was a glass sphere. A hot filament emitted electrons, bundled and accelerated in high vacuum by a strong electric field to impact the other electrode at high velocity. They were there suddenly decelerated, but basic laws of electromagnetism predict that when the velocity of electrically charged particles is reduced, they emit *braking* radiation (Bremsstrahlung). Deceleration of high velocity electrons produces X-rays. Their frequency spectrum is continuous, but there are also superposed narrow peaks, resulting from excitation of strongly bound electrons inside atoms of the anode. They return to their normal state by emitting photons of particular energy. These processes yield a beam of X-rays that is emitted at 90° when the flat anode is inclined at 45° with respect to the electron beam. Rife created a new system, represented in **Figure 8(a)**.

Actually, he replaced Geissler's tube by a hand-sized glass sphere and the hot filament of the Coolidge sphere by a cold metal plate. When the applied potential difference between the two electrodes exceeds a particular value, there appears a glow discharge. It results from the fact that a local space charge is created near the negative electrode and pushes some ions towards the cathode. It emits then electrons that are accelerated and ionize atoms of the noble gas. Its pressure is such that diffusion of excited atoms is limited, but the accelerated electrons are constantly slowed down and hit the anode at moderate energy. Being suddenly stopped, they produce braking radiation, but the energy of the emitted photons is lower than for Coolidge's X-ray tubes. The resulting *beam of radio waves* is also perpendicular to the electron beam and represented by points in **Figure 8(a)**. The lateral divergence of this beam is greater than for X-rays, because of the longer wave length.

The gas that surrounds the beam becomes luminous and such a diode is called a "phanotron". Rife tried different noble gases. He found that helium is preferable, since the impact of the lighter He^+ ions on the cathode increases its lifetime. **Figure 8(b)** indicates in a schematic way that the electric tension can be applied by modulating a signal of high-frequency F with rectangular pulses of lower
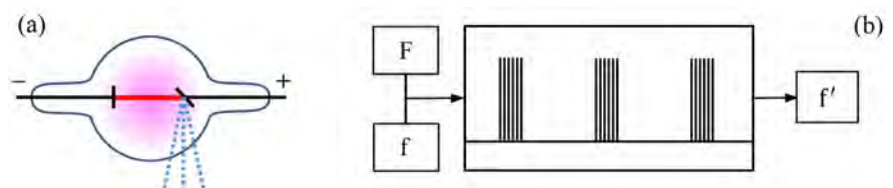
Figure 8. (a) Rife's *phanotron* is a gas-discharge diode, where an electron beam produces at 90° a beam of EM waves. (b) An electric signal of fixed high frequency F is combined with pulses at a particular audio-frequency f to produce sinusoidal oscillations of desired frequencies f'.

frequency f. Since avalanche phenomena distort these signals, the resulting EM wave is equivalent to a superposition of sinusoidal waves of various frequencies f' by Fourier transformation.

3.3. The Rife Frequencies and Evidence of Exploding Microbes

The history of the development of Rife's machine has been reconstructed in detail [47]. The report contains many photographs and includes new measurements. They were performed on rediscovered instruments or reconstructed ones, according to original schemes. This study was essentially concerned with engineering problems, but for us it is important that this system could produce electric fields that oscillate at any desired frequency f'. Rife provided a list of *resonance frequencies* for different types of microbes by observing their reaction with his microscope. Since they were definitively inactivated, he called them "mortal oscillatory rates".

He communicated his initial list in 1935 to the electronic engineer Philip Hoyland. He had been hired by Dr. Milbank Johnson who operated a "cancer clinic" that used Rife's method. Hoyland's mission was to construct a more compact version of Rife's machine. Electronics was constantly progressing, indeed. He determined also the resonance frequencies with Rife's microscope and Rife did control his measurements. He agreed with the fine-trimmed values of 1936. Table 1 provides the carefully established list. It appears in the report (p.103), but is rearranged here for increasing frequencies instead of the names the pathologies in alphabetic order.

To produce these frequencies, Rife bought commercially available equipment of top quality. He needed a sinusoidal carrier wave of authorized frequency and was allowed to emit at $F = 3,300,000$ Hz. This signal, modulated by rectangular pulses, was fed to the phanotron. The pulses were distorted by avalanche effects and possible frequencies were then determined by

$$F + nf = n'f' \tag{4}$$

The numbers n and n' can be 1, ±2, ±3, … The sidebands have decreasing intensities for greater values of these numbers. Table 1 tells us that the resonance

Table 1. The Rife-Hoyland list of resonance frequencies for different pathologies.

Frequency	against		
		549.07 kHz	Staphylococcus Albus
139.20 kHz	Anthrax	759.45 kHz	Typhoid Fever (rod)
191.80 kHz	Streptothrix	719.15 kHz	Streptococcus Pyrogen.
233.00 kHz	Gonorrhea	769.000 kHz	Tuberculosis (filterable)
234.00 kHz	Tetanus	769.035 kHz	Coli (filterable)
369.43 kHz	Tuberculosis (rod)	788.70 kHz	Syphilis
416.51 kHz	Coli (rod)	1.4452 MHz	Typhoid Fever (filterable)
426. 86 kHz	Spinal Meningitis	1.52952 MHz	Cancer Sarcoma (BY)
477.66 kHz	Staphylococcus Aureus	1.60745 MHz	Cancer Sarcoma (BX)

frequency for BX is 1607.45 kHz. It was thus produced by choosing f = 21.275 kHz, while n = -4 and n' = 2. This procedure is quite complicated, but similar to normal practice for broadcasting. It did also protect Rife's invention, without requiring patenting, since it was not easy to find the adequate value of f.

When Hoyland passed away, Verne Thomson became Rife's new engineer. He built several ray machines and verified that the fine trimmed resonance frequencies of Table 1 are correct. We see there that the resonance frequencies are different, but *unique* for any particular type of microbes. Rife attributed this fact to their "chemical constitution" (p. 20 of the report). It was not yet possible to be more explicit, but the empirical result was already very important.

Today, it is possible to use frequency generators and hand-held electrodes. We were surprised when we examined a system, promoted in a book (Frequenz Therapie, German Edition, 2014). It contains an enormous list of resonance frequencies, without explaining how they were determined. It states for instance that they are 21,275 Hz for the BX carcinoma and 20,080 Hz for the BY sarcoma. These values differ from those of Table 1. Moreover, the book preconizes for instance 11 frequencies against "lack of appetite". They are very low, since even 10 of them are situated between 20 and 1865 Hz, while 63 frequencies were listed to treat hepatitis C. This contradicts Rife's result: there is *only one* resonance frequency for every type of microbes. Another list of frequencies, claimed to be Rife frequencies [48] provides also many relatively low frequencies, without any detailed justification. Only 4 of the 11 frequencies of the previous list are given here for lack of appetite, but 52 frequencies are provided for cancer. They range between 120 Hz and 795.6 kHz. It is prudently stated that these frequencies are "only for experiments", but "you can see if they work for you". Anyway, the apparatus is sold with much publicity.

We are afraid, of course, that this kind of business can constitute a serious obstacle to scientific recognition of Rife's method and have to conclude that objective control and authorizations are needed, as for most professions and technical equipment. The biomedical engineer Marcello Allegretti reviewed medical applications of EM waves in several books, to make them understandable in general terms [49]. However, we never found an explanation of targeted destruction of microbes by resonance. It has to be possible for any real phenomenon.

Our first task was therefore to verify if there are visual proofs of the efficiency of Rife's method. In addition to the trustable test for curing cancer patients, Rife made numerous microphotographs and movies to document his observations [50], but nearly all of them were stolen or destroyed. Nevertheless, some proofs were saved. We recommend two easily available videos [51] to see with our own eyes what happens. The video "Royal Rife-in his own words" shows instruments, procedures and (at minute 6:58) the turquoise-blue nanobacteria that he discovered. "The Royal Rife story" shows several times bursting bacteria (6:45, 6:59, 7:12, 8:37 and 9:07). Other videos [52] provide more background information.

John Crane presents in "Dr. Royal Rife's 1939 lab film" the working place and equipment, used by Rife. The first pictures of the BX (14:33) were taken with

Rife's microscope of 1922. Bacteria are much larger and could already be observed with standard optical microscopes, even when they exploded (34:25, 34:45 and 35:15). The longer version of "Rife in his own words" displays turquoise-blue nanobacteria (7:39) and green ones (8:53). Drawings of the BX and the BY entities (15:23, 16:23) indicate the presence of pili on their surface. Nanobacteria can even be seen together with the corresponding bacteria (41:12). "The Rife story" includes more images of exploding bacteria (15:48, 16:02, 16:15, 1.56:03 and 1.56:14).

4. Explanation of Microbe Destruction by Resonance

4.1. Formulation of the Basic Problem

The first method that is customarily used when we are faced with unexplained phenomena is to make them plausible by referring to *analogies*. In a video of outstanding pedagogical quality, the music professor Anthony Holland used this method, since it is possible to shatter a wine glass by sound waves of adequate frequency [53]. The resonance frequency can be determined by tapping the wine glass or by rubbing its rim with a moist finger. The resulting stick-slip friction yields a continuous sound as for the bow and a vibrating string of violins. Though there are several modes of vibration for wine-glasses and bells, the dominant one corresponds to deformations of the rim along two orthogonal axes, as indicated in Figure 9(a). When the intensity of the exciting sound wave is strong enough, the glass is shattered, since it is quite brittle.

The relevant concept can be visualized in a more transparent way by means of a loop of steel wire, attached to a vertical vibrator that is activated by a frequency generator. There appear then "standing waves" with 4 knots for the lowest resonance frequency. More knots than in Figure 9(a) are also possible at higher frequencies. Figure 9(b) represents a "singing bowl". This is a very old musical instrument, still used in China, Tibet and other Asian countries. It was made of bronze and vibrates like a wineglass, but does not break. When it is partly filled with water, bouncing droplets appear for strong enough excitation [54]. Nevertheless, these systems provide merely examples of *normal* resonance phenomena. Small scale surface waves of water result from surface tension and it is well-known that cohesion can then lead to the formation of drops.
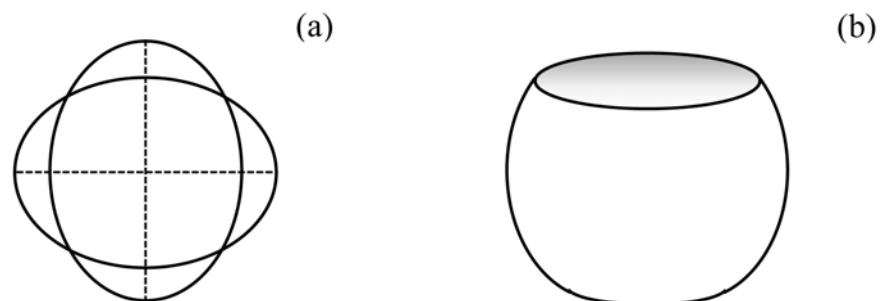
Figure 9. (a) Deformations of a vibrating wine glass. (b) A singing bowl or standing bell.

The spectacular collapse of the Tacoma Bridge is often cited as an example of resonance phenomena, but this resonance concerned a twisting vibration of the bridge that caused turbulent wind. This turbulence amplified the vibration and vice-versa, as visually explained in a video [55]. Positive feed-back can thus lead to *auto-amplification* and stronger resonances than normal ones. We will show that targeted destruction of viruses and other microbes results from such a mechanism and does also end with fatal disruption.

Anthony Holland did perform himself experiments concerning the effects of EM waves. He showed the results for a harmless unicellular organism, called "blepharisma". Its usual size is 75 - 300 μm and can thus easily be observed with a standard optical microscope. These entities are elongated and their surface is uniformly covered with short hair-like organelles (see Wikipedia). Holland's video [53] shows (at minute 10:43) that the membrane displays a blister before breaking up (11:13). It is interesting that another blister was forming at the other side (11:03) and that a small apparently exploring entity was unaffected at the imposed frequency. Holland showed then also exploding leukemia cells (13:00-13:24), by using the phanotron of a "Bare/Rife device".

James Bare is an MD, wanting to help patients. It is respectable that he tried to understand what happens, but it is instructive to examine his attempted explanations to become aware of possible pitfalls. The term "resonant light technology" is not adequate, since the resonance is due to an EM wave and not by the luminous electron beam. Dr. Bare knew that, but he thought that it constitutes a "small antenna". He mentions even "solitons" [56], but an antenna is only a conducting wire, where electrons are set in longitudinal oscillation to produce a standing wave with maximal amplitude at both ends. This is the usual way to create EM waves, but we explained already that Rife produced EM waves by deceleration of electrons in the anode.

Since the microscope revealed that the membrane of nearly spherical cells was locally broken up, Dr. Bare and collaborators thought that the resonance is due to the hole. A spherical vessel with a short neck constitutes a "Helmholtz resonator", since the air in any closed vessel acts like a spring on the oscillating air in the neck. The resonance does spontaneously appear when an airstream is blowing fast enough over the opening, since stationary waves are then excited by turbulence, as inside some flutes. However, there is only one resonance frequency for a given size of the vessel and its neck, since there is a single oscillator. For flutes, there are several possible standing waves of different frequencies. Actually, the hole in the membrane of an exploding cell is a consequence of Rife's resonances and not its cause.

To explain the destruction of viruses and microbes by resonance, it is necessary to start with adopting an adequate model. Holland's analogy with shattering a wine glass could suggest that Rife excited deformations of the cell body. This would yield an ensemble of resonance frequencies [57], while Table 1 attributes only one resonance frequency to any particular type of microbes. Another possi-

ble hypothesis would be an electric polarization of the cell body. This mechanism leads to a resonance for particles that are very small compared to the wavelength λ of EM waves. They are bathing in a homogeneous electric field that induces surface charges, creating a secondary electric field inside the particle. It leads to a resonance for dipole oscillations. This accounts for the blue sky, since the electric field of sunlight does polarize very small particles in atmospheric air. This resonance frequency is situated in the domain of UV light and energy is only *absorbed* at this resonance frequency, but scattered at neighboring frequencies. This so-called "Rayleigh scattering" of sunlight results from the induced polarization. It is more intense for blue than for red light. This theory applies also to collective oscillations of electrons in very small metal particles and allowed us to explain the "anomalous optical absorption" of thin granular metal films [58]. The same theory explains the resonance that radio-waves produce in red blood cells [59]. However, the mechanism of Rife's resonance phenomenon is different and has not yet been explained.

4.2. Structure and Function of Virus Spikes

The Covid-19 pandemic and images of the relevant viruses suggested to the author that their spikes might be set in oscillation and could perhaps lead to a devastating resonance. We will test this hypothesis by establishing the relevant equation and solving it, but first of all, we had to know more about the structure and function of virus spikes. They are not merely flower-like decorations, but very efficient weapons for attacking cells, in order to use their machinery to reproduce themselves in great numbers.

The so-called "Spanish flue" of 1918 was due to a virus. It infected some 500 million people and killed at least 20 million persons [60]. This virus became more lethal during the pandemic, since its mutation led to a second wave, where lungs were filled with blood. The Corina-19 virus appeared in China and was partially controlled by containment, but not stopped. Social proximity, increased population densities, worldwide mobility and interwoven economies are major factors of its spreading. We see also that the search and testing of vaccines take time. Even a vaccine cannot protect us against unpredictable new mutations and the possible appearance of more virulent forms. It would thus be irresponsible to neglect already existing evidence that an *efficient, safe and rapidly adaptable biophysical method* is possible.

Rife's method could have been tested at least by means of experimental procedures, but it was rejected since it seemed to be unbelievable. Nevertheless, it is also necessary to explain why the reported facts are true. We are thus confronted with a basic scientific problem. There are numerous examples, indeed, where something unexpected was discovered. It concerned still *hidden realities*. How can we get access to anything that is not directly observable? We have to imagine what might happen, draw logical consequences from this hypothesis and verify then if they are true or not. The first problem is thus to select a plausible hypo-

thesis, deserving rigorous analysis ...

It became possible at about 1980 to combine cryogenic electron microscopy with gene sequencing to understand the role of spikes. The resulting knowledge is summarized in Figure 10, but for clarity, we represent only one pair of macromolecules, while the flower-like hemagglutinin (HA) spikes contain 3 identical pairs. We are now accustomed to artistic representations, but they do not reveal what is essential. Figure 10(a) represents the normal state of the associated HA1 and AH2 proteins. The HA1 molecule contains negative charges (COO^-) that belong to small sialic acid molecules that can move inside the molecule. Because of their mutual repulsion, they create surface charges. Electrostatics tells us that its density depends on the configuration of the surface and has to be greater near the pointed tip of the HA1 molecule.

These charges polarize the electrically neutral HA2 molecule, which is a slender, helicoidally wound molecule. It tends to be straight, but is bent and kept in this state, because of the increased surface charges at the lower end of the HA1 molecule. The middle part of the coil spring is more irregular than indicated here, but it is only important that we get a *loaded spring trap*. It is anchored in the membrane of the virus. Tts extremity, represented in green in Figure 10(a), is situated on the other side of the membrane of the virus. It is electrically charged and thus hydrophilic. This is usually sufficient to secure the implantation, but not for very strong traction.

Figure 10(b) shows what happens in the vicinity of a cell. Its pores allow ion transport that maintains a potential difference between the inner and outer surface of its membrane. This leads to an increased density of H^+ ions near the external surface. When a virus comes close to the membrane, these protons reduce the surface charge density of the HA1 molecule, since $COO^- + H^+ \rightarrow COOH$. The remaining surface charge is then too small to keep the HA2 spring in its bent state. It is suddenly released and its tip carries a fusion protein, indicated in red. It penetrates the membrane and this occurs simultaneously for the three HA
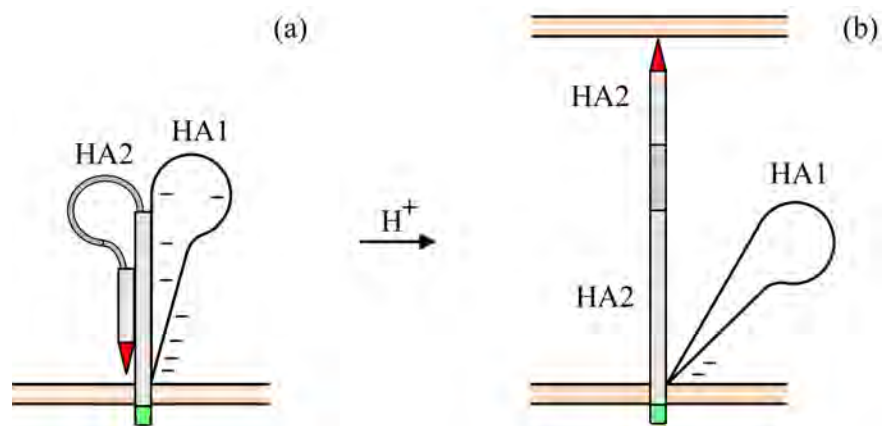
Figure 10. Schematic representation of one pair of HA1 and AH2 molecules, constituting spikes of viruses. (a) In the normal state, the helically wound molecule HA2 is bent and kept in place like a loaded spring. (b) It is released by neutralization of the HA1 molecule.

pairs. The redundancy strengthens the grabbing, as well as the rooting. Moreover, the structure of the HA1 part is modifiable by mutations to prevent the immune system from recognizing the potential invader. Viruses are terrorists, carrying jackknifes under a coat. They are ready for stabbing cells that are in reach and their camouflage can be modified to escape detection. The HA2 part is on the contrary strictly conserved. This ingenious system was elaborated by natural selection, governed by survival of the fittest.

The existence of this war machine was recognized in 1993 [61]. To highlight the rapidly expanding research on this subject, we mention the review of the virologist Suzuki and a molecular biochemist [62]. Professor Stephen Harrison of Harvard medical school presented this theory in an excellent video [63] and explained how the spikes help the virus to penetrate into the cell [64]. We insist more on explaining the mechanism of automatic triggering. It is known that spikes of the SARS-2 virus have a conical form [65]. It differs from usual representations, although it is also attached to the membrane by a thin stalk.

4.3. Other Spikes of Viruses and the Pili of Bacteria

So far, we described only virus spikes that are made of hemagglutinin (HA), but viruses do also have another type of spikes. They are constituted of 4 neuraminidase (NA) proteins, which are also electrically charged [66]. 18 variants of HA and 11 subtypes of NA are known [67]. The phylogenic tree of the Corona virus [68] indicates thus quite great variability. Viruses were modified to become more efficient. The influenza virion carries 300 to 400 HA spikes and 40 to 50 NA spikes. Their relative numbers have to be balanced [69], since they cooperate to help the virus to get inside the pirated cell. The diameter of the spherical core of usual viruses is about 120 nm. The length of HA spikes can be about 12.5 nm long, while the length of NA spikes is slightly smaller or greater.

Rotaviruses are different. They contain double-stranded RNA, instead of single-stranded one and are said to be non-enveloped. Actually, the lipid bilayer is replaced by a tightly fitting protein coat, but there are always spikes that undergo conformational changes and perforate the lipid bilayer of the target cell [70]. *Bacteria* are endowed with long corkscrew-like flagella. They allow for efficient propulsion, since they are activated by small individual motors, embedded in the cell membrane, but the whole surface of bacteria is covered with *pili*. The growth and molecular constitution of these hair-like structures are now well-known. The major part is a helical fiber with a sticky tip. This allows for adhesion and some stretching that causes retracting forces. The rod is hollow and can even allow for DNA transfer, but is also an electron conductor. The main function of pili or cilia of bacteria is to sense their environment and to facilitate sexual reproduction by fusion with the same type of bacteria. Antibacterial molecules interfere with this process, but do not prevent survivors from producing protective mutations. For us, it is essential that pili do also carry positive and negative parts [71], since that offers the possibility to act on them by means of an oscillating electric field.

4.4. The Normal Resonance and Parametric Amplifiers

To facilitate a rational understanding of Rife's resonance, we begin with analyzing the properties of a simple and familiar system. A pendulum is merely composed of a mass M, suspended at a fixed point by means of a string of constant length L. Figure 11(a) shows that an angular displacement θ with respect to the vertical implies a horizontal displacement $x = L\sin\theta$. The mass M is subjected to the gravitational force $F = Mg$. Its tangential component $F\sin\theta = Mgx/L$ is proportional to x, but opposite. This restoring force tends to reestablish equilibrium, but once the pendulum has started to oscillate, it has the tendency to remain in this state of motion. To show why and to make scientific reasoning accessible to non-specialist, also for later generalizations, we recall Newton's law. It states that the product of the mass M and its instantaneous acceleration $\ddot{x}$ is always equal to the sum of all applied forces. When air friction is negligible, we get thus for small angular displacements

$$M\ddot{x} = -\frac{Mgx}{L} \text{ or } \ddot{x} + \omega_o^2 x = 0 \text{ where } \omega_o^2 = \frac{g}{L} \tag{5}$$

Every dot indicates a derivation with respect to the time variable t. The solution of this equation is $x(t) = C\sin(\omega_o t + \varphi)$ and accounts for free oscillations. The (angular) frequency ω_o is determined by the value of the local gravitational acceleration g and the length L of the pendulum. The values of the amplitude C and the phase φ depend on the initial conditions. Indeed, a child that is sitting on a swing can initiate free oscillations by pushing with its feet on the ground. This means that $x(0) = 0$ and therefore $\varphi = 0$, but the initial velocity $\dot{x}(0) = \omega_o C$. The amplitude C depends then on the impulse for starting the oscillation.

If air friction were really negligible, the amplitude C would remain constant. Actually, the oscillation is progressively damped, since the mass M is subjected to air friction. This braking force is proportional to the instantaneous velocity $\dot{x}$ and depends on the cross-sectional area. However, the oscillations can be sustained by means of a push at the adequate rhythm. The mathematical treatment is simplified for a constantly applied driving force that oscillates at some frequency ω with constant strength S. The equation of motion is then
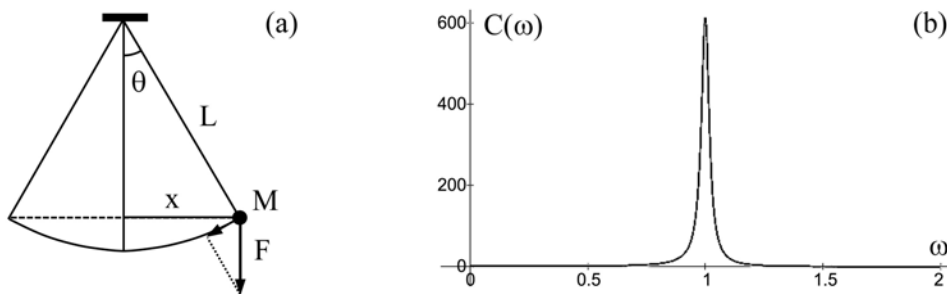
Figure 11. (a) Parameters needed to describe the motion of a simple pendulum. (b) The peak for possible amplitudes of forced oscillation is very high and narrow for low friction.

$$\ddot{x} + \omega_o^2 x + 2v\dot{x} = S\sin(\omega t) \tag{6}$$

Thus,

$$x(t) = A\sin\omega t + B\cos\omega t = C\sin(\omega t + \varphi) \tag{7}$$

The solution (7) describes *forced oscillations* that subsist when the initial conditions are not relevant anymore, because of damping. The mass M is oscillating at the imposed frequency ω, but the constants A and B are determined by substituting Equation (7) in Equation (6). We get then

$$(\omega_o^2 - \omega^2)A - 2v\omega B = S \quad \text{and} \quad (\omega_o^2 - \omega^2)B + 2v\omega A = 0$$

Thus,

$$A = \frac{(\omega_o^2 - \omega^2)S}{(\omega_o^2 - \omega^2)^2 + (2v\omega)^2} \quad \text{and} \quad B = \frac{-2v\omega S}{(\omega_o^2 - \omega^2)^2 + (2v\omega)^2}$$

Because of (7), $C^2 = A^2 + B^2$. The amplitude of the forced oscillation is therefore

$$C = \frac{S}{(\omega_o^2 - \omega^2)^2 + (2v\omega)^2} \quad \text{while} \quad \text{tg}\,\varphi = \frac{2v\omega}{\omega^2 - \omega_o^2} \tag{8}$$

These expressions describe the *normal* resonance phenomenon. Rife's resonance is more powerful, but the first relation (8) is already very useful to understand the physical meaning of resonances. The amplitude C of forced oscillations is maximal when the denominator is minimal, this happens when its derivative with respect to ω is zero and thus when $\omega = \omega_v$, where $\omega_v^2 = \omega_o^2 - 2v^2$. When friction is sufficiently small ($v \ll \omega_o$), the graph of $C(\omega)$ displays a symmetric peak that is centered on ω_o. The resonance frequency has thus the same value ω_o as for free oscillations. Figure 11(b) provides the graph of $C(\omega)$ when $S = 1$, $\omega_o = 1$ and $v = 0.02$.

In general, the height of the peak is $S/4v^2$ and its width at half height is equal to v. The resonance becomes thus sharper for decreasing friction. The amplitude C would even become infinite in the absence of friction. The second relation (8) predicts the phase difference φ for different values of ω. This function is represented in Figure 12(a) for $\omega_o = 1$ and $v = 0.02$. The change of sign means that the oscillator is able to follow the rhythm of the applied force when the imposed frequency is lower than ω_o, but it stays behind when it is too fast.

We are now ready to answer a simple question: is a child, sitting on a swing, able to sustain itself the oscillations without any external help? Probably, you found the answer yourself by trial and error. It is fun to make discoveries and to master a situation oneself. It is even much more interesting and surprising to understand why this is possible. The child has to straighten up when it is approaching the highest points and to incline backwards when it is moving towards the other side. The effective length L of the pendulum is thus modified as shown in Figure 12(b).
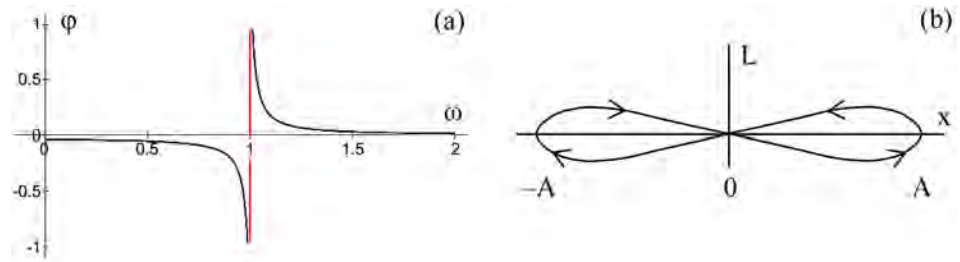
Figure 12. (a) The phase difference between the forced oscillation and the applied force. (b) This type of periodic variations of the effective length L of the pendulum yields a parametric amplifier.

The variation of L can be approximated by the function

$$L(t) = L_o \left(1 + 2\gamma \sin 2\omega t\right) \text{ when } x(t) = A \sin \omega t$$

The variation of the parameter L is adapted to the actual frequency of oscillation, but the equation of motion (6) is then modified. It yields

$$\ddot{x} + \omega_o^2 \left(1 - 2\gamma \sin 2\omega t\right) x + 2\nu \dot{x} = 0 \text{ when } S = 0 \tag{9}$$

To solve this equation, we note that

$$2 \sin 2\omega t \sin \omega t = \cos \omega t - \cos 3\omega t \tag{10}$$

This relation was proven in trigonometry, without mentioning its physical importance. The fact that the product of two oscillating functions is equivalent to a sum of two oscillating functions implies that Equation (9) is equivalent to

$$\ddot{x} + \omega_o^2 x + 2\nu\omega A \cos \omega t = \gamma \omega_o^2 \left(\cos \omega t - \cos 3\omega t\right)$$

The periodic variation of the length L produces thus two oscillating *driving* forces. The first one does exactly compensate friction when $\omega = \omega_o$ and $\gamma = 2\nu/\omega_o$. The other force has negligible effects, since the frequency 3ω is too far away from the resonance frequency. The child can thus sustain the oscillations by its own muscular forces. Greater values of γ will not only compensate energy losses, but increase the amplitude. The system becomes then a *parametric amplifier* until equilibrium is reached. This can easily be verified by attaching a small mass on a string that is partially wrapped around a pencil. It is sufficient to rotate the pencil towards the left and the right at the adequate rhythm. Trapeze artists apply this method at a human scale.

We transposed this theory to explain the mysterious phenomenon of *ball lighting* [72]. Since skeptics did simply attribute it to illusions, in spite of numerous testimonies of serious witnesses, it is useful to show how the explanation was found. The example is also adequate to illustrate the method of imagining what is hidden and verifying if the logical consequences do agree with all observed facts. We assumed that ball lightning is similar to a soap bubble, but that the membrane is luminous, since it contains ionized air. However, light emission results from recombination processes. The luminosity should decrease very rapidly, as for ordinary lightning. The difference is that the membrane allows for collective motions of the free electrons with respect to the heavier ions inside the

membrane. The frequency ω_o of this "plasma oscillation" is determined by the density of free electrons, but they are radially oscillating inside the membrane. This makes the external surface alternatively positive and negative. Ball lightning does thus alternatively attract electrons and positive ions that are present in the ambient air near its surface. This replenishes not only the stock of charged particles, but modulates also the oscillation frequency as in Equation (9). This leads to *auto-oscillations*. They are sustained without requiring constant excitation by an oscillating electric field of external origin.

How can we test the validity of this explanation? The answer is that it accounts for apparently mysterious observations. Indeed, ball lightning is usually moving around in an apparently erratic way. We can now "mentally see" that it is constantly attracted towards the greatest density of charged particles in the ambient medium. It behaves thus like a living being that survives by feeding itself. Moreover, ball lightning can suddenly disappear in midair, as if the light had been extinguished. This is due to entering a region where the ambient air was not sufficiently ionized. It can also happen that ball lightning explodes, even very violently. The invisible cause is a locally greater ionization of the ambient air, which led to fatal parametric amplification. Although this was a digression, it is useful to understand an essential feature of science and to be prepared for another intellectual adventure. It concerns the destruction of viruses and other microbes by means of resonances, but they are quite special.

4.5. The Peculiar Resonance of Virus Spikes

The analogy with shattering a wine glass [49] is useful as a first approximation. It begins also with determining the resonance frequency and an experienced singer is able to produce a sound wave of precisely the same frequency. With laboratory instrumentation, we can prove that there are several possible ones and select one of these frequencies to produce a resonance [73]. Spikes can also be set in forced oscillations, but the resulting resonance is more powerful than normal resonances. Figure 13(a) shows the outline of the spikes of the Corona virus, according to data obtained by means of cryo-electromicrography [74]. The spike is normally straight and we know that its upper part is negatively charged. Figure 13(b) reduces the spike to its essential elements. It is then similar to a *cantilever* that is implanted in a larger body, but can be bent, when its effective tip
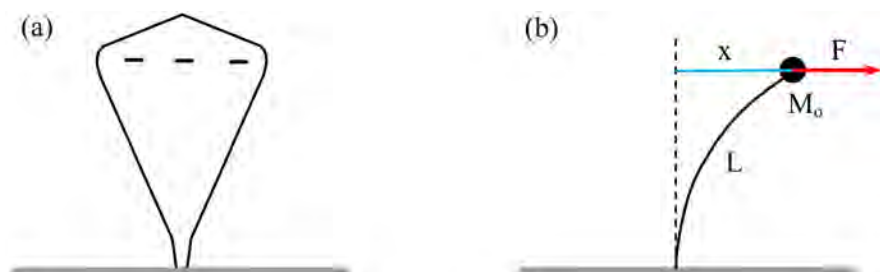
Figure 13. (a) The global shape of a Corona virus spike in its normal state. (b) The applied force produces a lateral displacement and allows for a powerful resonance.

mass M_o is subjected to a lateral force F. It produces then a displacement x with respect to the symmetry axis. How does it vary for an oscillating force?

Fortunately, Friswell's team established already in 2012 the equation of motion for *energy harvesters* [75]. They consist of a homogenous elastic beam that carries a tip mass and is implanted on a chariot. It is set in motion by random oscillations of a bridge and the resulting kinetic energy is transformed by detectors into electric energy. We adapt their equation to describe possible vibrations of virus spikes. The difference is only that their base remains fixed, while the oscillating force F is directly applied to the tip mass M_o. Although the stem of the spike is not homogeneous, we can keep the model of a uniform beam by defining average values. However, the spike is surrounded by a fluid instead of air and thus subjected to viscous friction. The equation of motion is then

$$M_o \ddot{x} = F(t) - \sigma \dot{x} - \left[k + a\left(\ddot{x} + \dot{x}^2\right)x + bx^2 \right]x \tag{11}$$

where

$$M_o = M + 0.227 L\mu + \frac{2.467}{L^2}I \quad \text{and} \quad k = \frac{3.044}{L^3}EI - \frac{1.234}{L}gM - 0.367 g\mu$$

$$a = \frac{1.523}{L^2}M + \frac{0.276}{L}\mu + \frac{6.091}{L^4}I \quad \text{and} \quad b = \frac{3.756}{L^5}EI$$

The effective mass M_o is thus defined by the real tip mass M, the length L of the beam and its averaged mass density μ. It is also necessary to account for the moment of inertia I of the spike with respect to the fixed point. The stiffness of the beam is mainly determined by the coefficient k, which depends on Young's modulus E of the constituting material, the length L of the cantilever and its moment of inertia I. For energy harvesters with a very flexible beam, the weights of the tip mass M of the beam will reduce the restoring force. This allows for two lateral equilibrium positions along a given direction. The nonlinear terms of Equation (11) lead then to *chaotic* behavior. where the tip mass can execute small oscillations around one of the possible equilibrium positions, but also pass from one side to the other. Indeed, very small changes of the instantaneous position and velocity at critical moments will produce qualitatively different motions. For spikes, surrounded by a fluid, we can neglect the weights because of buoyancy, but the nonlinear effects remain important. Actually, the equation of motion (11) is reduced to

$$\ddot{x} + \omega_o^2 x + 2\nu\dot{x} + 4\gamma\left[x\ddot{x} + \dot{x}^2 + \beta x^2\right]x = S\sin\omega t \tag{12}$$

$$\omega_o^2 = \frac{k}{M_o} = \frac{3.044 EI}{L^3 M_o}, \quad \gamma = \frac{a}{4M_o} = \frac{0.381}{3.467 L^2} \quad \text{and}$$

$$\beta = \frac{b}{aM_o} = \frac{2.466}{1.523}\frac{EI}{L^3 M_o} = \frac{1.619}{3.044}\omega_o^2$$

The spike does not simply behave like an inverted pendulum, since Equation (6) is generalized. The nonlinear terms depend on the instantaneous values of the displacement x, the velocity $\dot{x}$ and the acceleration $\ddot{x}$. When the tip mass is dominant, $I \approx ML^2$ and $M_o \approx 3.467 M$. Measuring the displacement x in units $L =$

1, we get then $\gamma = 0.110$ and $\beta = 0.532\omega_o^2$. Since forced oscillations occur at the imposed frequency ω

$$x = C\sin(\omega t + \varphi), \quad \dot{x} = \omega C\cos(\omega t + \varphi) \quad \text{and} \quad \ddot{x} = -\omega^2 x$$

The value of φ depends on v, but when $\alpha = \omega t + \varphi$, we get always

$$4x^3 = C^3(3\sin\alpha - \sin 3\alpha) \quad \text{and} \quad 4\dot{x}^2 x = \omega^2 C^3(\sin 3\alpha + \sin\alpha)$$

The nonlinear terms in Equation (12) are again equivalent to adding two forces. They oscillate at the frequencies ω and 3ω. The first one modifies the applied force and the second force can be neglected, since the frequency 3ω is too far off-resonance. To concentrate on essential features for the resonance, we assume that friction is negligible ($v = 0$ and $\varphi = 0$). The amplitude C of forced oscillations is then determined by Equation (12), which yields

$$\left(\omega_o^2 - \omega^2\right)C\sin\alpha + 2\gamma\left(\omega_1^2 - \omega^2\right)C^3\sin\alpha = S\sin\omega t$$

Indeed, $4\left(x\ddot{x} + \dot{x}^2 + \beta x^2\right) = \left(3\beta - 2\omega^2\right)C^3\sin\alpha$ and $\omega_1^2 = 3\beta/2 = 0.798\omega_o^2$. The amplitude C of forced oscillation is thus determined by the cubic equation

$$\left(\omega_o^2 - \omega^2\right)C + 2\gamma\left(\omega_1^2 - \omega^2\right)C^3 = S \tag{13}$$

Thus

$$C = C_o(\omega) = \frac{S}{\omega_o^2 - \omega^2} \quad \text{when} \quad \gamma = 0$$

without nonlinear effects, we get the *normal* resonance. It corresponds to (8), but is simpler, since $v = 0$. It is represented by the black graph in **Figure 14(a)** and represents the actual amplitude of forced oscillations with a change of sign below and above the resonance frequency. It differs from **Figure 11(b)**, which accounted only for the magnitude of $C(\omega)$ when $v = 0.02$, while the sign was determined by **Figure 12(a)**. Nonlinear effects do modify the response of spikes, since Equation (13) allows for 3 possible solutions and in particular for
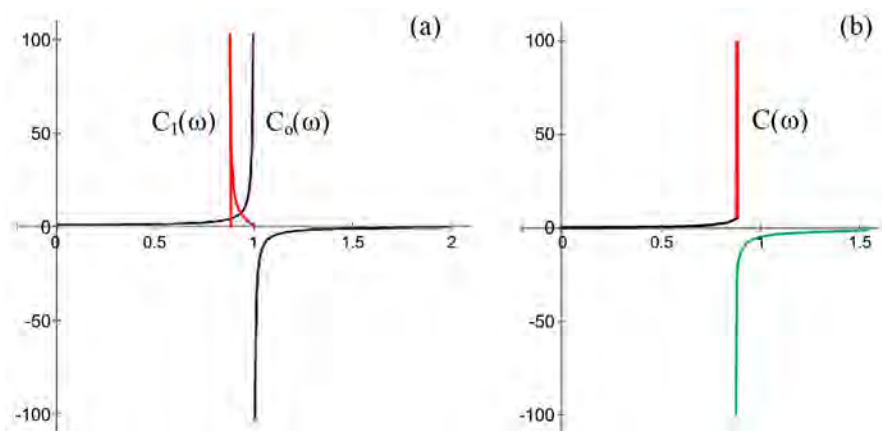
Figure 14. (a) The amplitude of forced oscillations of spikes would be $C_o(\omega)$ without nonlinear effects. The resonance frequency is then $\omega_o = 1$. Nonlinear effects allow for auto-oscillations, characterized by $C_1(\omega)$. (b). This leads to a *synergy* when it is combined with constant excitation and yields then $C(\omega)$.

$$C = 0 \quad \text{or} \quad C^2 = \frac{\left(\omega_o^2 - \omega^2\right)}{2\gamma\left(\omega^2 - \omega_1^2\right)} \quad \text{when} \quad S = 0$$

We expected, of course, that without excitation there is no response, but because of nonlinear effects, spikes are able to produce a driving force that yields *auto-oscillations*. This is similar to what happened for a pendulum, when its effective length was periodically modified, but the reason is different. Now, it does not compensate friction, since we considered even the case where $v = 0$. The stiffness of spikes allows them to oscillate by themselves, but only in a limited frequency domain, since C^2 has to be positive to yield a real value for the amplitude C. It is necessary that $\omega_1 \le \omega \le \omega_o$, The resulting function $C_1(\omega)$ is represented by the red curve in **Figure 14(a)**. It defines the amplitude of the auto-oscillation and diverges when $\omega = \omega_1 \approx 0.9\omega_0$. There is a resonance, but at a lower frequency than for the normal resonance. Equation (13) tells us what happens when the spike is constantly subjected to an excitation of strength S, oscillating at some given frequency ω. The normal resonance is then modified, since $C_o(\omega)$ has to be replaced by a function $C(\omega)$ that is represented in **Figure 14(b)**. It can only be defined by *real* solutions of (13). This yields 3 curves represented in different colors. They are simultaneously possible in a very small frequency domain (from 0.8933 to 0.89621 when $\omega_0 = 1$).

The rigorous treatment of this problem was necessary, because of past contestations. It is also instructing from a theoretical point of view, since it illustrates the usually hidden mechanism of nonlinear systems. Moreover it is and should be of great practical importance. We can now harvest the fruits. We measured displacements in units $L = 1$, but when the mass M is dominant, the moment of inertia I is proportional to L^2. The value of ω_1^2 is thus proportional to $1/L$. The resonance frequency is greater for short spikes, since they are stiffer. However, $\gamma \approx 0.11/L^2$. The amplitude of forced oscillations is thus proportional to $L^2 S$ and greater for long spikes than for short ones. Moreover, there is only *one* resonance frequency for every particular type of microbes, in agreement with Rife's measurements. Since its value ω_1 does not depend on the strength S of the applied force, it is sufficient to determine ω_1 for *one* particular strength S, although greater values of S do increase the amplitude of forced oscillations. Empirical discoveries can make sense, of course, without understanding the underlying mechanism. It is then only necessary to verify that the observed facts are trustable. When it turns out that they are real, they have to be explained, but that requires other methods and may be delayed.

4.6. The Mechanism of Targeted Microbe Destruction

Constructing a theory consists in choosing a plausible hypothesis and deducing logical consequences. Even a correct theory is only valid when its predictions agree with all known facts and further experimental verifications. **Figure 15(a)** represents a cantilever that is set in forced oscillation at a frequency ω that is close to the resonance frequency. When $\omega = \omega_1$, the amplitude C of the oscillation
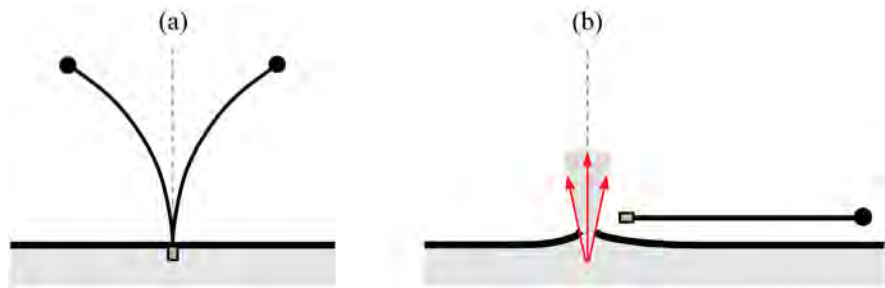
Figure 15. (a) Forced oscillations of a spike or pili. (b) At resonance, it is extracted and creates a hole in the membrane that destroys the microbe by extrusion of its content.

becomes quasi infinite, even when friction is not totally negligible. Resonance would thus imply enormous stretching of spikes or pili, if they were solidly implanted in the membrane or any equivalent structure. Normally, this would cause plastic deformations and eventually fracture, but that is replaced by extraction from the membrane and creation of a hole.

This causes expulsion of the content of the virus, as represented in **Figure 15(b)**. The virus is definitively destroyed. We recall that spikes are only fastened by the hydrophilic tail of their backbone, represented in green. This fixation is usually sufficient, but not secured, as can be achieved by means of bolts and screws. This system was invented in Antiquity at about 400 BC and it was recognized that the screw has to be well-tightened. The explanation is that dry friction between nonmoving surfaces is greater than kinetic friction and increased by pressure. This insight came much later and required even repeated discoveries [by da Vinci, Amontons and Coulomb, respectively at about 1500, 1700 and in 1785]. The fastening of spikes is improved by triple implanting, but not enough to resist at the resonance frequency. Even trees can be deracinated by strong wind, in spite of their distributed roots.

This theory applies also to *pili*, covering the surface of bacteria and nanobacteria. Since they carry electrical charges, they can also be set in forced vibrations by an oscillating electric field. They behave like cantilevers that can be elastically bent, but because of nonlinear effects, they allow for auto-oscillation and extremely great amplitudes of oscillation at their resonance frequency ω_1. The creation of a hole and destruction of microbes could be observed. Holland's video [53] shows even local *bulging* of the membrane of bacteria before the explosive eruption. This means that a bunch of pili was involved at a place, where the electric field was perpendicular to these structures. Bulging began also at the opposite side, where the electric field is also effective. Moreover, microbes are immobilized before breaking up, since the propelling function of pili is already disturbed. It does not only depend on motorized flagella.

The sophisticated spikes of viruses are highly efficient weapons, but they have an inherent weakness that can be exploited when we are aware of this possibility. Although pili of bacteria and nanobacteria have other functions, they lead also to total destruction, without survivors that could initiate securing mutations. It is

only necessary to impose a frequency that is precisely equal to the resonance frequency. It was a huge error to claim that the observed facts had to be bogus, even without verifying, since it deprived humanity from making use of a simple and secure method to fight sicknesses, plagues and even cancer.

Rife found not only that BX and BY bacteria are involved in cancer, but also that they are proliferating after radiotherapy. This merits special attention. It has been rediscovered that oscillating electric fields can be used for cancer therapy. A possible mechanism has been proposed [76] [77], but it is still a hypothetical one and should be reexamined in a larger context. Since pleomorphic transformations are reversible, it is plausible that the total number of pili is conserved in size reduction. Their surface density would then be increased for nanobacteria and explain why they become more virulent. Nevertheless, they remain vulnerable for Rife's resonances.

It should be noted that a cantilever, constituted of a steel wire, does also allow for another mode of oscillation, where a knot is created near the free end. However, the resonance frequency is significantly higher and this type of deformations can be excluded for virus spikes. We mention also that it is possible to use UV light for disinfecting surfaces. Low pressure mercury lamps produce UVC light at 254 nm. It is absorbed by RNA and produces there local defects [78], but this method is only applicable to viruses that are directly exposed to this radiation on a surface, in aerosol droplets or very thin liquid films. The FDA issued a warning, since UVC light damages the human skin and is dangerous for our eyes [79]. Rife's method is not dangerous at all and efficient for destroying virulent microbes anywhere inside our body.

5. Summary and Conclusions

Rife did prove that *optical* microscopes allow for much greater magnification and higher resolution than had been assumed. Since he constructed himself several supermicroscopes with purely classical means, his scientific creativity and accomplished craftsmanship deserve recognition and respect. With his instruments, he could clearly observe that when bacteria are exposed to stress, they reduce their size. They keep only what is essential to survive, but are more aggressive. Naessens did also prove the reality of pleomorphism, but some authorities did not like that. They declared that these pioneers are quacks, but refused to verify if the reported facts were real or not. This attitude is more than strange.

Moreover, Rife discovered already about 100 years ago that bacteria and nanobacteria can be destroyed by resonance. His phanotron was an ingenious instrument that produced the required electric field by means of braking radiation. Instead of emitting EM waves in all directions by means of an antenna, like Hertz did and is usual for broadcasting, his system generated a local beam of EM waves. The destruction of bacteria by resonance was already observable with standard optical microscopes, but Rife was also able to see exploding nanobacteria. Actually, he had to persevere during more than a decade to make these tiny

microbes visible. He did then prove that some of them are present in cancer tissue and that after being cultured, they do also cause cancer. He determined the resonance frequency for targeted destruction of various microbes. These values were confirmed by two collaborators, using different equipment.

The efficiency of his method for healing cancer was clinically tested, but even these results were declared to be bogus, since they required modifying cherished postulates. For those who had the power to crush Rife, it did not matter that the reported results might be true. Rife was prosecuted. His documents were stolen. Instruments were wrecked and all traces of his achievements were eradicated from official medical records. That was *profoundly unjust, truly antiscientific and detrimental* for the worldwide health system.

We solved the basic scientific puzzle with mathematical rigor by considering that spikes of viruses, as well as pili of bacteria and nanobacteria can be set in forced oscillation. Nonlinear effects make the resonance stronger and sharper than usual ones. There is only one resonance frequency for every particular type of microbes. It depends on the length of the oscillating structures and is thus specific. This theory is experimentally confirmed and leaves no rational reason to negate the possibility of targeted destruction of microbes. The author of this study has no financial interest whatsoever in a general implementation of this method. His concern is merely truth, justice, but also reduction of unnecessary suffering and death. Other persons and institutions have now to go on in the direction that was pointed out by Rife.

The Coronavirus pandemic and its social implications should make everyone attentive to the existence of a biophysical method that differs from the usual biochemical one, but is *effective, secure and rapidly adaptable*. It is only necessary to determine the adequate resonance frequency very carefully, but this can be done with inexpensive equipment and by means of direct microscopic observation. Even the constant threat of unpredictable mutations can rapidly be countered. The treatment of patients requires only a few minutes, at intervals of three days. Because of the sharp resonance, this method is selective and can eliminate side effects when it is objectively controlled like cars and traffic, for instance.

There is also rising evidence that our precious arsenal of antibiotics is endangered. *Multiple antibacterial resistances* are increasing [80]. The US Centers for Disease Control and Prevention concluded already in 2015 that "coordinated efforts to implement new politics, renew research efforts, and pursue steps to manage the crisis are greatly needed." This was thought to "require considerable investment of human and financial resources", but that is not true for Rife's method. Basically, it only required to change some habits of though.

We have to insist that dogmatism and concentration of power endanger scientific progress by blocking freedom of thought. When it is guided by observing reality and rational analysis, it is more efficient than *ideology*, but dictatorship and reckless use of power are always a temptation. In this context, we have to mention the research of the Russian chemist Tamara Lebedeva [81]. She

made intensive research on *trichomonade* parasites and proved that they can cause cancer. Their reproduction rate was found to be increased by radiotherapy, but Lebedeva's work was not recognized by medical authorities. Alfons Weber studied the impact on cancer of protozoa causing malaria [82]. He published his results in 1967 and promptly lost his approbation as medical doctor. It is now appearing that there are connections between malaria and cancer [83]. The plasmodium parasite is involved in both fields and cross-fertilization in medicine should be encouraged. The common feature of the research of Lebedeva and Dr. Weber was to consider that cancer is an infectious disease. We have to add that these types of parasites are not the only possible cause of cancer, but their effects should also be investigated.

To provide a concrete and still actual example of tenacious preconceptions related to medicine, we mention that Dr. Jacques Benveniste did experimentally prove the existence of "water memory" in the 1980th. Nevertheless, it was declared (even by a world-famous scientific journal) that this is impossible. This claim was based on the apparently obvious idea that when biologically active molecules are repeatedly dissolved in water, they cannot be active any more when all of them have been eliminated. Since Benveniste found that the final solution did produce the same effect as if these molecules were still present, this fact required an explanation. From a scientific and human point of view, it is shocking that it was accepted to pretend that Dr. Benveniste and his team were merely victims of an illusion. The real problem required to verify if the active molecules could be replaced by substitutes, resulting from structuring water. Is it really impossible that thermal agitation of water molecules in the liquid state could cause structuring of water molecules according to the initial template?

Since this concerns condensed matter physics, we tried to solve this problem and published in 2018 a rational explanation [84]. Since water molecules are dipolar, they can constitute very dense crystallites, where all these dipoles have the same orientation. We proved that they are spherical and so small that they could not be observed with standard optical microscopes. These nano-pearls are formed by the electric field of charged parts of biologically active molecules. Being also dipolar, these "water pearls" constitute chains, where they are set in rotation at the frequency of the vibrating charged part of active molecules. The resulting standing wave limits the length of these chains by preventing further growth. Since the length of these chains depends on the frequency of oscillation of the charged part of active molecules, they become relevant information carriers. Their existence is real.

They are even multiplied by successive dilutions, always accompanied by vigorous shaking, since some chains are then broken, but are reconstituted by the oscillating electric field of the majority of intact chains. This process yields numerous efficient substitutes of the active molecules. It explains also about a dozen other experimental observations, made in the meantime. It accounts even for *homeopathy*, which is at present under harsh attack by those who claim that these products can merely act as placebos. Without understanding the real me-

chanism, it is more difficult to abandon preconceptions, but it is surprising that even a high-level "Scientific Advisory Council" did participate in lobbying to eliminate homeopathy by legal procedures [85]. Ideology and financial interests can even overrule normal scientific procedures.

This fact has to be combined with objective evidence that pharmaceutical industries are radically and recklessly oriented towards big profits in a capitalistic way. This dreadful situation was recently documented by Luc Hartmann [86] and shows that Big Pharma is out of control. This is not always true, of course, but according to trustable authorities [86], they can indirectly pay institutions that should evaluate the efficiency, as well as already reported side effects. Political and legislating authorities should urgently react to avoid more scandals and flagrant injustices.

Rife made a great discovery. We did only explain why apparently unbelievable, but observed facts are true. Now it is up to other persons and institutions to carry on. The fast development of vaccines merits praise, but there is now much more at stake than protection of already gigantic industrial empires. We appeal therefore to the World Health Organization, all Ministers of Health and Governments, as well as the United Nations to initiate and organize also another way to cope with unnecessary suffering and death. That is possible and urgently needed.

Acknowledgements

Conflicts of Interest

The author declares no conflicts of interest regarding the publication of this paper.

References

[1] Lynes, B. (1987) The Cancer Cure That Worked! Fifty Years of Suppression. Bio-Med Publishing Group, South Lake Tahoe.

[2] Masters, B.R. (2010) The Development of Fluorescence Microscopy. Wiley Online Library. https://doi.org/10.1002/9780470015902.a0022093

[3] Anonymous (2017) Royal Rife's Universal Microscope (and Why It Can't Exist). Blog. http://sustainable-nano.com/2017/08/18/royal-rifes-universal-microscope-and-why-it-cant-exist

[4] Wade, G. (2014) The First Rife Microscope and the Gained Ability to Observe Viruses and the Fine Structure of Bacteria with an Optical Microscope. https://www.rife.de/observe-viruses-and-bacteria.html

[5] Kungliga Vetenskapsakademien (2014) The Nobel Prize in Chemistry 2014. Scientific Background.

https://www.nobelprize.org/prizes/chemistry/2014/advanced-information

[6] Seidel, R.E. and Winter, M.E. (1944) *Journal of the Franklin Institute*, **237**, 103-130.
http://www.pulsedtechresearch.com/wp-content/uploads/2013/04/New-Microscopes-SeidelWinter.pdf
https://doi.org/10.1016/S0016-0032(44)90203-6

[7] BRMI (2018) History—Dr. Royal Raymond Rife Jr.
https://www.brmi.online/royal-raymond-rife

[8] Comparet, B.L. (1960) Questions and Answers. Rife Research Europe: An Interview with Rife. https://www.rife.de/an-interview-with-rife.html

[9] Neuman, R.O. and Mayer, M. (1914) Atlas und Lehrbuch wichtiger tierischer Parasiten und ihrer Überträger.
https://jamanetwork.com/journals/jama/fullarticle/438846

[10] Kendall, A.K. and Rife, R.R. (1931) *California and Western Medicine*, **35**, 409-411.
https://europepmc.org/article/med/18741967

[11] San Diego Union (1929) Local Man Bares Wonders of Germ Life. New Apparatuses Unveil Hidden Microbe Universe to Human Eye.
https://rifevideos.com/local_man_bares_wonders_of_germ_life.html

[12] Rife, R.R. (1953) History of the Development of a Successful Treatment for Cancer and Other Virus, Bacteria and Fungi. Research Lab. Data, San Diego.
https://www.rife.de/files/history_rife_cancer_treatment.pdf

[13] Rosenow, E.C. (1932) *Science*, **76**, 192-193.
https://www.rife.de/observations-with-the-rife-microscope.html
https://doi.org/10.1126/science.76.1965.192

[14] Hess, D.J. (1996) *Medical Anthropology Quarterly*, **10**, 657-674.
https://doi.org/10.1525/maq.1996.10.4.02a00140

[15] Rife, R.R. and Crane, J. (1950) The Universal Microscope. RifeVideos.com.
https://www.rifevideos.com/dr_rife_talks_with_john_crane_about_his_universal_microscope.html

[16] Hell, S.W. (2014) Nobel Lecture.
https://www.youtube.com/watch?v=9BzGB1SUPGQ
https://www.nobelprize.org/uploads/2018/06/hell-lecture.pdf

[17] Vangindertael, J., *et al.* (2018) *Methods and Applications in Fluorescence*, **6**, Article ID: 022003. https://doi.org/10.1088/2050-6120/aaae0c
https://www.chem.kuleuven.be/pd/static/publications/Vangindertael2018.pdf

[18] Bonhams (2009) An Exceptionally Rare Rife Microscope.
https://www.bonhams.com/auctions/16871/lot/113

[19] Elswick, S.R. (1994) The Amazing Wonders of Gaston Naessens. Super Microscopes and Suppressed Cancer Treatments. Nexus Magazine.
http://www.whale.to/v/naessens.html

[20] Naessens, G. (2010) The Somatoscope.
https://www.youtube.com/watch?v=KGJW94ciq4c

[21] Claxton, N.S., *et al.* (2006) Microscopy, Confocal. Wiley, Hoboken.
https://en.wikipedia.org/wiki/Confocal_microscopy
https://doi.org/10.1002/0471732877.emd291

[22] Bird, C. (1991) The Persecution and Trial of Gaston Naessens. Tiburon-Kramer. 336 p.

[23] BRMI. History-Antoine Béchamp.

https://www.biologicalmedicineinstitute.com/antoine-bechamp

[24] Perrot, A. and Schwarz, M. (2014) Pasteur et Koch, un duel de géants dans le monde des microbes. Odile Jacobs.
https://www.youtube.com/watch?v=YuC3T3eesDU

[25] Henri, V. (1914) *Comptes rendus de l'Académie des Sciences*, **159**, 340-343, 413-415.
https://pubs.rsc.org/en/content/articlelanding/1914/ca/ca9140601112/Abstract#!divAbstract

[26] Almquist, E. (1922) *The Journal of Infectious Diseases*, **31**, 483-493.
https://doi.org/10.1093/infdis/31.5.483

[27] Naessens, G. (2010) The Somatid and Its 16 Stage Cycle.
https://www.youtube.com/watch?v=ttl5NBo3_Z4

[28] Klieneberger-Nobel, E. (1951) *Microbiology and Molecular Biology Reviews*, **15**, 77-103. https://mmbr.asm.org/content/mmbr/15/2/77.full.pdf
https://doi.org/10.1128/MMBR.15.2.77-103.1951

[29] Kurath, G. and Morita, R.Y. (1983) *Applied and Environmental Microbiology*, **45**, 1206-1211. https://doi.org/10.1128/AEM.45.4.1206-1211.1983

[30] Folk, R.L. (1994) Interaction between Bacteria, Nannobacteria and Mineral Precipitation in Hot Springs of Central Italy.
https://www.erudit.org/en/journals/gpq/1994-v48-n3-gpq1907/033005ar.pdf

[31] Kajander, E.O. and Ciftcioglu, N. (1998) *Proceedings of the National Academy of Sciences of the United States of America*, **95**, 874-879.
https://doi.org/10.1073/pnas.95.14.8274

[32] Ciftcioglu, N., *et al.* (2006) *Journal of Investigative Medicine*, **54**, 385-394.
https://doi.org/10.2310/6650.2006.06018

[33] Cantwell, A. (1990, 1995) The Cancer Microbe. The Hidden Killer in Cancer, Aids and Other Immune Diseases. Aries Rising Press, Los Angeles, 281 p.

[34] Cantwell, A. (2005) For Women against Cancer. Aries Rising Press, Los Angeles, 281 p.

[35] Wainwright, M. (1997) *Perspectives in Biology and Medicine*, **40**, 407-414.
https://doi.org/10.1353/pbm.1997.0038

[36] Kumar, C.A., *et al.* (2011) *Oral Medicine and Radiology*, **23**, 354-359.
https://doi.org/10.5005/jp-journals-10011-1168

[37] Schlieper, G., *et al.* (2011) *Nephrology Dialysis Transplantation*, **26**, 3436-3439.
https://doi.org/10.1093/ndt/gfr521

[38] Ciftcioglu, N. and McKay, D. (2010) *Pediatric Research*, **67**, 490-499.
https://doi.org/10.1203/PDR.0b013e3181d476ce

[39] Cantwell, A. (2014).
https://livebloodonline.com/breast-cancer-caused-pleomorphic-bacteria

[40] Duda, V.I., *et al.* (2012) *Microbiology*, **81**, 379-390.
https://doi.org/10.1134/S0026261712040054

[41] Luef, B., *et al.* (2015) *Nature Communications*, **6**, 6373.
https://www.nature.com/articles/ncomms7372
https://doi.org/10.1038/ncomms7372

[42] Krotz, D. (2015) First Detailed Microscopy Evidence of Bacteria at the Lower Size Limit of Life. https://newscenter.lbl.gov/2015/02/27/ultra-small-bacteria

[43] Mattman, L.H. (1974) Cell Wall Deficient Forms: Stealth Pathogens. CRC Press, Boca Raton, 448 p. https://doi.org/10.1201/b16928

[44] Ramijan, K., *et al.* (2019) *Nature Communications*, **9**, Article No. 5164.
https://www.nature.com/articles/s41467-018-07560-9.pdf

[45] Claessen, D. and Errington, J. (2019) *Trends in Microbiology*, **5**, 1025-1033.
https://www.cell.com/trends/microbiology/pdf/S0966-842X(19)30192-1.pdf
https://doi.org/10.1016/j.tim.2019.07.008

[46] Vassilatos, G. (2003) Ultra Microscope and Cure Rays: R. Raymond Rife. Lost Science (See Spears). http://customers.hbci.com/~wenonah/history/rife.htm

[47] Crane, J., March, J., *et al.* (2012) The Rife Machine Report: A History of Rife's Instruments and Frequencies. 149 p.
http://www.royal-rife-machine.com/the_rife_machine_report.pdf

[48] Spooky 2 (2018) Rife Frequency List. Compiled by Spooky2-mall .com, 2018.
https://s6c2n9k7.stackpathcdn.com/download/spooky2rifefrequencylist.pdf

[49] Allegretti, M. (2018) The Therapeutic Properties of EM Waves. 154 p.

[50] Dunn, H.H. (1931) Movie.
https://www.rife.de/movie-new-eye-of-microscope-in-war-of-germs.html

[51] Videos: Rife in His Own Words. The Royal Rife Story.
https://www.rife.de/rife-related-videos.html

[52] Rifevideos.com: 1939 Royal Rife Laboratory Film (John Crane, 35:34); Royal Rif in His Own Words (51:15); The Royal Rife Story (2.11:22).

[53] Holland, A. (2013) Shattering Cancer with Resonant Frequencies. TEDx Talks (17:08). https://www.youtube.com/watch?v=1w0_kazbb_U

[54] Terwange, D. and Bush, J. (2011) Tibetan Singing Bowls.
https://core.ac.uk/download/pdf/4434335.pdf

[55] Practical Engineering (2018) Why the Tacoma Bridge Collapsed. YouTube (8:48).

[56] Dubost, G., *et al.* (2008) Theoretical Low Frequency Acoustic Resonances of Various Rife-Bare Antennas. https://www.researchgate.net/publication/273886201

[57] Baladin, A.A. and Fonoberov, V.A. (2005) *Journal of Biomedical Nanotechnology*, **1**, 90-95. https://doi.org/10.1166/jbn.2005.005

[58] Rouard, P. and Meessen, A. (1977) *Progress in Optics*, **50**, 79-137.
http://www.meessen.net/AMeessen/optical_properties_of_thin_metal_films.pdf
https://doi.org/10.1016/S0079-6638(08)70477-3

[59] Polk, C. and Postow, E. (1986) CRC Handbook of Biological Effects of Electromagnetic Fields. CRC Press, Boca Raton.

[60] Barry, J.M. (2004) The Great Influenza: The Story of the Deadliest Pandemic in History. Penguin Books, London.

[61] Carr, C.M. and Kim, P.S. (1993) *Cell*, **73**, 823-832.
https://doi.org/10.1016/0092-8674(93)90260-W

[62] Sriwilaaijaroen, N. and Suzuki, Y. (2012) *Proceedings of the Japan Academy, Ser. B*, **88**, 226-249. https://doi.org/10.2183/pjab.88.226

[63] Harrison, S. (2015) Viral Membrane Fusion. Part 2.
https://www.youtube.com/watch?v=qcepGvFUM38

[64] Harrison, S. (2015) *Virology*, **479**-**480**, 498-507.
https://www.sciencedirect.com/science/article/pii/S004268221500183X
https://doi.org/10.1016/j.virol.2015.03.043

[65] Saplakoglu, Y. (2020).
https://www.livescience.com/coronavirus-spike-protein-structure.html

[66] McAuley, J.L., *et al.* (2019) *Frontiers in Microbiology*, **10**, 39-62.
https://doi.org/10.3389/fmicb.2019.00039

[67] Kosik, I. and Yewdell, J.W. (2019) *Viruses*, **11**, 346-364.
https://doi.org/10.3390/v11040346

[68] Biswas, A., *et al.* (2020) *Critical Reviews in Microbiology*, **46**, 182-193.

[69] Gaymard, A., *et al.* (2016) *Clinical Microbiology and Infection*, **22**, 975-983.
https://doi.org/10.1016/j.cmi.2016.07.007

[70] Harrison, S. (2015) Non-Enveloped Virus Entry.
https://www.youtube.com/watch?v=-1tSBwE1Wuk

[71] Chang, C., *et al.* (2019) *Proceedings of the National Academy of Sciences of the United States of America*, **116**, 18041-18049.
https://doi.org/10.1073/pnas.1907733116

[72] Meessen, A. (2010) Ball Lightning: Bubbles of Electronic Plasma Oscillations.
http://www.meessen.net/AMeessen/Ball-Lightning-Theory.pdf

[73] Harvard Natural Science, Lecture Demonstrations: Shattering Wineglass.
https://sciencedemonstrations.fas.harvard.edu/presentations/shattering-wineglass

[74] Wrapp, D., *et al.* (2020) *Science*, **367**, 1260-1263.
https://science.sciencemag.org/content/367/6483/1260
https://doi.org/10.1126/science.abb2507

[75] Litak, G., *et al.* (2012) Nonlinear Oscillations of an Elastic Inverted Pendulum. 4*th IEEE International Conference on Nonlinear Science and Complexity*, Budapest, 6-11 August 2012, 113-116. http://litak.pollub.pl/20_nsc2012.pdf
https://doi.org/10.1109/NSC.2012.6304737

[76] Kirson, E.D., *et al.* (2004) Disruption of Cancer Cell Replication by Alternative Electric Fields. *Cancer Research*, **64**, 3288-3295.

[77] Miller, J. (2007) Electric Fields Have Potential as Cancer Treatment. *Physics Today*, **60**, 19. https://doi.org/10.1158/0008-5472.CAN-04-0083
https://physicstoday.scitation.org/doi/10.1063/1.2774085

[78] Heßling, M., *et al.* (2020) Ultraviolet Irradiation Doses for Coronavirus Inactivation. *GMS Hygiene and Infection Control*, **15**, Doc08.
https://www.egms.de/static/en/journals/dgkh/2020-15/dgkh000343.shtml

[79] https://www.fda.gov/medical-devices/coronavirus-covid-19-and-medical-devices/uv-lights-and-lamps-ultraviolet-c-radiation-disinfection-and-coronavirus

[80] Ventola, C.L. (2015) The Antibiotic Resistance Crisis Part 1 Causes and Threats. Part 2 Management Strategies and New Agents. *Pharmacology & Therapeutics*, **40**, 277-283. https://www.ncbi.nlm.nih.gov/pmc/articles/PMC4378521
https://pubmed.ncbi.nlm.nih.gov/25987823/

[81] Lebedewa, T. und Driediger, E. (2001) Krebserreger Entdeckt. Driediger Verlag, Georgsmarienhütte.

[82] Weber, A. (1969) Über die Ursache der Krebskrankheit. Verlag Parcus, München.

[83] Nordor, A.V. (2018) *Open Biology*, **8**, Article ID: 180127.
https://www.ncbi.nlm.nih.gov/pmc/articles/PMC6223206
https://doi.org/10.1098/rsob.180127

[84] Meessen, A. (2018) *Journal of Modern Physics*, **9**, 2657-2724.
https://www.scirp.org/pdf/JMP_2018122814430215.pdf
https://doi.org/10.4236/jmp.2018.914165

[85] European Academies Science Advisory Council (2017) Homeopathic Products and

Practices.
https://easac.eu/fileadmin/PDF_s/reports_statements/EASAC_Homepathy_stateme nt_web_final.pdf

[86] Hartmann, L. and Lasco, C. (2020) Big-Pharma Labos Tout-Puissants. Arte, TV. Sept. 11, 2020.
https://www.telez.fr/actus-tv/big-pharma-labos-tout-puissants-sur-arte-le-juteux-b usiness-du-medicament/

Fuzzification of Feynman Path Integral and Its Effect on Field Theory and Quantum Gravity—Reformation and Redevelopment of Quantum Theory

Wenbing Qiu

Department of Physics, Faculty of Science, Shihezi University, Shihezi, China
Email: 2962546794@qq.com

Abstract

The quantum probability theory of fuzzy event is suggested by using the idea and method of fuzzy mathematics, giving the form of fuzzy event path integral, membership degree amplitude, fuzzy field function, Green function, physical quantity and fuzzy diagram. This theory reforms quantum mechanics, making the later become its special case. This theory breaks unitarity, gauge invariance, probability conservation and information conservation, making these principles become approximate ones under certain conditions. This new theory, which needs no renormalization and can naturally give meaningful results which are in accordance with the experiments, is the proper theory to describe microscopic high-speed phenomenon, whereas quantum mechanics is only a proper theory to describe microscopic low-speed phenomenon. This theory is not divergent under the condition of there being no renormalization and infinitely many offsetting terms, thereby it can become the theoretical framework required for the quantization of gravity.

Keywords

Quantum Probability, Fuzzy Event, Path Integral, Membership Degree, Membership Degree Amplitude, Fuzzy Graph

1. Introduction

Since Hawking offered the problem of black hole information loss [1], scholars have tried their best to save the conservation of information [2] [3] [4], because the non conservation of information will destroy the unitarity of quantum theory and bring a major crisis to quantum theory [5]-[12] in which brilliant

achievements have been made. However, here there exists a problem: quantum theory is a theory to describe reversible process, whereas black hole radiation is irreversible process [13]. How can the former fit describing the latter! The reason why black hole radiation is irreversible is that the heat capacity of black hole is negative and there is no stable heat balance between black hole and the outside world. There must be temperature difference between the black hole and the outside world, and the radiation process must be irreversible. Quantum theory is not suitable for describing irreversible processes, and it is incompatible with the second law of thermodynamics. Thereby, the reformation of quantum theory or a new theory has to be found to depict irreversible black hole radiation. This is the work of this paper.

In my first work [14] on fuzzy quantum probability, it is mentioned that there are two directions for developing quantum probability into fuzzy quantum probability: one is to introduce fuzziness into the event, whereas the probability (wave) is clear or determined, so as to obtain the quantum probability of fuzzy event; the other is to introduce fuzziness into the quantum probability, while the event is clear, so as to obtain the fuzzy quantum probability of the event. The literature [14] is dedicated to the work in the second direction, *i.e.* doing the work of "the fuzzification of quantum probability" with the method of fuzzy mathematics, whereas the work of the first direction will be done in this paper. This work will reform quantum theory and push quantum theory to a new stage.

In this paper, the form of the path integral of fuzzy event is established in Section 2. The quantum field theory of fuzzy event is discussed in Section 3. In Section 4, the mathematical form of membership degree amplitude of fuzzy path is discussed. Fuzzy diagram is also introduced and discussed in this Section.

2. The Path Integral of Fuzzy Event

As we know, quantum probability is calculated by "probability amplitude", whereas probability amplitude is calculated by "path integral". Thereby, if one attempts to create a theory about the quantum probability of fuzzy event, it is necessary to introduce fuzziness into path integration. For this, the three different probability theories about paths should be first reviewed.

In Figure 1, the point A is the particle source whereas a detector is placed at point B. $\vec{r}(t)$ represents a possible path from A to B. Then, the total probability of finding the particle at the point B can be computed from the viewpoints of several different probability theories.

First, from the viewpoint of classical probability theory, if there exists a probability distribution for the momentum values of the emitted particles, the particle has a certain probability to move along the path $\vec{r}(t)$ and are observed at point B. This probability is denoted as $P\left[\vec{r}(t)\right]$. Then, the probability that a particle will be observed at point B is

$$P(A \rightarrow B) = \sum_{\substack{\text{all } \vec{r}(t) \\ \text{from } A \text{ to } B}} P\left[\vec{r}(t)\right]. \tag{1}$$
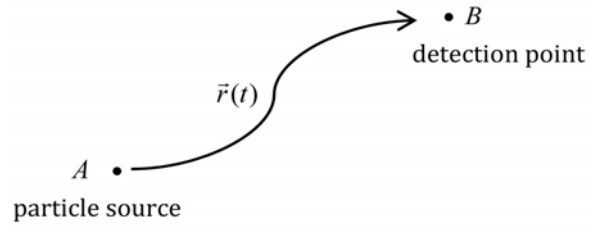
Figure 1. This figure shows the thought of path summation. For the probability theory of fuzzy event, the position (coordinate) of the particle at a certain moment is fuzzy or difficult to be judged accurately. The so-called "fuzziness of the coordinate" is different from the probability uncertainty of the coordinate, the former is the uncertainty of the judgment of the result that has occurred whereas the latter is the uncertainty of the prediction of the result that has not occurred.

Second, from the viewpoint of the probability theory of fuzzy event, considering the fuzziness of the position (coordinate) of the particle, the path of the particle also is unsharp. So, $A \to B$ is a fuzzy event, which can be denoted using a fuzzy set $\tilde{R}$. Every path belongs to this fuzzy set only in a certain degree of membership. For instance, the membership degree of the path $\vec{r}(t)$ is expressed as $\mu_{\tilde{R}}\left[\vec{r}(t)\right] \in [0,1]$. According to the probability formula of fuzzy event [15], the probability that a particle will be observed at point B is

$$P\left(\tilde{R} = (A \to B)\right) = \sum_{\substack{\text{all } \vec{r}(t) \\ \text{from } A \text{ to } B}} \mu_{\tilde{R}}\left[\vec{r}(t)\right] \cdot P\left[\vec{r}(t)\right]. \tag{2}$$

Third, from the viewpoint of quantum mechanics, considering the volatility of the particle, according to the principle of superposition, the probability amplitude for $A \to B$ is

$$K(A \to B) = \sum_{\substack{\text{all } \vec{r}(t) \\ \text{from } A \text{ to } B}} \psi\left[\vec{r}(t)\right].$$

Here $\psi\left[\vec{r}(t)\right]$ is the probability amplitude for the path $\vec{r}(t)$. According to the statistical interpretation of wave function, the total probability should be calculated using probability amplitude

$$P(A \to B) = \left|K(A \to B)\right|^2. \tag{3}$$

The logic vein among these three probability theories is shown in **Figure 2**.

The designed path summation form about fuzzy event is also exhibited in **Figure 2**. Is this kind of path summation form rational? The consideration can be made as follows:

1) When the interference terms

$$\sum_{\substack{\text{all } \vec{r}(t) \\ \text{from } A \text{ to } B}} \sum_{\substack{\text{all } \vec{r}'(t) \\ \text{from } A \text{ to } B \\ (\vec{r}'(t) \neq \vec{r}(t))}} \lambda_{\tilde{R}}^*\left[\vec{r}(t)\right] \lambda_{\tilde{R}}\left[\vec{r}'(t)\right] \times \psi^*\left[\vec{r}(t)\right] \psi\left[\vec{r}'(t)\right] \to 0,$$

i.e. wave effect disappears, the form of the quantum probability of fuzzy event changes into

$$P\left(\tilde{R} = (A \to B)\right) = \sum_{\substack{\text{all } \vec{r}(t) \\ \text{from } A \text{ to } B}} \left|\lambda_{\tilde{R}}\left[\vec{r}(t)\right]\right|^2 \times \left|\psi\left[\vec{r}(t)\right]\right|^2.$$
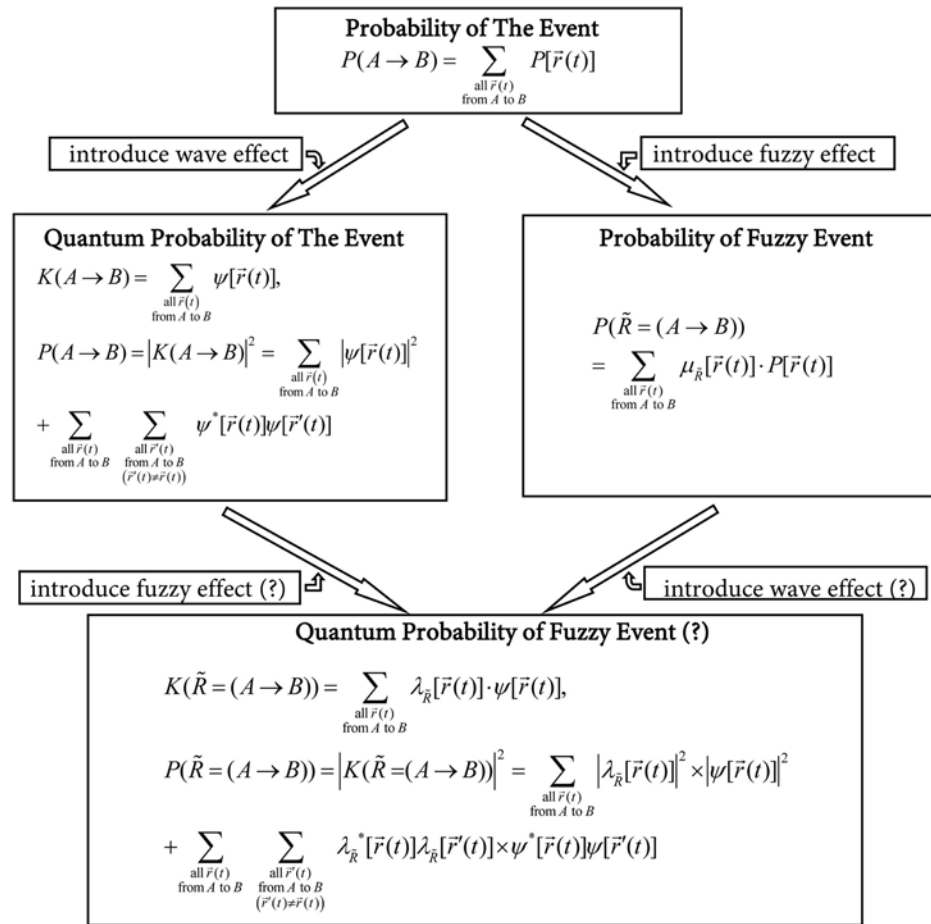
Figure 2. This figure shows the logical clues to the development of probability theory. It exhibits how fuzziness is introduced into the event. In the probability theory of fuzzy event, the property of the probability $P\big[\vec{r}(t)\big]$ of basic event has no change. Similarly, in the quantum probability theory of fuzzy event, the property of the probability amplitude $\psi\big[\vec{r}(t)\big]$ of basic event also has no change. Not only that, but the properties of the operator, eigenstate, eigenvalue etc. also are not changed. In the figure, $\big|\lambda_{\tilde{R}}\big[\vec{r}(t)\big]\big|^2 \in [0,1]$ represents the membership degree for the path $\vec{r}(t) \in \tilde{R}$, whereas $\lambda_{\tilde{R}}\big[\vec{r}(t)\big]$ is named "membership degree amplitude" just like the origin of the name of probability amplitude. In addition, it is worth being pointed that in the probability theory of fuzzy event, the conservation of probability does not hold. This is because $\sum_{\forall B \in \Omega} \sum_{\substack{\text{all } \vec{r}(t) \\ \text{from } A \text{ to } B}} \mu_{\tilde{R}}\big[\vec{r}(t)\big] \cdot P\big[\vec{r}(t)\big] < \sum_{\forall B \in \Omega} \sum_{\substack{\text{all } \vec{r}(t) \\ \text{from } A \text{ to } B}} P\big[\vec{r}(t)\big] = 1.$ Where Ω represents the whole space. Similarly, it can be imagined that in the quantum probability theory of fuzzy event, probability also is not conserved because of the introduction of the membership degree (amplitude).

This just accords with the form of the probability of fuzzy event.

2) When the membership degree amplitude

$$\lambda_{\tilde{R}}\big[\vec{r}(t)\big] \to 1, \quad \big(\text{for arbitrary path}\big)$$

i.e. fuzziness effect disappears, the form of the quantum probability of fuzzy event changes into

$$P\left(\tilde{R}=(A\to B)\right)=\sum_{\substack{\text{all }\vec{r}(t)\\ \text{from }A\text{ to }B}}\left|\psi\left[\vec{r}(t)\right]\right|^2+\sum_{\substack{\text{all }\vec{r}(t)\\ \text{from }A\text{ to }B}}\sum_{\substack{\text{all }\vec{r}'(t)\\ \text{from }A\text{ to }B\\ (\vec{r}'(t)\neq\vec{r}(t))}}\psi^*\left[\vec{r}(t)\right]\psi\left[\vec{r}'(t)\right].$$

This just accords with the form of the quantum probability of the event.

That is to say, under certain conditions, the quantum probability of fuzzy event can respectively transition to the probability of fuzzy event and the quantum probability of the event. So, the designed path summation form for fuzzy event in Figure 2 is rational.

According to the above thought and the explanation about Figure 2 (in the quantum probability theory of fuzzy event, the property of the probability amplitude $\psi\left[\vec{r}(t)\right]$ of basic event has no change), one can write out the path integral form of fuzzy event

$$K\left((\vec{r}_1,t_1)\to(\vec{r}_2,t_2)\right)=C\sum_{\text{all paths}}\lambda_{\tilde{R}}\left[\vec{r}(t)\right]\cdot\exp\left\{iS\left[\vec{r}(t)\right]/\hbar\right\}, \tag{4}$$

or

$$K\left((\vec{r}_1,t_1)\to(\vec{r}_2,t_2)\right)=\int\lambda_{\tilde{R}}\left[\vec{r}(t)\right]\cdot\exp\left\{iS\left[\vec{r}(t)\right]/\hbar\right\}D\left[\vec{r}(t)\right]. \tag{5}$$

Equation (5) also can be introduced in another way. Usually, it is thought that the position (coordinate) $\vec{r}(t)$ of the particle is clear and certain at one moment. However, according to the idea of fuzzy theory [16], it can be argued that those seemingly clear and certain quantities are actually not at all clear and certain, and they have fuzziness or they are difficult to be evaluated accurately and should be depicted using fuzzy numbers. Here, it is thought that the position of the particle at one moment is fuzzy or difficult to be evaluated accurately, and it should be depicted by fuzzy number $\tilde{\vec{r}}$ (fuzzy coordinate). Thus, the range (boundary) of the coordinate value of the particle is also fuzzy. According to the integral theory of fuzzy mathematics [17], an integral of non-fuzzy function over fuzzy interval $(\tilde{a},\tilde{b})$ can be defined

$$\begin{aligned}\tilde{K}\left((\vec{r}_1,t_1)\to(\vec{r}_2,t_2)\right)&=\int_{\tilde{a}}^{\tilde{b}}\exp\left\{iS\left[\vec{r}(t)\right]/\hbar\right\}D\left[\vec{r}(t)\right]\\ &=\lim_{\substack{N\to\infty\\ \varepsilon\to0}}\int_{\tilde{x}_{1a}}^{\tilde{x}_{1b}}\int_{\tilde{x}_{2a}}^{\tilde{x}_{2b}}\cdots\int_{\tilde{x}_{N-1,a}}^{\tilde{x}_{N-1,b}}C_N\exp\left\{iS_N\left[\vec{r}(t)\right]/\hbar\right\}\prod_{j=1}^{N-1}d^3x_j.\end{aligned} \tag{6}$$

This fuzzy integral can be computed in an alternate form

$$\begin{aligned}K\left((\vec{r}_1,t_1)\to(\vec{r}_2,t_2)\right)&=\lim_{\substack{N\to\infty\\ \varepsilon\to0}}\int_{-\infty}^{\infty}\lambda_{\tilde{R}}\left(\vec{r}_0,\vec{r}_1,\cdots,\vec{r}_N\right)C_N\exp\left\{iS_N\left[\vec{r}(t)\right]/\hbar\right\}\prod_{j=1}^{N-1}d^3x_j\\ &=\int\lambda_{\tilde{R}}\left[\vec{r}(t)\right]\exp\left\{iS\left[\vec{r}(t)\right]/\hbar\right\}D\left[\vec{r}(t)\right].\end{aligned} \tag{7}$$

Thus, (5) is obtained ((7) is just (5)). (7) can be regarded as the result of the non-fuzzification of (6).

Is the above design from (6) to (7) rational? An explanation can be made as follows:

From (6) and (7), it can be obtained respectively that

$$\left|\tilde{K}\left((\vec{r}_1,t_1)\to(\vec{r}_2,t_2)\right)\right|^2=\lim_{\substack{N\to\infty\\ \varepsilon\to0}}\int_{\tilde{x}_{1a}}^{\tilde{x}_{1b}}\int_{\tilde{x}_{2a}}^{\tilde{x}_{2b}}\cdots\int_{\tilde{x}_{N-1,a}}^{\tilde{x}_{N-1,b}}\left|C_N\exp\left\{iS_N\left[\vec{r}(t)\right]/\hbar\right\}\right|^2\prod_{j=1}^{N-1}\mathrm{d}^3x_j$$

$$+\text{ the interference terms,}$$

$$\left|K\left(\left(\vec{r}_1,t_1\right)\rightarrow\left(\vec{r}_2,t_2\right)\right)\right|^2 = \lim_{\substack{N\rightarrow\infty\\\varepsilon\rightarrow 0}}\int_{-\infty}^{\infty}\left|\lambda_{\tilde{R}}\left(\vec{r}_0,\vec{r}_1,\cdots,\vec{r}_N\right)C_N\exp\left\{iS_N\left[\vec{r}\left(t\right)\right]/\hbar\right\}\right|^2\prod_{j=1}^{N-1}\mathrm{d}^3x_j$$

+ the interference terms.

When the interference terms tend to zero (*i.e.* wave effect disappears), the above two equations change respectively into

$$\left|\tilde{K}\left(\left(\vec{r}_1,t_1\right)\rightarrow\left(\vec{r}_2,t_2\right)\right)\right|^2 = \lim_{\substack{N\rightarrow\infty\\\varepsilon\rightarrow 0}}\int_{\tilde{x}_{1a}}^{\tilde{x}_{1b}}\int_{\tilde{x}_{2a}}^{\tilde{x}_{2b}}\cdots\int_{\tilde{x}_{N-1,a}}^{\tilde{x}_{N-1,b}}\left|C_N\exp\left\{iS_N\left[\vec{r}\left(t\right)\right]/\hbar\right\}\right|^2\prod_{j=1}^{N-1}\mathrm{d}^3x_j, \quad (8)$$

$$\left|K\left(\left(\vec{r}_1,t_1\right)\rightarrow\left(\vec{r}_2,t_2\right)\right)\right|^2 = \lim_{\substack{N\rightarrow\infty\\\varepsilon\rightarrow 0}}\int_{-\infty}^{\infty}\left|\lambda_{\tilde{R}}\left(\vec{r}_0,\vec{r}_1,\cdots,\vec{r}_N\right)\right|^2\times\left|C_N\exp\left\{iS_N\left[\vec{r}\left(t\right)\right]/\hbar\right\}\right|^2\prod_{j=1}^{N-1}\mathrm{d}^3x_j. \quad (9)$$

According to the integral theory of fuzzy mathematics [17], (9) is just the alternative form of (8). This shows the rationality of (6) and (7).

3. Quantum Field Theory of Fuzzy Event

For the non-relativistic particle system (microscopic low-speed phenomenon) whose particle-number is certain, probability conservation is satisfied. So, there is no fuzziness, $\lambda_{\tilde{R}}\left[\vec{r}\left(t\right)\right]=1$. Thus, (5) becomes usual Feynman path integral.

But, for field theory (microscopic high-speed phenomenon), it is difficult to accurately determine the particle-number of every momentum value because of the generation and annihilation of the virtual particle pairs in vacuum. According to the fuzzy quantity theory of fuzzy mathematics [16], this kind of quantity, which is difficult to be assessed accurately, should be regarded as fuzzy variable represented by the membership function. That's to say, the microscopic vacuum state of field theory is unsharp (uncertain). It is also known that the determined microscopic state corresponds to the determined field function. Thus, the fuzziness of the microscopic state of vacuum directly leads to the fuzziness of the field function of vacuum (this can be called "fuzzy vacuum" or "fuzziness of vacuum"). Whereas the fuzziness of field function again leads to the fuzziness of the path integral of field theory. So, if (5) is used to describe field system, one can have $0\leq\left|\lambda\left[\varphi\left(x\right)\right]\right|^2\leq 1$ (here real scalar field $\varphi\left(x\right)$ is taken as an example).

Here it should be pointed out that if (6) and (7) are used to describe the field theory, (6) is based on the fuzziness of the field function and fuzzy field function should be written as

$$\tilde{\varphi}\left(x\right) = \frac{1}{\left(2\pi\right)^3}\int_{-\infty}^{\infty}\tilde{q}\left(\vec{k},t\right)\mathrm{e}^{i\vec{k}\cdot\vec{x}}\mathrm{d}^3k.$$

Where $\tilde{q}\left(\vec{k},t\right)$ indicates the fuzziness of microscopic state of the field. Whereas in (7), since (7) is the result of the non-fuzzification of (6), the field function $\varphi\left(x\right)$ also should be regarded as the result of the non-fuzzification of $\tilde{\varphi}\left(x\right)$ with the form

$$\varphi\left(x\right) = \left(1/\left(2\pi\right)^3\right)\int_{-\infty}^{\infty}\lambda\left(\vec{k}\right)q\left(\vec{k},t\right)\mathrm{e}^{i\vec{k}\cdot\vec{x}}\mathrm{d}^3k. \quad (10)$$

Where $q(\vec{k},t)$ is a possible value of $\tilde{q}(\vec{k},t)$, whose membership degree is maximum. $\lambda(\vec{k})$ is the relative membership degree amplitude of $q(\vec{k},t)$, and $\mu(\vec{k}) = |\lambda(\vec{k})|^2$ represents the relative membership degree for $q(\vec{k},t)$. For the non-vacuum field (the field of excited state), there is no fuzziness, $\mu(\vec{k}) = 1$; whereas for vacuum field (the field of ground state), there is fuzziness, $0 \le \mu(\vec{k}) \le 1$. Here it is might as well supposed temporarily that

$$\lambda(\vec{k}) = \sqrt{\Lambda^{2n} / (\vec{k}^2 + \omega_{\vec{k}}^2 + \Lambda^2)^n}. \tag{11}$$

This is a form satisfying the requirement of theoretical relativistic invariance. $\Lambda(\Lambda \in R)$ and $n(n \in N)$ are two undetermined parameters (constants). Of course, besides of (11), $\lambda(\vec{k})$ or $\mu(\vec{k}) = |\lambda(\vec{k})|^2$ also can take other forms (see **Figure 4**).

The introduce of $\lambda_{\tilde{R}}[\varphi(x)]$ into path integral of field theory will lead to the change of the forms of Green function and physical quantity. It is easy to prove that the expressions of the n-point Green function and physical quantity, which are corresponding to the fuzzy path integral, respectively are

$$
\begin{aligned}
G(x_1, \cdots, x_n) &= \langle 0 | T \{ \lambda_{\tilde{R}}[\varphi(x_1)] \hat{\varphi}(x_1) \cdots \lambda_{\tilde{R}}[\varphi(x_n)] \hat{\varphi}(x_n) \} | 0 \rangle \\
&= i^{-n} \frac{\delta^n W_F[J]}{\delta J(x_1) \cdots \delta J(x_n)} \Bigg|_{J=0},
\end{aligned}
\tag{12}
$$

$$\langle O \rangle = \frac{1}{Z} \int D\varphi O[\varphi(x)] \lambda_{\tilde{R}}[\varphi(x)] \exp\left\{ \frac{i}{\hbar} S[\varphi(x)] \right\}. \tag{13}$$

Where $W_F[J]$ is the generating functional based on the fuzzy path integral, $O[\varphi(x)]$ is the physical quantity under study, and Z is the fuzzy path integral about $\varphi(x)$ and its form is like (5).

It is worth being pointed out that in the quantum probability theory of fuzzy event, since probability conservation is broke, unitarity does not hold (because unitarity means probability conservation). Because unitarity also implies gauge invariance and information conservation, the breaking of unitarity will mean the breaking of gauge invariance and information (entropy) conservation. The unconservation of information (entropy) further means irreversibility. The breaking degree of unitarity can be depicted by the rate of the change of information (entropy): the change rate being large (corresponding to irreversible process) means large breaking degree, the change rate being small implies less breaking degree, and the change rate tending to zero (corresponding to reversible process) means that unitarity is not broken. Traditional quantum field theory, which argues unitarity, is applicable to the reversible process; whereas quantum field theory of fuzzy event in this paper, which negates unitarity, is suitable for the irreversible process.

The relations among these several conceptions are shown in **Figure 3**.
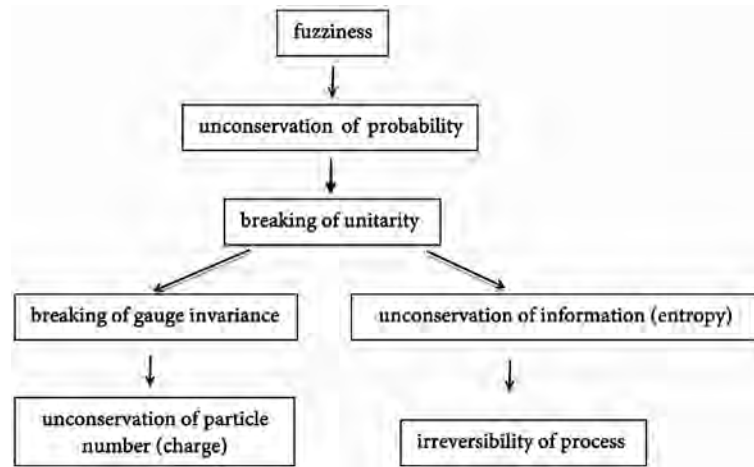
Figure 3. The breaking degree of unitarity can be depicted by such several approaches: 1) the rate of change of information (entropy), $\mathrm{d}I/\mathrm{d}t \to 0$, unitarity comes into true. 2) the breaking degree of gauge invariance, $k_\mu \Pi_{\mu\nu}(k) \to 0$ (here $\Pi_{\mu\nu}(k)$ is taken as an example), unitarity comes into true. 3) the breaking degree of probability conservation, $|P_{sum} - 1| \to 0$, unitarity comes into true. It can been seen that the so-called "unitarity", "gauge invariance", "probability conservation", "information conservation" and "reversible process" are all not strict principles but approximate ones under certain conditions. It will be seen in the next section that for black hole, these approximate principles no longer hold!

4. The Mathematical Form of Membership Degree Amplitude and Fuzzy Diagram

In the path integral of fuzzy event, what is the mathematical form of the membership degree amplitude $\lambda_{\tilde{R}}[\varphi(x)]$? This is a process of exploration.

For instance, for the scattering problem of the electron-photon interaction system, it can be ordered that

$$
\begin{aligned}
&\lambda_{\tilde{R}_1}\left[\bar{\psi}(x),\psi(x),A_\mu(x)\right] \\
&= F_1 \exp\left\{\frac{i}{\hbar}\int d^4x\left[\delta m\bar{\psi}(x)\psi(x)+\frac{1}{2}\delta\mu_A^2 A_\mu(x)A_\mu(x)\right]\right\}.
\end{aligned}
\tag{14}
$$

Where $d^4x = dx_1 dx_2 dx_3 dx_4$, $x_4 = it$ is virtual time. F_1 is a constant satisfying

$$
0 \le \left|\lambda_{\tilde{R}_1}\left[\bar{\psi}(x),\psi(x),A_\mu(x)\right]\right|^2 \le 1.
$$

$$
\delta m = \Sigma^*(p)\big|_{\gamma_\nu p_\nu = im}. \quad \delta\mu_A^2 \text{ satisfies}
$$

$$
-i(2\pi)^4 \delta_{\mu\nu}\delta\mu_A^2 = \Pi^*_{\mu\nu}(k \to 0).
$$

Since gauge invariance is broken in quantum field theory of fuzzy event, the square term of gauge field is introduced into (14). This square term breaks unitarity and probability conservation. The breaking degree is decided by the integral of this square term. When the integral is relatively large, the breaking degree of unitarity also is relatively large; when the integral is relatively small, the breaking degree of unitarity also is relatively small. When the integral tends to zero, the

square term of the gauge field can be ignored, and gauge invariance, unitarity, probability conservation and information conservation come into true.

By using (10) and (14), a S matrix element without divergence, from which the theoretical results can be computed in accordance with the experimental data, can be obtained from (12). The propagators in the S matrix element have the following forms:

$$S_F(p) = \mu(p) \times \frac{i}{(2\pi)^4} \frac{i\hat{p} - m}{p^2 + m^2 - i\varepsilon}, \quad (\text{for electron})$$

$$\delta_{\mu\nu} D_F(k) = \mu(k) \times \frac{-i}{(2\pi)^4} \frac{\delta_{\mu\nu}}{k^2 - i\varepsilon}. \quad (\text{for photon})$$

Here $\mu(p)$ and $\mu(k)$ are the membership degree factors of the propagators. Several Feynman diagrams are drawn in **Figure 4** to show the membership degrees of the vacuum propagators.

These diagrams in **Figure 4** are actually called "fuzzy graphs" [18] in fuzzy mathematics. It can been seen from these fuzzy graphs that in vacuum, the higher the order of the excitation is, the lower its degree of membership is. That is to say, the farther away from the influence of non-vacuum particles the vacuum is, the smaller the membership degree of its propagator is. In this way, it can be imagined that for a vacuum without the influence of non-vacuum particles, the membership degree of its propagator should tend to zero. Thus, for the vacuum without the influence of non-vacuum particles, n should be a very large value in (11). The vacuum energy (density) calculated with (10) and (11) will be a very small value, which can help to explain the problem of small cosmological constant.

Since there is no divergence in the quantum field theory of fuzzy events, the renormalization is not need (Some people think that the renormalization theory cannot be regarded as a completely correct theory even though it's supported by experiments. We should also seek a deeper understanding to explain the intrinsic nature of the agreement between the experimental results and the calculated results [19]. The quantum theory of fuzzy events may be an attempt at this understanding). Though generally renormalization is not need, the renormalization of the coupling constant can be carried out for some specific purposes, for instance, researching "asymptotic freedom".

It should be pointed out that under the condition of $\Lambda_1 = 6 \sim 10m$ and $\Lambda_2 < 1 \times 10^{-4} m$, the above fuzzy diagrams give

$$\delta\mu_A^2 \approx 0 \text{ and } k_\mu \left[\Pi_{\mu\nu}^*(k) - \Pi_{\mu\nu}^*(0)\right] \approx 0 \rightarrow k_\mu \Pi_{\mu\nu}^*(k) \approx -i(2\pi)^4 k_\mu \delta_{\mu\nu} \delta\mu_A^2 \approx 0.$$

Thus, gauge invariance, unitarity and the conservation of probability and information come into true in an approximate sense (it is mentioned above that these principles are only approximate ones).

Similarly, for the quark-gluon system, it can be ordered that

$$\lambda_{\tilde{R}_2}\left[\bar{\psi}(x), \psi(x), B_\mu^\rho(x), \bar{\eta}(x), \eta(x)\right]$$
$$= F_2 \exp\left\{\frac{i}{\hbar}\int d^4 x\left[\delta m_\psi \cdot \bar{\psi}(x)\psi(x) + \frac{1}{2}\delta\mu_B^2 \cdot B_\mu^\rho(x) B_\mu^\rho(x) + \delta\mu_\eta^2 \cdot \bar{\eta}^c(x)\eta^c(x)\right]\right\}. \quad (15)$$
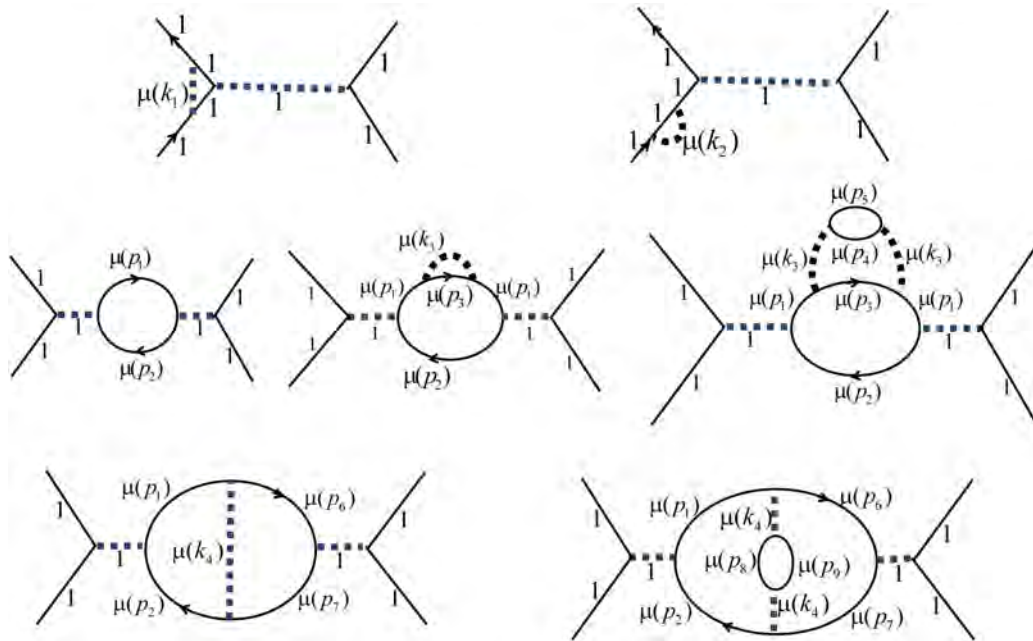
Figure 4. This figure shows the rules and laws of writing the (relative) membership degree factors of various propagators. The membership degree is assigned the value 1 for the non-vacuum propagator, $\Lambda_2^2 \big/ \left[\left(2p \pm k \right)^2 + \Lambda_2^2 \right]$ for the vacuum electron propagator of the first-level excitation and $\left[\Lambda_1^2 \big/ \left(k^2 + \Lambda_1^2 \right) \right]^2$ for the vacuum photon propagator of the first-level excitation (*i.e.* in (11), $n = 2$). Here, the so-called "first-level excitation" is pointing the vacuum propagator excited directly by the non-vacuum propagator. In addition, in the above digrams there are also second-level excitation, third-level excitation, fourth-level excitation, and so on. The "second-level excitation" is pointing the vacuum propagator excited directly by the vacuum propagator of the first-level excitation, and the "third-level excitation" is pointing the vacuum propagator excited directly by the vacuum propagator of the second-level excitation, and so on. In the above diagrams, the membership degrees of several vacuum propagators of the first-level excitation are respectively assigned the values as follows:

$\mu \left(k_1 \right) = \left[\Lambda_1^2 \big/ \left(k_1^2 + \Lambda_1^2 \right) \right]^2$,

$\mu \left(k_2 \right) = \left[\Lambda_1^2 \big/ \left(k_2^2 + \Lambda_1^2 \right) \right]^2$,

$\mu \left(p_1 \right) = \mu \left(p_3 \right) = \mu \left(p_6 \right) = \Lambda_2^2 \big/ \left[\left(2p_1 - k \right)^2 + \Lambda_2^2 \right]$,

Where $\Lambda_1 = 6 \sim 10m$, $\Lambda_2 < 1 \times 10^{-4} m$, m is the mass of electron. For the va-

$\mu \left(p_2 \right) = \mu \left(p_7 \right) = \Lambda_2^2 \big/ \left[\left(2p_2 + k \right)^2 + \Lambda_2^2 \right]$.

cuum propagator of the second-level excitation, the assignment of the membership degree should consider the influence of the fuzziness of the vacuum propagator of the first-level excitation. For instance, in the above diagrams,

$\mu \left(k_3 \right) = \left[\Lambda_2^2 \big/ \left(\left(2p_1 - k \right)^2 + \Lambda_2^2 \right) \right] \left[\Lambda_1^2 \big/ \left(k_3^2 + \Lambda_1^2 \right) \right]^2$,

$\mu \left(k_4 \right) = \left[\Lambda_2^2 \big/ \left(\left(2p_1 - k \right)^2 + \Lambda_2^2 \right) \right] \left[\Lambda_1^2 \big/ \left(k_4^2 + \Lambda_1^2 \right) \right]^2$ or $\left[\Lambda_2^2 \big/ \left(\left(2p_2 + k \right)^2 + \Lambda_2^2 \right) \right] \left[\Lambda_1^2 \big/ \left(k_4^2 + \Lambda_1^2 \right) \right]^2$. For the vacuum propagator of the

third-level excitation, the assignment of the membership degree should consider the influence of the fuzziness of the vacuum propagator of the second-level excitation. For instance, in the above diagrams,

$\mu \left(p_4 \right) = \left[\Lambda_2^2 \big/ \left(\left(2p_1 - k \right)^2 + \Lambda_2^2 \right) \right] \left[\Lambda_1^2 \big/ \left(k_3^2 + \Lambda_1^2 \right) \right]^2 \left[\Lambda_2^2 \big/ \left(\left(2p_4 + k_3 \right)^2 + \Lambda_2^2 \right) \right]$,

$\mu \left(p_5 \right) = \left[\Lambda_2^2 \big/ \left(\left(2p_1 - k \right)^2 + \Lambda_2^2 \right) \right] \left[\Lambda_1^2 \big/ \left(k_3^2 + \Lambda_1^2 \right) \right]^2 \left[\Lambda_2^2 \big/ \left(\left(2p_5 - k_3 \right)^2 + \Lambda_2^2 \right) \right]$,

$\mu \left(p_8 \right) = \left[\Lambda_2^2 \big/ \left(\left(2p_1 - k \right)^2 + \Lambda_2^2 \right) \right] \left[\Lambda_1^2 \big/ \left(k_4^2 + \Lambda_1^2 \right) \right]^2 \left[\left(\Lambda_2^2 \big/ \left(2p_8 + k_4 \right)^2 + \Lambda_2^2 \right) \right]$,

For the vacuum propagators of the higher-level exci-

$\mu \left(p_9 \right) = \left[\Lambda_2^2 \big/ \left(\left(2p_1 - k \right)^2 + \Lambda_2^2 \right) \right] \left[\Lambda_1^2 \big/ \left(k_4^2 + \Lambda_1^2 \right) \right]^2 \left[\Lambda_2^2 \big/ \left(\left(2p_9 - k_4 \right)^2 + \Lambda_2^2 \right) \right]$.

tation, and so on.

Where $\eta(x)$ represents ghost field. But, in the case of lattice gauge field, there is no ghost field. According to the above thought, under the condition of large momentum exchange, the perturbation S matrix element without divergence can be obtained whose theoretical results accord with the experimental data when

$$\begin{cases} \Lambda_3 \le 10^{-7} m_e, \ (\text{for the membership degree factor of the vacuum propagator of gluon}) \\ \Lambda_4 \le 10^{-8} m_e, \ \left(\begin{array}{l}\text{for the membership degree factor of the vacuum propagator of ghost} \\ \text{particle}\end{array}\right) \\ \Lambda_5 \le 10^{-9} m_e. \ (\text{for the membership degree factor of the vacuum propagator of quark}) \end{cases}$$

What is more, gauge invariance, unitarity, probability conservation and information conservation are all satisfied because

$$\delta\mu_B^2 \approx 0 \quad \text{and} \quad k_\lambda\left[\left(\Pi^*\right)_{\lambda\lambda'}^{aa'}(k) - \left(\Pi^*\right)_{\lambda\lambda'}^{aa'}(0)\right] \approx 0 \rightarrow k_\lambda\left(\Pi^*\right)_{\lambda\lambda'}^{aa'}(k)$$
$$\approx -i(2\pi)^4 k_\lambda \delta_{\lambda\lambda'} f_{abc} f_{a'bc} \delta\mu_B^2 \approx 0.$$

However, under the condition of extremely strong gluon field, the integral of the square term of gluon field cannot be ignored, and the breaking of unitarity also has to be considered.

Since the quantum field theory of fuzzy event need no renormalization and infinitely many offsetting terms and can naturally give meaningful results without divergence, it is the theoretical framework required for the quantization of gravity. For the system of gravity and scalar field, it is ordered that

$$\lambda_{\tilde{R}_3}\left[h^{\mu\nu}(x), \bar{\theta}^\alpha(x), \theta_\beta(x), \phi(x)\right]$$
$$= F_3 \exp\left\{(i/\hbar)\int d^4x\left[(1/2)\delta\mu_h^2 h^{\mu\nu}(x)h_{\mu\nu}(x)\right.\right. \tag{16}$$
$$\left.\left. + \delta\mu_\theta^2 \bar{\theta}^c(x)\theta_c(x) + \frac{1}{2}\delta\mu_\phi^2 \phi(x)\phi(x)\right]\right\}.$$

Where $\theta(x)$ is the ghost field, $h^{\mu\nu} = \left(gg^{\mu\nu} - \eta^{\mu\nu}\right)/\kappa$ is the gravitational field. $\delta\mu_h^2$ is a very small value (this is similar to $\delta\mu_A^2$ and $\delta\mu_B^2$ above). For weak gravity system, the gravitational square term in (16) is very small and thereby can be ignored, unitarity is tenable. But, for the black hole or the universe of very early stage, due to extremely strong gravity, the gravitational square term in (16) can no longer be ignored. So, the breaking of unitarity also can no longer be ignored, and information is no longer conserved.

5. Conclusions

In this paper the second kind of fuzzy quantum probability theory (quantum probability of fuzzy event) is proposed. This theory can be regarded as the reformation and redevelopment of usual quantum theory, making fuzzy events also be able to be described. Under certain conditions, the quantum probability theory of fuzzy event will transition to usual quantum theory. Thereby, traditional quantum theory is only the special case of the quantum probability theory of fuzzy event. Due to the introduction of fuzziness, this new theory breaks un-

itarity, gauge invariance, probability conservation and information conservation, making these principles become approximate ones under certain conditions. This new theory is a theory which can describe irreversible process, whereas quantum mechanics is only a theory to describe reversible process. This new theory, which needs no renormalization and can naturally give meaningful results in accordance with the experiments, is the proper theory to describe microscopic high-speed phenomenon, whereas quantum mechanics is only a proper theory to describe microscopic low-speed phenomenon.

The novelty of the work of this paper lies in: 1) bringing forward the conept and idea of "fuzzy vacuum" or "fuzziness of vacuum"; 2) putting forward that under the condition of extremely strong gauge field or gravitational field, usual quantum theory and unitarity will fail.

At present, seemly there are six directions for the quantum theory of fuzzy event to play roles:

1) Being helpful to meaningfully quantize gravity.

2) Being helpful to construct the unified theory of four basic forces.

3) Being helpful to solve the puzzle of cosmological constants.

4) Being helpful to research quantitatively the origin of the Big Bang.

5) Being helpful to understand the problem of black hole information loss.

6) Possibly providing a new idea and solution to the "abnormal" decay probability of B mesons in LHCb.

Conflicts of Interest

The author declares no conflicts of interest regarding the publication of this paper.

References

[1] Hawking, S.W. (1976) *Physical Review D*, **14**, 2460-2472. https://doi.org/10.1103/PhysRevD.14.2460

[2] Zhang, B.C., Cai, Q.Y., You, L., *et al.* (2009) *Physical Letters B*, **675**, 98-101. https://doi.org/10.1016/j.physletb.2009.03.082

[3] Zhang, B.C., Cai, Q.Y., Zhan, M.S., *et al.* (2011) *Annals of Physics* (*New York*), **326**, 350-363. https://doi.org/10.1016/j.aop.2010.11.015

[4] Zhang, B.C., Cai, Q.Y., Zhan, M.S., *et al.* (2013) *International Journal of Modern Physics D*, **22**, 1341014. https://doi.org/10.1142/S0218271813410149

[5] Hawking, S.W. (2005) *Physical Review D*, **72**, 084013. https://doi.org/10.1103/PhysRevD.72.084013

[6] Callan, C.G. and Maldacena, J.M. (1996) *Nuclear Physics B*, **472**, 591-608. *https://doi.org/10.1016/0550-3213(96)00225-8*

[7] Mathur, S.D. (2009) *Classical and Quantum Gravity*, **26**, 224001. https://doi.org/10.1088/0264-9381/26/22/224001

[8] Page, D.N. (1993) *Physics Review Letters*, **71**, 3743-3746. https://doi.org/10.1103/PhysRevLett.71.3743

[9] Ryu, S. and Takayanagi, T. (2006) *Physics Review Letters*, **96**, 181602.

https://doi.org/10.1103/PhysRevLett.96.181602

[10] Almheiri, A., Engelhardt, N., Marolf, D., *et al.* (2019) *Journal of High Energy Physics*, **2019**, 63. https://doi.org/10.1007/JHEP12(2019)063

[11] Almheiri, A., Mahajan, R., Maldacena, J., *et al.* (2020) *Journal of High Energy Physics*, **2020**, 13. https://doi.org/10.1007/JHEP03(2020)149

[12] Penington, G., Shenker, S.H., Stanford, D., *et al.* (2019) arXiv preprint arXiv: 1911. 11977

[13] Zhang, J., Hu, Y. and Zhao, Z. (2006) *Modern Physics Letters A*, **21**, 1865-1868. https://doi.org/10.1142/S0217732306019980

[14] Qiu, W. (2020) *Journal of Modern Physics*, **11**, 952-966. https://doi.org/10.4236/jmp.2020.116059

[15] Schwartz, D.G. (2015) On the Probability of a Fuzzy Event, with Application to Nonmonotonic Reasoning. 2015 *Annual Conference of the North American Fuzzy Information Processing Society* (*NAFIPS*) *Held Jointly with* 2015 5*th World Conference on Soft Computing* (*WConSC*), Digipen, WA, 17-19 August 2015, 1-6. https://doi.org/10.1109/NAFIPS-WConSC.2015.7284124

[16] Timothy, J.R. (2001) Fuzzy Logic and Its Engineering Applications. Publishing House of Electronics Industry, Beijing, 75.

[17] Didier, D. and Henri, P. (1980) Fuzzy Sets and Systems Theory and Applications. Academic Press, London, 110-111.

[18] Feng, D. and Long, S. (1985) Methods and Applications of Fuzzy Mathematics. Seismological Press, Beijing, 22-24.

[19] Yin, P. (1986) The Outline of Quantum Field Theory. Shnghai Scientific & Technical Publishers, Shanghai, 372.

Journal of Modern Physics

Journal of Modern Physics

Journal of Modern Physics **(JMP)** is an international journal dedicated to the latest advancement of modern physics. The goal of this journal is to provide a platform for scientists and academicians all over the world to promote, share, and discuss various new issues and developments in different areas of modern physics.

Editor-in-Chief

Prof. Yang-Hui He   City University, UK

Subject Coverage

Journal of Modern Physics publishes original papers including but not limited to the following fields:

Biophysics and Medical Physics	New Materials: Micro and Nano-Mechanics and Homogeneization
Complex Systems Physics	Non-Equilibrium Thermodynamics and Statistical Mechanics
Computational Physics	Nuclear Science and Engineering
Condensed Matter Physics	Optics
Cosmology and Early Universe	Physics of Nanostructures
Earth and Planetary Sciences	Plasma Physics
General Relativity	Quantum Mechanical Developments
High Energy Astrophysics	Quantum Theory
High Energy/Accelerator Physics	Relativistic Astrophysics
Instrumentation and Measurement	String Theory
Interdisciplinary Physics	Superconducting Physics
Materials Sciences and Technology	Theoretical High Energy Physics
Mathematical Physics	Thermology
Mechanical Response of Solids and Structures	

We are also interested in: 1) Short Reports—2-5 page papers where an author can either present an idea with theoretical background but has not yet completed the research needed for a complete paper or preliminary data; 2) Book Reviews—Comments and critiques.

Notes for Intending Authors

Submitted papers should not have been previously published nor be currently under consideration for publication elsewhere. Paper submission will be handled electronically through the website. All papers are refereed through a peer review process. For more details about the submissions, please access the website.

Website and E-Mail

https://www.scirp.org/journal/jmp   E-mail: jmp@scirp.org

What is SCIRP?

Scientific Research Publishing (SCIRP) is one of the largest Open Access journal publishers. It is currently publishing more than 200 open access, online, peer-reviewed journals covering a wide range of academic disciplines. SCIRP serves the worldwide academic communities and contributes to the progress and application of science with its publication.

What is Open Access?

All original research papers published by SCIRP are made freely and permanently accessible online immediately upon publication. To be able to provide open access journals, SCIRP defrays operation costs from authors and subscription charges only for its printed version. Open access publishing allows an immediate, worldwide, barrier-free, open access to the full text of research papers, which is in the best interests of the scientific community.

- High visibility for maximum global exposure with open access publishing model
- Rigorous peer review of research papers
- Prompt faster publication with less cost
- Guaranteed targeted, multidisciplinary audience

Scientific Research Publishing

Website: https://www.scirp.org
Subscription: sub@scirp.org
Advertisement: service@scirp.org